CRANFIELD INSTITUTE OF TECHNOLOGY

Department of Materials

PhD Thesis

V. T. de Abreu e Antunes

Creep Fatigue Analysis of a Nickel Superalloy over the Range 750 - 1040°C

Supervisor P Hancock

September 1979

Abstract

After the review of the predictive methods in the high temperature fatigue field the characterization of the low cycle fatigue behaviour of a nickel superalloy, MARM002, is carried out using one of those predictive methods, the Strainrange Partitioning method. The basic concepts and procedures of this method are reviewed and applied to MARM002 over the range 750° - 1040°C. These procedures involved the determination of the four basic life relationships at 850°C and 1040°C and their use in conjunction with a damage rule were then employed to assess the degree of insensitivity of the four basic strainrange versus life relationships to test temperature. Three damage rules and the assumptions behind them are discussed within the context of their application with the Strainrange Partitioning approach. An alternative analysis based on Ostergren's method is studied in a separate chapter and proved to be an easy and helpful method in predicting high temperature low cycle fatigue of several superalloys.

The characterization of the creep-fatigue behaviour of MARM002 was completed by separation of initiation and propagation periods within two temperature intervals. A situation of early formation of cracks at the higher temperature interval 950° - 1040°C with accelerated growth at lower temperatures 750° - 850°C showed that great care is necessary when applying MARM002 isothermal results to cases where temperature varies.

ACKNOWLEDGEMENTS

I am greatly indebted to Professor P Hancock for his friendly help, guidance and encouragement throughout the period of research leading up to this thesis. The leave of absence from DEMEC - FACULADE DE ENGENHARIA - UNIVERSIDADE DO PORTO and the encouragement from Professor Vasco de Sà to start this period of studies in Cranfield are also acknowledged.

Thanks are due to Dr G Harrison at National Gas Turbine Establishment and Mr T Clifton at Cranfield Institute of Technology for their helpful discussions and assistance.

I would like to thank the Junta Nacional de Investigação Cientifica & Tecnológica in Lisboa for the financial support given. I further want to thank Mr D Smith for his assistance with the experiments and Miss Elizabeth Bellamy for typing the text.

Finally a special mention to all my friends at Coffee House 28 without whom this stage at Cranfield would have been just passable.

C O N T E N T S

Page No

F I G U R E S

List of Tables

N O T A T I O N

D	Damage
D_f	Damage associated to fatigue
D_c	Damage associated to creep
$\frac{\delta D}{\delta N}$	Damage per cycle
E	Young Modulus
F_{ij}	Strain ratio of type ij
F_{pp}	Strain ratio of type PP
F_{cp}	Strain ratio of type CP
F_{pc}	Strain ratio of type PC
F_{cc}	Strain ratio of type CC
L	Load
m	Creep-rupture exponent
N	No of cycles
N_f	No of cycles to failure
N_5	No of cycles for 5% drop in tensile load
N_p	No of cycles in propagation
n'	Strain hardening exponent
N_t	Transition fatigue life
N_{OBS}	Observed life
N_{PRED}	Predicted life
RA	Reduction of area
t	Time
t_f	Time to failure
t_h	Time of hold period
T	Temperature

τ	Time per cycle
τ_t	Time per cycle in tension
τ_c	Time per cycle in compression
ν	Frequency
ν_c	Compression going frequency
ν_t	Tension going frequency
ϵ	Strain
ϵ_r	Strain at rupture
$\Delta\epsilon_t$	Total strain range
$\Delta\epsilon_e$	Elastic strain range
$\Delta\epsilon_p$	Plastic strain range
$\Delta\epsilon_i$	Inelastic strain range
$\Delta\epsilon_{pp}$	Inelastic strain range of the type PP
$\Delta\epsilon_{pc}$	Inelastic strain range of the type PC
$\Delta\epsilon_{cp}$	Inelastic strain range of the type CP
$\Delta\epsilon_{cc}$	Inelastic strain range of the type CC
$\dot{\epsilon}$	Strain rate
σ	Stress
$\Delta\sigma$	Stress range
σ_u	Ultimate tensile strength
σ_f	True fracture stress
σ_T	Tensile stress
σ_r	Creep rupture stress
σ_M	Maximum stress
$\bar{\sigma}$	Mean stress

1 - INTRODUCTION

Equipment that operates at elevated temperature is often subjected to a combination of transient and steady-state loading conditions. Many service components may undergo a thermally induced strain cycle during start-up and shut down or during variations in operating conditions. Under steady state conditions time dependent creep or stress relaxation on the material are most likely to occur at high temperatures. It is the likely interaction of the cyclic fatigue damage and the time dependent creep damage which brings most of the problems on the design of elevated temperature equipment. A survey of the literature dealing with the life prediction analysis of the creep-fatigue situations shows widespread difficulties in generalising each approach in order to take into account a variety of factors such as frequency, wave shape, tensile and compressive hold effects, environment-component interactions, varying temperature within a cycle, etc.

Common features of many high temperature fatigue tests are a very pronounced degradation in fatigue resistance when the frequency of cycling is low or long hold time periods are introduced. This degradation is closely dependent on how high is the working temperature range, upon how fast that range is crossed and where the hold period is introduced, tension compression or both. Moreover, these situations involve thermal fatigue occurring during start and shut down periods where high strains are generated due to different rates of heating and cooling in components within a certain structure. Included are aircraft gas turbines, nuclear pressure vessels, heat exchangers and fuel elements, steam turbines and power plant components, etc. The technological performance of components working in these exigent high temperature situations is largely dependent upon the development of new high temperature alloys and the accurate prediction of the fatigue life of the high temperature structure.

This last exercise usually consists of two major steps: calculation of the stress and strain history in critical regions and estimation of the lives of these regions. As far as this second point is concerned the usefulness of any life prediction method in these sort of situations in which fatigue and creep are superimposed depends in the first place on how good is the simulation of the tensile conditions. The use of isothermal strain controlled tests to simulate and study components subjected to thermal fatigue has been of widespread use because tests are easier to conduct with better control of the variables normally related to fracture: plastic and creep strains, stress and temperature. This simplification becomes even more attractive with any method promising some degree of temperature insensitivity to its basic life relationships since that would save generation of data for different temperatures. This simplification was offered by a recently developed life prediction method, Strainrange Partitioning which was chosen for the characterization of the high temperature, low cycle fatigue behaviour of MARM002, a recently developed nickel superalloy, within the

temperature range 750 - 1040^{o}C. This low cycle fatigue characterization of MARM002 is reported in chapter four of this thesis. An alternative method for life prediction is discussed in chapter six being the study extended in there to other six alloys.

The problems associated with the use of isothermal data to thermal fatigue situations are discussed in chapter seven. Since the initiation and propagation periods separation was found to be essential for the understanding of the results on those circumstances, the relative importance of initiation and propagation on the creep fatigue tests of MARM002 was assessed then in chapter seven, as a first step to approach the thermal fatigue situations using isothermal data.

Some of the damage rules involved on many life prediction methods are discussed separately in chapter five.

2 - REVIEW OF THE PREDICTIVE METHODS IN HIGH TEMPERATURE FATIGUE

The subject of high temperature low cycle fatigue can be approached from two directions. On one case the big emphasis is put on fatigue, with modification being made to the fatigue laws developed for room temperature in order to take into account creep effects. The alternative case considers the isostatic creep laws governing high temperature deformation and manipulates the laws in order to apply them to cyclic loading.

Looking back, there are two important developments over the past thirty years. Firstly, the COFFIN-MANSON relationship (1) marked an important transition from a stress to a strain approach and secondly the PARIS-ANDERSON concept relating stress intensity factors to fatigue crack growth rates (2). There were also several attempts to develop accurate and general methods of predicting cyclic lives at room and high temperatures. The MANSON-HIRSCHEBERG universal slopes method (3) was developed enabling room temperature cyclic lives to be estimated as a function of the total strain range using conventional short time tensile properties. It is followed by attempts to account for creep effects such as the so called 10% rule (4) and the creep modified 10% rule (5). The life fraction approach (6) tried to remedy the rather conservative results predicted by the former methods when large creep strains were involved. Finally the formation of the STRAINRANGE PARTITIONING method was proposed in 1971 promising to overcome many of the difficulties found with previous methods. Before going into detailed analysis of those methods with usefulness, advantages and limitations being analysed, a review of the testing variables found in high temperature low cycle fatigue will be done. Their effect on life, for different materials when possible, is presented.

2.1 - THE TESTING VARIABLES IN HIGH TEMPERATURE LOW CYCLE FATIGUE

At elevated temperatures the need for reliable procedures for life-time prediction is of increasing concern. Trying to solve the problem, a great number of prediction methods were developed. The difficulties associated with their application, becomes clear after studying the number and type of new variables appearing in this field. Moreover, there appears to be some doubt as to the effect of some variables in a certain cycle with sometimes opposite results for different materials. Take as an example the holdtime periods which is recognised as an important source of life degradation. It seemed till some time ago that the tensile holds were the most damageable ones with some visible healing effects with the introduction of a compressive hold because the crack path changed from intergranular to transgranular. However, later reports on some nickel superalloys showed the compressive holds as the most damageable. As soon as a material is cyclic stressed within its creep range, more variables are added or the relative importance of existing variables at room temperature are then

drastically changed, which is going to alter its behaviour at higher temperatures. For example processes of oxidation are greatly accelerated with the rate of thickening of some oxides increasing exponentially with increasing temperature and thermal activated processes bringing into play new deformation processes. It is believed that the different high temperature behaviour is to a certain extent the result of these new mechanisms of deformation operating at high temperature (grain boundary sliding, dislocation climb, vacancies, diffusion, etc). Plastic deformation can occur more readily, temperature, stress level and strain rate being the factors which determine what mechanisms will predominate.

An obvious danger associated with this rests on the fact that the short time accelerated laboratory tests may involve significantly different deformation modes when compared to the long time tensile conditions experienced by a component. The consequences can be a bigger ratio between predicted and observed lives which decreases the reliability of the prediction method.

2.1.1 - Temperature

The majority of materials exhibit reduced number of cycles to crack initiation and failure with increased temperature. For a given total strain amplitude, the number of cycles to failure are reduced as the temperature increases and the ratio inelastic strain to elastic strain increases due to the lower yield strength. Even for equal inelastic strain ranges the fatigue life is reduced with increasing temperature because of the easier initiation and propagation of microcracks when intergranular cracking mode becomes more likely (7). There are exceptions to this, in some ferrous materials and nickel superalloys experiencing strain ageing above room temperature (8,9). Under conditions of strain cycling the effect of increasing the test temperature is to reduce the strain range that leads to failure in a specified number of cycles; the curve of total strain amplitude versus cycles to failure moves generally downwards and towards the left. Using a representation for elastic and plastic strain ranges suggested by Manson at low temperatures (10), the total strain range can be found analitically by combining a frequency modified elastic and plastic strain ranges.

$$\Delta\varepsilon_t = \Delta\varepsilon_e + \Delta\varepsilon_p = \frac{A'}{E} N_f^{-\beta'} \nu^{k1} + C_2 (N_f \nu^{k-1})^{-\beta} \qquad (2.1)$$

where $\Delta\varepsilon_t$ - total strain range

$\Delta\varepsilon_e$ - elastic strain

$\Delta\varepsilon_p$ - plastic strain
N_f - cycles to failure
ν - frequency
E - YOUNG MODULUS
A', β', k', C_2, k, β - constants

Several features arise from the increasing temperature on fatigue phenomenology using this representation. First, higher temperatures seem to cause the plastic line to become steeper and the elastic line to be lowered. Secondly, with increasing temperature the transition fatigue life N_t (the life where the elastic and plastic strain range are equal) shift to lower values of life (11).

2.1.2 - Frequency

High temperature alloys used in gas turbine engines are subjected to fatigue stresses applied over a wide range of frequencies varying from the high vibrational frequencies experienced by the turbine blades ($\sim 2 \times 10^5$ cpm) to low frequencies associated with the period of engine operation (1 cycle per flight).

At low temperatures there is practically no effect of frequency on fatigue life except for frequencies approaching the ultrasonic range (12).

A decrease in frequency at elevated temperatures, where time dependent processes become important, tends to affect the number of cycles for crack initiation and propagation. Elevated temperature fatigue fracture can be essentially intergranular (along grain boundaries) or transgranular (across grains). The rate of crack initiation and propagation is much faster where it occurs intergranularly. Therefore, it is to be expected that there should be a reduction in cyclic life where factors such as temperature or strain rate favour the intergranular mode of fracture.

ORGAN and GELL (13) found for a wrought nickel superalloy working at 760°C a decrease in life by a factor of about 100 on reducing the frequency from 600 to 2 cycles/min as shown in Figure(2.1). The observed peak on the cyclic life vs frequency curve is believed to be the result of two competing processes.

(i) A reduction in the effects of creep and oxidation with increased frequency that tends to increase the life.

(ii) An increase in the heterogeneity of deformation with increased frequency that tends to reduce life.

It was found that at low frequencies crack initiation occurred at surface-connected grain boundaries: crack propagation was initially intergranular and then proceeded non-crystallographically normal to the stress axis. On the other hand, crack initiation at high frequencies occurred at subsurface brittle phases located at grain boundaries and crack propagation was entirely transgranular (13).

Tilly et al (14) found that for Nimonic 90 tested at temperatures above 600°C the fatigue life increased with increasing frequency between 0.1 and 8000 cpm and increasing frequency favoured transgranular compared to intergranular crack propagation.

For the same superalloy working at 700°C Northwood et al (15) found fatigue life increased as frequency was increased from 4400 to 8600 cpm and that crack leading to failure initiated within the specimen interior.

A number of phenomenological models have been developed that consider the effect of frequency on fatigue life. Eckel and Coles (16,17) have used the equation:

$$\nu^k t_f = C_1 \tag{2.2}$$

to evaluate the relative influence of creep fatigue in hold-time tests. The relationship includes the frequency ν expressed in cycles/min, the time to failure t_f being k and C_1, constants depending on the material and testing conditions.

Equation (2.2) can be rewritten as:

$$\nu^k t_f = \nu^k \frac{N_f}{\nu} = N_f \nu^{k-1} \tag{2.3}$$

The quantity $N_f \nu^{k-1}$, where N_f is the number of cycles to failure has been called the frequency modified fatigue life and has been used in (18,19,20) as a parameter for combining frequency and life in the so called frequency modified fatigue equations. These equations which are supposed to represent the material behaviour through the use of the plastic (inelastic) strain range and the frequency of the cycle are

$$\Delta\varepsilon_p = A(N_f \nu^{k-1})^{-\beta} \tag{2.4}$$

$$\Delta\varepsilon_e = A' N_f^{-\beta'} \nu^{k1'} \tag{2.5}$$

It has been proposed (21,22) that in air environment at elevated temperature three frequency regimes exist. These three regimes are shown schematically in Figure (2.2) on a plot of the frequency of cycling ν versus N_f, the cycles to failure.

Excluding any consideration of strain rate dependency on crack tip strain localisation it was suggested that at very high frequencies the time for which the fatigue crack is open is too short for any chemical effect to influence the crack growth processes and, therefore, the frequency of cycling has no effect on crack growth. In this regime from equation (2.4), $k = 1$. At very low frequencies it has been observed (21) that the fracture mode is mainly intergranular and that for a specific inelastic strain range the time for failure remains constant independently of the frequency of testing. This regime corresponds to $k = 0$. For intermediate frequencies $0<k<1$. This is the regime where most material work with a progressive change of transgranular to intergranular crack growth as the frequency is lowered. The transition frequencies are identified as ν_e and ν_m in Figure (2.2) which is assumed to be generally representative of a wide variety of high temperature alloys. Further, in Figure (2.2) is shown an upper bound horizontal line representing the fatigue life for a frequency independent transgranular failure mode situation. Eventually this upper bound can be extended to very low frequencies. It was determined (23) at 600^{o}C for AISI304 stainless steel tested in high vacuum that the fatigue life was not significantly altered whether the frequency of cycling was 1 cpm or 0.01 cpm.

Data of Berling and Slot (20) for the same steel in air plotted in Figure (2.3) shows a severe life degradation. Apparently the degradation of fatigue was mainly due to environment - specimen interactions. On the other hand there are materials which showed a decrease in life at low frequencies even in high vacuum as found by Solomon and Coffin (22) for A283. They observed that above a critical frequency identified on Figure (2.2) as ν_m, the failure was increasingly transgranular and the life became independent of frequency while below ν_m the fracture was intergranular and the behaviour was best described by $k = 0$ in equation (2.4).

It seems, however, that for most materials life degradation with decreasing frequencies of practical interest is due to both factors: environment-specimen interactions and the change of deformation modes. Thus like in Figure (2.2) three regimes are of practical interest: a high frequency time independent regime, and intermediate regime when environment sensitivity is controlling and a low frequency regime where the deformation mode and environment interact. The critical

frequency ν_e describes the bound between the higher frequency regimes while ν_m defines the transition where the deformation mode changes independent of the environment.

2.1.3 - Hold Periods

In strain cycling introducing a hold time into a cycle causes an effect similar to that of decreasing the frequency. The extent of the fatigue life reduction is generally noted to be related to the length of the hold periods. Most of the time the fatigue life is reduced as the hold periods in tension and (or) compression are longer.

Several authors (24,25,26) found that the incorporation of hold periods at the maximum tensile strain limit, induces stress relaxation producing internal grain boundary cracking with consequent reduction in endurance. Such hold times effects have been reviewed by Krempl (27).

Wareing et al (28) found that tests involving 5 minute tensile hold periods result in considerable reduction in fatigue life, particularly at the lower strain levels where all the failures were due to the steady growth of a surface nucleated crack. Jaske et al (29) found for total strain amplitudes larger than 0.5%, hold time in tension had significantly shortened cyclic lives comparatively to non-hold tests. However, for lower strain levels, a 10 minute tension hold period did not significantly affect the cyclic life. This result suggested the existence of a threshold strain level, below which, hold time has little or no detrimental influence on fatigue life. This threshold value found for 304 stainless steel is believed to be one for which there is no appreciable introduction of creep with increasing hold time period. In fact, the hold time periods involving stress relaxation, present a limit to the amount of creep introduced in the cycle. The theoretical limit will be precisely the elastic component associated to the peak hold period part of the cycle.

Berling and Conway (30) have tried to develop a relationship between strain rate and hold time effects. A linear relationship on logarithmic co-ordinates was noted between the time to fracture (ratio of the number of cycles over the test frequency) and the cycle period. If this relationship works for other materials and test conditions one could predict hold time results from a knowledge of continuous strain cycling data at several strain rate or frequency levels.

However, this approach was found to have limitations made clear in Figure (2.4).

(i) Plots of cycles to fracture vs time for one cycle can not be extrapolated to high strain rates (low times for one cycle), because there is a threshold value for the time for one cycle dependent on total strain below which the cycles to failure are constant. This threshold value is suggested to be the one for which all time dependent deformation is eliminated.

(ii) The time to fracture for the non-hold time tests is no longer colinear with the hold period data in the range of large cycle times. Two regimes are defined in this range: one within the fatigue life is independent of strain rate, and another wherein N_f is independent of hold period length. The use of low frequency continuous data to hold time tests may lead to non-conservative results.

However, the most interesting points about plots such as the one in Figure (2.4) are the saturation effects both at high and low frequencies. The fact that several plateaus were found at the lower frequency region according to the wave shape of the test (continuous, tensile hold) was noted by Manson et al (92) in introducing the Strainrange Partitioning concept which is based on four strainrange to life relationships which are no more than saturation lines for four different basic type of tests: high frequency tests, low tests with tensile holds, low frequency tests with compressive holds and low frequency continuous tests. While tensile strain hold periods were generally found to be more damaging than equal hold periods in tension and compression or of compression hold periods only (31,32,33), this last type of dwell has been found to be most damaging in some lower ductile, high strength alloys, particularly, for the cast nickel-base superalloys.

Berling and Conway (26) found for 304 stainless steel strained at 650^{0}C that, if the cycle contained 30 minute tensile hold only, there was a serious reduction in cyclic life being the mode of crack propagation intergranular. If a small 3 minute compressive hold was introduced on the former cycle, then a healing effect was observed, so that the loss in cyclic life was small and the mode of initiation was transgranular.

Wells and Sullivan (9) testing a nickel based alloy - Udimet 700 - at 760^{0}C, concluded that holding compressive strains was more damaging than holding tensile strains. Lord and Coffin (34) found the same eg., compressive strain

hold periods reduce the fatigue lives relative to high frequency continuous cycling, while tensile strain holds gave greater lives. Studying a nickel base as cast superalloy, René 80, at 870°C they found that the hysteresis loops from the hold time tests exhibited pronounced and opposite mean stresses, the tensile strain hold tests showing a compressive mean stress shift. The variable 'mean stress' was considered of vital importance in determining life to fracture by Coffin (35) when the range of strains in which the material is tested is such that a great elastic strain component comparative to the inelastic one is found. This is more likely the lower the temperature, the lower the ductility or the higher the strength of the material under testing.

In order to explain the influence of these mean stresses on creep fatigue life elastic crack growth, arguments are introduced utilizing crack closure. It is believed that a compressive mean stress is less damaging and tensile mean stresses is a more damaging situation, such that tensile holds are less damaging than compressive hold periods. As the inelastic strain increases relative to the elastic strain crack closure differences diminish and damage due to crack growth during tensile relaxation becomes the controlling factor (23).

In a recent report (36) of the strainrange partitioning behaviour of an automotive nickel superalloy - CA 101 - it was found that strain dwells retards both the initiation and propagation processes. It was proposed there that dwells can potentially retard the initiation process because of the enhanced dispersion of localized deformation due to the activation of secondary dislocation mechanisms, eg., stacking faults. Coffin (35) suggests that dwells can potentially retard crack growth because of crack tip stress relaxation due to local creep deformation. Either one or both of these facts can lead to longer cyclic lives in the presence of a dwell or hold time if no other factor overides them.

2.1.4 - Wave Shapes

Up to this point, it has been referred as possible laboratory test to investigate high temperature behaviour of a certain material, the stress controlled tests, the strain controlled tests with or without periods of strain or stress dwells. With the appearance and generalized use of the closed loop equipment in most part of the fatigue laboratories, large and more complicated form of wave shapes are now available. It is possible then in a much more precise way to simulate the service conditions. On the other hand, the large

amount of possible wave shapes and the different responses of the specimen to them are often responsible for apparent unexplicable fatigue results. Therefore, the wave shape becomes an important variable on any low cycle high temperature programme. Various wave shapes produced in closed loop testing equipment are shown in Figure (2.5).

The first type (a) is the widely used fully reversed straining type employing commonly a triangular wave shape. Other family involves a strain hold period (b) either in tension, compression, or both and introduces a stress relaxation during the hold. In Figure (2.5) (c) is shown a wave shape due to continuous stress cycling. Here a mean stress exists and ratcheting (progressive monotonic deformation), may take place, depending on the transition fatigue life (35). This form of ratcheting can be time independent and will occur at all temperatures depending only on the magnitude of the mean stress and the plastic strain range (37,38). At elevated temperature time dependent ratcheting can be expected due to creep effects. Another family of wave shapes also involves stress control (d). When the stress is fully reversed, but hold periods are introduced ratcheting may occur to increase the strain during each cycle. The creep during the hold period is responsible for the observed ratcheting effect. Another wave shape now receiving much attention is the one pictured in (e). Like in (d) a stress hold period is introduced either in tension, compression, or both, but this hold time is limited by a strain limit. Generally a mean stress is developed with the possible consequences in fatigue life already seen for case (b). Wave shapes in this category have been identified as CP or PC depending on whether the hold period is in tension or compression. The CC type will be related to a cycle with hold periods in tension and compression. The wave shape of (a) was identified as a PP type wave shape when cycling is sufficiently rapid that no creep deformation occurs.

Another category of wave shapes can be produced when temperature cycling is combined with mechanical cycling (f). Techniques for producing these conditions are now possible (39,40). In (f) the situation is the one in which the mechanical strain and thermal strain are in phase. The result is a rather unusual hysteresis loop with a CP appearance due to the tensile creep at high temperature. In the out of phase cases, it is noted a rather developed creep component in compression due to the high temperature now occuring concomitantly with the compression part of the cycle.

These mixed mechanical and thermal cycles have been studied by Sheffler (41) on A286 and 304 stainless steel utilizing high vacuum. Figure (2.6) refers to some of these tests and includes isothermal tests (ISOT), cycles involving an

interspersed mechanical strain change and temperature change, either in phase (raising temperature then increasing the strain), identified as TCIPs or out of phase cycling (raising the temperature then decreasing the strain) which are identified as TCOPs.

For A286 there was little difference between the fast and slow isothermal tests in vacuum, while an appreciable loss of life was found for the mixed thermal and mechanical cycling under out of phase conditons.

Another series of fatigue tests is reported by Coffin (42) using slow-fast, fast-slow and equal range rates on A286 and AISI 304 stainless steels in air and high vacuum. The overall frequency was kept constant for all the wave forms. Independently of the environment and for both metal, the slow-fast tests constituted the lower bound in life and the fast-slow the upper bound in life. These results indicate that specific wave shapes can lead to more or less damage independent of environmental influences.

2.1.5 - Mean Stress

It was already reviewed the importance of hold periods in fatigue cycles and their different consequences whether one is being situated on a purely low cycle regime (fat hysteresis loop), or in a regime where the elastic strains are predominant.

It is well known the effect of a mean stress on the degradation of fatigue life on a high cycle regime. Admitting the existence of a fatigue limit is generalised at the design level the use of relationships that take into account that effect. There is no theoretical reason for any of those relationships and one could only point as a safe rule to base design, is to carry out prior tests on the material of interest and determine its behaviour under similar conditions to those ones it would be expected in service. However, one thing is common th these equations. It is well established that if the mean stress becomes tensile, a lowering of the fatigue limit results. It is to expect for lives between the low cycle and high cycle regimes, to find the same effects although with the possibility of being attenuated by other factors to be considered at high temperature fatigue (environment, creep).

Microscopically a high compressive mean stress retards the amount of opening of a crack and lowers the growth rate, while a tension mean stress causes a greater crack opening and enhances crack growth (35). Mean compressive stresses have been reported to greatly retard the rate of Stage I

crack propagation in fatigue due to the increased frictional forces developed between rubbed crack faces (43). Others (44) put emphasis on the importances of the mean stress within the initiation period. It is proposed that the effect of the mean stress on crack initiation can be related to the amount of deformation within an individual slip band. As the density of deformation bands is increased by raising the mean stress, the deformation within each slip band is reduced. With the reduced slip activity within a given band, the rate of decrease of the cohesive energy will be slower, resulting in a longer time spent initiating a crack as the mean stress is increased. This is particularly important in cases where the initiation period takes a large slice of the fatigue life (small strains, wrought alloys, etc).

In summing up what has been said concerning hold periods and mean stresses and if one can assume that:

(i) The fatigue process is one of nucleation and propagation and that these processes are involved in all the testing methods already considered.

(ii) That elastic and inelastic strains can be separated.

(iii) Low and high cycle fatigue regimes can be identified and the transition between the two being defined by the transition fatigue life (Figure 2.7) - life corresponding to an hysteresis loop where the plastic component is equal to the elastic component.

(iv) Each regime exhibits distinct characteristics such as summarized in Figure (2.7), the low cycle regime being characterized best by the plastic strain range, the high cycle regime by the linear elastic fracture mechanics.

then some of the complexity of the hold time experiments may be removed.

It was observed for some superalloys that compressive strain hold periods were more damaging than tensile strain holds. It was further observed that concurrently with the compression hold a loop shift developed so as to produce a tensile mean stress while with tensile hold a compressive mean stress was found.

Lord and Coffin (34) proposed that since the lives were above the transition fatigue life the differences in life could account for the big role of the mean stress on crack growth. Below the transition fatigue life these mean effects are washed out and tensile dwells become more damaging as shown in reports from Berling (26), Manson (6), Hirschberg (45) and Halford (46).

Identification of regimes of applicability should, therefore, be helpful in sorting out some of the differences found when comparing hold period test results.

2.1.6 - Environment

It is well known that most of the times, fatigue crack nucleation occurs at the surface. It is important to recognise therefore, that environmental factors exert a marked influence on fatigue behaviour. Many fatigue cracks examined after a high temperature fatigue cycle are filled with oxides (39,40). The enhanced locally oxidized region then acts as a notch to further concentrate the strain and the development of a fatigue crack is made easier. Surface oxidation, therefore, is a critical factor in fatigue. When frequency is lowered there is a possibility of increased time dependent deformation but also there is more time to environment-surface interaction. The relative role of the two coexistent effects, creep and environment, is difficult to separate in these high temperature situations. There are cases where the environment seems to play the more important role in fatigue degradation, while for others, depending on temperature mean time testing and, of course, alloy, the creep deformation becomes the principal factor in degrading fatigue life.

For non-creep strengthened alloys at high temperature grain boundary sliding is the preferred deformation mode. Interaction of the strain localization at the grain boundaries with oxidation processes leads to the enhancement of grain boundary fracture (49). Another form of creep and environment interactions has been mentioned by Chang (50) and occurs for creep strengthened alloys like nickel-based superalloys. In this case prolonged exposure at 982°C led to grain boundary reactions which weakened the grain boundaries when subsequently at 871°C and led to lowered rupture ductility and high strain fatigue resistance.

Figure (2.8) illustrates a typical case where the environmental effect plays the principal role in decreasing lives between one and two orders of magnitude. But even here, vacuum, it can be detected a creep effect represented by the displacement relative to the principal data line of the two tests performed at lower frequencies (points A and B). McMahon and Coffin (47) found for a cast nickel based superalloy, Udimet 500, at 815°C localized oxidation at grain boundaries playing an important role in crack nucleation and propagation. Evidence was presented of surface ridging and pronounced grain boundary penetration due to oxidation, a divided zone adjacent to the oxide

and cracking of the oxide. Fleetwood et al (51) found that grain boundary oxidation affects significantly the nucleation in thermal fatigue of several cast nickel base alloys.

Sometimes a change in fracture mode is observed by changing the environment of a HTLCF test. That is what was found by Coffin (22) testing an iron base superalloy A286. In tests performed in vacuum the fracture was found basically transgranular and intergranular for tests conducted in air. However, Sheffler obtained results for the same alloy that show even in a vacuum a well defined creep effect (52, written discussion (44)). Coffin (16) suggests a model based in environment effects to explain the two slope of the function plastic strain range-frequency modified fatigue defined in equation 1.2. This parameter was introduced (16) in order to adapt to high temperature situations the Manson-Coffin equation. This one was proposed some twenty years ago (53,54) and relates plastic strain range $\Delta\varepsilon_p$ with the number of cycles to failure.

$$\Delta\varepsilon_p = AN_f^{-\beta} \tag{2.6}$$

This equation was modified for application at high temperatures to:

$$\Delta\varepsilon_p = A(N_f\nu^{k-1})^{-\beta} \tag{2.7}$$

A, β, k - Constants dependent on temperature
ν - Frequency of the test

At increasingly higher temperatures it is observed the increase of exponent β approaching unity (55). The coefficient A referred as being the fatigue ductility correlates less well with tensile ductility. It is found generally that extrapolations to $N_f = \frac{1}{4}$ exceeds the tensile ductility of the material. Therefore, there must exist a break on the slope of the curve $\Delta\varepsilon_p = \Delta\varepsilon_p(N_f)$ in order to approach more nearly the tensile ductility at $N_f = \frac{1}{4}$. The environment model suggested by Coffin assumes that low cycle fatigue is basically a crack propagation process; it is assumed also that the mode of crack propagation affects the fatigue life. For a given inelastic strain range an intergranular crack propagates more rapidly through the structure than a transgranular one since less distortion is involved. At low temperature where the fracture is entirely transgranular a single strainght line is obtained, Figure (2.9) while at high temperature where a change of fracture mode to intergranular failure is observed, the fatigue life is reduced.

To explain the intergranular failure mode, the steeper the slope and the slope break, the effect of the environment is introduced (18). It is generally accepted that the grain boundaries may be more aggressively attacked than grains themselves because their chemical complexity (precipitates, carbides, etc). At equal frequencies, the effect of oxidation damage on the fracture mode will depend on the strain amplitude. At low strains where the crack growth is small, the oxide-damaged region constitutes a large fraction of the cracked surface and the environmental effect is large. At high strains where the crack growth is large,oxide-damaged fraction of the crack advance is too small for such environment effect to occur.

A more extensive investigation of the influence of vacuum or inert environments on several materials subjected to a balanced hysteresis loops (equal ramp rates for each leg) was reported in (35). They are summarized in Figure (2.10). Here two types of tests are reported. Low cycle fatigue test results for room temperature together with high temperature tests run either in high vacuum or a highly purified argon atmosphere. Ductility differences were eliminated by normalizing the inelastic strain range to the inelastic strain range for failure at one cycle. Lines corresponding to various exponents β in equation (2.6) are also drawn shlowing that the test results fit within a scatter band of $|0.45 - 0.60|$. All fractures were reported to be transgranular. These facts supported well the view that at least for some materials oxidation effects are critically important in producing intergranular cracking and hence separating lives of cycles with different times per cycle, since in the absence of an agressive environment fractures tend to be transgranular and to be not significantly different.

2.2 - LIFE PREDICTION METHODS

The principal task to a designer engineer when he has to project a component subjected at the same time to cyclic variations (mechanical, thermal) and high temperature exposure (constant or variable) is to determine its shape and dimensions in order to accomplish the design life required by the service conditions. Generally he disposes of short time laboratory tests that jointly with rules, design codes when existent are used to the component. Here two fundamental questions can arise.

(i) In what measure can the service conditions be transferred to the laboratory specimens.

(ii) How do the short laboratory tests relate to the generally larger life service conditions.

In the first case it has been considered possible that a local and critical region of the component can be removed and investigated more effectively in laboratory by some suitable shape test specimen under well controlled simulated conditions.

The model shown in Figure (2.11) has been used throughout a lot of fatigue literature to describe the basic elements of the problem. The crack process is considered to involve three stages: nucleation and early growth, crack propagation through a plastic regime and crack propagation through an elastic regime. The previous model using the concept once called "smooth specimen simulation" (56) was first applied to pure fatigue and then mentioned for high temperatures by MOWBRAY (57) and Coffin (35) to relate laboratory data with actual component behaviour. The assumption behind the concept is that the laboratory specimen failure data are equated to crack initiation on the actual structure providing the strain gradient in the notch is small so that the plastic zone is large relatively to specimen size. Factors such as biaxility of stress or surface roughness being additional difficulties to the concept.

The assumption of this approach to the design of a high temperature fatigue component considers than that fatigue life is determined by crack initiation, that is, by the situation represented in Figure (2.11). This situation represents a designing philosophy completely opposed to an alternative approach with is finding increasing support with the advent of fracture mechanics concepts in design and which assumes the presence of a pre-existing flaw which negates any contribution from the initiation period. An intermediate approach takes both of the above design philosophies eg., every effort is taken to ensure that defects are absent from critically stressed regions and the structure is basically designed by crack initiation. However, a characteristic defect is assumed to slip through the inspection process and the respective life is so calculated in order to have the basis for determining the inspection frequency for crack detection of the component.

The second question has been tentatively approached for many years, but it has been found general difficulties to achieve good agreement between the predicted and the observed data, especially as the extrapolations are larger or the suggested methods or relationships are tentatively applied to increased universalized conditions. It is this sort of universal relationships that the researcher look for, on order to facilitate the task of normalization and design procedure.

A wide variety of predictive approaches have been developed over the years for application to designs for high temperature service. Many of these are fatigue modified methods where

modifications are made to the fatigue laws developed for room temperature situation in order to take into account high temperature effects.

2.2.1 - Life Prediction Methods in Pure Fatigue

The classic presentation of fatigue data is on the form of stress relationships for zero mean stress. These data are grouped on the well known Wholer curves. There are several empirical diagrams to take into account of a mean stress superimposed in a pure alternate fatigue cycle. Alternative methods of presenting mean stress data are covered in Ref (116).

The concept that cyclic life is related to the plastic strain range was first suggested by Manson (54) in an effort to estimate the importance of temperature on the thermal-stress fatigue of turbine buckets. This strain approach is particularly suitable for materials displacing sufficienty large plastic strains to be accurately measured. This is what happens with ductile materials or high temperature applications in general.

Consider a specimen that is subjected to axial reversed strain cycling. First, a positive strain (+ ε) is applied to the specimen; by reversing the load a negative strain (- ε) is obtained resulting in a total strain range of 2ε. The first observation made when a specimen is strained in this manner is that it requires different loads to accomplish a desired amount of strain, depending on the number of prior applications of the strain. This fact is illustrated in Figure (2.12). In the first cycle of loading the stress required to produce a fixed strain range say, 1.8% is represented by point A lying on the static stress-strain curve because by definition this static-strain curve provides the stress required to produce a given strain in the first quarter cycle of loading. However, if an attempt is made to apply the same strain in successive cycles it takes a greater stress range to maintain the strain range. This fact is illustrated in Figure 2.12 (b) along the line A'PA. In this case after about 600 cycles of loading the stress stabilizes and for the remainder of the test out to about 1400 the stress range remains constant. The assymptotic achievement is sometimes referred as "Saturation Hardening" (35). If this assymptotic stress range is plotted against strain range in Figure 2.12 (a) this point falls in A". In a similar way point B" is obtained for a total strain amplitude of 3.6%. The curve passing by A" and B" is known as the cyclic stress strain curve. In this case it lies considerably above the static stress strain curve; this material is thus referred to as a cyclic strain hardening material. The saturation hardening

is achieved after a small cyclic part of the total life always well before half the number of cycles to failure Figure (2.12 (c)). Figure (2.13) illustrates the behaviour of another class of materials described as cyclic strain softening. In this case for a strain range of 1.5%, the stress range required in the first cycle is represented by the point A but it quickly diminishes until a relatively few cycles, the stress range is only about half that of point A. The cyclic stress-strain curve here passes through A"B" being well below the static stress-strain curve. The degree of hardening or softening varies considerably among materials, temperatures and strain rates. Some materials even show hardening and softening in the same test (3).

Could the life of strain controlled tests be predicted using data for stress controlled tests? Or could the life of variable stress controlled tests be predicted from constant stress range data?

Miner (59) has dealt with this problem and considered that there is a linear accumulation with the number of stress cycles. If for a cycle stressed at ± Si the life is Ni the damage associated with the running of ni cycles at a stress range of ± Si is considered to be ni/Ni. For a multi level stress test with levels S_1, S_2 ... Si the total damaged is suggested to be:

$$\frac{n1}{N1} + \frac{n2}{N2} + \cdots + \frac{ni}{Ni} = \Sigma \frac{ni}{Ni} \qquad (2.8)$$

Miner considered that failure occurs when the total damage equals 1

$$\Sigma \frac{ni}{Ni} = 1 \qquad (2.9)$$

which is generally referred as Miner's Law. For a continuous stress spectrum equation it becomes:

$$\int \frac{ni}{Ni} = 1 \qquad (2.10)$$

This linear damage rule is many times used in design because of its simplicity. It has however, several shortcomings:

(i) It has been found experimentally that in a two step fatigue test high load followed by low load produces a cycle summation $\Sigma \frac{ni}{Ni}$ less than unity, while low

load followed by high load produces a cycle summation greater than unity.

(ii) It does not properly account for residual stress effects especially during the crack propagation stage. If the period of high load cycling is ended after the application of a tensile stress, residual compressive stresses remain at the root of a possible notch; on the subsequent application of lower load numerous stress cycles or perhaps a rest period may be required to overcome this residual stress field before the crack will start to propagate again.

(iii) Another important limitation is related to stress cycles below the initial fatigue limit of the material. Fatigue damages associated with stresses below the fatigue limit are always zero when Miner Law is applied ($N = \infty$), whereas in fact the effect of prior loading even at relatively low stress levels may reduce the fatigue limit, implying that cycle ratios of stresses below the initial fatigue limit should be accounted for.

(iv) The Miner's Law does not take into account 'coaxing' effects present in strain ageing materials (60) in which the appropriate sequence of loading may progressively raise the fatigue limit.

The most important concept trying to by-pass the difficulties found with fatigue as a function of the stress range specially in low cycle regimes, was proposed by Coffin and Manson (53,54) in 1952. Inherent to the relationship (2.6) is the resolution of the cyclic strain into elastic and plastic components and the recognition that only the plastic component is important to the fatigue process.

Equation (2.6) is applicable to low cycle fatigue cases that following the recommendation of Committee E9 of ASTM is characterized by the presence of macroscopic cyclic plastic strains as evidence by a stress-strain hysteresis loop. In terms of cycles to failure the upper limit of the low cycle regime may vary from a few cycles to 100.000 or more. Originally plastic strains of less than 10^{-3} were difficult to measure so that applicability was only for short lives. Recent reports employing recording equipment with much higher resolution, had increased ten fold that value showing that the Coffin-Manson equation is applicalbe to much lower plastic strains.

Initially proposed for axial fatigue tests, equation (2.6) has been found to be applicable to bend tests (61,62) and torsion tests (18,63).

Equation (2.6) has been found to be applicable for a wide range of tensile ductilities such as 3% for a tool steel (54) to as high as 99% for high purity tantalum (55).

Rather uncommon materials as Superplastic A-Zn (66), Ni-Co directionally solidified eutetic (67) and Zircaloy-2 fabricated from highlytexture plates (68) were found to obey to Manson-Coffin equation. Even high temperature, providing one uses a constant frequency, seems to be no restriction: Swindeman (69) for a Niobium base alloy at 1100°C and Sheffler (70) for two Tantalum base alloys at temperatures up to 1150°C found their data to obey to Coffin-Manson type equation. A number of theories have been proposed to the Coffin-Manson equation. It is generally observed that in LCF the regime that leads to failure, has a high ratio propagation over initiation periods. In other words, the physical process characterized by equation (2.6), is assumed to be that of high strain crack growth. Solomon has proposed a high crack growth law:

$$\frac{d\ell}{dN} = \emptyset\ \ell(\Delta\varepsilon_p)^{\alpha} \qquad (2.11)$$

where ℓ is the crack length, $\Delta\varepsilon_p$ the plastic strain range and $\emptyset$ and α are constants, based on direct measurements of growth of cracks, from which, by integration, equation (2.6) is produced.

Manson (3) suggests that the parameter $\Delta\varepsilon_p\sqrt{\ell}$ is significant in strain cycling as $\Delta\sigma\sqrt{\ell}$ is in stress cycling thus he assumed a power law relation between crack growth rate and $\Delta\varepsilon_p\sqrt{\ell}$

$$\frac{d\ell}{dN} = C(\Delta\varepsilon_p\sqrt{\ell})^{s} \qquad (2.12)$$

s , C being material constants

$$\frac{d\ell}{\ell^{s/2}} = C(\Delta\varepsilon p)^{s} dN \qquad (2.13)$$

and integrating between (ℓ_o, N_o) and (ℓ_f, Nf) where lo and No are any corresponding values of ℓ and N during which the crack growth law is valid and where ℓ_f is the crack length at the cyclic life at fracture N_f, results in

$$\frac{2}{2-s}\left(\ell_f^{\frac{2-s}{2}} - \ell o^{\frac{\ell-s}{2}}\right) = C(\Delta\varepsilon_p)^{s}(N_f - N_o) = C(\Delta\varepsilon_p)^{s} N_f\left(1-\frac{No}{N_f}\right) \qquad (2.14)$$

assuming N_o is small in comparison with N_f and ℓ_o is small compared with ℓ_f (high strain crack growth regime) equation (2.14) becomes:

$$C(\Delta\epsilon_p)^s N_f = \frac{2}{2-s}\,\ell_f^{\frac{2-s}{2}} \tag{2.15}$$

By further assuming that the crack length at fracture is approximately constant the plastic power law relationship

$$(\Delta\epsilon)^s N_f = \text{Constant}$$

follows immediately from equation (2.15)

Although the plastic strain is recognized to be the determinant factor in fatigue failure, sometimes it is difficult to measure it accurately and being the total strain, the strain that is known, it is difficult to estimate how much of the strain is plastic until the elastic component is known. Here, by substraction the plastic strain can be calculated.

The linearity of elastic strain vs cycles to failure in log-log scales was proposed first by Basquin (71).

The elastic strain-cycles to function was proposed to be of the form:

$$\Delta\epsilon_e = \frac{\Delta\sigma}{E} = \frac{B}{E} N_f^{-\beta'} \tag{2.16}$$

the total strain range $\Delta\epsilon_t$ is then obtained by the following sum

$$\Delta\epsilon_t = \Delta\epsilon_p + \Delta\epsilon_e = AN_f^{-\beta} + \frac{B}{E} N_f^{-\beta'} \tag{2.17}$$

where A, B, β, β' - constants
$\Delta\epsilon_e$ - elastic strain range
$\Delta\epsilon_p$ - plastic strain range
$\Delta\epsilon_t$ - total strain range
N_f - cycles to failure

In log-log scales both plastic and elastic relationships are straight lines, resulting the $\Delta\epsilon_t - N_f$ function being assymptotic to the plastic line at the lower cyclic life range and assymptotic to the elastic line at the higher cyclic life range.

Data obtained by Smith, Hirschberg and Manson (72) fit well the straight lines claimed to represent the fatigue behaviour of the several studied materials (Figure 2.14).

In Figure (2.7) it can be defined a life for which $\Delta\varepsilon_p = \Delta\varepsilon_e$. It is the transition fatigue life N_t . It was already mentioned that N_t serves as a very useful reference point for distinguishing in a given material whether the failure is one of low cycle fatigue, or one of high cycle fatigue. Implicit to this concept is the fact that high or low cycle fatigue is determined by the geometry of the obtained hysteresis loop instead of a certain predetermined number of cycles. In Figure (2.7) two regimes may be seen:

(i) The first corresponding to plastic strains larger than the elastic strains $\Delta\varepsilon_p > \Delta\varepsilon_e$ where the hysteresis loops are very 'fat', leading to lives smaller than

(ii) A zone corresponding to higher lives where the material reveals a loop which is essentially a straight line. Here the elastic component is dominant ($\Delta\varepsilon_p << \Delta\varepsilon_e$).

Coffin (35) proposed the definition of a material behaviour by its transition fatigue life N_t and by the corresponding strain $(\Delta\varepsilon)_t$. As a general trend the lower the strength and the higher the ductility the higher the transition fatigue life.

The two regimes present differencies concerning fracture process:

(i) Regime of High Cyclic Plastic Strain ($\Delta\varepsilon_p >> \Delta\varepsilon_e$). In this regime, the nucleation an early growth of fatigue cracks - Stage I - is generally accompanied by large amounts of slip at the surface which results in general surface rumpling (3). After the crystallographic growth (Stage I) of microcracks nucleated in grain boundaries, carbides, oxidated zones, etc., the growth progress is normal to the direction of the applied stress - Stage II - growth. With continued growth, smaller cracks are consumed by larger ones, until a few cracks remain to separate the specimen.

(ii) Regime of Low Plastic Strains ($\Delta\varepsilon_p << \Delta\varepsilon_e$). In this regime, the plastic strains are very small relatively to the elastic ones. Here, crack nucleation is a much more isolated event occurring by slipband extrusions or intrusions (73) due to cyclic plastic strain in a highly localized region by some surface or metallurgical defect. Most of the surface

remains undisturbed but a few microcracks are found, often just one which propagates by Stage I and Stage II growth to produce failure (74).

Consider now the life prediction methods for pure fatigue, all of them involving empirical relationships.

A - The Four Point Correlation Method

From a practical point of view it is extremely useful to know that both elastic and plastic strain data fall in straight lines when plotted vs cycles to failure in log-log scales.

It is possible to estimate these straight lines from a knowledge of more readily obtained material properties such as the results of uniaxial tensile tests.

Figure (2.15) summarizes the method suggested by Manson (3) in which the fatigue behaviour of an alloy is obtained by locating two points on each of the two proposed straight lines. A point is located on the elastic line at $\frac{1}{4}$ cycle with an ordinate of 2.5 σ_f/E where σ_f is the true fracture stress and E the young modulus. A suggested way to relate this true fracture stress with the more common and easy to determine, the ultimate stress, is reported in (3).

$$\sigma_f = \sigma_u \ (1 + D) \qquad (2.18)$$

where σ_f - true fracture stress
σ_u - ultimate tensile strength

$$D - \ell n \ \frac{100}{100-RA}$$

RA - reduction of area in %

Another point on this line is obtained at 10^5 cycles. For this abciss is suggested the ordinate 0.9 $\sigma u/E$. On the plastic line at a point at 10 cycles is suggested to have an ordinate of $\frac{1}{4}D^{\frac{3}{4}}$. The second point on the plastic line is obtained at 10^4 cycles. The point in Figure (2.15) shown by the star at 10^4 is first located on the elastic line and the observed ordinate is substituted into the following equation

$$(\Delta\varepsilon_p)_{10^4} = \frac{0.0132 - \varepsilon_e}{1.91} \qquad (2.19)$$

to obtain the corresponding ordinate.

The method is based in some experimental observations from which values and equation (2.19) are derived. For instance equation (2.19) is based on an assumption that the total strain at 10^4 cycles is approximately 1% (75). A fair agreement with experimental data was found for twenty-nine materials by Manson (58): only 60% of the data fall within a factor of two in life from the predicted value. It found its application on rapid estimations of fatigue behaviour room temperature applications. It is not a method to be applicalbe in design because of lack of sufficient accuracy and alternatively more accurate procedure to determine the four points experimentally which are not high time consumers, can improve its accuracy.

B - The Method of Universal Slopes

An alternative approach is to consider that the slopes of the elastic and plastic lines are the same for all materials at room temperature. In a statistical study (3) done for about thirty materials with reduction of area ranging from 1 to 94% and tensile strengths varying between 330 MN/m^2 and 3400 MN/m^2 it was found that the values - 0.6 and - 0.12 for the plastic and elastic relationships respectively were the more appropriate values for the $\Delta\varepsilon_p - N_f$ and $\Delta\varepsilon_e - N_f$ straight line when both plotted in log-log scales. The suggested values for the ordinates for $N_f = 1$ were $D^{0.6}$ and $3.5\sigma u/E$ for the plastic and elastic line respectively. The equation for the total strain becomes:

$$\Delta\varepsilon_t = \Delta\varepsilon_e + \Delta\varepsilon_p = \frac{3.5\sigma_u}{E} N_f^{-0.12} + D^{0.6} N_f^{-0.6} \qquad (2.20)$$

Figure (2.16) indicates a ready and easy method of construction of the elastic and plastic lines.

The agreement with experiment is approximately the same as that obtained by the four point method: 60% of data for 29 materials fall inside x2 bands life factor (3).

It is apparent from the preceding chapters that the nature of fatigue damage is complicated sufficiently without the inclusion of variables of time and temperature. The use of many empirical relationships reflects the difficulty of the problem. Unfortunately those factors are added to the already existing variables at low temperature to form probably one of the least understood aspects of fatigue: the fatigue at high temperatures. This situation is basically one of cummulative damage, one or more fatigue mechanisms governed by cyclic strain in conjunction with some creep mechanisms that depend upon the time under stress at elevated temperature. Because of the evolving physical understanding and the large number of variables which are necessary to take into account, the state of predictive methodology is one of constant change

and improvement. On the next sub-section methods with important roles in that improvement and newer methods currently under active study and evaluation are discussed.

2.2.2 - Life Prediction Methods for Fatigue at High Temperatures

Two basic situations for engineering components can be considered. The first is referred to as cyclic loads resulting in more or less plastic deformation. It was found that the plastic range or width associated with the fatigue hysteresis loop is an adequate parameter to relate to fatigue life providing it is sufficiently wide so that it can be accurately measured. The second situation is referred to as cases when a component suffers a time dependent deformation as a result of the application of a static load. The behaviour of one material could and has been commonly represented by parameters incorporating time and temperature into a single expression which in itself is a function of the stress (76,108,109).

Finally situations similar to those found in gas turbine applications ought to be considered. Here, besides the fatigue damage associated with time variation of strain, the material is now susceptible to time dependent deformation (creep) that contributes in itself to the damage already associated with fatigue.

One important feature of the creep failure is the large amount of intercrystalline cracking in contrast to the transcrystalline failure often found at temperature below the creep range. An immediate question which arises is in what measure these intercrystalline cracks influence the fatigue life of a material working at temperatures within the creep range. Could the high temperature fatigue behaviour be predicted taking similar procedures to the ones used at room temperature, for example, by applying the method of universal slopes? Obviously, in applying the tensile properties (strength and ductility) to high temperature situations, those tensile properties had to be measured at the temperature of interest and using strain rates similar to those ones employed in the fatigue tests. However, attempts to predict high temperature fatigue behaviour using similar expressions to those employed at room temperature brought to a much more conservative lives (7,60).

Figure (2.17) illustrates a high temperature crack hypothesis as suggested in (3). The importance of intercrystalline cracking in fatigue can be best visualized by considering the relative importance of crack initiation and propagation in fatigue. As it is illustrated, consider a

specimen which would last for 10^4 cycles at a temperature below the creep range, Figure (2.17(a)). During the 10^4 cycles the 'events' can be divided into two phases:

(i) Initiation
(ii) Propagation

the microstructural events associated with (i) are suggested to be (3):

a) Slip on a few well defined planes tends to produce internal discontinuities.

b) Substructure formations helping to maintain continuity, it results, however, in more centres of disorder.

c) Slip may affect the nature of the microstructure eg., breaking up dispersed particles (strain softening).

d) Slip not completely reversible results in internal and surface discontinuities.

For the development of the microcracks Manson (3) suggests the path outlined below:

a) The development of the former discontinuities are influenced by intial surface topography, intrusions, extrusions, inclusions, grain boundaries, etc.

b) Initial propagation direction is parallel to slip planes - Stage I - the growth is limited within individual grains, it can stop at grain boundary or other impediments.

c) Cracks penetrate grain boundaries; it assumes characteristic transcrystalline nature (Stage II).

d) The crack growth is done by a blunting and sharpening mechanism under alternated tension and compression as represented schematically in Figure (2.13).

Figure (2.17(a)) shows schematically cracks that have nucleated in the slip planes of individual crystals and linked to form a transgranular crack. Assume that the number of cycles required to initiate a crack is 85% of the total life to fracture ($0.85 \times 10^4 = 8500$). The remaining number of cycles (1500) are used to propagate the crack to a size leading to complete failure. Assuming that in the creep range intercrystalline cracks form much more readily than slip plane cracks, one must decide how much of that 85% of total life spent in initiating a microcrack of a few grains magnitude, is bypassed in the creep range by the ready formation of an

intercrystalline one. Suppose the extreme case in which such intercrystalline cracking occurs immediately upon the application of the first cycle of loading. In this first approximation 85% of the total life is by passed at high temperature as a result of the rapid formation of a precrack between grains. What percentage of crack propagation period is reduced as a result of the development of an intercrystalline crack? If one assumes that none of this period is reduced it is evident that a method of dealing with high temperature fatigue is:

(i) Take the lives at room temperature

(ii) Ignore all the initiation period and consider the propagation period to calculate the lives at high temperature.

This suggest a more general approach that takes into account the reductions in both the crack initiation and the crack propagation phase.

Can we adopt rules such as 0% - 100% meaning that the material employs only 100% of the propagation period observed at room temperature? And a 10% - 10% rule from which are retained only ten per cent of the cycles for each period?

Figure (2.19) shows several life prediction curves based on different assumptions regarding the crack initiation and crack propagation periods. The horizontal line constitutes the prediction based on the last 10% - 10% simple assumption. It is clear from Figure (2.19) that no single rule agrees with all the data points. The interpretation still based on an intergranular cracking hypothesis means that a single rule cannot cope with all situations concerning temperature and frequencies with totally different percentages of intergranular cracking. Obviously the material itself is the principal source of discrepancy with its own composition grain size, grain boundaries, composition, etc.

2.2.2.1 - Life Prediction Rules

1 - The 10% Rule

The 10% rule which attributes equal losses to both initiation and propagation is derived directly from what was said above. Manson (6) suggests that this over simplified rule possibly under corrects the crack initiation phase and over corrects the propagation period. With this simple rule it is impossible to represent all situations where the amount of intergranular fracture is tremendously variable.

Assuming that the computations based on tensile properties are some measure of the potential fatigue strength of a material, the less the intercrystalline cracking the smaller will be the coefficients of by-pass of the initiation and propagation period found at sub-creep temperatures. This shows that a trend to develop better materials for high temperature applications should include the search for mechanisms of strengthening, protecting or even removing the grain boundaries.

Manson (6) has considered the 10% rule very useful as a lower bound for cyclic creep lives. Later Halford (5) considered that a less optimistic lower bound was needed for cases where the stress rupture curve is very steep. This leads to the following method.

2 - Creep Modified 10% Rule

In this method (5) a linear damage law was applied wherein stress rupture damage is given by time ratios and fatigue damage by cycle ratios:

$$D_c + D_f = 1 \therefore \frac{N'f}{N_f} + \frac{t'}{t_r} = 1 \qquad (2.21)$$

where D_f - damage associated to fatigue
D_c - damage associated to creep
N'_f - number of cycles to failure under high temperature conditions
N_f - pure fatigue life in cycles to failure assumed to be given by equation (2.20)
t' - effective time of a test for which the peak stress acts
t_r - time to rupture at peak stress

Assuming that the effective time of a test for which the peak stress acts is given by

$$t' = \frac{k\ N'f}{\nu} \qquad (2.22)$$

where k - effective fraction of each cycle for which the material may be considered to be subjected to maximum stress

ν - frequency of stress application, cpm

and assuming that the stress rupture curve is given by a power function of the type:

$$\sigma_r = 1.75\ \sigma_u (t_r/A)^m \qquad (2.23)$$

where σ_u - ultimate tensile strength
A - coefficient characterizing the creep-rupture curve of the material at test temperature
m - slope of the creep-rupture line (negative value)

Substituting t' and t_r given by equation (2.22)and (2.23) respectively in equation (2.21) the equation to apply in actual fatigue-creep is obtained:

$$N'_f = \frac{N_f}{1 + \frac{k}{A\nu} N_f \frac{m + 0.12}{m}} \qquad (2.24)$$

The above analysis is presumed to have utility only when:

(i) a large creep effect (m>-0.12) is anticipated and $N_f/10$ is inadequate as a lower bound

(ii) $N'_f < 10^5$ cycles

The use of this predictive method can then be summarized as follows:

a) Determine the lower bound of life using either $N_f/10$ as computed from equation of universal slopes (2.20) or N'_f as computed from equation (2.24) which ever is lower

b) for average life use twice the lower bound life

c) for the upper bound of life use 10 times the lower bound life

Although a fair estimate of lives was achieved (59% of data within x2 bands - 90% of data with x4 bands) for a wide variety of materials (nickel base alloys, high and low alloy steels, stainless steels and aluminium base alloys), the above mentioned method is suggested to be better suited for quick approximate answers rather than for design purposes.

3 - Method of Characteristic Slopes

Berling and Conway (77) have proposed the following equations for predicting the relationship between total strain range $\Delta\varepsilon_t$ and cycles to fracture N_f:

$$\Delta\varepsilon_t = 2\varepsilon_{ef}\left(\frac{Nf}{10}\right)^{-n'/2} + \frac{D^2}{\dot{\varepsilon}_t}\left(\frac{N_f}{\nu}\right)^{-1} \qquad (2.25)$$

where ε_{ef} - elastic strain at fracture
$\dot{\varepsilon}_t$ - strain rate
n' - strain hardening exponent
D - fracture ductility = $\ln \frac{100}{100-RA}$
RA - reduction of area at fracture
ν - frequency

This very simple rule has been seen as a redefinition of the universal slopes equation. It refutes, however, the existence of slopes which are the same for all materials and test conditions. Instead terms defining elastic and plastic components are identified and are related to the short-term tensile behaviour of a given material at a given set of test conditions. The method based on expression 2.25 is based on two observations. First it was observed that for the stainless steels in study the slope of the logarithmic $\Delta\varepsilon_e$ vs N_f plot was essentially identical to one-half the strain hardening exponent obtained in short-term tensile tests at the same test conditions. Secondly it was noted that the value of $\Delta\varepsilon_e$ at N_f = 10 cycles was equal to twice the time elastic strain at fracture (represented by ε_{ef}) in a short-term tensile test at the same conditions of temperature and strain rate.

It is a method which has produced good agreement between predicted and observed lives for stainless steels at temperatures up to 650°C and covering strain rates from 4×10^{-5} to $4 \times 10^{-3} s^{-1}$. At temperatures of 816°C the prediction yields fatigue results higher than actual experimental values (77). Due to the type of assumption this method is based upon restricted applications only can be expected from it.

2.2.2.2 - Modified Fatigue Approaches

1 - Frequency Modified Strainrange Approach

In this approach the Coffin-Manson equation (eg., (2.6)) and the Basquin (eg., (2.16)) are modified so that time-frequency effects within the creep range could be taken into account. The high temperature relationships and the room temperature relations from which they derived are:

Room Temperature Form	Frequency Modified Form	
$\Delta\varepsilon_p = AN_f^{-\beta}$	$\Delta\varepsilon_p = A(N_f\nu^{k-1})^{-\beta}$	(2.26)
$\Delta\varepsilon_e = \frac{B}{E} N_f^{-\beta'}$	$\Delta\varepsilon_e = \frac{B}{E} N_f^{-\beta}\nu^{k_1'}$	(2.27)
$\Delta\sigma = C\Delta\varepsilon_p^{n'}$	$\Delta\sigma = C\Delta\varepsilon_p^{n'}\nu^{k_1}$	(2.28)

Where $C = BA^{n'}$, $n' = \beta'/\beta$, $k_1 = \beta n'(k-1) + k_1$

$A, B, \beta, \beta', k, k_1$ - material constants
$\Delta\varepsilon_p$ - plastic range
$\Delta\varepsilon_e$ - elastic range
N_f - number of cycles to failure
E - young modulus

The concept was introduced by Eckel (16) and further developed by Coles (17). In these reports fatigue lives were predicted for a specific plastic strain by the relationship:

$$\nu^k t_f = \text{constant} = f(\Delta\varepsilon p) \tag{2.29}$$

where ν - frequency in cpm
t_f - time to failure
k - constant only dependent on temperature

equation (2.29) can be written as:

$$\nu^k t_f = \nu^k \frac{N_f}{\nu} = N_f\nu^{k-1} \tag{2.30}$$

a quantity which has been called the frequency modified fatigue life.

The parameter $N_f\nu^{k-1}$ has been found convenient to relate to inelastic strain in a Coffin-Manson type of equation (19,20,73). In those reports the fatigue curve for one temperature is represented by data falling in one straight line when log - log scales of $\Delta\varepsilon_p$ and $N_f\nu^{k-1}$ are used, ie., the data obey to a relationship of the type:

$$\Delta\varepsilon_p = A(N_f\nu^{k-1})^{-\beta} \tag{2.31}$$

Sometimes equation (2.31) is rewritten in the form of:

$$\Delta\varepsilon_p \nu^{\beta}(k-1) = AN_f^{-\beta} \qquad (2.32)$$

The left part of equation (1.11) is called the frequency modified plastic strain and appears in many reports where it is plotted against cycles to failure (45,8).

The frequency modified equations (2.31 and 2.32) apply only to continuous cycling. Its range of applicability was extended to include hold time effects by defining the frequency ν as:

$$\nu = \frac{1}{t'_c + t_h} \qquad (2.33)$$

where t_h - time of hold period(s)
t'_c - $t_c - t_h$
t_c - time of a cycle

It must be emphasized that in this approach reference to a plastic term implies plastic deformation plus a creep contribution; the 'elastic term' no longer means pure elastic behaviour but elasticity eventually modified by a creep component. As was stated earlier increasing the temperature or decreasing the frequency steepens the plastic curve and moves it to the left. The point of intersection of the elastic and plastic curves - 'transition fatigue life' N_t - moves to lower values of number of failure. By equating equation (2.6 and 2.16) it can be expressed as:

$$N_t = \left(\frac{AE}{B}\right)^{\frac{1}{\beta-\beta'}} \qquad (2.34)$$

Coffin (35) considers N_t to be critical in determining the method of testing and the analytical procedures to be adopted. If the design life N_d is less than N_t then low cycle fatigue data and elasto-plastic solutions are required for design. If N_d is much greater than N_t then high cycle fatigue data and stress analysis are more relevant. This approach does not distinguish between tension and compression dwells and would predict the same cyclic life whether the hold period was in tension or compression which contradicts several isothermal tests tensile results by Berling and Conway (20), Ellison (79) and Coffin (42) and thermal mechanical tests conducted in high vacuums where pronounced cavity damage and intergranular cracking was reported. In all of these test hold periods were particularly damaging to specimen life in comparison to the compressive holds. In order to cope with these difficulties an extension of the

frequency modified fatigue approach described above was developed (42,80) where a separation of frequencies on each leg of the hysteresis loop into tension going and compression going was required. Two procedures are suggested whether the loop is balanced or not:

(i) Balanced loop conditions

In this first case the modification is fairly simple requiring only that the frequency term in equation (2.31) is replaced by that associated with damage, ie., the tension-going frequency νt.

In a balanced loop it can be written that

$$\tau = \frac{1}{\nu} = \tau_t + \tau_c$$

where τ_t and τ_c are the tension and compression going times

Being $\tau_t = \tau_c$ and $\tau_t = 1/\nu t$ $\tau_c = 1/\nu_c$

Thus for balanced conditions $\frac{1}{\nu} = 2/\nu_t$ or $\nu = \nu_t/2$

Equation (2.31) becomes

$$\Delta\varepsilon_p = A\left[N_f\left(\frac{\nu t}{2}\right)^{k-1}\right]^{-\beta} \qquad (2.35)$$

(ii) Unbalanced conditions

Considering the loops and nomenclature shown in Figure (2.20) it is assumed that the actual stress range for loops of unequal but constant ramp rates can be determined from the mean of the stress range for each leg of the loop.

Thus $\Delta\sigma SF = \Delta\sigma FS = (\Delta\sigma_S + \Delta\sigma_F)/2$ where the subscript refers to slow and fast, ie.,

$\Delta\sigma SF$ - stress range of a slow fast loop.
$\Delta\sigma FS$ - stress range of a fast slow loop.
$\Delta\sigma S$ - stress range of a slow slow loop.
$\Delta\sigma F$ - stress range of a fast fast loop.

From equations 2.26 and 2.27 it can be written

$$\Delta\varepsilon_e = \frac{\Delta\sigma}{E} = C'\Delta\varepsilon_p{}^{n'}\nu^{k1} \qquad (2.36)$$

C' - constant

Applying equation (2.36) to obtain the stress range for each frequency one gets:

$$\Delta\sigma SF = \Delta\sigma FS = \frac{C'}{2}\left[\left(\frac{\nu c}{2}\right)^{k1} + \left(\frac{\nu t}{2}\right)^{k1}\right]\Delta\varepsilon_p{}^{n'} \qquad (2.38)$$

Equation (2.38) is claimed to be verified to give reasonable predictions of the stress range for loops of unequal rates (23).

Next assumption is that if the stress range is known, life can be determined using equation (2.31). Substituting equation (2.38) in to equation (2.31) to determine the fatique life one finds:

$$N_f = \left(\frac{B'}{A\sigma_{SF}}\right)^{-1/\beta'}\left(\frac{\nu t}{2}\right)^{k_1/\beta'} \qquad (2.39)$$

Note that the coefficients $B' = \frac{B}{\Gamma}$, k_1 and β' are obtained form smooth bar equal rate tests as indicated earlier.

The applicability of the method has been checked in (42) for AISI 304 stainless steel at 595°C for the hold times and wave shapes indicated in Figure (2.29). Although early results found for the majority of materials that the tension hold times to be more damaging than equivalent hold times in compression (see 2.13) more recent testing of less ductile metals like CrMoV steel (81) and several nickel superalloys like Rene 80 (34), Rene 95 (82) and IN738 (83) and MARM002 (84) result in compression hold times as being the most damaging. Certainly for these alloys the frequency modified strainrange approach cannot lead to acceptable life predictions since equation (2.39) in which the method is based implies always, that tensile holds are more damageable (shorter lives) than compressive holds.

Coffin's frequency modified equation (2.26) and (2.27) have an implication which points out for some modification. According to these equations the frequency affects the elastic and plastic components as simple multipliers, therefore, as frequency is changed, the two components should simply be displaced parallel to themselves on a conventional log - log plot of strain component versus cyclic life. If changing the frequency produced a rotation of the line for each component

the equation should be altered so that frequency appears in the exponent of Nf. The convergency of lines at different frequencies found on the new numerous high temperature fatigue data stresses that need of modification.

2 - The Method of Ostergren

Ostergren (85) has recently proposed that hold time and frequency effects at elevated temperature can be accounted for by a damage function based on the net tensile hysteresis energy. The basic assumption of this method considers the net tensile hysteresis energy as a measure of fatigue damage. It can be shown that this damage measure is approximated by the quantity $\sigma_t \Delta\varepsilon_p$ where σ_t is the maximum stress in the cycle and $\Delta\varepsilon_p$ is the inelastic strain range. The use of the tensile stress quantity in conjunction with the plastic strain range provides means for accounting for loop unbalance, since, for the same inelastic a positive mean stress gives a greater tensile hysteretic energy than a compressive stress.

In order to determine fatigue life, the method requires the substitution of $\Delta\varepsilon_p$ by $\sigma_t \Delta\varepsilon_p$ in equation (2.6). In order to take account of wave shape effects, two cases are treated:

(i) Time-dependent damage is independent of wave shape

In this case the material responds equally to compressive and tensile hold as far as combined creep-fatigue damage is concerned. For most materials, the substitution in equation (2.6) above mentioned, leads to :

$$\sigma_t \Delta\varepsilon_p N_f^{\beta} \nu^{\beta(k-1)} = C \qquad (2.40)$$

For many nickel base superalloys like Rene 80, IN738, Rene 95 the tensile hysteretic energy $\sigma_t \Delta\varepsilon_p$ can be correlated with life to fracture without the frequency term which is equivalent to make k in equation (2.40) equal to 1 as reported in (85). This fact would suggest the occurrence of little time-dependent damage in these alloys which is in basic agreement with the metallographic observations reported in (34,83).

(ii) Time-dependent damage is dependent on Wave shape

This case refers to materials for which tension hold times lead to an increased degree of time-dependent damage which causes a change in the failure mechanism

(transgranular to intergranular) and hence to reduce life. Compression hold times do not cause a change in the failure mechanism or do not significantly reduce life.

$$\sigma_T \Delta\epsilon_p N_f^{\beta} \nu^{*\beta(k-1)} = C \qquad (2.41)$$

where ν^* named effective frequency substitutes the cyclic frequency ν in equation (2.40).

The frequency ν^* is defined as:

$\nu^* = 1/(To + T_T + Tc)$ for $T_T > Tc$

$\nu^* = 1/To$ for $T_T \leq Tc$

where To = time per cycle
Tc = compression hold time
T_T = tension hold time

By definition this empirical approach implies that the effective frequency is equal to the actual frequency when hold times occur only in tension; otherwise it is greater than the actual frequency giving expression (2.41) higher lives ie., showing the beneficial effects of compressive creep.

The method is fairly new and untested for wave shapes such as the named as fast-slow or slow-fast testing on the frequency modified strainrange approach.

The identification of the damage category for materials would seem somewhat difficult but the method promises to be a step forward on the life prediction of low ductility high strength alloys like the nickel base superalloys, which do show a significant influence of wave shape. The influence of wave shape on these alloys is to shift to positive or negative mean stresses their creep-fatigue loops as seen in 2.1.3 rather than to change the crack path like in other softer alloys. This method seems to be particularly helpful in differentiating and hence correctly predicts lives for these two cases. A chapter will be dedicated later on to this topic.

2.2.2.3 - Cumulative Fatigue and Creep Damage Models

1 - Linear Damage Summation Method

In this method a linear interaction relationship is established:

$$\sum_{j=1}^{P} \left(\frac{n}{Nd}\right)j + \sum_{k=1}^{9} \left(\frac{t}{td}\right)_k \leq D \qquad (2.42)$$

where D = total damage factor
n = number of applied cycles of loading condition j
Nd = number of design allowable cycles of loading condition j. Taken from rapid cycling fatigue curves
t = time duration of stress condition k
td = allowable time at a given stress k

This relation combines the damage summation of Miner (59) and Robinson (86) and was first proposed by Taira (87). It is of particular interest since it constitutes the basis of one out of two design methods contained in the Code Case 1592 of ASME SECTION III (88). The first method uses expression (2.42) requiring only stress rupture data and rapid cycling fatigue data. However, as shown in Figure (2.22) experience has shown that the sum of the two terms may be less than unity (89) and for this reason for design purposes the sum is set at some lesser value D, which is function of the relative amounts of creep and fatigue. For austenitic stainless steel the minimum value of D is 0.6. The great variation in D throws considerable doubt on the applicability of this cumulative damage approach. Alternatively, Code Case 1592 suggests a slow cycling fatigue design curves based on relatively short term tests, 2 - 3000 hours. There are doubts on the validity of these curves when applied to components intended to operate under combined creep-fatigue conditions for 20 - 30 years.

As it was said earlier the linear damage summation method involves the use of stress rupture curves for uncycled materials a procedure which has been questioned (29). In fact it is argued that since many alloys exhibited a significant amount of cyclic hardening at high temperatures much lower and possibly unconservative creep damage values would have been obtained from monotonic relaxation curves than the damage values based upon cyclically stable stress relaxation curves (29,89).

The following equation due to Gittus (90) was used in the same reports to describe the cyclically stable stress-relaxation behaviour of type 304 stainless steel and alloy 800 at temperatures between 430°C and 650°C for a hold time of duration t:

$$\ell n(\sigma max/\sigma) = \frac{A}{1+m} t^{1+m}$$

Values of A and m were computed from experimental tests reported on the same references (29,89).

For design purposes the allowable stress in the ASME approach for a given lifetime is 2/3 of the minimum experimental value. The fatigue design curves used in ASME are the average total strainrange versus life curves at the temperature of interest, reduced by a factor of two on strain or by twenty on life whichever is the larger.

2 - Non Linear Damage Summation Method

Polhemus et al (91) had suggested a model for cumulative damage analysis using an exhaustion of ductility concept in which the basic assumption is that a decrement of 'available ductility' resulting from a period cycling could be represented as an increment of creep extension.

A Coffin-Manson type equation was used to describe the fatigue behaviour:

$$\Delta\varepsilon t^{\alpha} Nf = (2\varepsilon_{fo})^{\alpha/4} \qquad (2.43)$$

where $\Delta\varepsilon_t$ = strain range (total)
N_f = cycles to failure
ε_{fo}, α = material constants

The values of these constants are determined from low cycle fatigue test results but they may also be approximated using static properties of the material.

If the specimen is strain cycled through a number of cycles at a strain range $\Delta\varepsilon t$ it can be shown that the original ductility has been reduced by an amount:

$$\Delta\varepsilon = \varepsilon_{fo}\left[1-\left(1-\frac{n}{N_f}\right)\right]^{1/\alpha} \qquad (2.44)$$

or substituting N_f given by (2.43)

$$\Delta\varepsilon = \varepsilon_{fo}\left\{1-\left[1-4n\left(\frac{\varepsilon t}{2\varepsilon_{fo}}\right)^{\alpha}\right]^{1/\alpha}\right\} \qquad (2.45)$$

Next this damage is transformed in terms of an equivalent creep time using the constant creep curve of the material assumed to be of the form:

$$\varepsilon_t = At^b \qquad (2.46)$$

where A,b - constants
t - time
ε_c - creep strain

The equivalent creep time will be represented by

$$teq = \left(\frac{\Delta\varepsilon}{A}\right)^{1/b} \tag{2.47}$$

To this increment of equivalent creep time an increment time tin of actual creep time is added.

The sum teq and t_{in} locates a point on the creep curve of the material. For instance the decrease in residual ductility after one cyclic increment plus one creep increment is given by:

$$\varepsilon_{FR1} = \varepsilon fo - A(teq + t_{in})^b \tag{2.48}$$

The general equation for decrease in ductility resulting from cycling is:

$$\Delta\varepsilon_n = \varepsilon_{FR_{n-1}}\left\{1-\left[1-4n_n\left(\frac{\varepsilon TRn}{2\varepsilon FRn-1}\right)^{\alpha}\right]^{1/\alpha}\right\} \tag{2.49}$$

where

$$\varepsilon_{FR_{n-1}} = \varepsilon_{fo} - A(teq_{n-1} + tin_{n-1})^b$$

and

$$teq_{n-1} = \left(\frac{\Delta\varepsilon_{n-1} + \varepsilon_{fo} - \varepsilon_{FR_{n-2}}}{A}\right)^{1/b}$$

The stepwise progression is followed until failure occurs during a strain cycling period in which the criterion of failure is:

$$1 \leqslant 4(\varepsilon_{TRf}/2\varepsilon_{FR_f})^{\alpha} \tag{2.50}$$

or during a creep period in which the criterion is:

$$\varepsilon_{fo} \leqslant A(teq_f + t_{in_f})^b \tag{2.51}$$

The subscripts stand for:

CR - pertains to creep

eq - equivalent

f - value at fracture
F - ductility
FR - remaining ductility
inc - increment
TR - total range

In evaluating thermal fatigue tests which included hold times at peak tensile stress, agreement between the experimental and calculated lives were well within a factor of two. On the other hand when a linear damage rule was used the lack of agreement was evident as shown in Figure (2.23). For the alloys studied, that plot showed that interaction was non linear and that the linear damage rule will be conservative in some cases (U - 700 W and U - 700C nickel superalloys) and unconservative in others (B1900 nickel superalloy).

2.2.2.4 - Other Methods

A wide variety of predictive approaches have been developed over the years for application to design for high temperature service. Many are simple rules better suited for quick approximate answers to particular situations and alloys rather than for general design purposes. Others, like the frequency separation on the frequency modified strainrange approach, Ostergren's method, Strainrange Partitioning (4) and Continuous Damage Approach (93) are more general and currently under active study and evaluation. These last two approaches deserve special mention here.

The Continuous Damage Approach corresponds to a new concept to predict life in a component. While all the previous methods had modelized only failure relations, this one promises to describe the progressive deterioration processes, taking between initial undamaged state (D=0) and final collapse (D=1) which corresponds approximately to initiation of the macroscopic crack in the structure as seen in model discussed in SECTION 2.2.

The Strainrange Partitioning Approach was chosen as the framework of a large cooperative evaluation programme in which it was evaluated the lability of the method to first correlate the creep-fatigue behaviour of gas turbine materials, and then to predict the creep-fatigue lives of laboratory specimens subjected to complex cycling conditions.

The programme started in 1975 and its culmination was in 1978 with the specialist's meeting and the publication of the correspondent Proceedings AGARD-CP243 (94).

One of the sixteen European and American Laboratories involved on this programme was the Department of Materials of the Cranfield Institute of Technology where the experimental work reported in this thesis was carried out. The SrP method will be given a detailed review in a separate section.

The Continuous Damage Approach was initially introduced by Kachanov (95) and Rabotnov (96) for problems dealing with creep rupture processes. It was extended to the fatigue process (97), monotonic tensile failure and more recently to creep-fatigue interaction (93). Under high temperature fatigue situation it considers two main deterioration processes: the time dependent creep deterioration connected to the initiation and propagation of microscopic intercrystalline cracks and the cycle dependent fatigue damage associated with sufficiently high frequency tests in order to preclude creep effects and where microscopic cracking is predominantly transgranular. When the two different processes are present the two associated damages have to be added. The general constitutive differential equation for damage growth is in this case:

$$dD = d_{creep}dt + d_{fatigue}dN \qquad (2.52)$$

$$\text{or} \quad dD = f(\sigma,D,T)dt + g(\sigma_M\bar{\sigma},D,T)dN \qquad (2.53)$$

Due to the prescence of D in the two terms non linear interaction can arise. Several functions have been suggested for $f(\sigma,D,T)$ and $g(\bar{\sigma},D,T)$ in (97,98) and the process of integrating (2.53) asks for complex numerical calculations which only a digital computer can cope. The Continuous Damage Approach covers a large range of test conditions, mean stress and strain effects, non linear cumulative effects but its application is limited to materials showing similar damaging influence for compressive and tensile loading and where cyclic hardening (softening) is not important otherwise $f(\sigma,D,T)$ becomes a function even more complex.

2.3 - THE STRAINRANGE PARTITIONING METHOD

The strainrange partitioning method has been developed by Manson and co-workers (92,45,46,52,99,100) at the Nasa Lewis Research Center over the last eight years. It is a general strain approach which predicts fatigue lives within the creep range, employing the concept that any conceivable inelastic strain range can be separated in four possible kinds of strainranges:

- tensile plasticity reversed by compressive plasticity
- tensile creep reversed by compressive plasticity
- tensile plasticity reversed by compressive creep
- tensile creep reversed by compressive creep

The basic steps are the experimental determination of the lives as a function of the four partitioned strainranges and the partition of the considered cycle. Even for cycles where the temperature is variable, it is claimed that the basic relationships $\Delta\varepsilon_{ij}$ - N_{ij} are not dependent of the temperature (46) and, therefore, the only influence of temperature on life is canalised through the partitioned components of the hysteresis loop. This fact brings a great simplification to the application of the method to thermal fatigue situations. The predictive process may ignore a great part of the analytical procedures inherent to the SrP approach, if one is only interested to know bounds for the fatigue lives. The method will eventually provide a lower and an upper bound for such lives. In general any case involving arbitrary variation of strain and temperature as a function of time can be handled by this life-predictive approach providing a partition of the respective hysteresis loop width can be performed properly.

2.3.1 - Basic Assumptions of the Strainrange Partitioning Method

The strainrange partitioning method is a strain approach geared to handle high temperature low cycle fatigue situations and whose basic premises are:

A - In any hysteresis loop there are a combination of just TWO DIRECTIONS OF STRAINING and TWO 'TYPES' of inelastic strains. The two directions are tension and compression; the two types of inelastic strain are time independent (plastic) strain.

By a combination of the two directions of strain with the two types of strain are obtained four possible kinds of strainranges:

(1) A strainrange 'caused' by plastic deformation in tension reversed in compression by plastic deformation. It is designated as a PP strainrange and it is represented by $\Delta\varepsilon_{pp}$.

(2) A strainrange caused by creep deformation in tension reversed in compression by plastic deformation. It is designated as a CP strainrange and is represented by $\Delta\varepsilon_{cp}$.

(3) A strainrange caused by plastic deformation in tension reversed in compression by creep deformation. It is designated as a PC strainrange and it is represented by $\Delta\varepsilon_{pc}$.

(4) A strainrange caused by creep deformation in tension reversed in compression by creep deformation. It is designated as a CC strainrange and it is represented by $\Delta\varepsilon_{cc}$.

In any hysteresis loop obtained by cycling a material between strain levels (strain approach) the method is totally focused to what happened inside the hysteresis loop. In other works it is concerned with the inelastic strains associated with hysteresis loop not with the limit strains of the loop. As it will be shown later the inelastic strainrange associated to any conceivable hysteresis loop can be built of one, two or three combinations of the four basic types already seen.

B - Supposing that it is possible to generate in laboratory the four basic loops already seen, for each type of loop different inelastic strains (hysteresis loop width) might lead to different lives. It is assumed in the strainrange partitioning method that the relationship between each of those different inelastic strains (within the same basic type) and the respective cyclic lives obey to a Manson-Coffin type relationship:

$$\Delta\varepsilon_{ij} = AN_{ij}^{-\beta} \tag{2.54}$$

i = P or C
j = P or C

It is proposed, therefore, that the Manson-Coffin relationship (which represents the inelastic strainrange vs life behaviour for materials below the creep limit) is expanded to four relationships for dealing with temperatures within the creep range:

$$\Delta\varepsilon_{pp} = A1\ N_{pp}^{-\beta} \tag{2.55}$$

$$\Delta\varepsilon_{cp} = A_2\ N_{cp}^{-\beta} \tag{2.56}$$

$$\Delta\varepsilon_{pc} = A_3\ N_{pc}^{-\beta} \tag{2.57}$$

$$\Delta\varepsilon_{cc} = A_4\ N_{cc}^{-\beta} \tag{2.58}$$

C - Given a certain hysteresis loop the first task must be to partition it, or to determine how much of it is composed of a PP component, or (and) CP component or (and) PC component or (and) CC compenent. These procedures of partitioning the loop width leads to the building of the ratios Fij i=P or C j= P or C

$$Fpp = \frac{\Delta\varepsilon pp}{\Delta\varepsilon_i} \qquad Fcp = \frac{\Delta\varepsilon cp}{\Delta\varepsilon_i} \qquad (2.59)$$

$$Fpc = \frac{\Delta\varepsilon pc}{\Delta\varepsilon_i} \qquad Fcc = \frac{\Delta\varepsilon cc}{\Delta\varepsilon_i}$$

The predicted life N_{PRED}, for the hysteresis loop defined by the inelastic strainrange $\Delta\varepsilon_i$ and ratios Fij, is then calculated using a damage rule. The authors of strainrange partitioning method have recently proposed the so called interaction damage rule:

$$\frac{1}{N_{PRED}} = \frac{Fpp}{Npp} + \frac{Fcc}{Ncc} + \frac{Fpc}{Npc} + \frac{Fcp}{Ncp} \qquad (2.60)$$

Where Npp is calculated substituting $\Delta\varepsilon pp$ by $\Delta\varepsilon i$ in equation (2.55), Ncp substituting $\Delta\varepsilon_{cp}$ by $\Delta\varepsilon_i$ in equation (2.56) and so on.

As it can be concluded by now the determination of relations (2.55) - (2.56) - (2.57) - (2.58) prior to any predictions is essential in Strainrange Partitioning.

Summing up it is this total process of generating the individual failure life relationships (equation 2.54) partitioning an hysteresis loop in its component strainranges and combining the effects of these components to determine life that has been called the method of strain range partitioning.

2.3.2 - Generation of the Basic Strainrange versus life Relationships

This approach is built around a series of experiments to establish strain-cycle life relationships for a given material and temperature. In these experiments the two directions of straining are combined to the two types of inelastic strain (plasticity and creep) to form the four basic types of strain.

In a first approximation plasticity can be regarded as the sum of all inelastic strain components which occur immediately upon application of stress, while creep will be seen as that part of the inelastic strain that results from the sum of all time dependent components. It is assumed that the high temperature low cycle fatigue behaviour will depend basically on how these two modes of deformation can interact, not only regarding their existence in tension or in compression, but also and principally, how

tensile components of strain are balanced by a compressive component to close the hysteresis loop.

Consider the hysteresis loop of Figure (2.24). This hysteresis loop can be obtained by loading rapidly to stress level (B) holding this stress for a certain period of time in order to get a certain amount of creep C_1. The stress is reversed to a compressive value (CC'E), holding the stress corresponding to E to close the loop with the amount of creep C_2. While in tension the loop is characterized by an inelastic strain composed of a plastic part A'B' and a creep component B'C', in compression the inelastic strain can be divided in a plastic component C'E' plus a creep component E'A'. In the tensile portion of the cycle there is more creep than in compression while the plastic component is lower in tension than in compression. So, there is a reversed plastic component $\Delta\varepsilon_{pp}$, a reversed creep component $\Delta\varepsilon_{cc}$ and also a strain component wherein tensile creep is reversed by compressive plastic flow $\Delta\varepsilon_{pc}$. This partition may be visualized by rotating 180^{o} the compressive part of Figure (2.24) to form Figure (2.25). Here the partition can be done noting the way the several inelastic strain bits are crossed in tension and compression. For example the A'B' bit can be achieved in tension by plastic deformation or in compression by plastic deformation too. It is a $\Delta\varepsilon_{pp}$ component. The segment (E') (A') corresponds to an inelastic component resulting from creep in tension or creep in compression. It is an $\Delta\varepsilon_{cc}$ component. The segment B'(E') is the result of a creep component in tension or a plastic component in compression. It is a $\Delta\varepsilon_{cp}$ component. Following SrP notation for the several types of inelastic strain $\Delta\varepsilon_{ij}$, where the first index i is refered to tension and the second j to compression, the width A'C' of Figure (2.24) can be partitioned as follows:

$$A'B' = \Delta\varepsilon_{pp}$$
$$A'E' = \Delta\varepsilon_{cc}$$
$$B'E' = \Delta\varepsilon_{cp}$$

A simple rule can also be applied to Figure (2.24) to partition the inelastic strain represented by the hysteresis loop width A'C':

- $\Delta\varepsilon_{pp}$ → smaller value of the plastic strain in tension or compression
- $\Delta\varepsilon_{cc}$ → smaller value of the creep strain in tension or compression

- $\Delta\varepsilon_{cp(pc)}$ → $\Delta\varepsilon_{cp}(pc) = \Delta\varepsilon_{i} - (\Delta\varepsilon_{pp} + \Delta\varepsilon_{cc})$ = creep in tension - creep in compression = plasticity in compression - plasticity in tension.

If the creep in tension is greater than the creep in compression, the former partitioned term is a CP component; if the reverse is true the component is PC.

Summing up, four basic strain components must be considered:

Notation		Tensile Strain		Compressive Strain
$\Delta\varepsilon_{pp}$	-	Plastic	-	Plastic
$\Delta\varepsilon_{pc}$	-	Plastic	-	Creep
$\Delta\varepsilon_{cp}$	-	Creep	-	Plastic
$\Delta\varepsilon_{cc}$	-	Creep	-	Creep

In any hysteresis loop it is only possible to have a maximum of three components since by definition a CP component can not coexist with a PC component.

After the definition of the $\Delta\varepsilon_{ij}$ strains, the next assumption with the SrP method is that the functions relating each one of basic types of strains $\Delta\varepsilon_{ij}$ with cyclic lines N_{ij} are straight lines when plotted on log-log scales. In other words they obey to a Manson-Coffin type relationship.

$$\Delta\varepsilon_{ij} = A_k N_{ij}^{-\beta k} \qquad ij = \begin{cases} pp \\ pc \\ cp \\ cc \end{cases} \qquad k = 1,2,3,4 \quad (2.61)$$

A_k, β_k = constants

Finally the method assumes the existence of a process of combining the effect of several strainranges $\Delta\varepsilon_{ij}$ resulting from the partitioning of a more or less complex hysteresis loop as follows. The authors of SrP had suggested till now two damage rules to accomplish this final step. In an early paper about SrP (92) it was proposed to apply within its technology the so called Linear Damage Rule in which:

$$\Sigma \frac{1}{N_{ij}} = \frac{1}{N_{PRED}} \qquad ij = \begin{cases} pp \\ pc \\ cp \\ cc \end{cases} \qquad (2.62)$$

where N_{PRED} is the predicted life in cycles to failure for a loop of inelastic strain $\Delta\varepsilon_i$:

$$\Delta\varepsilon_i = \Sigma\Delta\varepsilon_{ij} = \Delta\varepsilon_{pp} + \Delta\varepsilon_{pc} + \cdots\cdots$$

At this stage of application of the method, the four $\Delta\varepsilon_{ij}$ - N_{ij} relationships through their coefficients A_k, β_k must be already determined:

$$\begin{cases} \Delta\varepsilon_{pp} = A_1 N_{pp}^{-\beta_1} \\ \Delta\varepsilon_{cp} = A_2 N_{cp}^{-\beta_2} \\ \Delta\varepsilon_{pc} = A_3 N_{pc}^{-\beta_3} \\ \Delta\varepsilon_{cc} = A_4 N_{cc}^{-\beta_4} \end{cases} \qquad (2.63)$$

In equation (2.62) the lives N_{ij} are calculated substituting the partitioned strain bits $\Delta\varepsilon ij$ in (2.63). Then:

$$N_{ij} = \text{Antilog}\left(-\frac{\log \frac{\Delta\varepsilon ij}{Ak}}{\beta k}\right) \qquad (2.64)$$

$$ij = \begin{cases} PP \\ PC \\ CP \\ CC \end{cases} \qquad k = 1,2,3,4$$

These values substituted in (2.62) give us the predicted life N_{PRED}.

Later (45,99) a new damage rule was proposed, it is the so called 'Interaction Damage Rule' where

$$\frac{1}{N_{PRED}} = \Sigma \frac{Fij}{Nij} \qquad Fij = \frac{\Delta\varepsilon ij}{\Delta\varepsilon i} \qquad ij = \begin{cases} PP \\ PC \\ CP \\ CC \end{cases} \qquad (2.65)$$

For this damage rule the lives Nij are calculated substituting in equations (2.63) the partitioned strains $\Delta\varepsilon_{ij}$ by the inelastic strain $\Delta\varepsilon_i$. The general expression for the N_{ij} lives come:

$$N_{ij} = \text{Antilog}\left(-\frac{\log \frac{\Delta\varepsilon i}{Ak}}{\beta k}\right) \qquad (2.66)$$

Figure (2.26) shows graphically the difference in one application of the two damage rules. Lives predicted by application of the two damage rules do not differ greatly (52). Three different damage rules used with the SrP method will be discussed in a later chapter.

Ideally the hysteresis loops to produce experimentally the strainrange vs life relationships would be as follows:

(a) $\Delta\varepsilon_{pp} = \Delta\varepsilon_{pp}(N_{pp})$
In this case the hysteresis loop should contain just plastic strains (Figure 2.27 a)

(b) $\Delta\varepsilon_{cp} = \Delta\varepsilon_{cp}(N_{cp})$
For this relationship the cycle must display an inelastic component achieved in tension by creep and by plasticity in compression (Figure 2.27 b)

(c) $\Delta\varepsilon_{pc} = \Delta\varepsilon_{pc}(N_{pc})$
Here the cycle must be such that displays an inelastic component achieved in tension by plasticity and in compression by creep (Figure 2.27 c)

(d) $\Delta\varepsilon_{cc} = \Delta\varepsilon_{cc}(N_{cc})$
In this relationship both directions of straining (tension and compression) should only cause creep Figure 2.27 d)

while the PP type can be generated in a conventional manner the other types require some less conventional testing procedures.

(a) - PP Type Tests

In this type of test no creep strain is permitted. In order to achieve this requirement at high temperatures it is necessary to employ a sufficient high frequency to preclude a significant introduction of creep. This minimum frequency depends upon the material and temperature used and can be determined experimentally by conducting a series of tests at progressively higher frequencies, till a plateau in stress-strain response or in cyclic life is achieved. The strain ranges for the PP type should be selected so as to give lives covering the range between approximately 50 to 50,000 cycles to failure. In some cases of high temperatures, high strength, low ductility alloys that upper limit is reduced in order to make possible the accurate measurement of the inelastic strains involved in those tests. A plot should be constructed of $\Delta\varepsilon_{pp}$ vs cycles to failure N_f in log-log scales. The required straight line will be the one that fits best the experimental data (Figure 2.28 a).

(b) - CP Type Tests

There are three practical cycles that can be performed in order to produce a hysteresis loop formed basically of a CP component. In the first one, (Figure 2.28 b) a constant tensile creep stress is used to produce a preset amount of strain. The cycle is reversed in the compressive part by

using a sufficiently high strain rate to prevent the occurrence of any creep. The test can be executed under servo-load control with external strain limits superimposed. The value of the tensile stress to be used must be low enough in order to provide a hysteresis loop where the creep strain is the dominant strain. It should, however, be large enough that the creep time per cycle is not too large. This creep time can change drastically due to cyclic strain hardening or softening. In this case, the stress level should periodically increased or decreased. Another type of cycle suggested to perform the CP tests is shown in Figure (2.28 c). It is a strain hold cycle involving stress relaxation occurring by a creep mechanism. The creep strain obtained by this method is limited by the amount of elastic strain which can be readily transformed in creep strain. This test cycle should only be used when the inelastic strainrange is very small, otherwise the plastic component in tension will become preponderant. A third testing technique employs a continuous strain cycling but now involving a low strain rate in tension to introduce creep and a high strain rate in compression to prevent it. Although this type of cycle is relatively simple to use, the interpretation of how much is creep and how much is plasticity in tension is not just straight forward as in the former techniques. In this case, the tensile strain should be partitioned into its component strains by means of independent techniques which will be dealt with later on.

All these practical cycles introduce a PP component contrarily to the ideal cycle seen in Figure (2.27 b) . This PP component should be kept below 50% in cycles used to determine the $\Delta\varepsilon_{cp} - N_{cp}$ relationship (99).

Before the $\Delta\varepsilon_{cp} - N_{cp}$ relationships can be plotted the damage due to the presence of any pp type strainrange must be considered. Here a damage rule must be used in a reverse manner. For the interaction damage rule we have:

$$\frac{Fpp}{Npp} + \frac{Fcp}{Ncp} = \frac{1}{N_{OBS}} \qquad (2.67)$$

Here the experimentally observed life N_{OBS} substitutes the predicted life N_{PRED} and equation (2.67) is solved for the unknown Ncp. Before any attempt to plot the $\Delta\varepsilon_{cp} - N_{cp}$ relationship it is necessary to establish first the $\Delta\varepsilon_{pp} - N_{pp}$ function (Figure 2.28 b).

c - PC Type Tests

The appropriate tests for the determination of the PC tests are identical to the CP tests. The creep portion of the cycle is here in compression. All that was said for the

CP tests is valid for the PC ones, providing the tensile and compression notations were interchanged. The practical cycles to perform the PC tests are shown in Figure (2.29, e,f,g).

d - CC Type Tests

The three basic testing techniques to generate CC type cycles where creep should be predominant in tension and compression are shown in Figure (2.29,h,i,j). The most widely used cycle involves a cyclic creep rupture test (101) where a constant tensile stress is servo controlled until a preset tensile strain limit is reached. When this limit is reached the stress is rapidly reversed and a constant compressive strain limit (equal to the tensile one) is reached. Again it may be necessary to change periodically the stress levels in tension and compression to maintain a desired creep strain or time per cycle.

An alternative test (Figure 2.29,i) is a rapid strain cycling with hold strain periods superimposed. The tensile and compressive stresses are allowed to relax and the elastic strain is converted into creep. If the two amounts of creep are equal in both directions there is no unbalanced CP or PC component. Generally this does not happen and an unbalanced type of strain is introduced. Here there is a necessity to take into account the possible damage effect of a PP component and of a CP or PC component. This is achieved using the interaction damage rule in a reverse way:

$$\frac{Fpp}{Npp} + \frac{Fpc}{Npc}\left(\frac{Fcp}{Ncp}\right) + \frac{Fcc}{Ncc} = \frac{1}{N_{OBS}} \qquad (2.68)$$

The $\Delta\varepsilon_{cc}$ - N_{cc} relationship is the last to be determined because it needs the knowledge of the $\Delta\varepsilon_{pp}$ - N_{pp}, $\Delta\varepsilon_{cp}$ - N_{cp} and $\Delta\varepsilon_{pc}$ - N_{pc} relationships (Figure 2.28 d).

A third means of producing a creep strain cycle CC is simply to perform a reversed strain cycle at a very low frequency, in order to introduce sufficient creep in both directions (Figure 2.29 j).

Figure (2.30 provides examples for six alloys of the four basic partitioned strainrange versus life relationships.

2.3.2 - Techniques for Separating Inelastic Strains

The concept underlying strainrange partitioning is that the creep-fatigue interaction is related to the manner in which creep and plasticity reverse each other. They can be

differentiated and detected in a certain cycle because of the dependency of the first one compared with the time dependency of the second one. This separation is not always simple and easy. Here two types of cycle must be distinguished.

(i) A first type of cycle composed of continuous cycling at sufficiently high strain rate to prevent creep with the superimposition of one or more hold periods during which creep occurs.

(ii) Continuous cycling at which simultaneously creep and plasticity occur.

In the first type of cycle with hold periods in which creep is introduced within the cycle consider a CP type cycle shown in Figure 2.31 b. The three main variables are:

- limit strains
- stress levels in tension and compression
- strain rates in tension and compression

Choosing a sufficiently high compressive hold stress, the compressive strain limit is attained first by-passing the preset hold stress period in compression, Figure (2.31 a). Schematically it shows how to separate strains from the stress-time and strain-time plots. The total strain is represented on the graph strain vs time by the vertical distance between points D and C. The inelastic strainrange is given by the vertical distance between A and E. This inelastic strain can be also calculated substracting from the total strain $\Delta\varepsilon_T$ the elastic strain given by ratio of the cycle stress amplitude over the young modulus. Within the hysteresis loop creep is developed between C and D, therefore, $\Delta\varepsilon_{cp}$ is represented by the vertical distance between C and D on the strain-time graph. The PP strain type can be calculated knowing that:

$$\Delta\varepsilon_i = AE = AC' + CD \qquad \Delta\varepsilon_{pp} = \overline{AE} - \overline{CD}$$

Considering continuous cycling, partition is not so straight forward. It is impossible now, to separate a creep component from a plastic component because the two strain types occur not only on the same direction but also within the same time increment.

Three methods are suggested on the strainrange partitioning literature for dealing with these situations.

(1) Rapid Cycling Between Two Stress Peaks

In Reference (52) a method was presented for separating the strain components in symmetrical cycles to involving only $\Delta\varepsilon_{pp}$ plus $\Delta\varepsilon_{cc}$ components. Figure (2.32) shows the principle involved and the results obtained for a stainless steel. As the cycling was done at a constant strain rate the obtained plastic strains were equal in tension and compression. This resulted in a partition of the inelastic strain amplitude in only two components $\Delta\varepsilon_{pp}$ and $\Delta\varepsilon_{cc}$. After the establishment of a stable hysteresis loop at one of the four frequencies considered, (wider of the hysteresis loops at A,B,C, and D), it is necessary to traverse the peak stress rapidly in order to prevent the introduction of creep. Once the peak stresses were established the cycle is changed to stress control and the frequency is increased resulting in a non creep thinner hysteresis loop shown at A,B,C and D. Their width represents the $\Delta\varepsilon_{pp}$ strainrange for each of the four cases. The plasticity loop is extremely thin at the low frequency but it comprises almost the entire width at the high frequencies. Therefore, the inelastic strainrange is almost composed of a $\Delta\varepsilon_{cc}$ component at low frequencies and $\Delta\varepsilon_{pp}$ at high frequencies which is the expected partition in both cases.

Accordingly fatigue lives approach N_{cc} at the lowest frequencies and N_{pp} at the highest frequencies. In fact this method is not applicable to cycles including more than two components $\Delta\varepsilon_{ij}$. This method separates $\Delta\varepsilon_{pp}$ being the remainder strainrange calculated by substraction of the inelastic strain $\Delta\varepsilon_{i}$.

However, the same principle can be applied in treating each half cycle separately to determine its individual components - creep and plasticity. This constitutes the basis of the following method.

(2) The Half-Cycle Rapid Load-Unload Method

This method was proposed in (100) to deal with unsymmetric cycles displaying a $\Delta\varepsilon_{pp}$, $\Delta\varepsilon_{cc}$ and an unbalanced type $\Delta\varepsilon_{pc}$ or $\Delta\varepsilon_{cp}$, Figure (2.33) illustrates the procedure. Basically a rapid strainrate is imposed on the half of the cycle presenting time dependent strain. The application of the method shown for the tensile part can be used similarly for the compressive part.

For the case shown in Figure (2.33) a stable hysteresis loop ABCDEF must be first established. Then the specimen is brought to point A and followed by the straining within the same strain limits but employing a high strain rate in tension. The rapid loading from A to C' produces only plastic strain AC". The compressive half of the cycle might be likewise analysed. The loop should be stabilized before

each rapid loading to washout the effects of prior rapid loading effects. The method cannot be applied to materials presenting negative strain rate sensitivity.

(3) The Step-Stress Method

The previous process can be generalised by increasing the number of steps from and to which the stress is rapidly changed; the new method is illustrated in Figure (2.34). The method uses the measurement of the steady creep rate at a number of stress levels from which the overall creep can be determined. In Figure (2.34) the stress levels E,A,B,C, D are chosen at the centres of the five intervals of equal strain into which the hysteresis loop width is arbitrarily divided. In Figure (2.35a) the first task is to determine how much creep occurs in tension. After the stabilization of the original hysteresis loop one must stop at A and determine the steady creep rate by holding the stress at that level Figure (2.35b). Once the effective creep rates have been established at the selected values of stress, a plot of the rates vs time should be drawn. The area under the obtained curve is the total tensile creep.

By this method the concept of a creep component is somewhat modified because the time dependent transient creep is considered as plasticity rather than creep. It seems reasonable to consider all the steady state creep as creep to apply in the SrP approach in the sense that there is a high probability of different deformation mechanisms operating relative to plasticity. However, the precision of how much of the transient creep should be considered as 'effective creep' remains an insoluble question. This is an important aspect of a partition process as the ratio between the transient creep and steady creep within a cycle increases. From the knowledge of the creep component in tension and the creep component in compression calculated by a similar process, the partition of the hysteresis loop width can be effectivated as in the previous cases: the smaller of the tension and compression creep components is assumed to be the $\Delta\varepsilon_{cc}$ strainrange, the smaller of the plastic components $\Delta\varepsilon_{pp}$, the remainder of the inelastic strainrange being $\Delta\varepsilon_{cp}$ or $\Delta\varepsilon_{pc}$ component.

2.3.4 - Advantages of the SrP Method

It was seen that the material characterization was done by means of four relationships each one involving a few tests to define it. Supposing that a mean value of five points for each of the basic relationships $\Delta\varepsilon_{ij} - N_{ij}$ are sufficient to establish confidence on the respective straight lines in log-log plots, twenty tests would be necessary to characterize the fatigue-creep behaviour of the material

being studied. Besides test temperature (which will be dealt with separately in a later subsection) the SrP approach through the $\Delta\varepsilon_{ij}$ - N_{ij} relationships is able to take into account several effects such as:

- testing frequencies
- applied wave shapes (strain or stress dwells)

Therefore, the first advantage of SrP method is its high degree of generality. Designers will have to determine the type and magnitude of the strain being applied to their structure but the failure curves as represented by the four partitioned strainrange versus life relationships $\Delta\varepsilon ij$ - Nij are general and can be applied to any specific situation.

2.3.4.1 - The Establishment of Bounds on Life

During the design process, it is likely that the inelastic strains were known at critical points such as the root of a turbine blade. It is, however, unlikely at least with a sufficient degree of accuracy to know how much of that inelastic strain is of PP,CP or CC type. The SrP approach in cases where the partition of the hysteresis is difficult or impractical provides upper and lower bounds on fatigue life. In considering the case of Figure (2.36) where the CP, CC, PC and PP life relationships are in decreasing order of lives for the same inelastic strainrange, the higher the life can possibly be is N_{pp}. On the other hand, if $\Delta\varepsilon_i$ was made up entirely of the most damaging type of strainrange $\Delta\varepsilon cp$ the life could be no less than Ncp. Additional information concerning the type of cycle suffered by that component can narrow those bounds. For example certain thermal fatigue problems the designer might know that certain strain types are unlikely, say the CP type. This information eliminates the CP failure and thereby alters the lower bound from Ncp to Ncc. For some materials two or more of the four relationships $\Delta\varepsilon ij$ - Nij can be quite close to each other Figure (2.30). In such a case the partition of a hysteresis loop might not be justified and greatly reduce the analysis required for life prediction processes.

2.3.4.2 - Temperature Insensitivity

One of the first and more important claims for the strainrange partitioning approach was the temperature insensitivity of the four partitioned strainranges versus life relation-

ships. Halford et al (46) found for two stainless steels tested in ranges between 595 - 815°C that the $\Delta\varepsilon_{ij}$ - N_{ij} functions were not significantly affected by varying the temperature within the mentioned range. Figure (2.37) compares the observed and predicted lives at different temperatures. These predicted lives were calculated using data shown by open circles. In these examples temperature variations (closed circles) do not influence the results. A maximum factor of 2 was found between observed and predicted lives.

It is suggested (46) that the effects of the temperature on the fatigue failure is not so sensitive as the well known temperature effect on the flow behaviour. The role of temperature on the failure behaviour is to alter the partitioning within a cycle but not the basic failure relationships $\Delta\varepsilon_{ij}$ - N_{ij}. If this is observed to be true at least for certain ranges of temperatures, the generality of the approach is considerably improved because fewer tests are required to characterize the high temperature low cycle fatigue behaviour of a material. Analysis of cycles including changes of temperatures is greatly simplified. What is needed is, as in an isothermal case, to partition the cycle, calculate lives N_{ij} and apply a damage rule to predict the fatigue life. There are some obvious limitations to such temperature insensitivity. It is not expected to find temperature independent relationships when the material is metallurgically unstable or when the creep and plastic ductilities are sensitive functions of the temperature or testing time.

2.3.4.3 - Frequency Effects

As it was seen, the frequency is an important variable within the creep range because with the temperature it is the main factor in determining how much creep is going to be introduced in a fatigue cycle. With sufficiently high frequency of straining, insufficient time will be available for significant creep to occur. On the other hand as one decreases the frequency of straining, more creep is introduced within the cycle, modifying its partitioning. In the first case it is expected that the corresponding life should be N_{pp}. At extremely low frequencies one can expect that the inelastic strainrange will be formed almost entirely of the $\Delta\varepsilon_{cc}$ component, therefore, with the corresponding life approaching the N_{cc} life. In this sense the effect of decreasing the frequency is the same as to increase the temperature. In both cases the amount of creep is larger. This can be seen from Figure (2.38) for a stainless steel. Here to increase the frequency or decrease the temperature, other

conditions being constant, display the results from the upper bound N_{pp} to the lower bound N_{cc}. This fact suggests another advantage of the SrP approach. The life relationships can be determined accurately at a single elevated temperature at extreme frequencies in order to establish bounds in life. If the bounds are close to each other fewer tests are required. If the lives for the respective bounds are widely separated or highly divergent a more accurate estimate of cyclic life is required including the normal determination of the four $\Delta\varepsilon_{ij} - N_{ij}$ functions.

2.3.4.4 - Hold Time and Relaxation Effects

At high temperature creep always occurs during a tensile or compressive hold. The introduction of holding periods may develop a $\Delta\varepsilon_{cp}$ or $\Delta\varepsilon_{pc}$ component if creep is reversed by plasticity on the opposite direction or may develop a $\Delta\varepsilon_{cc}$ component if creep is reversed by creep. On the Strainrange Partitioning approach, the influence on life of these hold periods is taken into account through the damage associated with a PC,CP or CC component.

2.3.4.5 - Ratcheting Effects

An internal ratcheting effect was suggested (52,100) to explain the sometimes rather reduced lives of cycles incorporating unbalanced strainranges $\Delta\varepsilon_{cp}$ or $\Delta\varepsilon_{pc}$. Here it is considered that the tensile strain is achieved within one deformation system and the compressive strain is obtained within another system. Suppose that the cycle incorporates a creep component in tension obtained by a mechanism of deformation based on grain boundary sliding and a plastic component in compression where the deformation is supposed to be achieved by plane slip. Although externally there was no practical net geometrical change, after each cycle the internal effect may be substantial. A repetitive $\Delta\varepsilon_{cp}$ cycle becomes more like a monotonic tensile creep test since every cycle adds more tensile creep deformation. In the same way a repetitive $\Delta\varepsilon_{pc}$ simulates a conventional tension test. If the mechanism of deformation is repeated totally (PP and CC components) or partially it should be expected that a certain amount of healing will take place during every cycle since the reversed strain is 'undoing' some of the damage due to the strain that had occurred in the forward half of the cycle. On the other hand if the reversed strain takes place in another system that healing cannot occur and the development of a crack is made easier. In these cases where failure occurs by ductility exhaustion, the creep

ductility D_c (CP cycles) and the tensile ductility Dp (PC cycles) are the important variables in determining the exhaustion and, therefore, the fatigue life. It is interesting to note that in an ideal case where the two reversed strains occurred in two completely different systems, let us say creep exclusively by grain boundary sliding, plasticity exclusively by slipping along crystallographic slip planes, the exponent of the $\Delta\varepsilon cp$ and $\Delta\varepsilon pc$ versus life relationships would be -1. In fact being Dp and D_c the plastic and creep ductilities the lives would be given by:

$$N_{cp} = \frac{D_c}{\Delta\varepsilon_{cp}} \qquad \Delta\varepsilon_{cp} = D_c N_{cp}^{-1} \qquad N_{pc} = \frac{D_p}{\Delta\varepsilon_{pc}} \qquad \Delta\varepsilon_{pc} = D_p N_{pc}^{-1}$$

If some healing is to be expected or in another way if some deformation mechanism is shared by the tension and compression side it would be expected coefficients less than 1. In cycles where healing will be expected to occur, like on the balanced cycles PP or CC, one could expect under this point of view power exponents for the respective relationships.

This ratcheting effect is particularly important under circumstances where the temperature and strain rates favour grain boundary sliding and also important in thermal cycling, where the effect is accentuated by changing the temperature in such a way that the hot part coincides with the imposition of hold periods (creep strain-grain boundary sliding) and the cold part coincides with the fast reversal (plastic strain-slip).

2.3.4.6 - Thermal Fatigue

As it was pointed out in previous sections thermal fatigue play nowadays is an important role within the field of the high temperature low cycle fatigue. In this sort of fatigue problems, large temperature fluctuations cause creep and plastic strains to occur in more or less constrained parts resulting in the occurence of critical points where a crack can develop. Although some good results in treating thermal fatigue employing other predictive methods were obtained (102) the strainrange partitioning approach is a sufficient generic method to take into account several thermal histories, and distinguish between compressive and thermal creep damages.

How strainrange partitioning can help in dealing with several thermal situations is schematically shown in Figure (2.39). Here the schematic assembly of two thin

outside bars designated as 'edges' and the massive interior bar designated as 'inside', simulates a turbine blade wherein the outside bars represent the edges of the balde and the inside bar represents the massive centre of the b de. When the turbine blades are subjected to the hot gases coming from the combustion chamber, the outside edges are the first to heat. Their expansion is, however, constrained by the massive part which is slower to heat, resulting in the development of compressive stresses on the edges. During the cooling from a uniform temperature the reverse is observed as the edges tensioned because they tend to cool faster. Several cases are considered in Figure (2.39) and all of them can be associated to a particular strainrange type already seen for the strainrange partitioning approach. The case illustrated in Figure (2.39 a) simulates faster rates of heating and cooling preventing an appreciable variation of the massive part which constraining the edges makes these ones alternate between tensile and compressive plastic strains. The developed inelastic strainrange is in this case of the PP type. The case b) involves a hold period sufficiently small to prevent an appreciable heating of the massive part. Compressive plastic flow occurs immediately after heating. During the hold period strain relaxes. The tensile plasticity happens during cooling but no creep can occur because meanwhile the temperature is too low. The case c) represents the typical case of an uncooled turbine blade subjected to extended steady operation at high temperatures. Compressive plastic flow occurs on the edge bar while its temperature increases but the inside bar temperature has not yet begun to rise (AB). Here, no time is allowed for creep. Immediately the interior part begins to heat and a tensile component of strain is developed followed by stress relaxation during the temperature 'plateau' for both parts. The predominant strain for this cycle type is therefore $\Delta\varepsilon_{pp} + \Delta\varepsilon_{cp}$. Finally case d) is similar to case c) but here a lag period is introduced during which time the edge temperature is maintained at a high value while the inside bar is still cold. The strainranges present are $\Delta\varepsilon_{pp} + \Delta\varepsilon_{cc}$ as shown in Figure (2.39d).

Prediction of lives for cycles similar to these ones is made easier in applying the SRP method providing it can be determined the amplitude and type of strains being involved. Once this is done whatever was the complexity of the cycle, the strainrange partitioning has an inherent ability to handle any thermal cycle by solving a 'damage expression' such as those mentioned in section 2.3.2.

2.3.4.7 - Difficulties with the Strainrange Partitioning Method

The numerous data generated mainly after 1975 on the evaluation of the Strainrange Partitioning Method showed clearly that there are some difficulties associated with the generation of the basic data. Basically these difficulties are related to the accuracy in measurements of the parameters of interest (inelastic strain), identification of the type of strain in very narrow loops or with subjacent techniques to the method ie., the damage rules which the approach demsnds. However, there are other questions raised by this predictive approach which deserve perhaps more attention because they are related to the basic assumptions of the method.

One is that the method predicts two bounds - one at high frequency, the other at low frequency. This situation is depicted in Figure (2.40). The upper bound or high frequency saturation of fatigue life is consistent with the model shown in Figure (2.2) while the lower is not.

Hold time saturation effects have not been studied extensively but the behaviour pattern can be established now for some materials. Conway (30) found that beyond a certain hold tensile period duration (about 50 min for AISI304 stainless steel specimens tested at 650^{0}C between strain levels ± 1%) the relaxed stress level is so low that the additional creep damage resulting from an increased duration was negligible (see Figure 2.4). This would be rather important on experimental investigation because once the saturation limit is reached for a given material and general test conditions the use of longer hold period tests would be eliminated or at least drastically reduced. The two plateaus B and C from Figure (2.4) mean that two saturation effects can be separated. The plateau B whose results correspond practically to the CC line and the plateau C corresponding to the CP line represent two saturation effects. The first can be viewed as a strain rate or frequency effect and any reduction below plateau B is a true hold effect such as happens with plateau C.

However, the existence of these plateaus sometimes cannot be established which casts doubts on extrapolations to predict them. In some cases on two or more plateaus for the same type of cycle are obtained, resulting in more than one strainrange vs life relationship for one cycle of SrP. That is the case found for 1 Cr'lo steel (103) where stress dwells and strain dwells were found to induce different CP lines. This was explained by the existence of sharply defined ductile/brittle transition

stress. While on the load controlled tests (stress dwells) the tensile hold was always greater than the transition stress and hence produced fractures on the ductile regime on the strain controlled tests (strain dwells), the tensile load relaxed very rapidly down to values below the transition stress and into the brittle regime producing lower lives than those found for creep produced by stress dwells.

Another question relates when the creep processes are unimportant relative to environmental damage. In this case not only such plateau on life vs time per cycle cannot be expected to happen and hence the CP, CC or PC lines have no significance but also the damage instead of being reflected by time is reflected by the ratio of inelastic strains $\Delta\varepsilon_{ij}/\Delta\varepsilon_{i}$ which is not sufficiently sensitive enough to represent damage specially at very long dwells. This problem can be enhanced as temperatures are lowered ie., in the regime where mechanical strain and environment alone interact and where different hold times although not producing basic percentages of creep induced completely different periods of initiation and hence inducing different lives which the different creep within the cycle would not predict.

2.3.5 - Scope of the Thesis

Since 1969 cyclic creep behaviour studies of Nimonic alloys have been made at Cranfield. Past studies have involved stress cycled push-pull creep in Nimonic 108 (104) and metallurgy and fracture behaviour in MAR1002 (105). The development of these new as cast nickel superalloys results from the demand of stronger alloys under the creep-fatigue point of view and they are aimed to perform reliably in exigent high temperature situations such as those found for disc, vanes and blades in gas turbines. Due to either externally applied stresses or to thermal stresses arising from constraint during heating and cooling cycles, damage on those components, should be described by a life prediction method sufficiently generic to deal with those different mechanical and thermal histories.

The Strainrange Partitioning was thought to be helpful in this regard. MAR1002 a recently developed as cast nickel superalloy was used in a programme which aimed basically to characterize high temperature low cycle fatigue behaviour of that alloy. According to that programme three important aspects of the creep-fatigue interactions in that alloy were suggested to be studied:

(i) Complete characterization of the high temperature low cycle fatigue of MARM002 using the strainrange partitioning approach at two basic temperatures 850 and 1040°C.

(ii) Determination of the effect of test temperature on the strainrange versus life relationships established in (i).

(iii) Relative importance of initiation and propagation on the high temperature low cycle fatigue tests on MARM002.

These three topics will be dealt with in separate chapters with a fourth one dedicated to the analysis of the damage rules which the SrP method uses in its technology.

3 - EXPERIMENTAL

The low cycle fatigue tests were conducted on a high temperature fatigue laboratory having as basic facilities:

(1) A servo hydraulic tension-compression machine with a maximum capacity of 3 tons.

(2) Strain and load control systems.

(3) Temperature control system

(4) Measurement and recording systems.

The tension and compression rig was purpose built in the Department of Materials of Cranfield Institute of Technology to reproduce deformation problems associated with thermal fatigue of turbine blades (104) and to study cyclic creep of nickel superalloys (105). The main adaptation necessary for the strainrange partitioning work on MARM002 was a new wave generator capable of reproducing the wave shapes necessary to the basic SrP tests.

3.1 - TENSION-COMPRESSION RIG

The fatigue machine consists of a double acting hydraulic jack mounted into a fixed lower head rigidly attached to the lower block as shown schematically in Figure (3.1). The jack load is reacted through a lead screw into the top block. The botton block supported on a rigid angle frame holds the fixed lower head. The jack load is controlled by a "dowty moog" servo hydraulic valve fixed directly into the jack body. The hydraulic pressure is gauged at the inlet to the servo-valve and an accumulator placed after the reducing valve, provides an oil reservoir to smooth out any pressure variations. Two safety switches limit the course of the jack piston cutting off the supply pressure and venting the jack to the hydraulic return line.

3.2 - LOAD AND STRAIN CONTROL

The load is supplied by a double acting hydraulic ram controlled by an electrically activated precision spool valve. The load cell is a conventional ring employing four semi-conductor strain gauges connected as a four-arm bridge.

Specimen strain is measured by a variable reluctance transducer mounted on the water cooled end of a scissor type of extensometer. The extensometer is located into the specimen by ceramic inserts spring loaded into V-ridges machined on the specimen. More details of the extensometer are available in Reference (106).

3.3 - TEMPERATURE CONTROL

The specimen temperature is measured by a Land Optical Pyrometer connected via an amplifier to a Bristol Strip chart recorder. The recorder provides a control signal to a saturable reactor proportional to the difference between specimen temperature and the set temperature.

The saturable reactor is in series with a step down transformer which provides the current through the specimen. Provision is made on the saturable reactor for band width and reset control.

Chart (3.2) provides the function control signal versus temperature. The specimen were all resistance heated in air through rods attached directly to the specimen as shown in Figure (3.3). The diameter of these rods is slightly inferior than the diameter of the specimen on its gauge length. The input rods reach a higher temperature pumping heat into the specimen rather than extracting it. Longitudinal variations of less than $3^{o}C$ at $900^{o}C$ over the gauge length were achieved with this set up.

3.4 - SPECIMENS AND WAVE GENERATION

Specimens were obtained in the as-cast condition from the National Gas Turbine Establishment. They were machined to shape and subsequently heat treated for 16 hrs at $870^{o}C$, furnace cooled anf finally grinded before testing. The standard equipment for the more conventional tests includes a FARNELL function generator, two channel X-Y recorder and an U.V. recorder for the high frequency fatigue tests. In order to perform the PC, CP and CC tests a wave generator was constructed. It is shown schematically in Figure (3.4). Here the strain signal from the extensometer is connected into two voltage comparitors. The reference voltage to comparitor 1 is set to the tension strain limit and the reference voltage to comparitor 2 is set to the compression strain limit. When the strain input signal reaches these preset limits the bi-stable circuit operates a change over relay. The two inputs to the change over relay are connected to the input of a ramp generator. The output voltage of the ramp generator feeds into the Moog Valve Amplifier as demand signal. The machine control system is connected in a load feedback mode.

In operation the programme work is as follows:

when the start switch is depressed the ramp generator operates and produces a signal at a preset rate until a preset maximum value. When the strain reaches the value set or the comparitor the relay operates and the ramp generator ramps down through zero to a preset value in the opposite polarity and sits on this value until the strain reaches its other preset value.

The second comparitor operates immediately and reverses the ramp generator. The programme then repeats the cycle.

Charts (3.5) and (3.6) provide graphs of equivalent voltages for the strain limits in tension and compression and for the loads at tensile and compressive hold periods. The control system (strain or load) is shown schematically in Figure (3.7).

4 - STRAINRANGE PARTITIONING BEHAVIOUR OF MARM002 OVER THE TEMPERATURE RANGE 750 - 1040°C

This section investigates the high temperature, strain cycling fatigue resistance of MARM002 (CAST MARM246 + Hf) an alloy proposed for turbine discs and blades in gas turbine engines. Experience with gas turbine engine components has indicated that low cycle fatigue is often the life limiting factor. Strainrange Partitioning, an advanced life prediction analysis procedure, was used then to quantify the low cycle fatigue behaviour of MARM002. Axially strain controlled tests of each of the four generic types were performed at two temperatures 850°C and 1040°C. These results were then used to predict specimen life at other temperatures 750°C and 950°C.

Before the fatigue tests at high temperature, standard tensile tests were conducted to document the more conventional mechanical properties of MARM002.

4.1 - STATIC PROPERTIES OF MARM002

The alloy investigated in this programme was the cast nickel superalloy, MARM002. The chemical composition of MARM002 is given in Table (4.I) along with the composition of the other superalloys mentioned in this chapter.

The alloy was cast for the Department of Materials of Cranfield Institute of Technology by the National Gas Turbine Establishment and arrived in the form of cast test bars as shown in Figure (4.1 a). They were subsequently machined to shape Figure (4.1 b) then heat treated for 16 hrs at 870°C, furnace cooled and finally ground before testing.

Views of the cast structure and of the microstructure of the test bars after the heat treatment are shown in Figures (4.2) and (4.3) respectively.

Tensile properties including the ultimate tensile strength, yield strength (0.2% offset), per cent reduction of area and final elongation were obtained for at least two strainrates.

Plots of strength and ductility versus temperature are provided in Figure (4.4). Plots of strength and ductility versus strain rate, at 850°C and 1040°C are shown in Figure (4.5). Figure (4.6) provides a plot of the static Young Modulus versus temperature.

Table 4.II presents the tensile properties of MARM002. Creep tests were performed at 850°C and 1040°C at stress levels similar to those used on the basic high temperature low cycle fatigue tests. The 850°C and 1040°C stress rupture data is plotted in Figure (4.7) and Table (4.III) presents these data plus additional results at intermediate temperatures.

The tensile properties of MARM002 confirm the expected increase in ductility and decrease in strength as the temperature rises. Strain rate has a marked influence on these properties specially at the higher temperatures. An increase of 70% on ultimate tensile strength and a decrease of 70% in reduction of area was found when the strain rate was increased 30 times at 1040^{o}C. When compared with other cast superalloys, MARM002 was among the stronger and more creep resistant alloys. Within the Nimo cast series its stress rupture properties were matched only by the alloy PD21 which, however, presented lower tensile ductilities than MARM002 (4% reduction of area at 1000^{o}C).

4.2 - DETERMINATION OF THE FOUR BASIC STRAINRANGE VERSUS LIFE CURVES AT 850^{o}C AND 1040^{o}C

The four basic failure lines were obtained from data collected from thirty tests performed at two temperatures - 850^{o}C and 1040^{o}C. Experimental lines corresponding to the non partitioned strains were determined as follows:

(i) PP Tests
High frequency, completed reversed strain controlled fatigue tests using a triangular wave form.

(ii) CP Tests
Tensile load hold tests in which a hold period of about half a minute was applied. They were strain controlled fatigue tests using a trapesoidal stress versus time wave form with superimposed limit strains.

(iii) PC Tests
As for the CP tests except the load hold which was introduced in compression.

(iv) CC Tests
Same as PC and CP with load holds in both strain directions.

These cycles are illustrated in Figure (4.8) which also depicts schematically the corresponding stress-strain loops. The specimens were cycled until 50% drop in tensile load was observed or until the separation of the two parts of the specimen, if happened first than that offset. Strain-time and stress-time graphs were obtained using an U V recorder at cyclic intervals throughout the life of the specimens. The total number of cycles Nf to complete the specimen failure, as defined above were recorded.

Before running the basic tests, the minimum frequency required to exclude creep strain was calculated by conducting one test at each temperature at progressively higher frequencies until

a plateau in stress-strain response was reached as shown in Figures (4.9) and (4.10). All PP tests were then conducted at the minimum frequencies leading to such plateau, ie 0.6 Hz at 850°C and 1 Hz at 1040°C. For these frequencies MARM002 cyclically hardened over the temperature range 700 - 1040°C. From stabilized PP loops were used to determine the cyclic curves at the two baseline temperatures 850°C and 1040°C and 750°C. These cyclic curves are compared with the static ones which were obtained plotting the tensile data out of the first cycle of each PP test, in Figures (4.11, 4.12) and (4.13). The fitting of a power function of the form:

$$\frac{\Delta\sigma}{2} = k'\left(\frac{\Delta\varepsilon p}{2}\right)^{n'} \qquad (4.1)$$

where $\Delta\sigma$ - stress range
$\Delta\varepsilon_p$ - plastic strain range

to the cyclic stress-strain curves resulted in values for k' and the cyclic exponent n' which are reported in Table (4.IV). The relationship (4.1) is presented in log-log scales in Figure (4.14) for the three temperatures above mentioned.

The strainrange partitioning method concerns itself with the non elastic behaviour. Nevertheless all engineering information which may facilitate the analysis of material response to complex cycles must be considered. That is the case for the total strain versus life relationships at 800°C and 1040°C. Cyclic lives as a function of the total strainrange of the four basic cycles employed on the SrP approach, are presented in Figure (4.15) and (4.16). In general increases in temperature result in decreases in life at the same total strain amplitude a direct consequence of the 53% decrease in yield strength between 850°C and 1040°C as shown in Table (4.II).

Figure (4.17) shows the four partitioned strainranges versus life relationships for 850°C and Figure (4.18) depicts the same relationships at 1040°C. Test conditions and results of all basic low cycle fatigue tests are presented in Table (4.V). According to linear regression analysis made for each group of data, the equations representing the basic strainrange partitioning are:

(1) 850°C

$$\begin{aligned} \Delta\varepsilon_{pp} &= 0.26\ N^{-0.94} \\ \Delta\varepsilon_{pc} &= 0.24\ N^{-1.05} \\ \Delta\varepsilon_{cp} &= 0.015\ N^{-0.38} \\ \Delta\varepsilon_{cc} &= 0.073\ N^{-0.66} \end{aligned} \qquad (4.2)$$

(ii) $1040^{o}C$

$$\Delta\varepsilon_{pp} = 0.042\ N^{-0.55}$$
$$\Delta\varepsilon_{pc} = 0.050\ N^{-0.58}$$
$$\Delta\varepsilon_{cp} = 0.021\ N^{-0.46} \qquad (4.3)$$
$$\Delta\varepsilon_{cc} = 0.018\ N^{-0.34}$$

Taking the results of Figures (4.17) and (4.18) which presented the strainrange partitioned data grouped isothermally two salient features emerged.

(i) In the $850^{o}C$ plots, the PC tests failed before any others at a given inelastic strainrange and the position of the CP line has a shallower slope and is placed far to the right (higher lives) of the others.

(ii) In the $1040^{o}C$ plots, all the types of tests showed similar N_{jj} - $\Delta\varepsilon_{jj}$ relationships except for the CC line which displayed slightly higher lives for the same inelastic strains. Nevertheless, one line could represent sufficiently well all the $1040^{o}C$ data. A correlation factor $r = 0.84$ was found for the best fitting equation:

$$\Delta\varepsilon = 0.030\ N^{-0.48} \qquad (4.4)$$

and all the $1040^{o}C$ as shown in Figure (4.19). Before going into a detailed analysis and discussion of these tests, important aspects brought up by the creep-fatigue tests independently of the type of cycle, ought to be discussed.

4.3 - INELASTIC STRAIN IN THE CREEP-FATIGUE TESTS

For a life prediction method which uses the inelastic strain as the relevant variable to relate to fracture, lives cannot be predicted accurately for strains of the order or smaller than the strain resolution. The accuracy of the measurement of strains with the best available equipment is not better than 10^{-4} therefore, lives involved in any prediction are limited by the value $N = N(\Delta\varepsilon = 10^{-4})$. Table (4.VI) includes this life for several alloys to which the method of Strainrange Partitioning has been applied to predict lives at high temperatures. In column 6 of this table the smallest of the low cycle fatigue lives (PP, PC, CP, CC) for an inelastic strain range of 10^{-4} is reported.

Considering a design life of 25000 cycles only the first three alloys in table (4.VI) and MARM002 at 1040°C, are well within the limit of strain resolution for that design life. Any life prediction method using inelastic strain to relate to fracture and intended to be applied for the other alloys in table (4.VI) ought to rely on extrapolated results. In this case uncertainties of strain calculation or measurements could result in unacceptable errors in life.

A concept which can bring some difficulties on Strainrange Partitioning applications, is concerned with the definition of the variables on which the concept of damage is based. Those variables are the time independent strain or plasticity and the time dependent strain or creep. There are problems in separating the two, specially in situations where there is a great percentage of transient creep and (or) anelastic creep. In this case should the transient creep be considered as plasticity or creep, the calculated lives could be rather different depending upon the choice made. Manson et al (100) studying a stainless steel at 700°C arrived at the conclusion that the most appropriate assumption that is the assumption leading to the best predictions was to consider the time dependent strain as being the sum of the steady state creep plus 10% of the transient creep. However, it was recognized as well, that this percentage cannot be generalized for other materials and test conditions. In the absence of any other information about the damage mechanisms of those forms of creep, it will be safe to consider them as being part of the most damageable part of the inelastic strain ie., creep.

In order to interpret the MARM002 results at both temperatures the concepts of low and high cycle fatigue have to be clarified. The knowledge a priori of the area in which a certain alloy is going to operate would help in determining the best methods of testing that alloy. It is known the importance of the maximum tensile and mean stresses as the variables to relate to life in the high cycle fatigue regime. Here, the great majority of test data is load controlled. On the other hand, the inelastic strain has received much attention as the variable to relate to fracture on the low cycle fatigue field. The Manson-Coffin failure law has been considered as an appropriate one to describe the low cycle fatigue behaviour of a material where creep effects are unlikely either because the temperature is low or the frequency is high enough. Generally the characterization of this behaviour is obtained through data from strain controlled tests requiring somewhat more sophisticated and hence more expensive equipment. Failure by low cycle fatigue has been commonly considered to occur for lives less than 10^4 or 10^5 cycles. For lives of this order of magnitude, significant plastic strain can occur for metals which are sufficiently ductile at the temperature of testing. Particularly with the development of the high strength low ductile superalloys it was apparent that a more rational definition for the two fatigue fields was

necessary. For these alloys sometimes plasticity can be neglected for a few thousand of cycles. The concept of transition fatigue life (life where plastic strain $\Delta\varepsilon_p$ equals the elastic component $\Delta\varepsilon_e$) has been helpful in distinguishing between the two regimes. It has been considered that if N_d is the design life and N_t the transition fatigue life, low cycle fatigue test techniques are required if $N_d << N_t$ while if $N_d >> N_t$ high cycle fatigue information will be more meaningful.

Another type of information which might help to determine the fatigue regime is the importance of initiation and propagation for a given set of working conditions. It is known that the gross plastic strains present on the low cycle regimes induce early nucleation of cracks. The ratio of the initiation over the propagation periods $\frac{No}{Np}$ becomes smaller as the load amplitude is raised so that in the extreme low cycle range of fatigue the entire life is spent in crack propagation.

The relative importance of initiation and propagation period will be reported for MARM002 in chapter 7 of this thesis.

4.4 - DISCUSSION AND INTERPRETATION OF THE STRAINRANGE PARTITIONING DATA FOR MARM002 AND OTHER ALLOYS

From Table (4.VI.) some interesting correlations can be made.

4.4.1 - Regime Versus Transition Fatigue Life

The first and perhaps the more important information for the listed high temperature alloys is related to the fatigue regime operating at a given life. In column 5 of Table (4.VI) presents together with the transition fatigue lives, the lives N_{t10} corresponding to PP loops where the elastic strain is ten times the plastic strain. If for comparing purposes, it is considered that any stress-strain conditions leading to lives greater than N_{t10} put the tested alloy in what is called a high cycle fatigue regime, at a design life of 20,000 cycles only the stainles steels will still be well within a low cycle fatigue regime ie., the plastic strain will be still measurable. There are three alloys, CA101, IN738LC and MARM002 at 850°C which will show plastic strains so small for that design life that a high cycle regime with elastic effects predominating over the plastic ones will be more likely for these alloys. In between there are alloys like MARM002 at 1040°C where a transition regime may be anticipated.

4.4.2 - Tensile Properties versus Transition Fatigue Life

This correlation could be anticipated through the meaning of the constants entering the definition of N_t.

By definition

$$\Delta\varepsilon_e = A' N^{-\beta'}$$

$$\Delta\varepsilon_p = A\ N^{-\beta}$$

A, A', β,β' - material constants

Therefore: $$N_t = \left(\frac{A'}{A}\right)^{1/\beta'-\beta}$$

Since A is a measure of strength, A' a measure of ductility and $\frac{1}{\beta'-\beta}$ is negative, increasing strength and decreasing ductility lower the transition fatigue life. The situation for MARM002 is pictured in Figure (4.20) where the lives have been normalized relatively to the transition fatigue life at each temperature. Here the rather lower strength and higher ductility of this alloy at 1040°C influenced strongly the value of N_{t10} = 3500 cycles which is considerably superior to that found at 850°C (N_{t10} = 518 cycles). Test lives have not exceeded 2000 cycles at 800°C and 5000 cycles at 1040°C. The exception was test no 19 with a life of almost 10,000 cycles but there the strain resolution was largely exceeded, therefore, the point was ignored when drawing the PP line. For a PP life of 2000 cycles the ratio elastic/plastic strains were 24 at 850°C while for a PP life of 5000 cycles at 1040°C that is 8. These two numbers suggested stronger elastic effects at the lower temperatures. These elastic effects are again apparent when the position of the strainrange vs life relationships are discussed next for MARM002 and other alloys.

4.4.3 - The Order of Decreasing Damage - Fatigue Regime - Crack Path Correlations

A difficult problem facing the high temperature fatigue designer is how to deal with extended hold periods. Degradation in fatigue under such circumstances can be quite severe as many investigations have shown (92,26,28). The introduction of creep specially in tension produced a higher crack growth rate generally associated with an intergranular crack and (or) evidence of degradation of fatigue properties with increasing dwell times due to increased localized oxidation.

The importance of this oxidation on crack growth is discussed in Reference (31) taking as main variables the crack path, strainrange,frequency and temperature. The deleterious effect of frequency and hold time on the austenitic steels fatigue behaviour was shown by the fact that the PP line constituted the upper bound among the strainrange vs life relationships being one of the cycles involving creep, normally the CP, the lower life bound.

This order of increasing damage with the amount of creep within a creep-fatigue loop is changed for some low ductility high strength alloys. They present very low transition fatigue lives with very low inelastic strainranges for lives around 10,000 cycles which can be considered as a lower bound of design lives of the high temperature components of gas turbines. The main consequence for the position of the $Nij - \Delta\varepsilon ij$ relationships is that the PP line does not constitute anymore the upper bound among the four strain life relationships. Normally cycles with lower tensile stresses like the CP or CC took its place.

The PC line constitutes for these alloys the lower bound as shown in column 7 of Table (4.VI). This fact has been associated with the fact that the PC cycles in these alloys shifted the loops to tension, high tensile mean stress being developed in these cycles. MARM002 was no exception in this class of alloys particularly when working at the lower temperatures and the order of the $Nij - \Delta\varepsilon ij$ lines reflect that, as shown in Figure (4.16).

4.5 - THE VALIDATION TESTS AT 750°C AND 950°C

One of the most important claims for Strainrange Partitioning method lay in the insensitivity of its strainrange vs life relationships to temperature. In fact for some materials working at certain temperature ranges (45,46) a unique set of strainrange vs life relationships could be employed without appreciable loss in life prediction ability of the method. In other cases, however, when those temperature ranges were extended completely different strainrange vs life relationships were obtained at different temperatures (36,111). To check on the extrapolative ability of the method as far as temperature is concerned, some tests were performed at an intermediate temperature - 950°C - and at a lower temperature 750°C. From the very beginning and due to the relative position of the basic strainrange vs life relationships at both temperatures it was apparent that the basic data at 850°C could not be used successfully to predict the results at 1040°C. Ratios of predicted

over observed lives as high as five were found when the basic 850°C data were used to predict the 1040°C results as shown in Figure (4.21). However, it was found that the 750°C results could be predicted within a factor ± 2 by the basic data developed at 850°C and the 950°C results could be predicted with similar accuracy from the 1040°C basic SrP data as shown in Figure (4.22). These results divided automatically the temperature range into two intervals (750 - 850°C) and (950 - 1040°C) where SrP could be applicable safely providing the adequate set of strainrange vs life relationships were applied. This confirmed the previous idea of different regimes operating at the two basic temperatures 8500C and 1040°C.

A final point was checked and this one was related to the type of crack path over the range of temperatures and test conditions used in this study. Detailed metallographic studies were made of the fracture surfaces. Longitudinal sections made on fractured specimens showed no evidence of intergranular (interdendritic) failure even at the higher temperatures with cycles involving creep in tension, situation which is known to be more prone to intergranular cracks and hence higher crack growth rate. Figures (4.23, 4.24, 4.25) show microphotographs of some of those longitudinal sections. It seems that even though there is a time dependent deformation going on for MARM002 the basic mechanism for this is not appreciably different than for plastic deformation. As regard the partitioning of strain cycles of MARM002 including creep in tension and (or) compression it was observed that high percentages of transient creep were present in those cycles. As shown in Figure (4.26) a CP cycle run at 1040°C shows 36% of plasticity, 64% of creep, 30% of which is transient creep.

In this cycle the steady state creep is, therefore, only 45% of the total inelastic strain. This high percentage could be put forward as the main reason for the creep damage not going into the grain boundaries. Tests reported in Table(4.VI) with dwells of 3 minutes with higher percentages of steady state creep did not however, introduce any intergranular damage. Lives of these additional data depicted in Figure (4.19) as solid symbols are well within the range of accurate predictions made by the basic strainrange vs life relationships.

Another point in connection with this is that the material oxidizes heavily at 1040°C specially during tests with long dwells. Even the severe oxidation does not decrease its life significantly. On the contrary the trend seems to be to higher lives as points representing the long dwell tests 1C and 3B, are on the right(higher lives) of the respective basic lines as shown in Figure (4.19) . Due to this strong air specimens interaction the longer lives at 1040°C for the same inelastic strain cannot be attributable to higher initiation periods.

Only different propagation periods can account for the difference in lives at the two main temperatures. The relative importance of the initiation and propagation periods at two intervals 750 - 850°C and 950 - 1040°C will be assessed in chapter 7.

4.6 - CONCLUSIONS

(i) Strainrange Partitioning measurements of MARM002 over the temperature range 750 - 1040°C have been made and the strainrange vs life relationships established at 850°C and 1040°C.

(ii) Different regimes were found to operate at the lower and higher temperatures. Higher elastic to plastic strain ratios were found on the tests at the lower temperatures. The limit of resolution of strain was attained for lives of two thousand cycles at 850°C and five thousand cycles at 1040°C. For these life levels elastic to plastic ratios were twenty four (24) at 850°C and eight (8) at 1040°C.

(iii) The order of damage of the strainrange vs life relationships for several alloys including MARM002 was explained in terms of transition fatigue life and crack path. For wrought fairly ductile alloys tensile creep damage has been induced within the grain boundaries resulting in lower lives for the cycles presenting creep in tension (CP or CC).

For the low ductility high strength alloys the transition fatigue lives were very low and in most of then including MARM002 it could not be found evidence of creep damage going into the grain boundaries. The tensile or compressive shift of the PC or CP loops was found to be for MARM002, like in other strong low ductile alloys, the main reason for the displayed order of the strainrange vs life relationships: the PC line was found to be the lower bound and the CP line the upper bound at 850°C. The effect of the maximum tensile and mean stresses at the higher temperature 1040°C, was apparently washed out in the sense that their effects on separating the basic SrP line almost disappeared at these higher temperatures.

The easier nucleation of cracks at this temperature due to environment-specimen interaction and the higher plasticity at these temperatures and hence easier relaxation of the mean stress at the crack tips can explain this effect. Only the assessment of the importance of the intiation and propagation periods at the two temperatures can confirm, however, this theory. This will be done in chapter 7.

(iv) The application of a unique set of strainrange vs life relationship to the whole range of temperatures (750 - 1040^{o}C) resulted in unacceptable errors in life prediction. Ratios as high as five of predicted over observed lives were found when 850^{o}C basic data was used to predict the 1040^{o}C results. However, Strainrange Partitioning approach led to satisfactory life predictions over limited temperature ranges. Lives within a factor of $\pm$ 2 could be predicted over the separate ranges 750^{o}C - 850^{o}C and 950^{o}C - 1040^{o}C using different sets of strainrange vs life relationships for each temperature interval.

5.- INTERPRETATION OF DAMAGE RULES EMPLOYED WITH THE STRAINRANGE PARTITIONING METHOD

5.1 - INTRODUCTION

The use of Strainrange Partitioning (92) as a method to characterize the high temperature low cycle fatigue is based upon the experimental determination of four basic rupture curves. Each curve is related to one of the possible four components of the inelastic strain and named PP, PC, CP and CC after separation of creep and plastic strains occurring in tension or (and) compression. If ε_p is the plasticity in tension and $\varepsilon p'$ the plasticity in compression in any loop characterized by its width $\Delta\varepsilon_i$, the partition of that loop for the SrP method is made using the following relations:

$$\Delta\varepsilon_{pp} = \text{minimum } (\varepsilon_p, \varepsilon_p')$$

$$\Delta\varepsilon_{cc} = \Delta\varepsilon_i - \text{maximum } (\varepsilon_p, \varepsilon_p')$$

The inelastic strain $\Delta\varepsilon_i - \Delta\varepsilon_{pp} - \Delta\varepsilon_{cc}$ will be named $\Delta\varepsilon_{pc}$ if $\varepsilon_p > \varepsilon_p'$ and $\Delta\varepsilon_{cp}$ if $\varepsilon_p < \varepsilon_p'$. Obviously if $\varepsilon_p = \varepsilon_p'$ the loop will be composed of a PP and CC component as $\Delta\varepsilon_{pc} = \Delta\varepsilon_{cp} = 0$. The method uses a number of special strain controlled tests with hold times in tension (CP tests), in compression (PC tests) in both directions (CC tests). The only line which can be drawn directly from data obtained in these tests is the PP line which is calculated on tests performed at sufficiently high frequency to prevent creep both in tension and compression. Some type of damage rule is needed to calculate the other strainrange vs life relationships since any of the experimental loops contains bits of PP strain and one or two of the other strain components. So far three damage rules have been proposed:

(A) The linear damage rule

The linear damage rule is given by:

$$\frac{1}{N_f} = \frac{1}{N_{pp}} + \frac{1}{N_{cc}} + \frac{1}{N_{cp(pc)}}$$

where N_f = cyclic life under some complex hysteresis loop.

N_{ij} = cyclic life expected for a loop of width equal to the bit $\Delta\varepsilon_{ij}$ and entirely of the type ij.

(B) The interaction damage rule

This damage rule is given by:

$$\frac{1}{N_f} = \frac{F_{pp}}{N_{pp}} + \frac{F_{cc}}{N_{cc}} + \frac{F_{cp}}{N_{cp}} \left(\frac{F_{pc}}{N_{pc}}\right)$$

Where N_f = cyclic life under a complex hysteresis loop defined by its width $\Delta\varepsilon_i$ and by its constitutive fractions
$F_{ij} = \Delta\varepsilon_{ij}/\Delta\varepsilon_i$ being $\Delta\varepsilon_{ij}$ the inelastic strain of the type ij.
N_{ij} = cyclic life of a loop of width $\Delta\varepsilon_i$ when it is 100% ij type.

(C) Alternative damage rule

$$N_f = F_{pp}N_{pp} + F_{cc}N_{cc} + F_{cp}N_{cp}(F_{pc}N_{pc})$$

where N_f, F_{ij} and N_{ij} have the same meaning as in the interaction damage rule.

The assumptions behind these damage rules will be analysed and also the implications of using each one during the two steps in which SrP technology needs a damage rule to extrapolate or interpolate lives will be discussed.

5.2 - THE CONCEPT OF DAMAGE BEHIND THE DAMAGE RULES

When the Strainrange Partitioning method was first proposed by Manson (92) the linear damage rule was used to establish the strainrange vs life relationships. It was considered there that since in a practical loop there is always a strain component of the type PP, a way to remove this component on a complex loop containing other strain components was to assume a linear life fraction rule. Moreover, the damage which was attributed to any type of strain component $\Delta\varepsilon_{ij}$ was considered to be given as N/N_{ij} when N is the life of a loop, $\Delta\varepsilon_i = \Sigma\Delta\varepsilon_{ij}$ and N_{ij} the life of a loop 100% of the type ij and width $\Delta\varepsilon_{ij}$. In a cycle with the purpose of drawing the CP line, the linear fraction damage rule assumed the following aspect:

$$\frac{N}{N_{pp}} + \frac{N}{N_{cp}} = 1$$

This equation is solved to give the unknown N_{cp}. This linear damage rule was later substituted by the so called interaction damage rule which was considered to be simpler to apply (52) because working in a unique strain level - $\Delta\varepsilon_i$ - its assumption is easier to understand: in the presence of other strainrange components the life relationship for each strainrange is displaced by an amount dependent on the slope of that life relationship and the fraction F_{ij} of that other component. The great majority of reports on Strainrange Partitioning have used this rule to combine the effect of several concurrent strainranges.

The alternative damage rule was first proposed in Reference (36) where it was concluded that the alternative rule predicts longer life compared to the Interaction damage rule when both are used to interpolate the life of a loop composed of 50% of one type of strain and 50% of any other strain type. The alternative damage rule was used to provide a basis for comparison with the interaction damage rule and as a tentative substitute of it in cases where the computations using the interaction rule resulted in negative values for the predicted life. The problem of computed negative lives when using SrP was found in other reports where the observed life of the complex loop N_f was bigger than the life N_{pp} relative to a loop of the same width but completely of the PP type. It is suggested in Reference (45) that when determining a strainrange vs life line of the type ij the fraction ratio F_{ij} must be predominant against the other different strain ratios. For instance, in a cycle drawn to calculate the CP line $F_{cp} > 0.5$ in order to get meaningful results and to prevent the prediction of negative lives. As it can be seen in Figure (5.1) the condition on F_{ij} can be even more restrictive, if ratio N_{ob} over N_{pp} is sufficiently high (very small F_{pp} ratios therefore high time consuming tests).

The justification to use one of the possible damage rules can only be given if the assumptions behind each of them are clear. In order to clarify these assumptions the concept of damage D_{ij} associated with an inelastic strainrange $\Delta\varepsilon_{ij}$ is used. From the function $D_{ij} = D_{ij}(N)$ only two points are known:

$$\begin{array}{ll} N = 0 & D = 0 \\ N = N_f & D = 1 \end{array} \qquad (5.1)$$

However, with only these two points it is possible to define the average damage per cycle $\frac{\delta D}{\delta N} = \frac{1}{N_f}$. The assumption that this damage per cycle is only a function of the inelastic strain $\Delta\varepsilon_{ij}$ in a way that

$$\frac{\delta D_{ij}}{\delta N} = \frac{1}{C_{ij}} \Delta\varepsilon_{ij}^{\gamma_{ij}} \qquad \begin{matrix} i = P \text{ or } C \\ j = P \text{ or } C \end{matrix} \qquad (5.2)$$

C_{ij}, γ_{ij} - material constants

Integrating equations (5.2) taking into account (5.1)

$$\int_0^1 \delta D_{ij} = \int_0^{N_{ij}} \frac{1}{C_{ij}} \Delta\varepsilon_{ij}^{\gamma_{ij}} \qquad 1 = \frac{N_{ij}}{C_{ij}} \Delta\varepsilon_{ij}^{\gamma_{ij}}$$

and therefore $N_{ij} = C_{ij}\Delta\varepsilon_{ij}^{-\gamma_{ij}}$ which constitutes a basic assumption the strainrange partitioning method is based upon: all the four strainrange vs life relationships follow a straight line where life and inelastic strainrange are drawn in log-log scales. If a cycle has got two or three strain types $\Delta\varepsilon_{ij}$ being their summation $\Sigma\Delta\varepsilon_{ij}$ equal to the loop width $\Delta\varepsilon_j$, an arising problem is how to relate the damage per cycle within that multi strain type and the individual damages per cycle corresponding to the bits $\Delta\varepsilon_{ij}$

$$\frac{\delta D}{\delta N} = \frac{\delta D}{\delta N} \left(\frac{\delta D_{ij}}{\delta N}\right)$$

The assumption that the total damage per cycle is equal to the summation of the partial damages,

$$\frac{\delta D}{\delta N} = \Sigma \frac{\delta D_{ij}}{\delta N} \qquad (5.3)$$

leads directly to the linear damage rule

$$\frac{1}{N} = \Sigma \frac{1}{N_{ij}} \qquad (5.4)$$

In order to find the interaction damage rule a second assumption on top of (5.3) is necessary. This second assumption is:

$$\frac{\delta D}{\delta N} (\Delta\varepsilon_{ij}) = \frac{\delta D}{\delta N} (\Delta\varepsilon_{ij} = \Delta\varepsilon_j) \times \frac{\Delta\varepsilon_{ij}}{\Delta\varepsilon_j} \qquad (5.5)$$

or the damage per cycle relative to a partial strain $\Delta\varepsilon_{ij}$ is equal to the damage per cycle of a strain $\Delta\varepsilon_{ij}$ with magnitude equal to loop width $\Delta\varepsilon_j$ times the ratio $F_{ij} = \frac{\Delta\varepsilon_{ij}}{\Delta\varepsilon_j}$.

In terms of lives (5.5) can be written

$$\frac{1}{N_{ij}(\Delta\varepsilon_{ij})} = \frac{1}{N_{ij}(\Delta\varepsilon_{ij})} \times \frac{\Delta\varepsilon_{ii}}{\Delta\varepsilon_i} \tag{5.6}$$

Substituting on the linear damage rule expression or which is the same thing, considering that assumption (5.3) is valid here as well as (5.4) it can be written

$$\frac{1}{N} = \Sigma \frac{1}{N_{ij}(\Delta\varepsilon_i)} \times \frac{\Delta\varepsilon_{ii}}{\Delta\varepsilon_i} = \Sigma \frac{F_{ii}}{N_{ij}(\Delta\varepsilon_i)}$$

which constitutes the interaction damage rule.

In the same way it can be shown that the assumptions behind the alternative damage rule are:

$$\left(\frac{\delta D}{\delta N}\right)^{-1} = \left(\Sigma \frac{\delta D}{\delta N}_{ij}\right)^{-1} \tag{5.7}$$

and

$$\left[\frac{\delta D}{\delta N}\ (\Delta\varepsilon_{ij})\right]^{-1} = \left[\frac{\delta D}{\delta N}\ (\Delta\varepsilon_i)\right]^{-1} \times F_{ij} \tag{5.8}$$

leading to $N = \Sigma F_{ij} N_{ij}(\Delta\varepsilon_i)$

ie., the alternative damage rule.

The physical meaning of these damage rules can, at this stage, be compared through their implicit assumptions. Starting with the alternative damage rule through its assumptions (5.7) and (5.8) it can be shown that each one of these equations lead to unacceptable consequences if eventually the combination of the two assumptions may lead to a plausible result.

In fact following assumption (5.7), the addition of a component $\Delta\varepsilon_{ij}$ to an already existent $\Delta\varepsilon_{pp}$ can only add to the specimen or component life. In terms of lives (5.7) can be written

$$N = \Sigma N_{ij}(\Delta\varepsilon_{ij}) \qquad \text{which is not true}$$

In the same way condition (5.8) means in terms of lives

$$N(\Delta\varepsilon_{ij}) = N(\Delta\varepsilon_i) \times F_{ij} \tag{5.9}$$

Equation (5.9) means that for a ratio $F_{ij} = 0$ the corresponding life N_{ij} equals zero, when theoretically it should be infinite. Summing up the alternative damage rule is based on two unacceptable assumptions, perhaps the two compensating each other to give plausible but certainly meaningless results.

Two other relations are involved in the two other damage rules:

(i) Assumption (5.3) for the linear damage rule

(ii) Assumption (5.3) plus (5.5) for the interaction damage rule.

In considering assumption (5.5) first it can be shown that its degree of accuracy depends on the material constant γ_{ij} (equation (5.2)) which is the slope of the strainrange $\Delta\varepsilon_{ij}$ vs life N_{ij} line when plotted in log-log scales.

In fact, starting from the set of equations $N_{ij} = C_{ij}\Delta\varepsilon_{ij}^{-\gamma_{ij}}$ it can be written:

$$\frac{N_{ij}(\Delta\varepsilon_i)}{N_{ij}(\Delta\varepsilon_{ij})} = \frac{C_{ij}(\Delta\varepsilon_i)^{-\gamma_{ij}}}{C_{ij}(\Delta\varepsilon_{ij})^{-\gamma_{ij}}} = \frac{C_{ij}(\Delta\varepsilon_i)^{-\gamma_{ij}}}{C_{ij}(\Delta\varepsilon_i F_{ij})^{-\gamma_{ij}}} = F_{ij}^{\gamma_{ij}} \qquad (5.10)$$

Therefore, only if γ_{ij} approaches 1 assumption (5.6) is about right. It was reported in Reference (112) that a value for $\gamma_{ij} = 1.67$ can better represent the average trend of the available data. Therefore, it appears that the relation (5.5) could be advantageously changed to

$$\frac{\delta D}{\delta N}(\Delta\varepsilon_{ij}) = \frac{\delta D}{\delta N}(\Delta\varepsilon_i) \times \left(\frac{\Delta\varepsilon_{ij}}{\Delta\varepsilon_i}\right)^{1.67} \qquad (5.5')$$

The 'modified interaction damage rule' would be:

$$\frac{1}{N} = \Sigma\frac{F_{ij}^{1.67}}{N_{ij}} \qquad (5.11)$$

The comparison of these two interaction damage rules for CP data at 850°C of a nickel superalloy - MAR1002 (Section 1) shows that the difference between computed lives can be important particularly at low strain levels. The CP line is described by the equation $N_{cp} = 2.69\ \Delta\varepsilon_{cp}^{-2.64}$(%) when the standard interaction damage rule

was applied to the non partitioned data. If equation (5.11) is applied to the same data the CP line will come out as:

$$N_{cp} = 2.69\Delta\epsilon_{cp(\%)}^{-2.44}$$

CP lives for inelastic strains around 0.02% (resolution limit) and when computed according to the damage rules discussed above, differ by a factor of 2.2. This factor decreases as inelastic strain increases, being 1 for a CP loop width of 1%.

However, the first assumption for both linear damage rule and interaction damage rule is assumption (5.3). It leads directly to the linear damage rule or jointly with the assumption stating that the ratio between the damages for cycle of a loop of width $\Delta\epsilon_{ij}$ and a loop of width$\Delta\epsilon_i$ is equal to the ratio of strains $F_{ij} = \Delta\epsilon_{ij}/\Delta\epsilon_i$ to the interaction damage rule. The linear damage rule was first proposed by Palmgren and later again by Miner to deal with cases where the structure of component were operating under a spectrum of loading. It assumes that during any stage of the loading history of the material, a stress range is applied for n_i cycles at a condition where failure would occur if N_i cycles were applied, the percentage of life used-up is n_i/N_i. Moreover the summation of the ratios $\frac{n_i}{N_i}$ equals one. This linear law often results in erroneous predictions of fatigue life. It is well known that the order of stressing or straining is going to affect the value for the sum of ratios $\frac{n_i}{N_j}$. Thus summation tends to be greater than one of a lower level of stress (strain) is applied first, or a value smaller than one if the higher level is applied first.

The application of linear damage rule to the Strainrange Partitioning method involves damages $D_{ij} = \frac{n_{ij}}{N_{ij}}$ associated to each strain $\Delta\epsilon_{ij}$. The summation $\Sigma\frac{N}{N_{ij}}$ at N_{ij} fracture will equal a value which in the linear damage rule is considered to be one. In general $\Sigma\frac{N}{N_{ij}} = \alpha(F_{ij})$ which is equivalent to saying that the damage summation as defined above will depend upon not only the type of strains combined in a loop but also their relative magnitudes. In fact, there is no reason why different combinations of different strain types will not induce different damage summation at fracture. Although for practical purposes damage has been associated with life ratio, the empirical concept involves mainly physical damage in the form of cracks or discontinuities caused by each strain type. Unfortunately damage involves more than crack length but also residual stresses near the propagating crack(s), metallurgical changes, presence of other cracks and their degree of coalescence, surface oxidation, etc.

5.3 - DAMAGE RULES OF THE TYPE $\Sigma N/N_{ij} = \alpha$

As it was suggested before, the value α or $\Sigma\frac{N}{N_{ij}}$ can not only be different from one but can vary according to the ratios $F_{ij} = \frac{\Delta\varepsilon ij}{\Delta\varepsilon i}$. For example, take the hypothetical case in which one wants to know the damage function applicable to two strains of the same type. In other words, the problem is to know which damage rule is best to combine the effects of two strains $\Delta\varepsilon_1$ and $\Delta\varepsilon_2$, knowing that the corresponding strainrange vs life relationships $N_1 = N_1(\Delta\varepsilon 1)$ and $N_2 = N2(\Delta\varepsilon 2)$ are coincident. In SrP terms the problem can be solved for any of the $N_{ij} = N_{ij}(\Delta\varepsilon_{ij})$ relationships. Taking the PP line, for example, the question is how to combine two PP inelastic strains $\Delta\varepsilon_{pp1}$ and $\Delta\varepsilon_{pp2}$ inside a loop of width $\Delta\varepsilon_{pp}$. To calculate the damage function the only assumption to be used, will be that for any $\Delta\varepsilon_{pp}$, a corresponding life N_{pp} will be obtained using a Manson-Coffin type of equation $\Delta\varepsilon_{pp} = A\, N_{pp}^{-\beta}$. Both partials $\Delta\varepsilon_{pp1}$ and $\Delta\varepsilon_{pp2}$ will fall in the same line defined by the equation above. As the three strains must follow the line above it can be written:

$$N_{pp1}^{-1} = \left(\frac{1}{A}\right)^{1/\beta}(\Delta\varepsilon_{pp1})^{1/\beta} \tag{5.12}$$

$$N_{pp2}^{-1} = \left(\frac{1}{A}\right)^{1/\beta}(\Delta\varepsilon_{pp2})^{1/\beta} \tag{5.13}$$

Summing (5.12) and (5.13)

$$N_{pp1}^{-1} + N_{pp2}^{-1} = \left(\frac{1}{A}\right)^{1/\beta}(\Delta\varepsilon_{pp})^{1/\beta}\left[\left(\frac{\Delta\varepsilon_{pp1}}{\Delta\varepsilon_{pp}}\right)^{1/\beta} + \left(\frac{\Delta\varepsilon_{pp2}}{\Delta\varepsilon_{pp}}\right)^{1/\beta}\right]$$

$$= N_{pp}^{-1}\left[(F_{pp1})^{1/\beta} + (1 - F_{pp1})^{1/\beta}\right]$$

being $F_{pp_1} = \frac{\Delta\varepsilon_{pp1}}{\Delta\varepsilon_{pp}}$ $\qquad F_{pp2} = 1 - F_{pp1} = \frac{\Delta\varepsilon_{pp2}}{\Delta\varepsilon_{pp}}$

Putting $\alpha = (F_{pp1})^{1/\beta} + (1 - F_{pp1})^{1/\beta}$ (5.14)

it can be written $$N_{pp1}^{-1} + N_{pp2}^{-1} = \alpha\, N_{pp}^{-1} \tag{5.15}$$

where α is a function of strain ratio F_{pp1} and the slope β.

For a certain β, α reaches a minimum for $F_{pp1} = F_{pp2} = 0.5$. In fact differentiating (5.14) with respect to F_{pp1}.

$$\frac{d\alpha}{pp1} = 1/\beta(F_{pp1})^{1/\beta-1} - 1/\beta(1 - F_{pp1})^{1/\beta-1}$$

$$\frac{d\alpha}{pp1} = 0 \text{ for } F_{pp1} = 1 - F_{pp1} \qquad F_{pp1} = 1/2$$

For this case of equal partial strains $F_{pp1} = 1 - F_{pp1} = 1/2$

$$\alpha = (1/2)^{1/\beta} + (1/2)^{1/\beta} \qquad \alpha = 2^{\frac{\beta-1}{\beta}} \tag{5.16}$$

From the expression giving α in function the slope β and strain ratio F_{pp1} it can be seen $\alpha \leq 1$ for any value of the strain ratios and $\beta \leq 1$.

Moreover α reaches a minimum $\alpha = 2^{\frac{\beta-1}{\beta}}$ when $F_{pp1} = F_{pp2} = 0.5$.

Figures 5.2 and 5.3 visualize these two functions $\alpha = \alpha\ (F_{pp})$ β = constant and $\alpha = \alpha(\beta)$, F_{pp} = ct . In Figure 5.2 it can be seen that the lower the slope of the strainrange vs life line, the shorter will be α or the lower β the greater will be the deviation relative to the linear damage rule. This rule will be obeyed for any strainrange only when the slope β approaches unity. Figure 5.3 visualizes the way the coefficient α varies with the slope for three values of F_{pp1} = 0.1, 0.3, 0.5. The coefficient α is highly dependent on the slope β when $F_{pp} = 0.5$.

The graphic construction of the damage rule for a slope $\beta = 0.6$ is shown in Figure 5.4. Equation (5.14) was used to determine α and hence the damage rule which equation (5.15) represents. Any values of F_{pp1} and F_{pp2} compatible with $F_{pp1} + F_{pp2} = 1$ can be chosen by selecting any point of the straight line shown in area A. The functions $(F_{pp1})^{1/\beta}$ and $(F_{pp2})^{1/\beta}$ are shown in areas B_1 and B_2 for a slope of $\beta = 0.6$. Finally in area C these values are added to determine the value α. Values of α for slopes of 0.9 and 1 are shown as well in Figure 5.4.

The calculations were done for a PP loop but can be repeated for any line providing its slope is known. Let us consider the CP line as the upper bound with the shallowest slope of all basic SrP lines as shown in Figure 5.5.

In this CP line any partial strains $\Delta\varepsilon_{cp1}$ and $\Delta\varepsilon_{cp2}$ will induce damages $\frac{N}{N_{cp1}}$ and $\frac{N}{N_{cp2}}$ which determine a point of the damage

rule function represented schematically in Figure 5.6 by the lower bound. The same function can be determined for each basic SrP line assuming as all SrPcalculations do, that each generic type follows a Manson-Coffin type of strainrange vs life relationship.

In any loop composed of an inelastic strain of a generic type ij_1 and other type ij_2 there are damages per cycle $\frac{\delta Dij1}{\delta N}$ and $\frac{\delta Dij2}{\delta N}$ which can be associated with each strain.

$$\Delta\varepsilon_{ij_1} + \Delta\varepsilon_{ij_2} \rightarrow \left(\frac{\delta D_{ij1}}{\delta N}\right) + \left(\frac{\delta D_{ij2}}{\delta N}\right)$$

If the two considered partitioned strains ij1 and ij2 are of the same type (say PP or CP) the damages per cycle $\frac{\delta D}{\delta N}$ are given as:

$$\Delta\varepsilon_{pp1} + \Delta\varepsilon_{pp2} \rightarrow \frac{\delta D_{pp1}}{\delta N} + \frac{\delta D_{pp2}}{\delta N} = \alpha_{pp}\frac{\delta D_{pp}}{\delta N} \qquad (5.17)$$

or
$$\Delta\varepsilon_{cp1} + \Delta\varepsilon_{cp2} \rightarrow \frac{\delta D_{cp1}}{\delta N} + \frac{\delta D_{cp2}}{\delta N} = \alpha_{cp}\frac{\delta D_{cp}}{\delta N} \qquad (5.18)$$

However, if they are of different kind, say PP + CP, the ratio between

$$\Sigma\frac{\delta D_{ij}}{\delta N}\left(\frac{\delta D_{pp1}}{\delta N} + \frac{\delta D_{cp}}{\delta N}\right) \text{ and } \frac{\delta D}{\delta N}, \text{ eg } \alpha(pp + cp) \text{ is unknown.}$$

However, some lower and upper bound can be imposed on α. Taking the hypothetical case still of a PP + CP loop where CP strains produce the lower lives it can be said that

$$\frac{\delta D_{pp}}{\delta N} < \frac{\delta D}{\delta N} < \frac{\delta D_{cp}}{\delta N}$$

or the damage per cycle of a mixed loop PP + CP will be between the damage per cycle $\frac{\delta D_{pp}}{\delta N}$ of a loop completely PP and the damage per cycle $\frac{\delta D_{cp}}{\delta N}$ of a loop completely CP. Moreover, if the non partitioned data (say 0.5PP + 0.5CP) falls in a Manson-Coffin type of equation, α(PP + CP) is going to be between α_{pp} and α_{cp}.

In fact from equations 5.3 and 5.16

$$\alpha_{pp} = \frac{\sum_{k=1}^{2} \frac{\delta D_{pp}}{\delta N} K}{\frac{\delta D_{pp}}{N}} = 2 \frac{\beta_{pp} - 1}{\beta_{pp}} \qquad (5.19)$$

$$\alpha_{cp} = \frac{\sum_{k=1}^{2} \frac{\delta D_{cp}}{\delta N} K}{\frac{\delta D_{cp}}{\delta N}} = 2 \frac{\beta_{cp} - 1}{\beta_{cp}} \qquad (5.20)$$

$$\alpha = \frac{\frac{\delta D_{pp1}}{\delta N} + \frac{\delta D_{cp2}}{\delta}}{\frac{\delta D}{\delta N}} = 2 \frac{\beta - 1}{\beta} \qquad (5.21)$$

Being β_{pp}, β_{cp} and β the slopes in log-log scales of the PP data, CP data and PP + CP data (50%-50%) respectively and assuming that $\beta_{pp} < \beta < \beta_{cp}$ hence $\alpha_{pp} < \alpha < \alpha_{cp}$. (5.22)

5.4 - THE USE OF A DAMAGE RULE OF THE TYPE $\Sigma \frac{N}{N_{ij}} = \alpha$ IN SrP TECHNOLOGY

In Strainrange Partitioning technology two cases ought to be distinguished when damage rules have to be applied:

(A) Extrapolation case

(B) Interpolation case

(A) The damage rule is used to extrapolate lives during the determination of the generic SrP curves. First to be determined is the PP line which does not need any extrapolation because it is possible to simulate in laboratory, 100% PP loops. Generally the second line to be determined is the PC or CP one. The loops which are used to determine experimentally these curves contain some percentage of a PP component. To take that into account some damage rule ought to be applied to extrapolate to a 100% PC or CP life.

Contrary to those damage rules which were developed on the previous subsections, here one has to combine damages produced by different strains.

In a hypothetical PP + CP loop, taking into account relations (5.22) two cases might happen:

(i) The slope $\beta_{cp} < \beta_{pp}$ where β_{cp} and β_{pp} are the slopes of the strainranges versus life relationships.

As shown in Figure (5.6) the exact slope of the CP line is not known but the trend, ie., whether it is a steeper or shallower slope can be assessed by the non partitioned data (PP + CP).

In this case the damage rule relative to PP strains should be applied because it constitutes a safer bound (shorter extrapolated lives) as is apparent in Figure 5.7. If $\beta_{pp} < 1$ the application of the linear damage rule would lead to too pessimistic results (N_{cp3}).

(ii) $\beta_{cp} > \beta_{pp}$
It is the case shown schematically in Figure 5.8. In this case the CP line slope will determine a safe bound for damage rule application. The linear damage rule can be safely applied providing β_{cp} has not a slope bigger than 1.

(B) Interpolation Case

The optimum damage rule to apply will depend upon the ratios F_{ij}. Ideally the damage rules corresponding to different F_{ij} should be known as shown schematically in Figure 5.9.

In the absence of this experimental information the damage corresponding to the shallower slope should be used since it leads to the safer (shorter) lives in these interpolative cases.

In fact, in an hypothetical case where one has to predict a life of a PP + CP loop the life N will be calculated according to:

$$\frac{\alpha}{N} = \frac{1}{N_{pp}} + \frac{1}{N_{cp}} = K \qquad N = \frac{\alpha}{K}$$

As α decreases with shallower slopes as shown in Figure 5.4, the point made above it is proved, ie., it is preferable to use rule with smallest α for safest prediction. Finally it must be said that in calculating the $\Delta\varepsilon_{ij}$ - N_{ij} relationships for MARM002 (see Chapter 4) case A(i) was applicable. The PP slope was approximately 1 hence the application of the linear damage rule would be about right. The use of the interaction damage rule gives slightly different extrapolated lives as shown in Figure 5.10, where it is shown the extrapolated CP lines using several of the damage rules mentioned in this discussion.

The use of the modified interaction damage rule has already been discussed in comparison with the interaction damage rule. In any case the relative position of the $\Delta\varepsilon_{ij} - N_{ij}$ relationships was not altered.

5.5 CONCLUSIONS

Three damage rules which have been used with the Strainrange Partitioning method were discussed and the concept behind them analysed. Tha analysis of the assumptions behind those rules allowed some conclusions to be drawn about their physical significance. The so called alternative damage rule was found to be based upon assumptions which were found unacceptable according to that analysis. The linear damage rule was based upon the assumption that the damage per cycle of a loop of width $\Delta\varepsilon_i$ composed of two or three partial strains $\Delta\varepsilon_{ij}$ (as defined on the SrP method) is equal to the summation of the partial damages relative to those strains. This assumption and another one considering that the damage per cycle of a strain $\Delta\varepsilon_{ij}$ is directly proportional to the relative magnitude of this strain inside the width loop $\Delta\varepsilon_i$, lead directly to the so called interaction damage rule. Considering that any SrP data of the same type follow a Manson-Coffin type of equation it was possible to conclude that:

(1) The interaction damage rule should be modified in order to take into account the average trend of the available SrP data. The modified interaction damage rule will be of the form

$$\frac{1}{N} = \Sigma \frac{F_{ij}}{N_{ij}}^{\gamma_{ij}}$$ where γ_{ij} is the inverse of the slope

of the strainrange vs life relationships $N_{ij} = N_{ij}(\Delta\varepsilon_{ij})$. A constant value for all relationships

$\gamma = \frac{1}{0.6} = 1.67$ was suggested to represent better the trend of the available SrP data than the $\gamma = 1$ which leads to the previous interaction damage rule.

(2) The linear damage rule was considered to be part of a more general group of damage rules of the form

$$\Sigma \frac{N}{N_{ij}} = \alpha$$ where α is dependent upon the types of strains

$\Delta\varepsilon_{ij}$ and upon the the ratios F_{ij}. The value α and therefore

the damage rule function was determined for a case where two PP strains' damages ought to be combined. The value of α is dependent on the slope β_{pp} of the PP line and strain ratios

$$F_{pp1} = \frac{\Delta\varepsilon_{pp1}}{\Delta\varepsilon_i} \quad \text{and } F_{pp2} = 1 - F_{pp1} \text{ of the}$$

two partials over the loop width $\Delta\varepsilon_i$. The same could be done for any type of strain $\Delta\varepsilon_{ij}$. It was concluded that in a loop composed of two strains (say PP + CP) an upper and lower bound on α could be anticipated if the non partitioned (PP + CP) data follow a Manson-Coffin type of relationship.

6 - A MODIFIED STRAINRANGE PARTITIONING METHOD FOR LOW CYCLE FATIGUE BEHAVIOUR CHARACTERIZATION OF SUPERALLOYS

6.1 - INTRODUCTION

Most low cycle fatigue predictive techniques at elevated temperatures have been derived from the well known Manson Coffin equation:

$$\Delta\varepsilon_p N_f^{\beta} = C \tag{6.1}$$

where $\Delta\varepsilon_p$ is the plastic strain range, N_f is the number of cycles to specimen failure and β and C material constants. These predictive techniques can be divided into two basic groups according to the employed material deformation parameter required for measuring damage.

(i) The first group used inelastic strain and time (frequency) combined together as relevant variables to relate to fracture. Perhaps the most representative of this group is the frequency modified failure equation suggested by Coffin (115)

$$\Delta\varepsilon_p N_f^{\beta} \nu^{\beta(k-1)} = C \tag{6.2}$$

ν - frequency

β, k, C - material constants

(ii) The second group used different types of inelastic strains combined together as variables to measure damage and hence to predict lives. The Strainrange Partitioning (SrP) method is within this group.

$$\Delta\varepsilon_{ij} = CN_{ij}^{-\beta_{ij}} \tag{6.3}$$

ij - plastic(tension) - plastic(compression)
- plastic - creep
- creep - plastic
- creep - creep

C, β_{ij} - material constants

A pronounced effect on cyclic life of strain-controlled high temperature tests was found for parameters such as:

(i) inelastic strain
(ii) frequency
(iii) hold times
(iv) time dependent damage

This time dependent damage for many materials consists of intergranular cracking and accelerated crack growth from environmental interactions.

The transition of transgranular to intergranular crack propagation has been put forward as the major source of the substantial life-reducing effects of hold times specially where they are introduced in tension.

Early test results reported in table (6.I) found tension hold times to be more damaging. More recent testing with strong low ductility alloys changed the pattern of increased damage: compression holds were found to be the most damaging. Moreover differences in crack path failed to explain the new situation. Instead a combination of tensile stress, mean stress effects on the fatigue loops are mentioned (9,34). Contrary to the low cycle fatigue tests without hold time, unequal hold times or frequencies in tension or compression, lead to loops with a tensile mean stress when compressive holds were applied and to compressive mean stress under tensile hold loops (9,34,36). Associated with this last hysteresis loop behaviour were alloys with high strength and low ductility like the cast nickel superalloys which when tested between prefixed strains, presented high ratios of elastic to inelastic strains for lives as short as 10^3 cycles. No method was available which could take account of this new stress effect on the low cycle fatigue loops of the high temperature alloys. Recently a damage function which includes stress as well as inelastic strainrange was proposed by Ostergren (85) as the basic measure of low cycle fatigue damage at elevated temperatures.

6.2 - THE OSTERGREN METHOD

The basic assumption of the Ostergren method considers the net tensile hysteresis energy as a measure of fatigue damage. It can be shown that this energy can be represented approximately by the product $\sigma_T \Delta\varepsilon_i$ where σ_T is the maximum tensile stress and $\Delta\varepsilon_i$ is the inelastic strain. It is postulated that this variable is related to life by an equation similar to the Manson Coffin relation:

$$\sigma_T \Delta\varepsilon_i N_f^{\beta} = C \qquad (6.4)$$

At this stage the effect of frequency should be taken into account, therefore, it is suggested that equation (6.4) should be modified to:

$$\sigma_T \Delta\varepsilon_i N_f^{\beta} \nu^{\beta(k-1)} = C \qquad (6.5)$$

following closely the frequency modified failure relationships proposed by Coffin (115). However, this could not take account of different damages of hold times in tension or compression. Therefore, when the time dependent damage was dependent on wave shape a third equation was suggested as:

$$\sigma_T \Delta\varepsilon_i N_f^{\beta} \nu^{*\beta(k-1)} = C \qquad (6.6)$$

where ν^* instead of being the cyclic frequency as in expression (6.5) is defined as:

$\nu^* = 1/(To + T_T + Tc)$ for $T_T > Tc$ (effective frequency)
$\nu^* = 1/To$ for $T_T \leq Tc$
To - time per cycle
Tc - compressive hold time
T_T - tensile hold time

With this definition of effective frequency, cycles with tensile hold times would last less than cycles with dwells in compression or cycles with dwells in both directions in which cyclic damage is considered to be a pure frequency effect. In fact, for cycles where the dwell in tension is shorter than the dwell in compression equations (6.6) and (6.5) coincide.

Equations (6.4,6.5,6.6) are claimed to represent any case of high temperature low cycle fatigue. It can be shown that equation 6.4 can be reduced to the Manson Coffin law if mean stresses are not present on the cycle. Moreover, for many superalloys k = 1 in equation 6.5 or in other words lives can be predicted without the frequency term. Equation 6.4 is therefore applicable. This supports the occurrence of little creep damage in these alloys which is in agreement with metallographic observations reported for Rene 80 (34), Rene 95 (82) and MARM002 in chapter 4 of this thesis. Cracks propagation was observed to remain transgranular even for cycles involving hold times in tension.

Correlation using equation 6.5 were used with sucess for CrMoV steel data at 538^{0}C (85), equation 6.6 for AISI 304 stainless steel data at 640^{0}C (85), and equation 6.4 for Rene 80 (34) and for IN738LC data (83). The failure relationships developed by Ostergren follow closely the Coffin frequency modified approach but like these, difficulties were found in separating tensile creep damage from compressive creep damage which proved to have for some materials completely different importance.

The Strainrange Partitioning method bypassed the problem of distinguishing between tensile creep and compressive creep damage by introducing as basic variables the following types of inelastic strains: plastic - plastic (PP), creep - plastic (CP), plastic - creep (PC) and creep - creep (CC). A strainrange-life relationship ought to be drawn for each strain type. The Ostergren's modification of the Coffin's frequency modified approach has the advantage of including stress and strain parameters which could help to explain the influence of maximum and mean stresses on the low cycle fatigue of some high temperature alloys. This suggests a modification of the SrP approach in order to take into account the elastic (stress) effects.

6.3 - MODIFIED STRAINRANGE PARTITIONING METHOD

The suggested modification of the SrP method consists of considering the variable $\sigma_T \Delta\varepsilon_{ij}$ instead of $\Delta\varepsilon_{ij}$ like on the SrP approach as the variable to relate to fracture. The four new relationships will have similar form as those employed on the Strainrange Partitioning method:

$$\sigma_T \Delta\varepsilon_{ij} = A_{ij} N_f^{-\beta_{ij}} \qquad (6.7)$$

σ_T - tensile stress

A_{ij}, β_{ij} - material constants

$\Delta\varepsilon_{ij}$ - inelastic strain of the type ij

i - plastic or creep

j - plastic or creep

N_f - number of cycles to failure

Again on the left hand side is the damage function $\sigma_T \Delta\varepsilon_{ij}$ which is suggested in Ostergren's method as a sufficiently accurate approximation of the proposed measure of fatigue damage - the tensile hysteretic energy.

The procedure to draw the four energy vs life relationships will follow the Strainrange Partitioning steps closely. An extrapolation to a hysteresis loop 100% CP,PC or CC will have to be calculated first or in other words, the energy versus life relationships have to be determined as for the SrP method. The stress levels which will be employed to draw the new lines are either determined experimentally or extrapolated from experimental cycles as shown in Figure (6.1)

However, the most attractive application of this modified SrP method should be for cases where little creep damage here identifiable as grain boundary damage can occur at the

temperatures of interest. In this case the set of four equations (6.7) will be reduced to one relationship:

$$\sigma_T \Delta\varepsilon_i = A N_f^{-\beta}$$

In these cases even though there is a time dependent deformation mode going on, its basic mechanism is not going to be markedly different than for plastic (time independent) deformation. The different SrP types of inelastic strain will produce the same damage on the material, therefore, there is no need to distinguish than as was necessary in relationships (6.7). If loops with the same inelastic strain but different types produce different lives it is because the maximum tensile stresses involved on those cycles are different and hence the tensile hysteretic energies are different as well.

6.4 - APPLICATION OF THE MODIFIED SrP METHOD TO THREE ALLOYS

The high temperature low cycle fatigue behaviour of three alloys was analysed using the suggested modified Strainrange Partitioning approach where plotted in log-log scales their tensile hysteretic energies $\sigma_T \Delta\varepsilon_i$ can be correlated with life using only one line.

Figure (6.2) shows the function $N = N(\sigma_T \Delta\varepsilon_i)$ which correlates rather well (correlation factor $r = 0.95$) the tensile energy with life for any type of hysteresis loop of a titanium alloy (Ti - 6Al - 4V) studied in reference (110). Data from reference (82) of a nickel superalloy RENE 95 was plotted in Figure (6.3) using again $\sigma_T \Delta\varepsilon_i$ as the variable to relate to fracture. About forty points were used to calculate the energy-life line. The best fitting equation $\sigma_T \Delta\varepsilon_i = 461\ N_f^{-0.86}$ could correlate data with life rather well ($r = 0.91$). This equation was used in Figure (6.4) to predict the results of twenty five validation tests including cyclic creep tests, unbalanced strain hold tests, slow rate strain cycles and slow-fast and fast-slow strain cycles.

Taking into account the diversity of tests, the predictability of the method has to be considered good. Seventy three per cent of the validation tests could be predicted with an error in life less than two and 100% of data with an error less than three.

A third alloy to be used to test the method was the alloy under investigation MARM002, a nickel superalloy tested within the range of temperatures 750 - 1040°C. First the 850°C data reported in chapter 4 was used to draw the energy-life relationships. It was found that a unique line could be drawn

through these data with a correlation factor of 0.92. That confirms that for this alloy little damage is done by the introduction of creep in tension or compression. The reason that the strainrange vs life relationship at 850°C reported in chapter 4 are different is because of the influence of the maximum stress and mean stress make them diverge. The regression analysis for the 850°C data gave:

$$\sigma_T \Delta\varepsilon_i = 158\ N_f^{-0.94} \qquad (6.8)$$

when this line, Figure 6.5, was used to predict lives at three temperatures 750°C, 950°C and 1040°C the predictability was rather better than the one found for SrP. For the SrP method itself only 57% of the same data fell inside x2 bands in life when the 850°C basic strainrange vs life relationships were used to predict the tests conducted at 750°C, 950°C and 1040°C.

The function $\sigma_T \Delta\varepsilon_p = 158 N_f^{-0.94}$ has increased that percentage to 85% as shown in Figure (6.6). In such a large range of temperatures it is an encouraging result for the method.

6.5 - THE METHOD OF OSTERGREN VERSUS STRAINRANGE PARTITIONING

On the previous three alloys the use of the tensile hysteretic energy to relate to life resulted in only one function $N = N(\sigma_T \Delta\varepsilon_i)$ to represent their creep-fatigue behaviour. The advantages of using the new method in these circumstances are obvious.

(1) The somewhat unusual position of the strainrange vs life relationships for some alloys can then be explained in terms of maximum and mean stresses by passing the apparent paradox of creep strains being beneficial for those alloys.

(2) The use of damage rules both to extrapolate to the 100% CP, PC and CC lives or to interpolate between lives in complex cycles is avoided. Therefore, the difficulties and uncertainties caused by the choice of damage rule and application as discussed in chapter 5 are avoided.

(3) Exclusively PP data can be used to draw the energy vs life relationship. As these data are a lot easier and less time consuming to produce the advantage over the SrP method is obvious.

Most of these advantages over the SrP method disappear when the introduction of creep either in tension or compression is

'detected' by the material as a particularly damageable strain and, therefore, if fracture changes from transgranular to an intergranular mode as creep becomes an appreciable factor, instead of one energy versus life relationship one has to deal with more than one as in the SrP method. That happened with Nimonic 90 data reported in reference (111). As different energy life relationships were obtained for the PP, PC and CP data at 810°C, a pronounced effect of creep on fracture mode can be anticipated for this alloy. Figure 6.7 shows different lives for the isothermal tests at 810°C and different PP lives at 650, 810 and 900°C. As all the PP tests were run at the same frequency (0.4 Hz) it is possible that some creep was involved on these tests at the higher temperature 810 and 900°C. The degradation of fatigue properties at these temperatures could be caused, therefore, by the use of not sufficiently high frequencies to preclude creep from the higher temperature PP loops.

But even if the use of higher frequencies might make the PP lines coincide in Figure 6.7, the CP and PC will be different. This as has already been said, brings difficulties already found on the SrP method, such as the partitioning of certain inelastic strains and the use of damage rules to extrapolate to 100% PC,CP or CC lives. Therefore, the main contribution of the method using both the Strainrange Partitioning and Ostergren's methods has to be into those cases where, if the $N_{ij} - \Delta\varepsilon_{ij}$ are separated, it is because a maximum and mean stress effects are present. Whether or not the maximum and mean stresses play an important role in determining creep-fatigue lives, it has to be checked for each case. However, there are several factors which might suggest if one can or cannot neglect this effect. First is the amount unbalance which results from the introduction of a hold time. This shifting of the loops to tension or compression will depend upon the strength - ductility characteristic of the material.

A helpful parameter in this regard will be the elastic to plastic ratios found for the first high temperature low cycle fatigue tests. High ratios will favour that shifting if a dwell is imposed, low ratios will mean that the mean stress which can be supported is very low. Alternatively the effect of this stress effect can be predicted in terms of the transition fatigue life, that is the life when elastic and plastic strains are equal.

The more the life exceeds the transition fatigue life the greater is the tendency to support a mean stress. Summing up, high elastic to plastic ratios (thin-long loops), low transition fatigue lives, unbalanced loops when dwells are applied, suggests that stress might play an important role in determining lives.

Secondly, is the relative importance of initiation and propagation, being this factor related closely to the one previously discussed. In fact, the larger the elastic to plastic ratios the larger normally will be the initiation period. It is known that in regimes where the elastic strain is a small fraction of the total strain the propagation period predominates. When elastic strains are a big fraction of the total strain like on the high cycle regime fatigue, almost all the life is spent in crack nucleation. Stress has been used successfully in high cycle fatigue as the relevant variable to determine life which is spent almost entirely in nucleating a crack. When plastic strains are large enough to be measured accuractely, they have been used successfully to determine life at temperatures where time dependent strain cannot be induced. The bigger these plastic strains the more important becomes the propagation periods of cracks leading to fracture.

When temperature is high enough to induce creep other variables come into the problem of predicting life as:

(i) Creep strain and direction of its application

(ii) Time effects (creep damage plus environment effects)

(iii) Stress effects in loops where different times spent in tension and compression induced pronounced positive or negative mean stresses.

Each factor will play a more or less important role depending upon the material temperature and regime in operation. The main hope is really that in the future a knowledge of the regime or conditions in which the material is going to operate will determine the choice of predictive methods best suited to the situation. It seems that the ideas put forward both by the Strainrange Partitioning technology and Ostergren method will help to describe the high temperature low cycle fatigue behaviour of many cast nickel superalloys like MARM002.

6.6 - CONCLUSIONS

(i) A method based on Strainrange Partioning and the method of Ostergren has been suggested for materials working in regimes where both inelastic strain, wave shape and stress could influence life.

(ii) The method was found particularly simple to apply when applied to some high temperature alloys as its four energy vs life relationships are reduced to one. This suggested little difference between the creep damage and plastic damage for those alloys. This fact was supported by metallographic evidence which showed that transgranular fracture was observed under

all testing conditions and frequency degradation of fatigue resistance by intergranular cracking did not occur even at high temperature with the longest hold times used.

For those alloys that do show a pronounced difference in fracture mode with frequency and wave shape, four energy vs life relationships have to be used as in the SrP method.

(iii) The method was applied to three high temperature alloys. As one energy vs life relationship could represent the high temperature low cycle fatigue behaviour of each alloy, the method was simpler to apply than Strainrange Partitioning. For these cases the life prediction ability of the method was found to be better than the SrP approach.

7 - RELATIVE IMPORTANCE OF INITIATION AND PROPAGATION ON HIGH TEMPERATURE LOW CYCLE FATIGUE TESTS ON MARM002

7.1 - INTRODUCTION

Thermal fatigue is one of the primary failure modes which must be taken into account when designing highly stressed hot components in gas turbine engines. Thermal fatigue of these components occurs during start and shutdown periods when high strains are generated due to different massivity. The usefulness of any life prediction method in these kinds of situation where fatigue and creep are superimposed, depends in the first place on how good the simulation of the service conditions is.

The use of isothermal strain controlled tests, to simulate and study components operating in such service conditions has been of widespread use because they are easier to conduct with in general better control of the variables of interest - plastic and creep strains, stress and temperature. This procedure becomes even more attractive with methods like Strainrange Partitioning offering some degree of temperature insensitivity for its basic strainrange versus life relationships. However, the comfortable situation of having strainrange versus life relationships independent of temperature, over large temperatures intervals normally does not arise. In the case of MARM002 it was found that the basic relationships were independent of temperature but over limited temperature ranges as discussed in chapter 4.

Even supposing that data can be generated to cover the temperature range of interest, an approach to thermal fatigue based on isothermal information covering the temperature range of interest can be dangerous. Recent work by Taira (113) showed that great care is necessary when isothermal data is used to predict thermal fatigue lives. The observed crack growth in air above and below the creep range leads to the following situation for a nickel superalloy:

(i) Many cracks are formed early in life at high temperatures but they propagate slowly.

(ii) At the lower temperatures a single dominant crack is formed late in life but propagates rapidly.

They concluded that the particularly detrimental effects of a thermal fatigue cycle involving tensile stress holds at the highest temperature were due to the early formation of cracks at the higher temperatures with accelerated growth by lower temperature deformation processes. Earlier, high temperature low cycle fatigue characterization of MARM002 over the range 750°C - 1040°C, was reported in chapter 4.

Later the position of the strainrange versus life relationships at the two temperature ranges was rationalized with the help of a concept used by Ostergren (85) introducing both inelastic strain and maximum tensile stress as multipliers in an energy parameter which was used then to relate to fracture.

This stress effect which explained the separation of the basic SrP lines at 850°C was washed out at 1040°C. Although significant mean stresses were present at the 1040°C loops as well, the basic strainrange versus life relationships at this temperature practically clustered together as seen in chapter 4. One hypothesis put forward then, was that due to higher plastic to elastic strain ratios, the bigger plasticity at these temperatures would induce easier relaxation of the mean stress at the crack(s) tips and, therefore, produce similar crack growth rates independently of the mean stress present on the loop ie., independently of the type of SrP cycle.

The clarification of this point needs an assessment of the importance of the initiation versus propagation periods at both temperatures. Also, this assessment will allow us to know how to use the isothermal data for MARM002 to variable temperature applications bearing in mind the already mentioned findings of Taira et al.

7.2 - EXPERIMENTAL PROCEDURES

The general experimental procedures were similar to those used to determine the strainrange versus life relationships of MARM002 and were already reported in chapter 4. All creep-fatigue tests were performed at a constant axial strainrate under completely reversed strain cycling. Again, either the direction of straining was reversed immediately upon reaching a predetermined strain limit or a constant load was maintained for a period of time until the predetermined strain limit was reached. Each test was divided into two parts separated by a period of homogenization at 870°C for ½ hour without applying stress. This series of mixed tests were divided into four sections:

(1) PP test at 850°C on the first part plus a CP test at 850°C on the second part.

(2) CP test plus a PP test at constant temperature of 850°C.

(3) PP test at 850°C plus PP test at 1040°C.

(4) PP test at 1040°C plus PP test at 850°C.

In each section an average of four tests were performed, varying the percentage of exhausted life N_1 where N_1 is the number of cycles imposed on the first part N_{p1} of the test and N_{p1} the predicted total number of cycles the specimen would last. The damage D which was done on the first part of the test was assessed on the second part running a number of cycles N_2 until fracture occurs. This number of cycles N_2 is then used with the predicted number of cycles that a virgin specimen would last N_{p2}, to compute the damage D given as

$$D = 1 - \frac{N_2}{N_{p2}} \qquad (7.1)$$

The extrapolated value of $\frac{N_1}{N_{p2}}$ for D = 0 was considered to be the initiation point of the tests run on the first part. Obviously these initiation points as defined above are only valid for the average conditions (inelastic strain levels, temperature) used on the first part of these mixed tests. It can be expected that for bigger inelastic strains (shorter lives) the propagation period will start earlier decreasing the $\frac{N_1}{N_{p1}}$ for D = 0 ie., lowering the percentage in life considered to be the initiation point.

The justification for the choice of the particular type of tests used on the previous four sections of mixed tests and the clarification of the concept of initiation in these tests will be dealt with in detail in the sub-section dedicated to the discussion of the mixed tests results.

7.3 - INITIATION VERSUS PROPAGATION ON CREEP-FATIGUE TESTS OF MARM002

Before describing and commenting on the set of mixed tests, additional information which is thought to be helpful as far as the separation of nucleation and propagation on the MARM002 basic tests will be reported. It will take two aspects, the first related with the type and number of secondary cracks existing after fracture on the specimens used to draw the four basic lines for the two temperature ranges, (750°C - 850°C) and (950°C - 1040°C) and the second related to the qualitative assessment of initiation and propagation within the same intervals. Here the tensile load monitoring of the PP and PC tests will allow to register the 5% drop in tensile load point which will be seen as a first sign that a crack(s) are present ie., it will be identified in a first step with the beginning of the propagation period.

7.3.1 - Secondary Crack Pattern

When MARM002 specimens were viewed in a binocular microscope at 3 to 10X magnification with the illumination shallowly inclined to the external cylindrical surface, sharply defined ridges were observed at numerous locations. These ridges were the result of localized oxidation and they acted most as nucleating sites for cracks as shown in Figures (7.1,7.2).

This type of surface damage was enhanced by higher temperatures on low frequency tests as expected for an oxidation phenomenon. In these oxidation induced cracks it was observed an oxide layer bonding the crack and a reaction zone (deplected γ'zone) between the oxide and the base structure as shown in Figure (7.3).

The analysis of secondary cracking in the longitudinal sections of the specimens used to draw the basic SrP relationships produced the following results:-

(a) Crack nucleation seemed to occur at surface connected weak points like pores and preferential oxidation points as shown in Figures (7.4,7.2).

(b) The number of very small cracks (<10μ) in longitudinal sections of about 25mm^2 is increased either with temperature or frequency as shown in Figure (7.2).

(c) The ability of these secondary cracks to grow seemed to decrease with higher temperatures as shown in Figure (7.6). The picture here seems to be that the higher the temperature the higher the number of secondary cracks but they are shorter than those found in smaller numbers at lower temperatures.

(d) Internal cracks were comparatively fewer and shorter than surface induced ones and seem to initiate at stress raisers like sharp carbides and propagated through $\gamma - \gamma'$ interfaces as shown in Figure (7.7).

(e) The number of grains in a longitudinal section ($\sim$25 mm^2) was very low (3 - 5 grains). As already reported in chapter 4 fracture profiles of these sections were found to be rather flat with no evidence of intergranular cracks.

The observation of the fracture surfaces using macroscopic light fractography and SEM revealed that:

(1) At higher strain limits (shorter lives) the failures were essentially ductile and often exhibited

characteristic cup and cone features even though the material was tested at stresses below the UTS.

(2) At lower strain limits fatigue was the predominant mode of failure. Optically this appeared as a darkened zone due to oxidation of the fracture surface. It was possible to detect in some specimens tested at low temperature bracket areas containing striactions as shown in Figures (7.8,7.9). At higher temperatures a thick oxide layer had hidden such fine features as the fatigue striactions as shown in Figure (7.10).

7.3.2 - The 5% Drop in Tensile Load as a Measure of Relative Importance of Initiation and Propagation

Within the four basic SrP type of cycles there are two PP and PC where the monitoring of the tensile load can serve as a rough indication of the existence of crack(s) within the specimen. Since the creep - plastic (CP) and creep - creep (CC) cycles employ stabilization between fixed load values the existence of a crack will only modify the partitioned strains in a cycle but the load plateaus. Hence what it is here to be considered as an initiation condition cannot be determined by a load drop technique for CP and CC cycles.

The life period $N_p = N_f - N_5$ where N_f is the total number of cycles until fracture and N_5 is the number of cycles for 5% drop in tensile load, was considered to be a measure of the propagation period. This criterion was applied at both temperature intervals and results for some PP and PC tests are shown in Figure (7.11). Here the ratio N_5/N_p is plotted against total life N_f. The ratio initiation of propagation as represented by N_5/N_p was found to be smaller at the higher temperature range. This suggested smaller initiation periods at these higher temperatures. At the low temperature bracket initiation periods were bigger specially as life increased as shown in Figure (7.11).

Based on those results which are reported in table (7.I) a check on the relative position of the strainrange versus life relationships based on the N_5 lives instead of the total number of cycles was possible. As shown in Figures (7.12) and (7.13), the relative position of the lines representing the strain versus lives based on 5% drop in tensile load, were not altered.

At the same inelastic strain level lives N_5 continued to be significantly longer at higher temperatures (points A and B in Figures (7.12) and (7.13)). For a life of two

thousand cycles there is a bigger period of propagation $N_f - N_5$ at higher temperatures (points C and D). This shows more clearly that at low temperature once the specimens reach a state where damage can be detected by a 5% drop in tensile load collapse is nearer. The rationalization of this can be based on the fact that at lower temperatures the material is less ductile, therefore, smaller critical crack lengths are to be expected then. Critical crack lengths between 0.5 and 2 mm were found for the $750^{o}C$ - $850^{o}C$ range and between 2 and 4 mm at the higher temperature range depending on inelastic strain level.

7.3.3 - Mixed Tests

Both main conclusions of the studies concerned with secondary cracking statistics and the detection of the 5% drop in tensile load pointed out a major qualitative assessment of the importance of initiation and propagation in some SrP cycles at two ranges of temperatures. Nucleation of many cracks differs earlier at higher temperatures but they propagate at a relatively slower rate. Nucleation for PP and PC in the lower temperature bracket (750 - 850) happens through the formation of fewer cracks but they propagate faster than the corresponding cycles at higher temperatures. That confirmed in general early work by Taira et al (113).

In order to check this qualitative assessment, a series of mixed tests were conducted at $850^{o}C$ and $1040^{o}C$. Basically the aim was to determine the maximum percentage $\frac{N1}{Np_1}$ of life that could be exhausted on the first part of the test without 'damaging' the specimen. That percentage was then considered to be the initiation point for a cycle like the one used on the first part, that 'damage' was assessed on the second part of the test and was considered to be $D = 1 - \frac{N2}{N_{p2}}$ where N_2 was the number of cycles the specimen took for fracture on the second part and N_{p2} the predicted life for the second part of the mixed test.

Using the inelastic strains $\Delta\varepsilon_{i1}$ and $\Delta\varepsilon_{i2}$ of the first and second part of the tests, N_{p1} and N_{p2} could be calculated using the strainrange versus life relationships for the PP and CP cycles at $800^{o}C$ and PP cycles at $1040^{o}C$ as reported in Chapter 4. They were

$$\Delta\varepsilon_{pp} = 0.26\ N_{pp}^{-0.94} \qquad (850^{o}C) \qquad (7.2)$$

$$\Delta\varepsilon_{cp} = 0.015\ N_{cp}^{-0.08} \qquad (850^{o}C) \qquad (7.3)$$

$$\Delta\varepsilon_{pp} = 0.042\ N_{pp}^{-0.55} \qquad (1040^{o}C) \qquad (7.4)$$

The choice of these three cycles was based upon:

(a) Since at 1040^{o}C there are no major differences in life for the different SrP cycles (chapter 4), the PP tests were chosen because they are the easiest and least time consuming of all SrP tests.

(b) The PC and CP cycles constituted the lower and upper bounds of the strainrange versus life relationships at 850^{o}C. Since there was no major difference between the PC and PP lives and taking into account that the last ones are the easiest to conduct, the investigation on the initiation points was done on the PP line and on the upper bound on lives at 850^{o}C, eg., CP line.

In table (7.II) data of the mixed tests are reported. As can be seen in this table, strain levels for the first part of the tests were around 10^{-3} for CP - 800^{o}C and PP - 1040^{o}C tests and 4 x 10^{-4} for the PP - 800^{o}C. If carried until fracture it would lead to lives between 500 and 1000 cycles. Plots of ratios N_1/N_{p1} of exhausted over predicted lives against the 'damage' $D = 1 - N_2/N_{p2}$ are shown in Figure (7.14). Data used in these graphs were computed from table (7.II) and are given in table (7.III).

Values of 20% 60% on life were obtained in those plots as extrapolated values for D = 0 which were considered as the initiation points I_{pp850} and I_{cp850} for the PP850^{o}C and CP850^{o}C SrP tests. The extrapolated point I_{pp1040} was found to be negative. That shows that even before the first part of the test at 1040^{o}C starts, there is some 'damage' imposed on the material estimated to be here, around 28% on life (point Do).

In other words, the ¼ hour or so at 1040^{o}C, time allowed before the first part of test (PP1040^{o}C) is started, to stabilize temperature and make last checks is sufficient to 'damage' the material in so far as 28% of the PP850^{o}C lives that follow are by passed.

The results of the mixed tests involved the prediction of two lives N_{p1} and N_{p2}. They are calculated using the strain-range versus life relationships represented by equations (7.2,7.3,7.4). Obviously there are errors associated with these predictions. Table (7.IV) presents data computed from table (4.V). These data were used to calculate a mean value for the error ΔN of the experimental results relative to those predicted by the best fitting lines described by equations (7.2,7.3,7.4). This value computed from table (7.IV) was found to be ΔN = 11%. The influence of this uncertainty on the ratios N_1/N_{p1} and N_2/N_{p2} can then be calculated. If N/N'_{p1}, is the exact value of the ratio N/N_{p1}

it can be written $N/N'_{p1} = N/N_{p1} + D1$ being $\Delta 1$ the value of the error on N/Np1 due to the uncertainty in predicting N_{p1}.

Therefore,

$$\Delta 1 = \frac{N_1}{Np'_1} - \frac{N_1}{Np_1} = \frac{N}{Np_1 \pm \Delta N Np_1} - \frac{N_1}{Np_1}$$

As ΔN was estimated to be around 11%

$$\Delta_1 = \pm\ 0.1\ \frac{N}{N_{p1}} \qquad (7.5)$$

The same sort of error Δ_2 can be estimated for the ratio N/N_{p2}

$$\Delta_2 = \pm 0.1 \frac{N}{N_{p2}}$$

Uncertainties in the initiation points I on Figure (7.14) are to be expected as a consequence of those errors $\Delta 1$ and Δ_2. It can be shown using equation (7.5) that $I_{cp850} = 0.58 \pm 0.06$ and $I_{pp850} = 0.21 \pm 0.02$ being the values 0.58 and 0.21 consequence of linear regressions performed on data from table (7.II). The respective equations D = D ($N_1/Np1$) are reported in Figure (7.14).

7.4 - DISCUSSION OF RESULTS

What one chooses to call initiation depends both on the problem under investigation and the techniques available for examination. The mechanisms of fatigue in the creep range have been reviewed for nickel superalloys and in brief here, initiation could be considered as a statistical process by which nucleation of dislocations at discontinuities such as Mc carbides, pores, etc., result in microcracks. In reports dealing with life prediction methods almost all events have been taken as crack initiation point, the first sighting of a crack(s) using a microscope.

First noticeable drop in load range, drop in fixed percentage of tensile load even the complete separation of the small laboratory specimens. Earlier on, results based on 5% drop in tensile load criterion showed earlier initiation at 1040°C with longer initiation periods for tests (PP and PC) at 850°C) As lives were greater at 1040°C a situation of earlier initiation - slow propagation at 1040°C and faster propagation at 850°C could be anticipated. This situation could be particularly dangerous at cycles involving varying temperatures between those values, since

as already mentioned this could lead to particularly short lives. The set-up of the mixed test programme had as main objectives to draw a lower bound for initiation at the higher temperatures and an upper bound for initiation at the lower temperatures since this combination would lead, in tests with varying temperature, to the most damagable situation. In order to find the initiation points corresponding to the CP tests at 850°C and the PP-1040°C tests, special PP-850°C tests were used on the second part of the mixed tests. Since initiation should be detected as early as possible PP tests with longer lives were used (average 3500 cycles).

On the other hand since an upper bound in initiation were required for the CP-850 tests the same PP tests were used but with much shorter lives (average 350 cycles). Obviously the values of 0% and 60% for the initiation points at 1040°C and CP-850°C tests respectively, are valid only for the strain (life) levels used on the first part of the tests (around 500 cycles). Higher lives (or lower strain levels) will tend to put, if possible, even more emphasis on initiation. The initiation point for the PP-850°C cycles was estimated to be around 20% on life. The life level in question was around 1000 cycles. Based on these values for the initiation points, new propagation lines, PP' and CP' were drawn in Figure (7.15). First a new PP line at 850°C was drawn assuming that the transition fatigue life N_t = 16 cycles is spent in first propagation and at a level N_f = 1000 cycles, 20% are initiation and 80% propagation as found earlier. This line is represented as PP'850°C in Figure (7.15). For a CP life of around 500 cycles (point B) it was calculated that 60% is initiation, therefore, substracting this percentage from the total life point B' is obtained.

This lies practically on the PP line. Therefore, assuming the linearity of the propagation SrP lines it can be concluded that only the different periods of initiation are responsible for the separation of PP and CP lives at 850°C. The new propagation line for the PP and CP cycles can be described approximately by:

$$\Delta\varepsilon_{pp'} = 0.30 N_{pp}^{-0.99}$$

and it constitutes accordingly to the previous considerations the lower bound for cycles involving PP and CP components, in which the temperature varies over the range 750 - 1040°C.

The 850-PC tests presented the most damagable cycles of all, as seen in chapter 4. The PC loops presented a higher maximum stress and positive mean stress when compared with other types of loops of the same width. Even supposing that due to their positive mean stress nucleation of cracks is very rapid this fact cannot take account of the exceptionally low lives as shown in Figure (7.15). Fast propagation, therefore, must be a reason as well for these low PC lives.

The isothermal results of MARM002, together, with the initiation versus propagation studies of the same alloy, have clearly demonstrated the problems involved. The risk is implicit on the very early development of cracks initiation either at 1040°C due to surface-environment interactions or at 850°C for cycles involving high tensile mean stresses, and with their rapid growth for any type of cycle at lower temperatures.

Further improvement on the knowledge of the high temperature low cycle fatigue of MARM002 and similar alloys could be achieved with the study of thermal fatigue tests over the temperature regime of interest.

7.5 - CONCLUSIONS

(i) A situation of early formation of cracks at the more elevated temperatures (950 - 1040°C) with accelerated growth on the lower temperature bracket (750 - 850°C) showed that great care is necessary. MARM002 isothermal results are applied to thermal fatigue cases or more generally, to any cases where temperature changes either during a cycle or during the specimen or components' lives.

Values for the initiation points of the PP cycles at 850°C, CP cycles at 850°C and CP cycles at 1040°C were calculated using mixed tests. These points were estimated to be %20 and 60% of the respective lives for cycles of the type PP at 1040°C, PP at 850°C and CP at 850°C respectively.

(ii) The relative position of these initiation points were confirmed by secondary crack statistical studies made on longitudinal sections of the basic SrP test specimens and through studies on the monitoring of the 5% drop in tensile load of PP and CC specimens tested at 750, 850, 950 and 1040°C. Many surface connected secondary cracks were found on the test specimens at the higher temperatures but they were shorter than similar secondary cracks at the lower temperature range.

The 5% drop on tensile load method revealed as well, quicker propagation period at the lower temperature bracket. The results of these tests were in qualitative agreement with those found for the mixed tests. That is earlier propagation of a great number of cracks mainly due to oxidation happening at higher temperatures and more or less late propagation, depending on SrP type of cycle, for a comparatively fewer number of cracks happened on the low temperature range of tests.

(iii) The separation in nucleation and propagation periods for some of the Strainrange Partitioning basic lives helped to explain the relative position of the basic strainrange versus life relationships which defined the high temperature low cycle fatigue behaviour of MARM002 within the range (750 - 1040°C). For example, the divergence of PP and CP lines at 850°C were consequences of longer initiation periods for the CP cycles. When from the PP and CP cycles the initiation period were substracted these lines clustered together.

This fact is coherent with previous finding about the crack paths in MARM002 SrP cycles which were found to be consistently transgranular.

8 - MAIN CONCLUSIONS AND SUGGESTIONS FOR FURTHER WORK

8.1 - MAIN CONCLUSIONS

This section recalls the salient features of this programme. References to the sections in which a particular topic was discussed are given parenthetically.

(i) Strainrange Partitioning is a viable life prediction analysis procedure that was successful in predicting specimen life under strain controlled cycling within the temperature range 750 - 1040°C. Strainrange Partitioning measurements of MARM002 over that temperature range have been made and the strainrange versus life relationships established at 850°C and 1040°C. Good agreement between predicted and actual cyclic lives at 750°C and 950°C demanded the use of two sets of inelastic strain versus life relationships. Lives, within a factor a ± 2, could be predicted for specimens tested at 750°C using the strainrange versus life relationships at 850°C and for specimens tested at 950°C using similar data at 1040°C (Chapter 4).

(ii) For a given inelastic strainrange PC type test cycles exhibited shorter cyclic lives than other test cycles at 850°C. The CP type life was the upper bound of the four strainrange versus life relationships.

The linear regressions describing the N_{ij} - $\Delta\varepsilon_{ij}$ relationships at 1040°C showed coincident PP, PC and CP lines with slightly higher CC lives (Chapter 4). Metallographic evaluation indicated that microstructural damage did not vary with cycle type and test temperature. All the specimens exhibited a transgranular type of fracture mode (Chapters 4 and 7). Hence cyclic life differences among the lower temperature interval (750 - 850°C) tests and between these and the higher temperature tests 950 - 1040°C could not be explained by different fracture modes.

(iii) Different regimes were found to operate at the two different temperature intervals and they were responsible for the differences in life mentioned above. The characterisation of the fatigue regime over the lower temperature range was based upon:

(a) Large elastic versus plastic strain ratios $\Delta\varepsilon_e/\Delta\varepsilon_p$ For a PP life of two thousand cycles this ratio was twenty four. Viewed differently a ratio $\Delta\varepsilon_e/\Delta\varepsilon_p = 10$ occurs for a life $N_{pp} = 518$ cycles (Chapter 4)

(b) Initiation periods between 20% and 60% of the specimens life depending on test type (Chapter 7). Transgranular propagation of one or a few cracks occurred at this temperature interval (Chapter 7).

The characterisation of the fatigue regime over the range 950 - 1040^{o}C could be summed up as:

(a) Relatively lower elastic to plastic strain ratios. For a PP life of two thousand cycles this ratio was six. Viewed differently a ratio $\Delta\varepsilon_e/\Delta\varepsilon_p$ = 10 occurs for a life N_{pp} = 8512 cycles.

(b) Initiation period completely bypassed by strong environment-specimen surface interaction (Chapter 7). Transgranular propagation of multiple cracks occurred at this temperature interval (Chapter 7).

(iv) Arguments to explain the position of the strainrange versus life relationship of MARM002 at 850^{o}C were based upon relative large elastic to plastic strain components, which allowed very different maximum tensile and mean stresses to be built up within each of the four typical SrP loops and hence inducing different fatigue lives. Like in other low ductile high strength superalloys the MARM002 N_{ij} - $\Delta\varepsilon_{ij}$ relationships at 850^{o}C showed a CP line far to the right (greater life) and a PC line constituting the lower bound of all creep-fatigue lives. The lives of the symmetrical PP and CC cycles were placed between those of the PC and CP loops. The damage order was explained at any given inelastic strain level by lower maximum tensile and negative mean stresses of the CP loops when compared with the higher maximum tensile and positive mean stresses showed by the PC loops (Chapter 4).

The loop unbalancing on non symmetrical cycles at 850^{o}C was less severe at higher temperatures. The clustering of the 1040^{o}C SrP lives was believed to be based upon that fact, which would be accentuated nearby the crack(s) tips where the higher plasticity tended to induce relaxation of the mean stress (Chapter 4).

(v) An alternative analysis based on Ostergren's method provided good correlations between tensile hysteretic energy and creep-fatigue-life for MARM002, the other three superalloys and a titanium alloy (Section 6). This approach generally demanding four energy versus life relationships before a life prediction of a complex cycle can be made was found to be particularly useful and simple to apply to some superalloys where maximum tensile stress effects on life could be anticipated. In two superalloys, a Titanium alloy and MARM002, over the range 750 - 1040^{o}C only one energy versus life

relationship could correlate well all the tests carried out over the previous temperature interval. It was concluded that like in MARM002 where creep deformation mechanisms is not going on within the grain boundaries this alternative approach presented advantages over the strainrange partitioning approach (Chapter 7). One of the main advantages was to avoid the use of damage rules whose difficulties in application and uncertainties on rule choice were discussed in one of the previous sections (Chapter 5).

(vi) A situation of early formation of cracks at the higher temperature interval with accelerated growth at lower temperatures showed that great care is necessary when applying MARM002 isothermal results to thermal fatigue cases or more generally to any cases where temperature changes either during a cycle or during a specimen or component's life (Chapter 7).

The role of the environment, especially at the higher temperatures and the role of stress at lower temperatures, are areas in which further work is needed. These areas and the one of thermal fatigue are suggested in topics for further study as means of achieving a better understanding of the creep-fatigue phenomena in superalloys and in deciding whether thermal or isothermal fatigue is critical for a given component.

8.2 - SUGGESTIONS FOR FURTHER WORK

Further work is suggested in the following areas:-

8.2.1 Effects of Strain and Stress Dwells on Life

Except for the PP tests, all the cycles used to draw the basic Strainrange Partitioning (SrP) relationships in the present investigation involved a stress dwell, either in tension or (and) compression. The reason why stress dwell tests were chosen was because they were less time consuming than the tests with strain dwells, when a certain percentage of creep was required on the hysteresis loop.

As discussed in Chapters 4 and 6, the important variables related to fracture of MARM002 were not only inelastic strain magnitude and type (PP, PC ...) but also maximum and mean stress values. The emphasis on one or more of these variables will depend upon the material and general test conditions such as temperature, frequency, inelastic strains, etc. As discussed in Section 6, the inelastic strain and maximum tensile stress variables could explain

the different lives found for MARM002 over the temperature range 750 - 1040°C. As the introduction of strain and stress dwells will produce different maximum tensile stresses, the observed lives could be dependent on dwell type and therefore alter the position of the generic strain-range versus life relationships in the SrP procedure. Moreover, the different times per cycle caused by the introduction of one or the other type of dwell may induce differences in experimental lives especially at temperatures where environmental effects are relevant to either initiation or (and) propagation periods. An investigation comparing the effects of strain and stress dwells would be useful additions both to SrP technology and Ostergren's method as discussed in Chapter 6.

8.2.2 - Environment Versus Creep on the Degradation of Fatigue Properties with Increased Time

There has been a great deal of discussion about the extent to which the environment and the time dependent strain (creep) are responsible for the degradation of the fatigue properties in cycles involving stress or strain dwells. In other cases like in many superalloys which present rather strong resistance to creep damage, it is not creep versus environment effects which ought to be separated but the effects of different stresses (maximum tensile, mean) resulting from the introduction of plasticity or creep on the fatigue loops and the environmental effects which might influence both initiation and crack propagation rates.

Methods involving variables such as time or test frequency to relate to fracture, are naturally best equipped to deal with cases where damage is produced as a result of the interaction of time sensitive factors (creep, environment). That is the case of the frequency modified strainrange method and others inspired by it. On the other hand, methods like Strainrange Partitioning which rely on inelastic strain (plasticity and creep) and on the direction (tension or compression) where it is imposed for the prediction of lives, are best equipped for cases where damage is mainly associated with the relative amounts of plasticity and creep and the direction where they are applied. High temperature low cycle fatigue tests performed on MARM002, discussed in Sections 1 and 3, showed two patterns of results. The first, relative to tests on the temperature range 750 - 850°C was characterised by significant differences among the strainrange versus life relationships, specially between the PC and the CP lines which represented the lower and upper bound respectively. The unbalanced hysteresis PC and CP loops exhibited pronounced and opposite mean stresses which accounted qualitatively for the observed behaviour. In Chapter 7, tests conducted on MARM002 suggested that environment-material interactions have cut short the initiation

period at the highest temperature but, as the lives to fracture increased it is possible that the environment, also had a strong influence on crack propagation rates.

A more precise picture of what is the balance of creep and environment effects on life, requires a programme of tests conducted in a neutral atmosphere.

Fracture studies on test specimens under these conditions will be easier to interpret since oxidation of the fracture surfaces will be reduced to a minimum.

8.2.3 - Thermal Fatigue

Another subject in need of considerable attention is that of thermal fatigue. Attempts to apply isothermal data to cases where temperature varies have resulted in unacceptable life prediction errors.

The ability of SrP or any other predictive method to deal with complex cycles in which temperature varies throughout the cycle depends upon:

(i) Temperature sensitivity of the methods basic relationships.

(ii) Regimes in which the material operates over the temperature range of interest.

Indications about the degree of temperature sensitivity of the strainrange versus life relationships and about operating regimes over the range 750 - 1040^{o}C were given in Chapters 4 and 7 for MARM002.

The use of its strainrange versus life relationships in a thermal fatigue situation could be dangerous as discussed in Chapter 7. There, evidence was found that accelerated intiation periods at the highest temperatures of the cycles, could combine with rapid propagation during the lower temperature part of the cycle to produce exceptionally short lives.

A programme of thermal fatigue cycles on MARM002 would be a helpful addition both to the understanding of the previous high temperature tests and on the characterisation of the high temperature fatigue of MARM002.

REFERENCES

1. COFFIN, L.F. A study of the effects of cyclic thermal stresses on a ductile metal, Trans. Am. Soc. Mech. Engrs., 1954, 76, pp 923 - 949.

2. PARIS, P.C. The fracture mechanics approach to fatigue. Proceedings of the 10th Sagamore Army Materials Research Conference, New York, August 1963, pp 107 - 132.

3. MANSON, S.S. Fatigue, complex subject - some simple approximations. Exp. Mech. Vol. 5, No. 7, July 1965, pp 193 - 226.

4. MANSON, S.S. Interfaces between fatigue, creep and fracture. Intl. J. of Fracture Mechanics, Vol. 2, 1966, pp 327 - 363.

5. HALFORD, G.R., MANSON, S.S. Application of a method of estimating high temperature low cycle fatigue behaviour of materials. ASM, Vol. 61, 1968, pp 94 - 102.

6. MANSON, S.S., SPERA, D.A., HALFORD, G.H. The role of creep in high temperature low cycle fatigue. Chapter 12 in Advances in Creep Design, A.I. Smith of A.H. Nicholson, eds., Appl. Science Publ. Ltd., London 1971, pp 229 - 249.

7. DIETER, G.E. Jr. Mechanical Metallurgy, McGraw Hill, 1961.

8. HENRY, M.F., SOLOMON, H.D., COFFIN, L.F. A comprehensive characterization of the high temperature fatigue behaviour of A286. Int. Conf. on Creep and Fatigue in Elevated Temperature Applications 1973, Paper C182/73.

9. WELLS, C.H., SULLIVAN, C.P. The effect of temperature on the low cycle fatigue behaviour of Udimet 700. ASM, Transactions Quarterly 60, 1967, pp 217 - 222.

10. MANSON, S.S. Behaviour of materials under conditions of thermal stresses. NASA TN2932, 1952.

11. COFFIN, L.F. Jr. Fatigue at high temperature, ASTM STP520, American Society for Testing and Materials, 1973, pp 5 - 34.

12. STEPHENSON, N. Memo No. 320, National Gas Turbine Establishment, Pyestock, Hants, June 1958.

13. ORGAN, F.E., GELL, M. The effect of frequency on the elevated temperature fatigue of a nickel superalloy. Metallurgical Transactions, 2, 1971, pp 943 - 952.

14. TILLY, G.P. Fracture behaviour of two creep resistant materials subjected to cyclic loading at elevated temperature. Proc. Inst. Mech. Engrs., 1965 - 66, Part 1 No. 46, pp 405 - 1056.

15. NORTHWOOD, J.E., SMITH, R.S., STEPHENSON, N. Memo No. M325, National Gas Turbine Establishment, 1959.

16. ECKEL, J.F. The influence of frequency on repeated bending life of lead. Proc. Am. Test. and Materials, 1951, 51, pp 745 - 756.

17. COLES, A., HILL, G.J., DAWSON, R., WATSON, S.J. The high strain fatigue properties of low alloy creep resisting steels. Int. Conf. on Thermal and High Strain Fatigue, p 270, The Metals and Metallurgy Trust, London, 1967.

18. COFFIN, L.F. A note on low cycle fatigue laws. J. Materials, 1971, 6, pp 388 - 402.

19. COFFIN, L.F. A generalized equation for predicting high temperature low cycle fatigue including hold times. Proc. Conf. on Fatigue and Fracture of Aircraft Structures and Materials, Miami Beach, 1969, pp 301 - 309.

20. BERLING, J.T., SLOT, T. Effect of strainrate on low cycle fatigue resistance of AISI 304, 316 and 348 stainless steels at elevated temperature. Symp. on Fatigue at High Temperatures, 1968, ASTM465, pp 3 - 30.

21. SOLOMON, H.D. Frequency dependent low cycle fatigue crack propagation.
Metallurgical Transactions, 4, 1973, pp 341 - 377.

22. SOLOMON, H.D., COFFIN, L.F. Effects of frequency and environment on fatigue crack growth in A286 at 1100^{o}F. Fatigue at Elevated Temperatures, ASTM STP 520. Americal Society for Testing and Materials, 1973, pp 112 - 133.

23. COFFIN, L.F. Fatigue at high temperatures. J. of Fracture, Vol. 1, ICF4, Waterloo, Canada, June 1977, pp 19 - 24.

24. SHEFFLER, K.D. Vacuum thermal-mechanical fatigue testing of two iron bore high temperature alloys. NASA CR-134524, January 1974.

25. DAWSON, R.T., ELDER, W.J., HILL, G.T., PRICE, A.T. High strain fatigue of austenitic steels. The Thermal and High Strain Fatigue, The Metals and Metallurgy Trust, London 1967, pp 239 - 69.

26. BERLING, J.T., CONWAY, J.B. Effect of hold time on the low cycle fatigue resistance of AISI 304 stainless steel at 1200^{o}F. First Int. Conf. on Pressure Vessel Technology, Delft, 1969.

27. KREMPL, E., WUNDT, B.M. Hold-time effects in high-temperature low cycle fatigue, ASTM STP489, Americal Society for Testing and Materials, September 1971.

28. WAREING, J., TOMKINS, B., SUMMER, G. Extent to which materials properties control fatigue failure at elevated temperature. ASTM STP 520, 1973, pp 123 - 138.

29. JASKE, C., MINDLIN, H., PERRIN, J.S. Combined low cycle fatigue and stress relaxation of alloy 300 and type 304 stainless steel at elevated temperature. ASTM STP 520, pp 365 - 376.

30. CONWAY, J.B., BERLING, J.T., STENTZ, R.H. Strainrate and hold time saturation in low cycle fatigue. ASTM STP 520, 1973, pp 637 - 647.

31. GELL, M., LEVERANT, G.R. Mechanisms of high temperature fatigue. ASTM STP 520, 1973, pp 37 - 67.

32. CONWAY, J.B., BERLING, J.T. A new correlation of low cycle fatigue data involving hold periods. Metallurgical Transaction 1, (1), pp 324 - 5, January 1970.

33. JASKE, C., MINDLIN, H., PERRIN, J.S. Influence of hold time and temperature on the low cycle fatigue of Incoloy 800. J. of Eng. for Industry, Trans. of ASME, 94, 3, 1972, pp 930 - 4.

34. LORD, D.C., COFFIN, L.F. Low cycle fatigue hold-time behaviour of cast René 80. Met. Trans., 1973, 4, pp 1647 - 54.

35. COFFIN, L.F. Fatigue at high temperature, prediction and interpretation. Proc. J.M.E. Vol. 1889/74 pp 109 - 127.

36. ANNIS, C.G., VAN WANDERMANN, M.C., WALLACE, R.M. Strainrange partitioning behaviour of an automotive alloy. NASA CR 134974, 1976.

37. COFFIN, L.F. The influence of mean stress on the mechanical hysteresis loop of Al 1100. J. Bas. Eng. 1964, 86D, p 673.

38. YAMANOUCHI, H., ASADA Y, WAKMATSU, Y. Ratchetting under cyclic axial strain with torsional stress. Symp. on Fatigue at Elevated Temperature ASTM STP 520, 1973, pp 552 - 562.

39. CARDEN, A.E. Thermal fatigue evaluation. Manual on Low Cycle Fatigue Testing. ASTM STP 465, 1968, pp 163 - 188.

40. HIRSCHBERG, M.H. A low cycle fatigue testing facility. Manual on Low Cycle Fatigue Testing. ASTM STP 465, 1968, pp 67 - 86.

41. SHEFFLER, K.D. Vacuum thermal-mechanical fatigue testing of two iron bore high temperature alloys. NASA CR-134524, January 1974.

42. COFFIN, L.F.

Symposium on Creep-Fatigue Interactions - Winter Annual Meeting of American Society of Mechanical Engineers, New York, December 1976.

43. BURK, L.H., SULLIVAN, C.P. Fatigue of glass bead blasted Nickel-Base Superalloy. Metallurgical Transaction Vol. 1, 1970, pp 1595 - 1600.

44. SHEFFLER, K.D., DOBLE, G.S. Thermal fatigue behaviour of T111 and ASTAR 811C in ultra high vacuum. ASTM STP 520, 1973, pp 491 - 499.

45. HIRSCHBERG, M.H., HALFORD, G.R. Use of strainrange partitioning to predict high temperature low cycle fatigue. NASA TND8072, 1976.

46. HALFORD, G.R., HIRSCHBERG, M.H., MANSON, S.S. Temperature effects on the strainrange partitioning approach for creep fatigue analysis. ASTM STP 520, 1973, pp 658 - 667.

47. McMAHON, C.J., COFFIN, L.F. Mechanisms of damage and fracture of a cast nickel superalloy. Metallurgical Transactions, 1970, 1, pp 3443 - 3450.

48. HILL, C.J. The fatigue of wrought 1 Cr - Mo - V steels in reversed bending high strain fatigue at 550°C. International Conference on Thermal and High Strain Fatigue 1967, the Metals and Metallurgy Trust, London, pp 312 - 327.

49. COFFIN, L.F. The effect of high vacuum on the low cycle fatigue law. Metals Transactions 1972, 3, pp 1777 - 1788.

50. CHANG, W. Tensile embrittlement of turbine blades alloys after high temperature exposure. MCIC Report 72 - 10, September, 1972, PV-1.

51. FLEETWOOD, M.J. The distribution of chromium around grain boundary carbides in Nimonic 80A. J.I.M., 90, 1962, p 429.

52. MANSON, S.S. The challenge to unify treatment of high temperature fatigue - a partisan proposal based on strainrange partitioning. ASTM STP 520, 1973, pp 744 - 782.

53. COFFIN, L.F. A study of the effects of cyclic thermal stresses on a ductile metal. Trans. Am. Soc. Mech. Engrs., 1954, 76, pp 923 - 946.

54. MANSON, S.S. Behaviour of materials under conditions of thermal stresses. NASA TN 2933.

55. ASHBY, M.F. A first report on deformation mechanism maps . Acta Metal, Vol. 20, July 1972, pp 882 - 897.

56. MORROW, J., WETZEL, R.M., TOPPER T.H. Effects of environment and complex load history on fatigue life. ASTM STP 462, 1969, p 74.

57. MOWBRAY, D.F. and McCONNELEE, J.E. Cyclic stress-strain behaviour analysis, experimentation and failure prediction. ASTM STP 519, 1973.

58. HALFORD, G.R., NACHTIGALL, A.J. Strainrange partitioning behaviour of the nickel base superalloys, René 80 and IN 100. AGARD Conference Proceedings No. 243, Aalborg, 1978, pp 2-1 - 2-14.

59. MINER, M.A. Cumulative damage in fatigue. J. Appl. Mech., 12, 3, A159 - A167, September 1945.

60. COFFIN, L.F. Cyclic strain and fatigue behaviour of metals in the creep range. Int. Conf. Fracture - Senday Japan, 1965.

61. DORN, J.E. Creep and recovery, ASM, 1975, p 254.

62. COFFIN, L.F. Low cycle fatigue : a review. Appl. Mat. Research, 1962, 1, pp 129 - 141.

63. ZAMRIK, S.Y. The application of strainrange partitioning method to torsional creep fatigue interaction, NASA CR 134817, 1975.

64. LANDGRAF, R.W. The resistance of metals to cyclic deformation ASTM STP 467, pp 3 - 35.

65. HILL, P.T., LA FORCE, R., BERNING, R.F., COFFIN, L.F. High temperature low cycle fatigue behaviour of Tantalum. 1970 General Electric Report 70 - C207.

66. ALDRICH, J.N., AVERY, D.H. Alternating strain behaviour of a superplastic metal. 16th Sagamore Army Materials Research Conference. August 22, 1969.

67. HENRY, M.F., STOLOFF, W.F. High strain fatigue in a Ni(Cr) T_aC fibrous eutectic. Symposium on the Fatigue of Composite Materials, ASTM, 1973.

68. LEED, D. The role of plastic anisotropy in the fatigue behaviour of zircalloy. Metals Trans. 1972, 3, pp 315 - 322.

69. SWINDEMAN, R.W. Low cycle fatigue study of Colombim alloy D-43. Symposium on Fatigue at High Temperatures, 1968, ASTM STP 459, pp 31 - 41.

70. SHEFFLER, K.D., DOBLE, G.S. Influence of creep damage on the low cycle thermal mechanical fatigue behaviour of two tantalum base alloys. NASA CR121001, 1972.

71. BASQUIN, O.H. The exponential law of endurance tests. Proc. Am. Soc. Test. Mater., 1910, 10, pp 625 - 630.

72. SMITH, R.N., HIRSCHBERG, M.H., MANSON, S.S. Fatigue behaviour of materials under strain cycling in low and intermediate life range. NASA TND 1574.

73. COTTRELL, A.H., HULL, D. Extrusion and intrusion by cyclic slip in copper. Proc. Roy. Soc. (London), Vol. 242A, 1957, pp 211 - 213.

74. GROSSKREUTZ, J.C. Fatigue mechanisms in the subcreep range. Metal Fatigue Damage Mechanism, Detection Avoidance and Repair. ASTM STP 495, pp 5 - 60.

75. MANSON, S.S., HIRSCHBERG, M.H. Fatigue behaviour in strain cycling in the low and intermediate cycle range. Fatigue - An Inter-Discipliniary Approach ed. by J.J. Bruise, N.C. Reed Weiss. Syracuse University Press, 1974, pp 133 - 173.

76. MANSON, S.S., HAFERD, A.M. A linear time-temperature relation for intrapolation of creep and stress rupture data, NACA TN 2890.

77. BERLING, J.T., CONWAY, J.B. A new approach to the prediction of low cycle fatigue data. Met. Trans. 1 (1), April, 1970, pp 805 - 809.

78. COFFIN, L.F. The effect of frequency on the cyclic strain and low cycle fatigue behaviour of Cast Udimet 500 at elevated temperature. Met. Trans. 12, September 1971, pp 3105 - 13.

79. ELLISON, E.G., PATTERSON, A.G.F. Creep-fatigue interactions in 1 Cr Mo V steel. The Institute of Mechanical Engineers, 190, 1976, p 333.

80. COFFIN, L.F.

Proc. International Conference on Materials. Boston, 1976, p 866.

81. LEVEN, M.M. The interaction of creep and fatigue for a rotor steel. Exp. Mech., September 1973, pp 353 - 371.

82. HYZAK, J.M., BERNSTEIN, H.L. An analysis of the low cycle fatigue behaviour of the superalloy Rene 95 by strainrange partitioning. AGARD Conference Proceeding No. 243, Aalborg, 1978, pp 11-1, 11-25.

83. DAY, M.F., THOMAS, G.B. Creep-fatigue interaction in alloy IN738LC AGARD Conference Proceedings No. 243, Aalborg, 1978, pp 10-1, 10-13.

84. ANTUNES, V.T.A., HANCOCK, P. Strainrange partitioning of MARM002 over the temperature range 750°C - 1040°C. AGARD Conference Proceedings No. 243, Aalborg, 1978, pp 5-1 - 5-9.

85. OSTERGREN, W.J. A damage function and associated failure analysis for predicting hold time and frequency effects in elevated temperature low cycle fatigue. Journal of Testing and Evaluation, Vol. 4, No. 5. September 1976, pp 327 - 339.

86. ROBINSON, E.L. Effect of temperature variation on the long-time rupture strength of steels. Transactions of ASME, Vol. 74, No. 5, July 1952, pp 777 - 781.

87. TAIRA, S. Lifetime of structures subjected to varying load and temperature. Creep in Structures, Hoff Nicholas, Academic Press, New York, 1962, pp 96 - 124.

88. ASME Boiler and Pressure Vessel Code, Case Interpretations Code Case 1592, The American Society of Mechanical Engineers, New York, 1974.

89. CAMPBELL, R.D. Creep-fatigue interaction correlation for 304 stainless steel subjected to strain controlled cycling with hold times at peak strain. Journal of Engineering for Industry, Transactions of the ASME Vol. 93, No. 4, November 1971, pp 887 - 892.

90. GITTUS, I.H. Implications of some data on relaxation creep in Nimonic 80A. Phil. Mag. 1964, 9, pp 749 - 753.

91. POLHEMUS, J.F., SPAETH, C.E., VOGEL, W.H. Ductility exhaustion model for prediction of thermal fatigue and creep interaction. ASTM STP 520. pp 628 - 636.

92. MANSON, S.S., HALFORD, G.R., HIRSCHBERG, M.H. Creep-fatigue analysis by strainrange partitioning. NASA TMX 67838, 1971.

93. CHABOCHE, J.L., POLICELLA, H., KACZMAREK, H. Applicability of the SrP method and creep-fatigue damage approach to to LCHTF LIFE prediction of IN-100 alloy. AGARD Conference Proceedings No. 243, Aalborg, 1978, pp 4-1 - 4-20.

94. AGARD Conference Proceedings No. 243 - Characterization of low cycle high temperature fatigue by the strainrange partitioning method, Aalborg, April 1978.

95. KACHANOV, L.M. Time of the rupture process under creep conditions I2V.ANAD.NAUK.SSR. Otd Tekh. NAUN No. 8, 1958, pp 26 - 31.

96. RABOTNOV, Y.N. Creep problems in structural members. North Holland Pub. Comp. Amsterdam-London, 1969.

97. CHABOCHE, J.L. Une loi differencielle d'endommagement de fatigue avec cumulation non lineaire. Revue Francaise de Mecanique. N50-51, 1974.

98. LECKIE, F.A., HAYHURST, D.R. Creep rupture of structures. Proc. Royal Soc. of London, Vol. 340, No. 1622, 1974, pp 323 - 347.

99. HIRSCHBERG, M.H., HALFORD, G.R. Strainrange partitioning - a tool for characterizing high temperature low cycle fatigue, NASA TMX-71691, 1975.

100. MANSON, S.S., HALFORD, C.R., NACHTIGALL, A.J. Separation of the strain components for use in strainrange partitioning. NASA TMX 71737, 1975.

101. HALFORD, G.R. Cyclic creep rupture behaviour of 3 high temperature alloys. NASA TN-D 6309, 1971.

102. SPERA, D.A. Comparison of experimental and theoretical thermal lives for 5 Ni bore alloys. ASTM STP 520, 1973, pp 648 - 657.

103. ELLISON, E.G. Strainrange partitioning in cyclic creep of 1 Cr Mov. steel. AGARD Conference Proceedings N1. 243, Aalborg, 1978, pp 14-1 - 14-19.

104. MAYES, P. PhD Thesis, Cranfield Institute of Technology, 1973.

105. BADDELLEY, D. Cyclic creep of a nickel base superalloy. MSc Thesis, Cranfield Institute of Technology, 1975.

106. CLIFTON, T.E. Creep and fatigue studies of Nimonic 108. Cranfield Institute of Technology, Cranfield. Memo 94, Part 1.

107. GELL, M. DUGUETTE, D.J. Corrosion fatigue. National Association of Corrosion Engineering, 1973.

108. LARSON, F.R., MILLER, J. A time temperature relationship for rupture and creep stress. Trans. of the ASME, July 1952, pp 765 - 775.

109. ORR, R.L., SHERBY, O.D., DORN, J.E. Correlations of rupture data for metals at elevated temperatures. Trans. of the ASM, Vol. 46, 1954, pp 113 - 127.

110. NOWACK, H. Strainrange partitioning applied to Ti-6A1-4V AGARD Conference Profeedings No. 243, Aalborg, 1978, pp 13-1 - 13-12.

111. HARRISON, G.F., WEAVER, M.J. The low cycle fatigue behaviour of Nimonic 90 at elevated temperature. AGARD Conference Proceedings No. 243, Aalborg, 1978. pp 6-1 - 6-19.

112. HALFORD, G.R., SALTSMAN, J.F., HIRSCHBERG, M.H. Ductility normalized - strainrange partitioning life relations for creep-fatigue predictions. NASA TM 73737, 1977.

113. TAIRA, S., FUJINO, M. Studies on thermal fatigue fracture of metallic materials. J. of the Soc. of Materials Science Japan, Vol. 25, No. 270, March 1976, pp 218 - 229.

114. WELLS, C.H., SULLIVAN, C.P., GELL, M. Mechanisms of fatigue in the creep range. Metal Fatigue Damage - Mechanism, Detection, Avoidance and Repair, ASTM STP 495, 1971, pp 61 - 122.

115. COFFIN, L.F.

in Proceedings of the Air Force Conference on Fracture and Fatigue of Aircraft Structures, AFDL TR 70-144, Air Force Development Laboratory, Dayton, Ohio, 1970, p 301.

116. ANTUNES, V.T.A., M.Sc. Thesis, Cranfield Institute of Technology, 1976.

PAGE
NUMBERS
CUT OFF
IN
ORIGINAL

Table 4.II - Tensile Properties of MARM002

Test No	Specimen Identification	Temp (°C)	Strain Rate ($\%s^{-1}$)	UTS (MN/m^2)	0.2 YLD Stress (MN/m^2)	Reduction of area (%)	Elongation (%)
8	NJ 14/3	20	0.2	1068	940	10	8
1	NJ 26/1	850	0.2	889	785	15	10
5	NJ 13/1	850	3.2	1116	868	13	9
3	NJ 25/5	1040	0.2	462	365	23	10
6	NJ 25/3	1040	3.5	756	703	16	8
7	NJ 18/1	1040	6.5	840	340	7	6

Table 4.III - Creep Properties of MARM002

Temperature	Stress (MN/m^2)	Time to Failure (hr)	Strain at Fracture (%)
850	590	4.8	6.3
850	464	25.7	3.0
1040	200	3.9	4.8
1040	185	4.7	4.4.

Temperature (°C)	Stress (MN/m^2) for Failure in *	10 hrs	100 hrs	1000 hrs
750		815	735	590
800		730	590	440
850		580	435	325
900		437	330	217
950		320	233	138
1000		223	158	91
1050		146	101	58

* Data supplied by NGTE

Table 4.IV - Data for the cyclic curves of MARM002 at 750°C, 850°C and 1040°C

Test	Temperature (°C)	$\Delta\varepsilon p$ (%)	$\Delta\sigma$ (MN/m^2)	$\log \frac{\Delta\varepsilon p}{2}$	$\log \frac{\Delta\sigma}{2}$	n'	b	k'
7A	750	0.018	622	-3.745	2.794	0.244		
8A	750	0.016	565	-3.796	2.752		3.69	
9A	750	0.052	771	-3.284	2.887			4.91×10^3
10	850	0.019	490	-3.710	2.690	0.277		
13	850	0.085	716	-3.071	2.855		3.71	
18	850	0.013	415	-3.903	2.618			5.14×10^3
21	1040	0.090	343	-3.046	2.535	0.319		
22	1040	0.031	292	-3.502	2.465		3.52	
24	1040	0.017	457	-2.767	2.660			33.31×10^3
25	1040	0.022	212	-3.657	2.326			

$$\frac{\Delta\sigma}{2} = k' \left(\frac{\Delta\varepsilon p}{2}\right)^{n'} \qquad \log \frac{\Delta\sigma}{2} = \log k' + n' \log \frac{\Delta\varepsilon p}{2}$$

$$b = \log k'$$

TABLE 4.V — BASIC LOW CYCLE FATIGUE TESTS

Test No.	Specim. Identif.	Temp. (°C)	Cycle Definition	Total Strain $\Delta\varepsilon_T$(%)	Inelastic Strain $\Delta\varepsilon_i$(%)	F_{ij} of $\Delta\varepsilon_{ij}/\Delta\varepsilon_{in}$ PP	PC	CP	CC	Cycles to Failure N	N_{ij} (4)	Tensile Stress (MN/m^2)	Mean Stress (MN/m^2)	Stress Range $\Delta\sigma$ (MN/m^2)	Time to Failure (hr)
10	NJB2/1	850	PP-0.6Hz	0.685	0.039	1	-	-	-	825	825	447	-43	980	0.4
13	NJB2/2	850	PP-0.6Hz	1.065	0.170	1	-	-	-	220	220	754	+37	1432	0.1
14	NJB25/4	850	PP-0.6Hz	2.02	0.844	1	-	-	-	10	10	1102	+33	2146	0.005
18	NJB1/2	850	PP-0.6Hz	0.544	0.025	1	-	-	-	1790	1790	420	+ 4	831	0.8
19	NJB2/3	850	PP-0.6Hz	0.304	0.004	1	-	-	-	10960	10960	325	0	650	5
21	NJB1/3	1040	PP 1 Hz	0.705	0.180	1	-	-	-	370	370	320	-24	686	0.1
22	NJB15/1	1040	PP 1 Hz	0.502	0.067	1	-	-	-	1640	1640	292	0	584	0.5
24	NJB3/3	1040	PP 1 Hz	0.977	0.341	1	-	-	-	95	95	443	-14	914	0.03
25	NJB3/1	1040	PP 1 Hz	0.349	0.044	1	-	-	-	4600	4600	202	-10	423	1.3
37	NJB6/4	850	CP(1)	0.600	0.063	0.15	-	0.85	-	1896	3050	351	-187	1076	11.2
30	NJB5/2	850	CP	0.731	0.092	0.27	-	0.73	-	1076	2744	377	-169	1091	6.4
29	NJB5/1	850	CP	0.996	0.220	0.30	-	0.70	-	166	169	480	-189	1338	1
39	NJB4/1	850	CP	0.863	0.094	0.27	-	0.73	-	805	1306	430	-191	1243	4.9
40	NJB4/2	1040	CP	0.402	0.124	0.25	-	0.75	-	451	412	161	-53	507	2.6
26	NJB3/4	1040	CP	0.724	0.279	0.27	-	0.73	-	88	77	245	-94	577	0.5
27	NJB3/2	1040	CP	0.538	0.153	0.36	-	0.64	-	347	313	172	-79	502	2
32	NJB5/5	850	PC(2)	1.000	0.211	0.32	0.68	-	-	92	76	940	+142	1595	0.5
33	NJB5/4	850	PC	0.707	0.074	0.38	0.62	-	-	408	363	723	+143	1160	2.5
38	NJB6/1	850	PC	0.487	0.011	0.09	0.91	-	-	1261	1182	574	+156	842	7.8
31	NJB5/3	1040	PC	0.928	0.515	0.30	0.70	-	-	53	57	531	+123	816	0.3
34	NJB6/2	1040	PC	0.550	0.177	0.26	0.74	-	-	402	435	414	+109	610	2.3
42	NJB4/5	1040	PC	0.315	0.066	0.39	0.61	-	-	1985	1965	311	+102	417	11.6
35	NJB6/3	850	CC(3)	0.796	0.211	0.30	-	0.16	0.54	180	188	573	+47	1262	2
44	NJB7/2	850	CC	0.489	0.052	0.05	-	0.05	0.90	1326	1304	467	+27	880	15
47	NJB7/5	850	CC	0.586	0.113	0.26	-	-	0.74	571	776	477	+14	925	6.6
36	NJB6/5	1040	CC	0.891	0.456	0.29	-	0.01	0.70	57	56	310	+11	597	0.6
41	NJB4/4	1040	CC	0.700	0.350	0.26	-	0.04	0.70	119	147	293	+5	575	1.4
45	NJB7/2	1040	CC	0.398	0.200	0.12	-	0.08	0.80	502	769	147	-6	308	5.8
46	NJB7/4	1040	CC	0.297	0.121	0.08	-	0.13	0.79	1237	1885	141	-8	295	14
6A	NJB14/4	750	PP	0.573	0.00(6)	1	-	-	-	9614	7395	520	+22	995	5.4
7A	NJB13/3	750	PP	0.771	0.036	1	-	-	-	1516	1099	656	+34	1244	0.8
8A	NJB14/2	750	PP	0.648	0.032	1	-	-	-	1977	1246	607	+41	1129	1
9A	NJB12/1	750	PP	0.872	0.104	1	-	-	-	327	356	753	-18	1543	0.2
10A	NJB12/3	750	PC	0.600	0.016	0.50	-	0.50	-	1674	1589	613	+76	1073	10
11A	NJB12/4	750	CP	0.670	0.040	0.45	0.55	-	-	2173	2010	429	-101	1060	11.3
12A	NJB13/4	750	CC	0.700	0.048	0.66	-	-	0.34	1377	1021	614	+24	1191	15.8
1B	NJB9/4	950	PP	0.664	0.155	1	-	-	-	511	403	461	+18	886	0.15
2B	NJB9/5	950	PC	0.423	0.072	0.57	0.43	-	-	1511	1594	415	+129	552	8.7
4B	NJB9/3	950	CC	0.360	0.086	0.16	-	0.07	0.77	1996	3290	217	0	434	21

(1) Stress Dwells of approximately 20 seconds (Tension).

(2) Stress Dwells of approximately 20 seconds (Compression)

(3) Stress Dwells of approximately 20 seconds (Tension and Compression)

(4) $\frac{1}{N} = \Sigma \frac{F_{ij}}{N_{ij}}$

Table 4.VI - Transition fatigue leves for several alloys

Material	Temperature (^{o}C)	UTS MN/m^2 (1)	Ductility (%) (2)	$N_t - N_{t_{10}}$ (3)	$N(10^{-4})$ (4)	Order of Decreasing Damage	Source
316 Stainless Steel	705	390	102	>4385 - 960,000	182,580	CP-CC-PC-PP	(35)
1Cr-1Mo-$\frac{1}{4}$V steel	565	500($0.4\%s^{-1}$)	160	1,912 - 53,800	~100,000	CP-PC-CC-PP	(103)
Titanium Alloy (Ti6A14V)	450	729	67	302 - 6,770	89,470	PC-PP-CP-CC	(110)
IN100	925	622	10	24 - 9,742	5,390	PC-CP-PP-CC	(58)
Nimonic 90	810	712($10\%mm^{-1}$)	22	249 - 17,581	25,840	PC,CP-CC-PP	(111)
RENE 95	650	1,448	13	72 - 1,322	2,650	PC-CC-CP-PP	(82)
CA101	927	638	8	2 - 146	1,713	PC-PP-CC-CP	(36)
IN738LC	850	885	4	7 - 664	~10,000	PC-PP-CP,CC (5)	(83)
MARM002	850	889($0.2\%s^{-1}$)	16	16 - 518	1,657	PC-PP-CC-CP	
MARM002	1040	482($0.2\%s^{-1}$)	26	17 - 8,512	45,019	PC,CP,PP-CC	

(1) When available, strainrate indicated in brackets.

(2) As defined by $\ln \frac{100}{100 - RA}$ where RA - Reduction of area.

(3) Two lives are indicated N_t - transition fatigue life; life for a PP loop $\Delta\varepsilon_p = \Delta\varepsilon_e$

$N_{t_{10}}$ - life for a PP loop $\Delta\varepsilon_p = \frac{\Delta\varepsilon_e}{10}$

$\Delta\varepsilon_p$ - plastic strain

$\Delta\varepsilon_e$ - elastic strain

(4) The smallest of the $N_{ij} = N_{ij}(\Delta\varepsilon_{ij})$ lives for an inelastic strainrange of 10^{-4}.

(5) Non partitioned data.

Table 4.VII - Complementary SrP tests

Test	Specimen Identification	Cycle Definition	Temp (°C)	Total Strain (%)	Inelastic Strain (%)	F_{ij} F_{pp}	F_{pc}	F_{cp}	F_{cc}	N_f	N_{ij} (2)	Tensile Stress (MN/m^2)	Mean Stress	Stress Range	Time Failure (hrs)
13A	NJB14/5	PP-1Hz	850	0.578	0.030	1.00	–	–	–	1483	1483	544	+ 9.5	1070	0.42
1C	NJB10/5	$CC_{(1)}$	1040	0.400	0.168	0.12	–	–	0.88	382	387	173	+13.5	319	31
3B	NJB9/1	$PC_{(1)}$	850	0.427	0.010	0.30	0.70	–	–	2675	2302	538	- 113	849	23

(1) - Stress dwells of approximately three minutes

(2) - $\frac{1}{N_{obs.}} = \Sigma \frac{F_{ij}}{N_{ij}}$

Table 6.I - Comparison of the relative position of the basic SrP lines for several alloys

Material	Temperature (°C)	Order of Decreasing Damage (Inelastic Strain Level 10^{-3})
Rene 80 case	871	PC-CP-CC-PP
IN 100 gatorized	760	PC-PP-CC-CP
IN 100 cast	925	PC-PP-CP-CC
Nimonic 90	810	PC,CP-CC-PP
Waspalloy	750	PC-CC,CP-PP
IN738LC	850	PC,PP-CP,CC
Rene 95	650	PC-CC,CP-PP
Narloy Z*	538	CP-CC-PC-PP
AMZIRC*	538	CP-CC-PC-PP
Ti-6Al--4V	450	PC-PP-CP-CC
1 CrMoV steel	565	CP-PC-CC-PP
316 stainless steel	705	CP-CC-PC-PP
2¼ Cr - 1Mo	595	PC-CC-CP,PP
A286	595	CP-PC-CC-PP
H 13 steel	595	PC-PP,CC,CP
T111	1150	CP-CC-PC-PP
MARM002	850	PC-PP-CC-CP
MARM002	1040	CP,PC,PP-CC
CA 101	927	PC-PP-CC-CP

* Tested in Argon

TABLE 7.I - 5% drop in tensile load data for MARM002

Test No	Test Type	N_f	N_5	$N_p = N_f - N_5$	N_5/N_p
3B	PP 850°C	2673	2100	573	3.70
7A	PP 750°C	1516	1000	516	1.90
33	PC 850°C	408	200	208	0.96
10A	PC 750°C	1674	1020	654	1.56
6A	PP 750°C	9614	8410	1204	6.98
22	PP 1040°C	1640	700	940	0.75
21	PP 1040°C	370	75	295	0.25
2B	PC 950°C	1511	500	1011	0.50
34	PC 1040°C	402	100	302	0.33

Table 7.II - Basic data for the mixed tests

Test Type	Spec. Ident.	Temp. (°C)	Cycle	$\Delta\varepsilon_1$ (%)	$\Delta\varepsilon_{i1}$ (%)	$\Delta\sigma$ MN/m^2	N_1	N_{p1}	Temp. (°C)	Cycle	$\Delta\varepsilon_2$ (%)	$\Delta\varepsilon_{i2}$ (%)	$\Delta\sigma$ MN/m^2	N_2	N_{p2}
1E	NJB 27/6	850	PP	0.777	0.048	1158	350	809	850	CP	0.785	0.114	1005	341	552
2E	NJB 27/5	850	CP	0.691	0.111	1078	250	550	850	PP	0.788	0.124	1295	397	295
3E	NJB 27/1	850	PP	0.566	0.033	1126	500	1206	1040	PP	0.567	0.127	626	403	579
4E	NJB 27/4	1040	PP	0.487	0.129	587	515	563	850	PP	0.418	0.006	714	1132	6792
5E	NJB 27/2	850	PP	0.763	0.041	1140	590	952	850	CP	0.756	0.102	1034	208	651
6E	NJB 27/3	850	PP	0.769	0.042	1149	770	904	850	CP	0.731	0.108	984	32	583
7E	NJB 27/1	850	PP	0.773	0.046	1155	180	850	850	CP	0.762	0.103	1042	598	604
8E	NJB 15/2	850	CP	0.769	0.109	1043	340	562	850	PP	0.992	0.110	1394	314	334
9E	NJB 15/6	850	CP	0.792	0.114	1072	415	514	850	PP	0.969	0.097	1378	149	382
10E	NJB 15/8	850	PP	0.665	0.032	1000	390	1222	1040	PP	0.565	0.116	620	604	679
11E	NJB 15/5	850	PP	0.691	0.035	1038	630	1145	1040	PP	0.578	0.126	625	268	582
12E	NJB 15/3	1040	PP	0.562	0.115	617	360	683	850	PP	0.509	0.013	785	1263	3322
13E	NJB 15/7	1040	PP	0.559	0.114	614	210	704	850	PP	0.534	0.020	813	1166	2011
14E	NJB 15/4	1040	PP	0.608	0.132	658	80	541	850	PP	0.527	0.018	802	1332	2221

$\Delta\varepsilon_1$ - Total strain on the first part of the mixed tests.

$\Delta\varepsilon_2$ - Total strain on the second part of the mixed tests.

$\Delta\varepsilon_i$ - Inelastic strain.

$\Delta\sigma$ - Stress range.

Table 7.III - Exhausted lives for the mixed tests

Test No.	Type	N_1	N_{p1}	N_1/N_{p1}	N_2	N_{p2}	N_2/N_{p2}	$1-N_2/N_{p2}$
1E	PP_{850} + CP_{850}	350	809	0.43	341	552	0.62	0.38
5E	PP_{850} + CP_{850}	590	952	0.62	208	651	0.32	0.68
6E	PP_{850} + CP_{850}	770	904	0.85	32	583	0.05	0.95
7E	PP_{850} + CP_{850}	180	850	0.21	598	604	0.99	0.01
2E	CP_{850} + PP_{850}	250	550	0.45	397	295	1.34	0
8E	CP_{850} + PP_{850}	340	562	0.60	314	334	0.94	0.06
9E	CP_{850} + PP_{850}	415	514	0.81	149	382	0.39	0.61
3E	PP_{850} + PP_{1040}	500	1206	0.41	403	579	0.69	0.31
10E	PP_{850} + PP_{1040}	390	1222	0.32	604	679	0.89	0.11
11E	PP_{850} + PP_{1040}	630	1156	0.55	268	582	0.46	0.54
4E	PP_{1040} + PP_{850}	515	563	0.91	1132	6792	0.17	0.83
12E	PP_{1040} + PP_{850}	360	683	0.53	1263	3322	0.38	0.62
13E	PP_{1040} + PP_{850}	210	704	0.30	1166	2011	0.58	0.42
14E	PP_{1040} + PP_{850}	80	541	0.15	1332	2221	0.60	0.40

Table 7.IV - Predicted versus observed lives of some basic SrP tests

Test No.	Type	Temperature (°C)	$N_{pred.}$	$N_{obs.}$
10	PP	850	1009	825
13	PP	850	210	220
18	PP	850	1620	1790
19	PP	850	11383	10960
21	PP	1040	320	370
22	PP	1040	1957	1640
24	PP	1040	99	95
25	FP	1040	4227	4600
37	CP	850	2243	1896
30	CP	850	886	1076
29	CP	850	159	166
39	CP	850	854	805

$N_{obs.}$ - Observed lives.

$N_{pred.}$ - Predicted lives using the Strainrange vs. Life Relationships reported on Chapter 4.

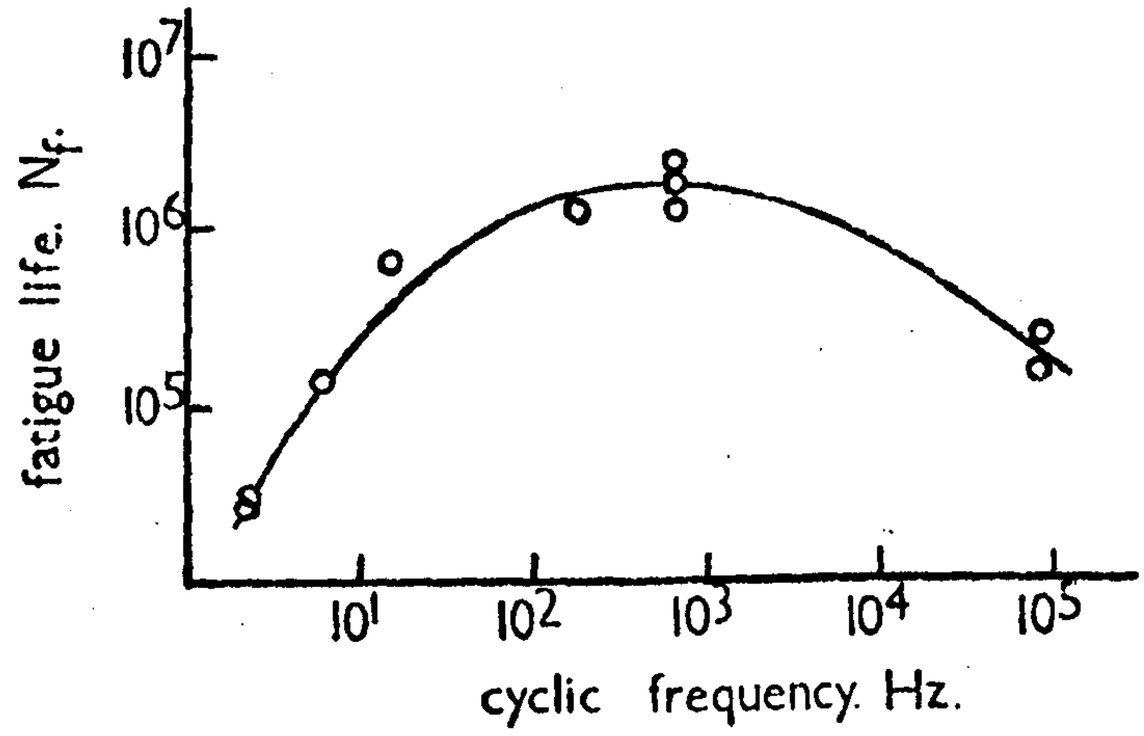

Figure 2.1 The effect of frequency on the fatigue life of wrought Udimet 700 at 760°C (13)

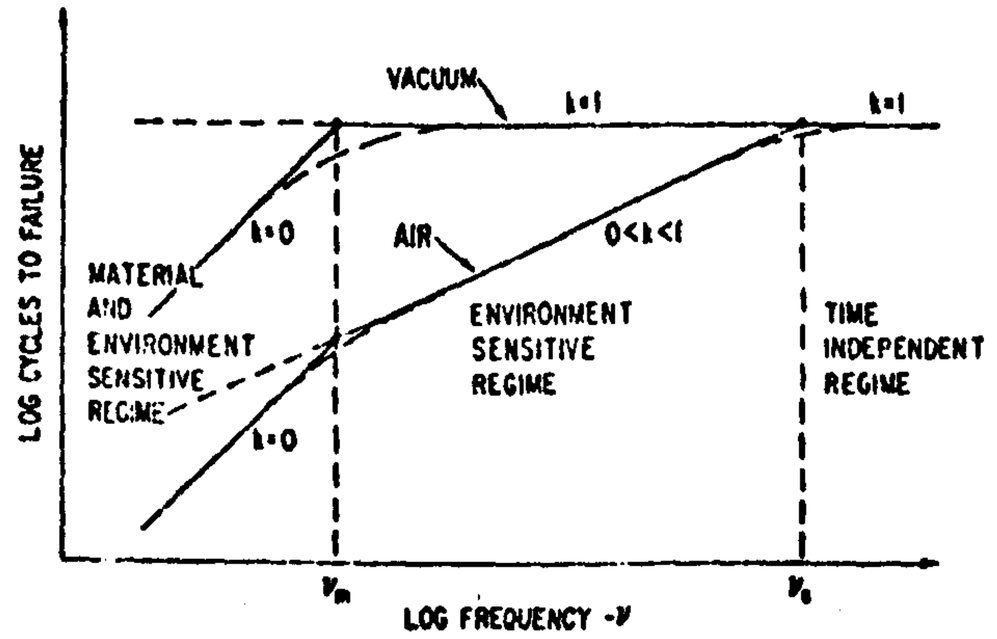

Figure 2.2 Model of effect of frequency on fatigue life at constant inelastic strainrange at high temperatures (22)

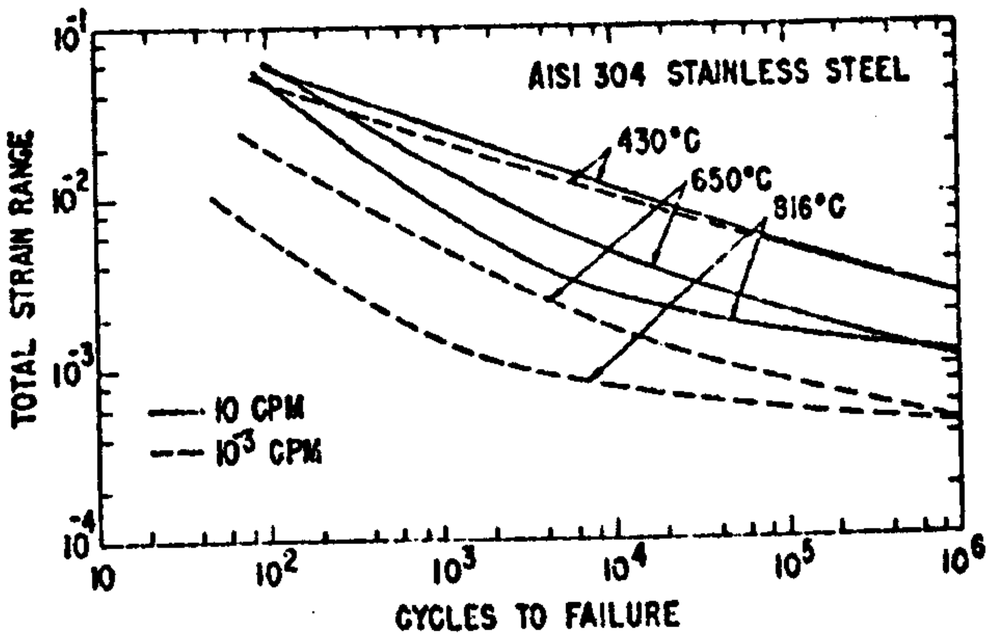

Figure 2.3 Effects of frequency on life of 304 stainless steel at 430, 650 and 816°C. (24)

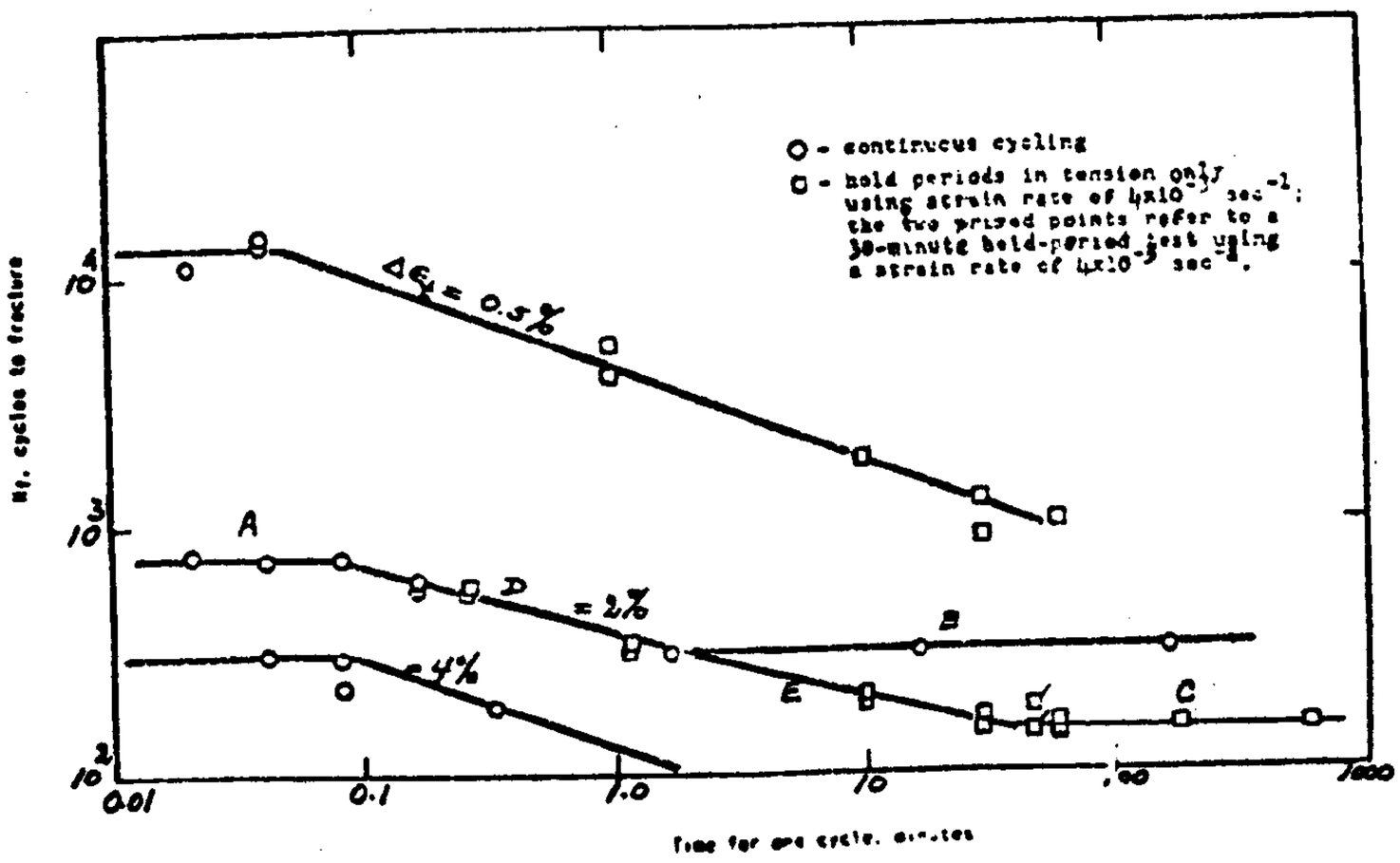

Figure 2.4 Plot of N_f versus cycle time of AISI 304 tested in air at 650°C (30)

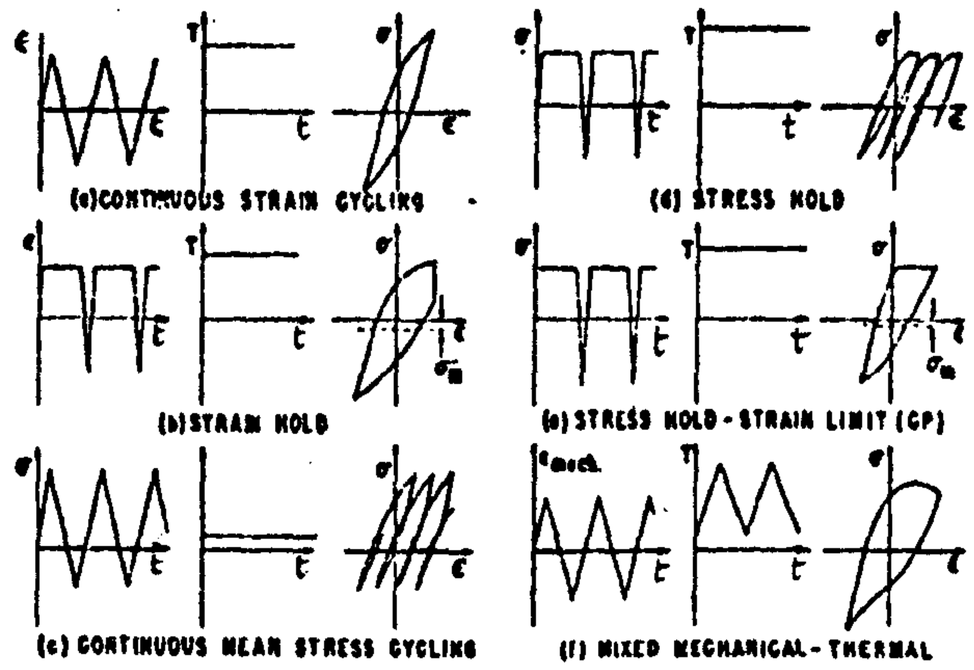

Figure 2.5 WAVE SHAPES which can be produced in close loops testing for life prediction testing

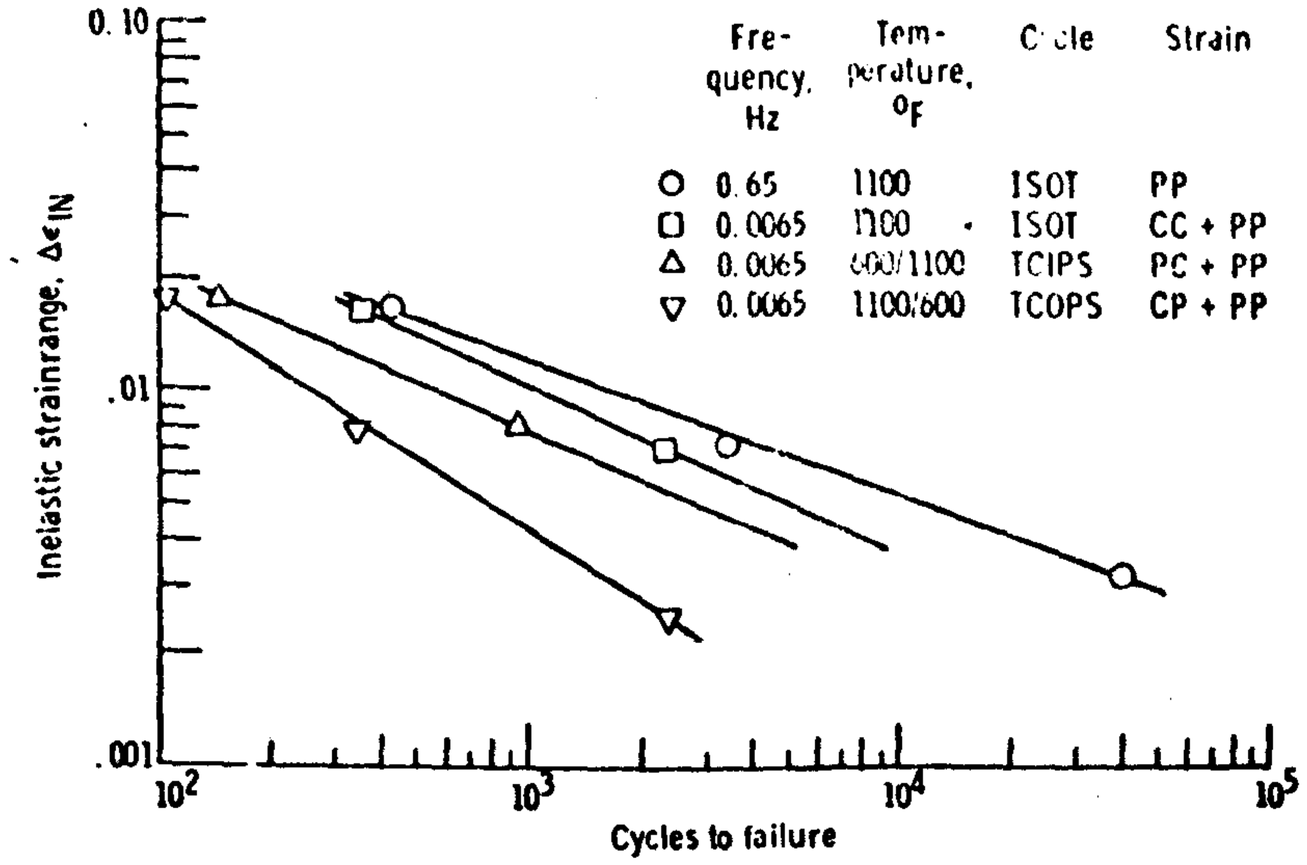

Figure 2.6 Inelastic strain effects in high vacuum during low cycle fatigue of aged A286 (41)

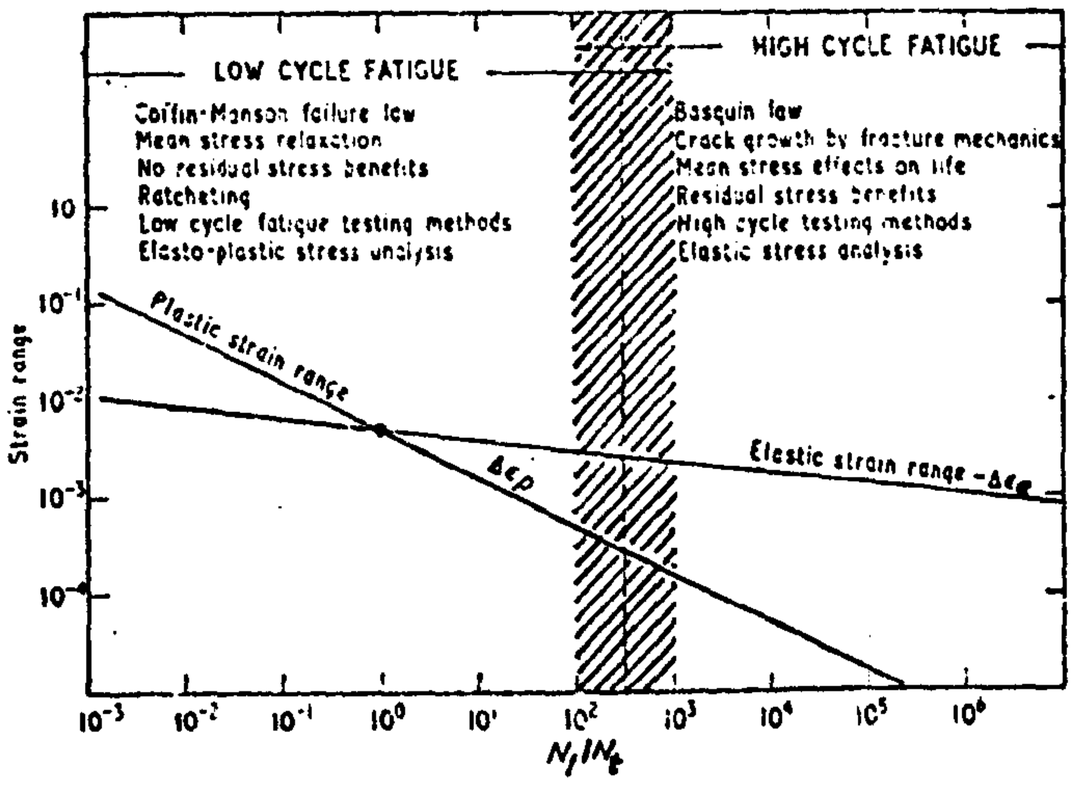

Figure 2.7 Identification of high and low cycle fatigue regimes using the transition fatigue life

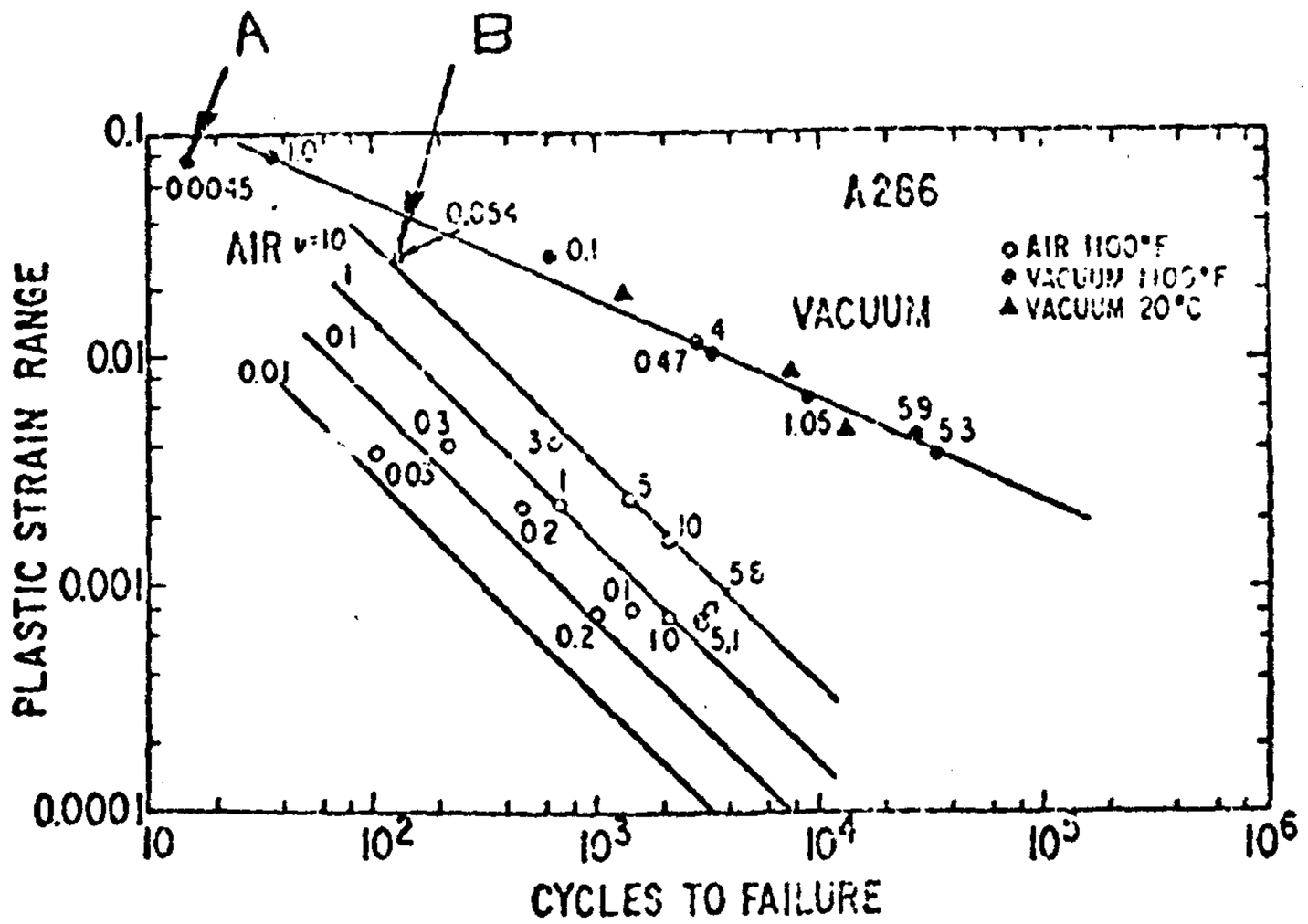

Figure 2.8 Inelastic strainrange versus fatigue life for A286 in air and vacuum at 593°C (55)

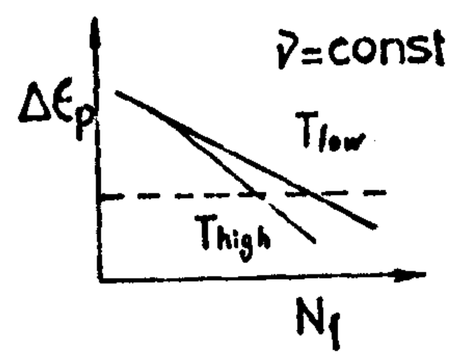

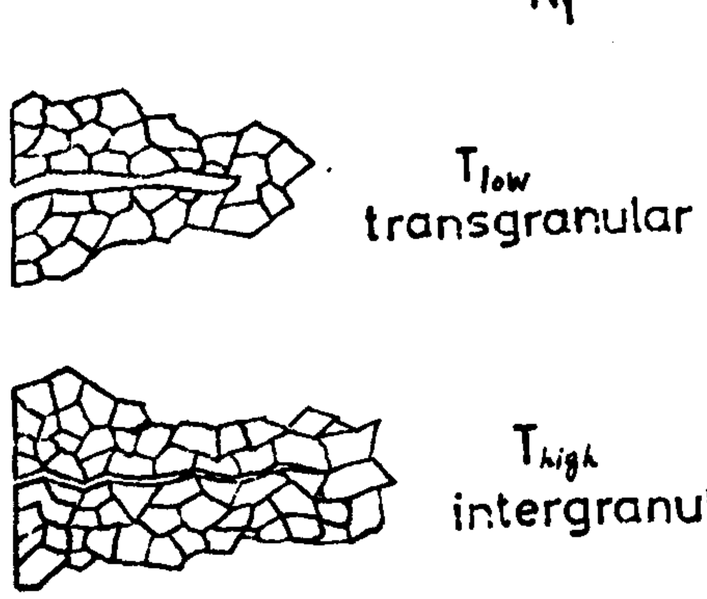

Figure 2.9 Schematic representation of fracture mode change with temperature and plastic strainrange

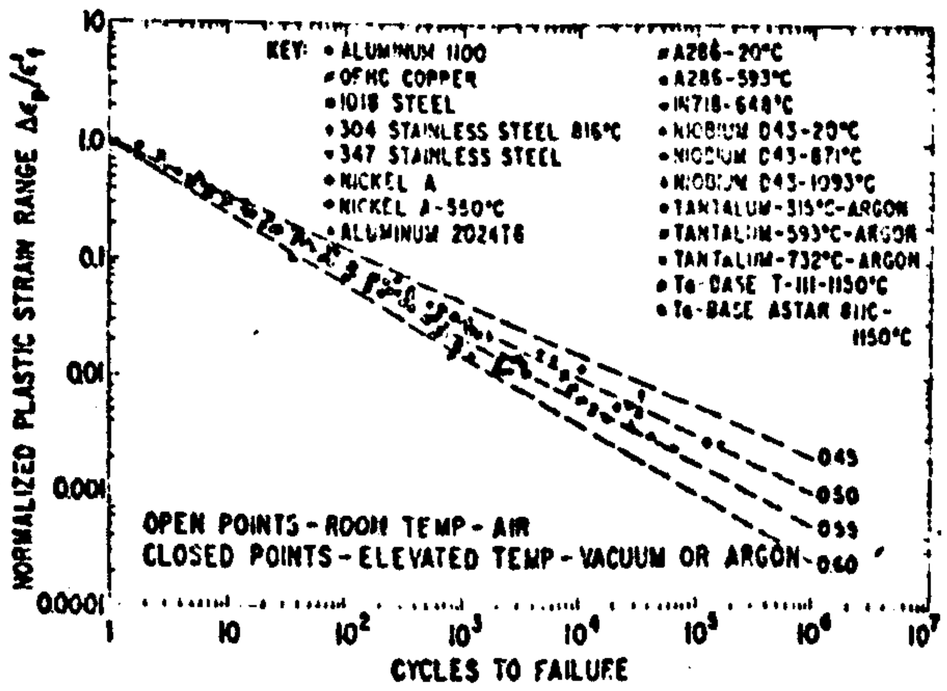

Figure 2.10 Summary plot of plastic strainrange versus cycles to failure for several metals in vacuum or argon. The plastic range is normalized to fatigue ductility (23)

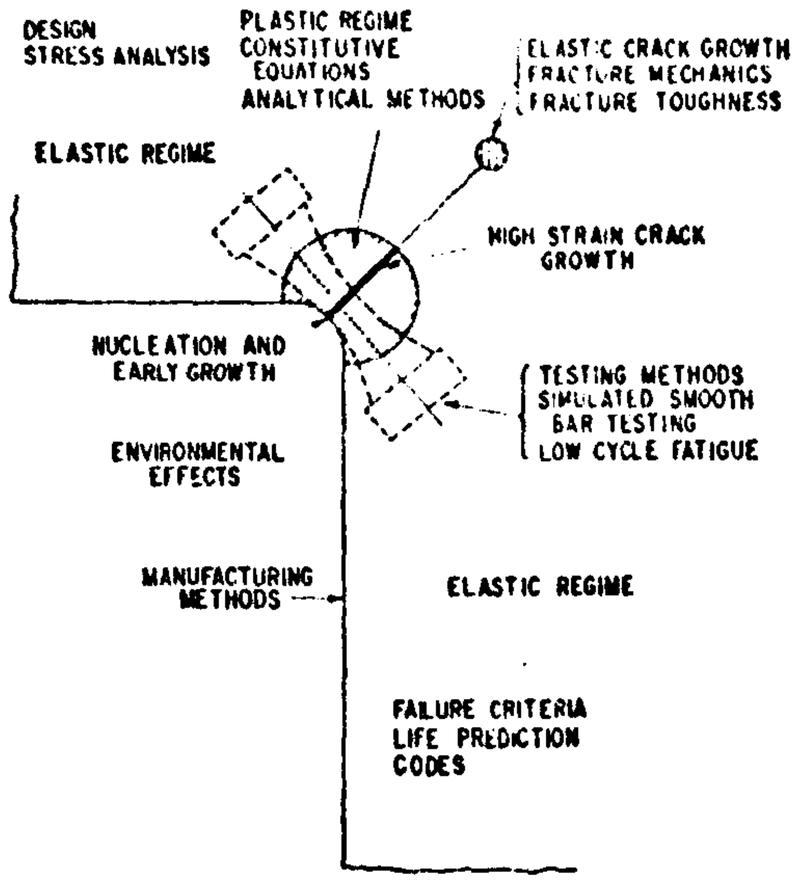

Figure 2.11 Model for crack initiation and propagation

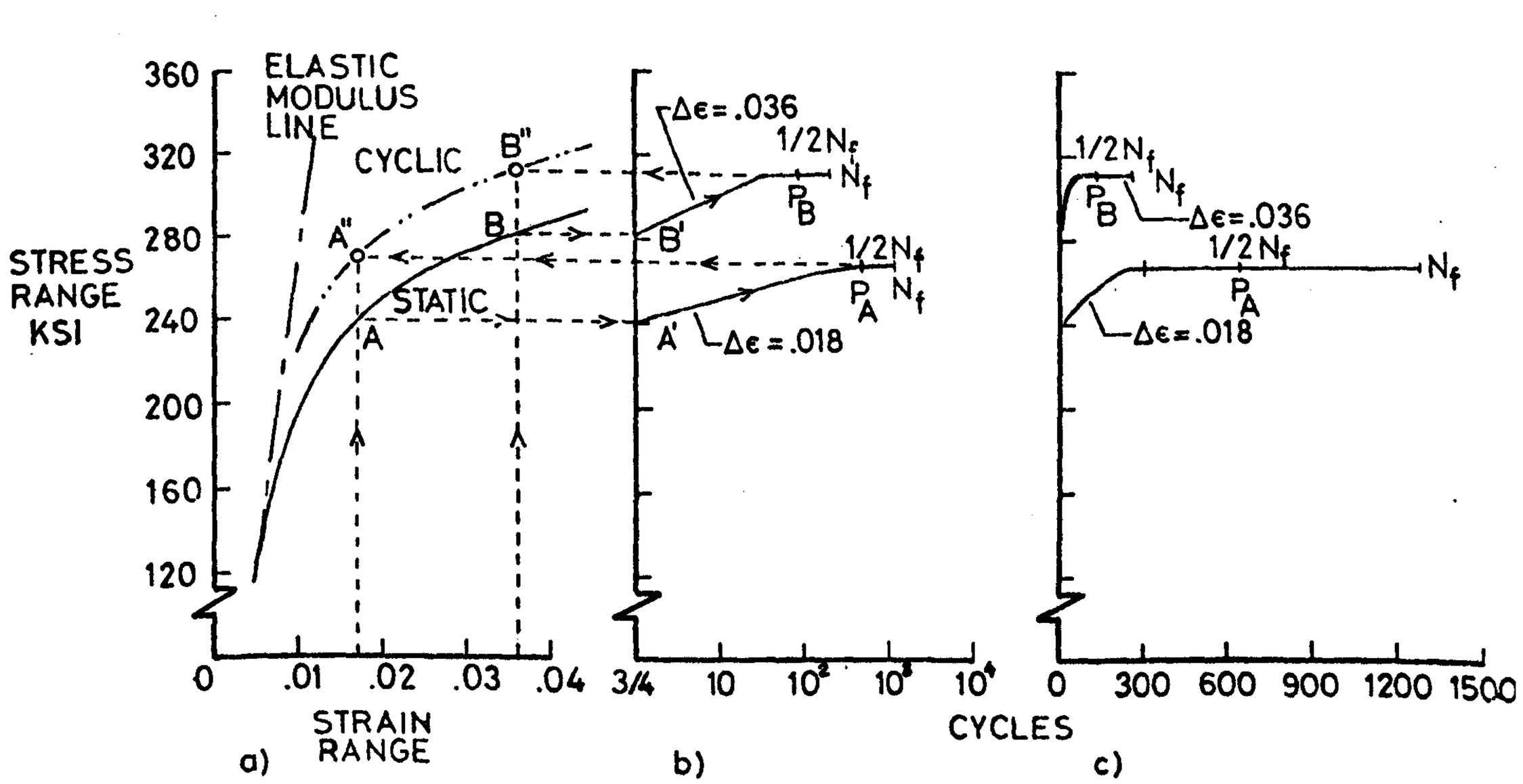

Figure 2.12 STATIC and cyclic stress characteristics of a hypothetical cyclic strain hardening material

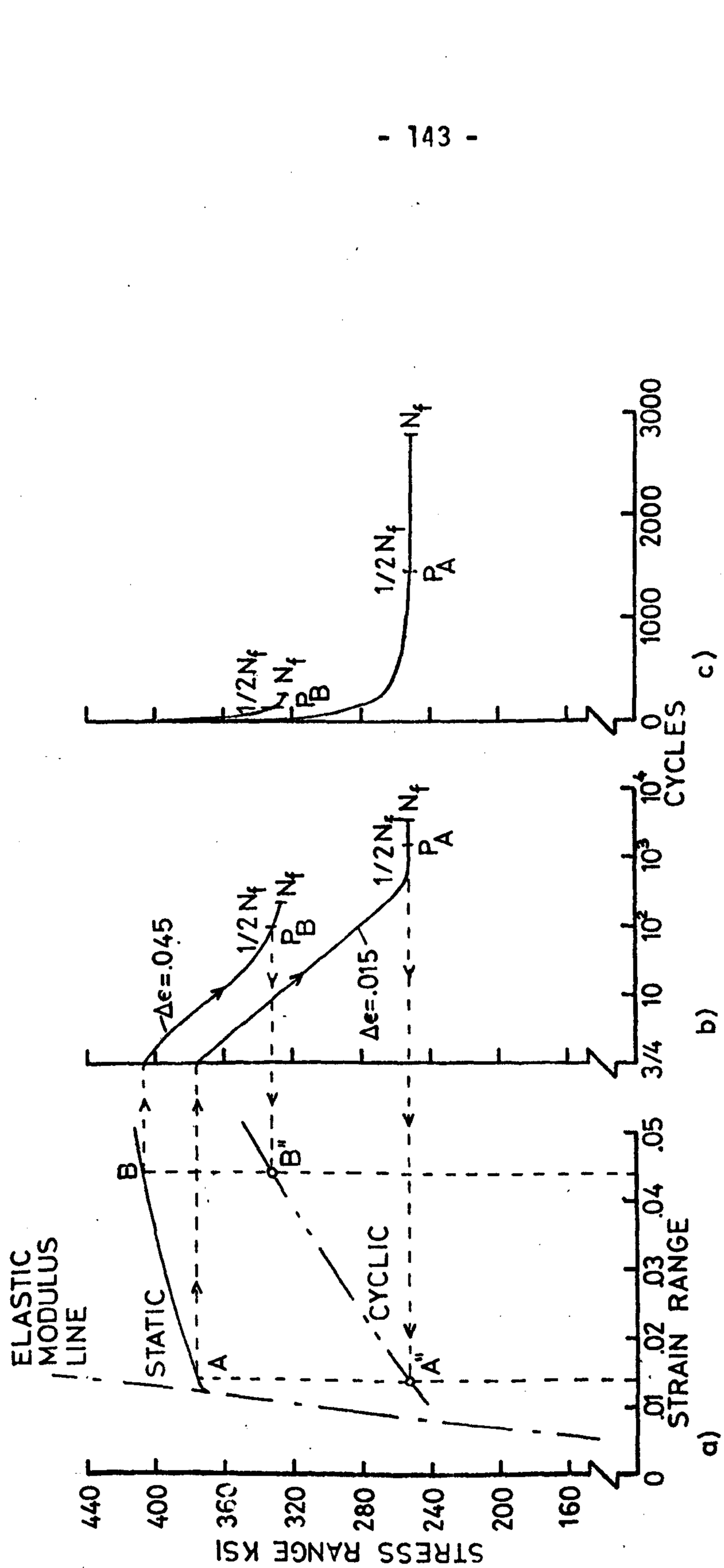

Figure 2.13 STATIC and cyclic stress characteristic of a hypothetical cyclic strain softening material

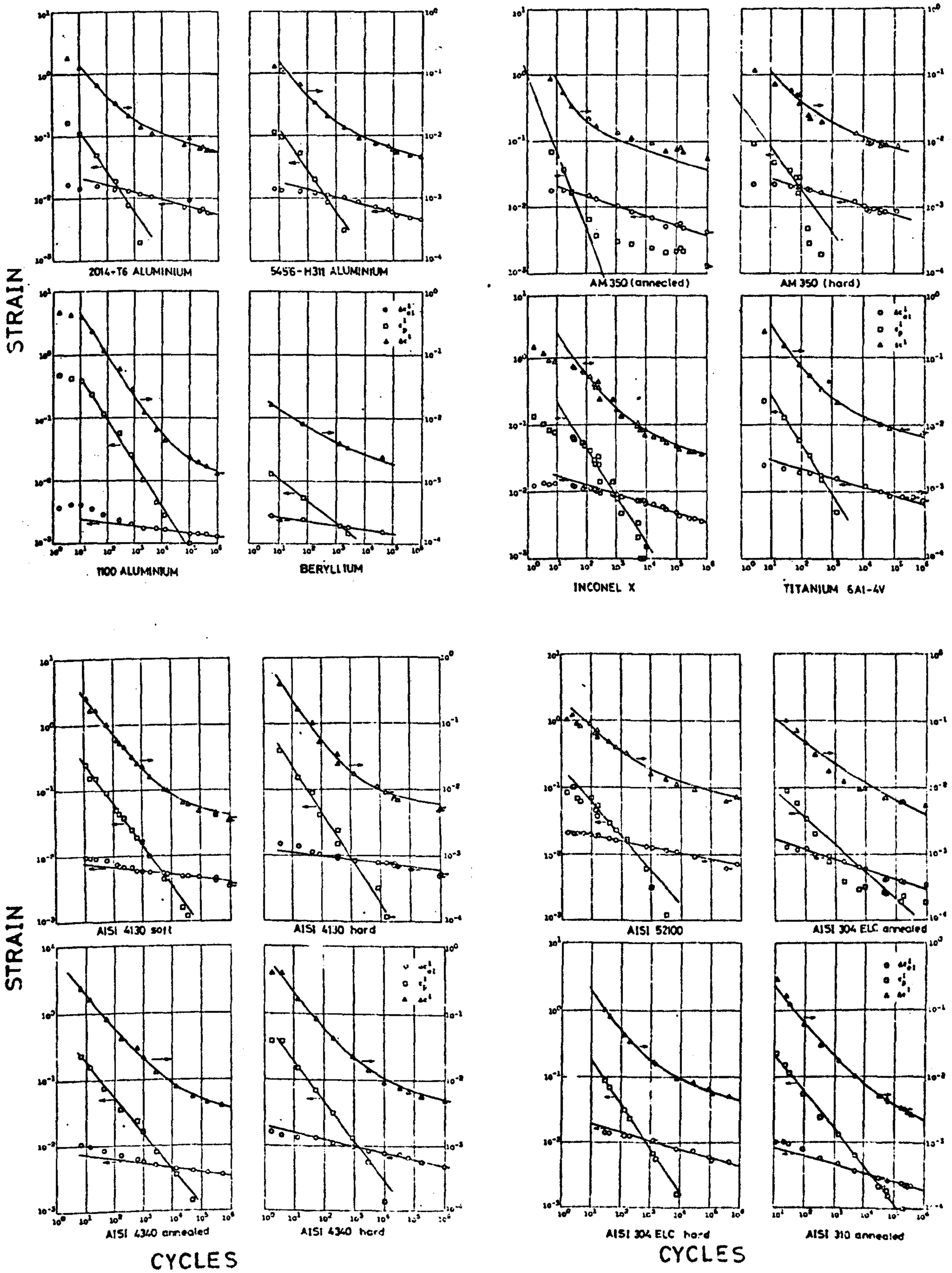

FIG. 2.14 - ELASTIC, PLASTIC AND TOTAL STRAINRANGE VARIATIONS WITH CYCLIC LIFE FOR 16 ALLOYS AT ROOM TEMPERATURE (72).

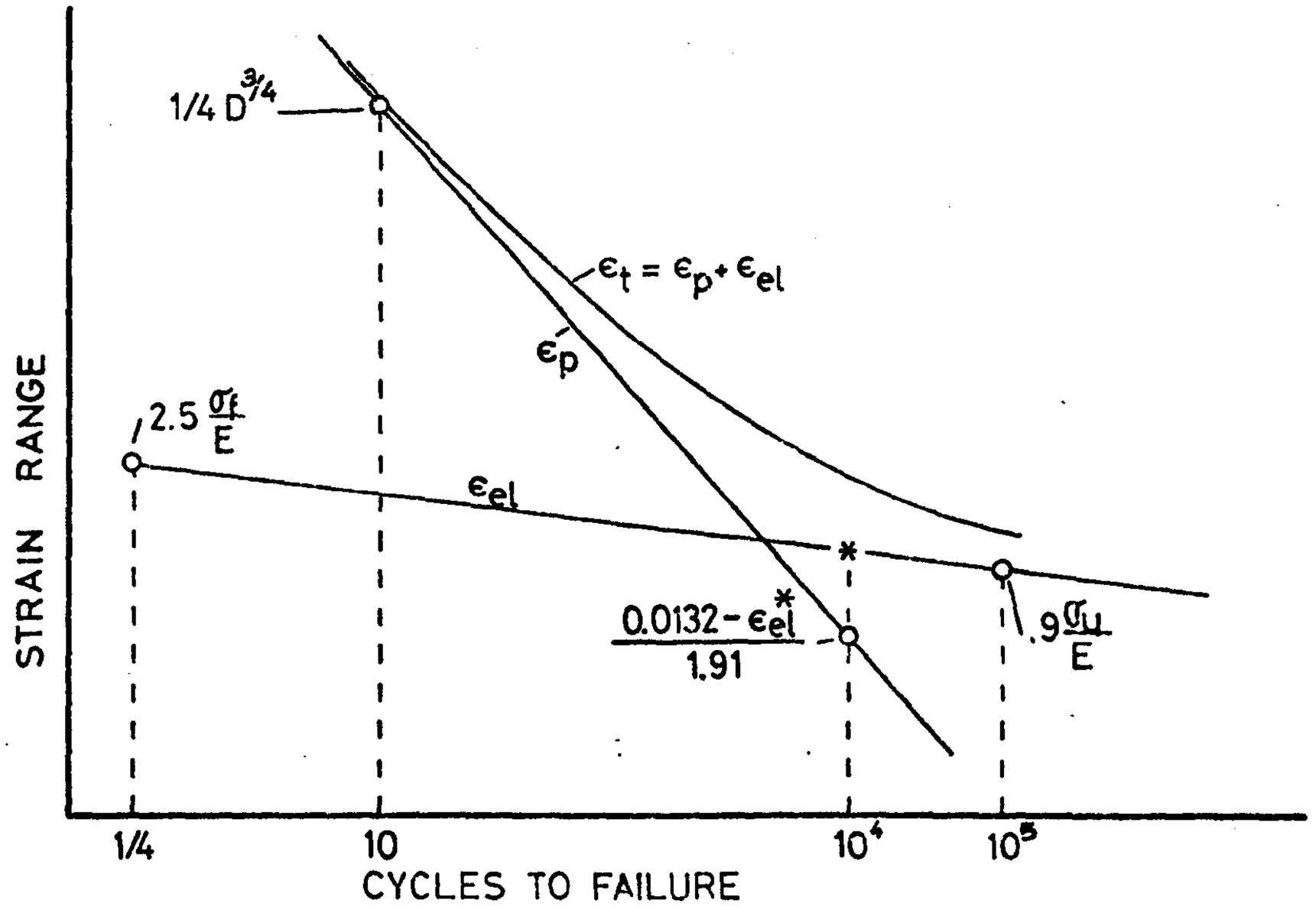

Figure 2.15 Model for the four point correlation method (3)

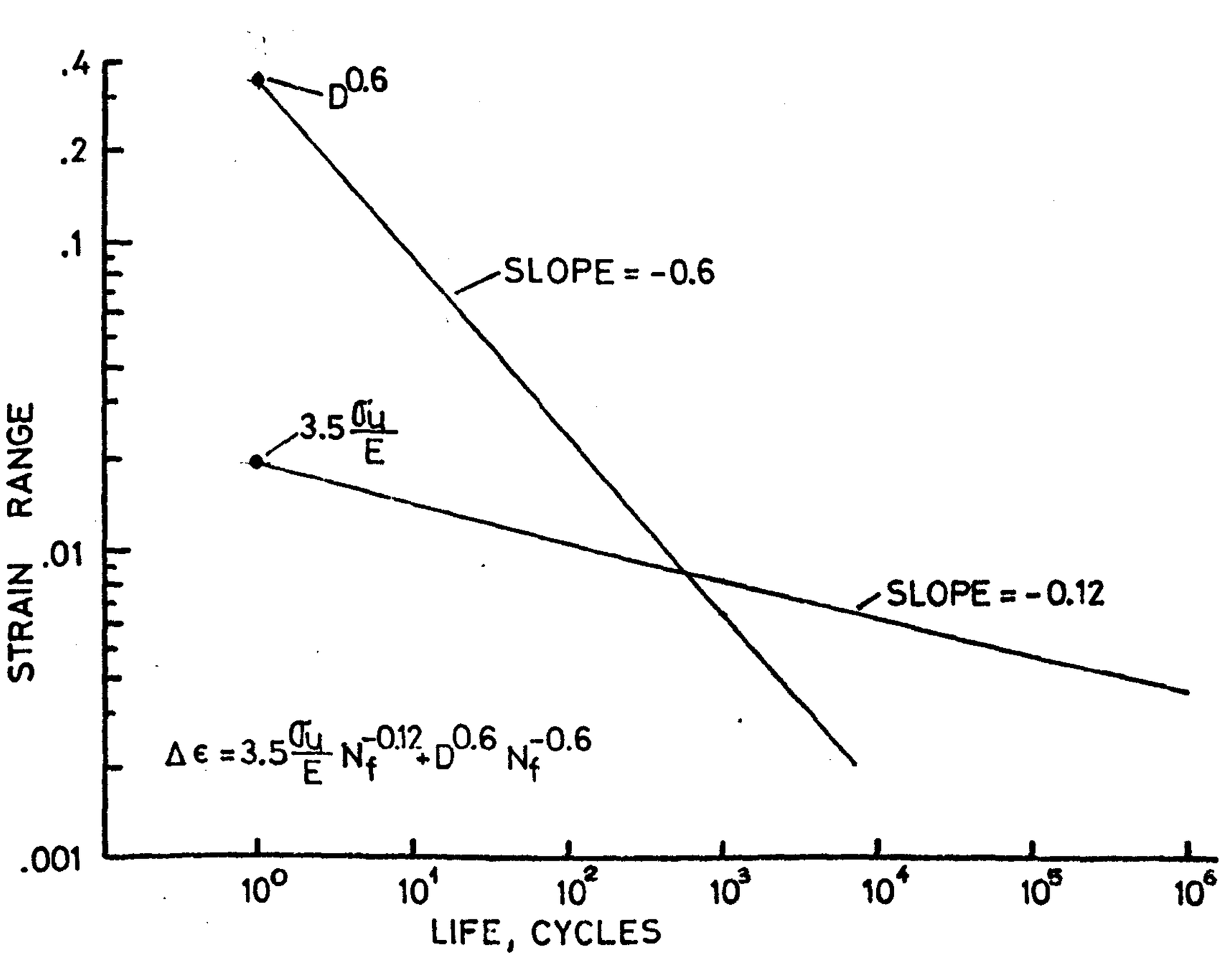

Figure 2.16 Model for the method of the universal slopes

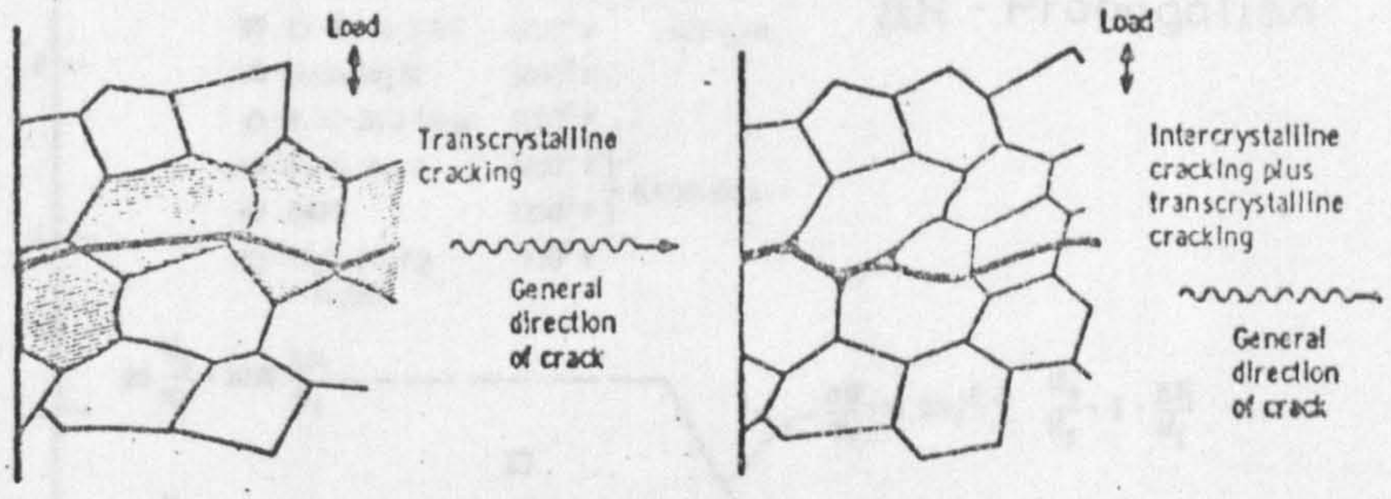

Figure 2.17 Illustration of a high temperature crack initiation hypothesis

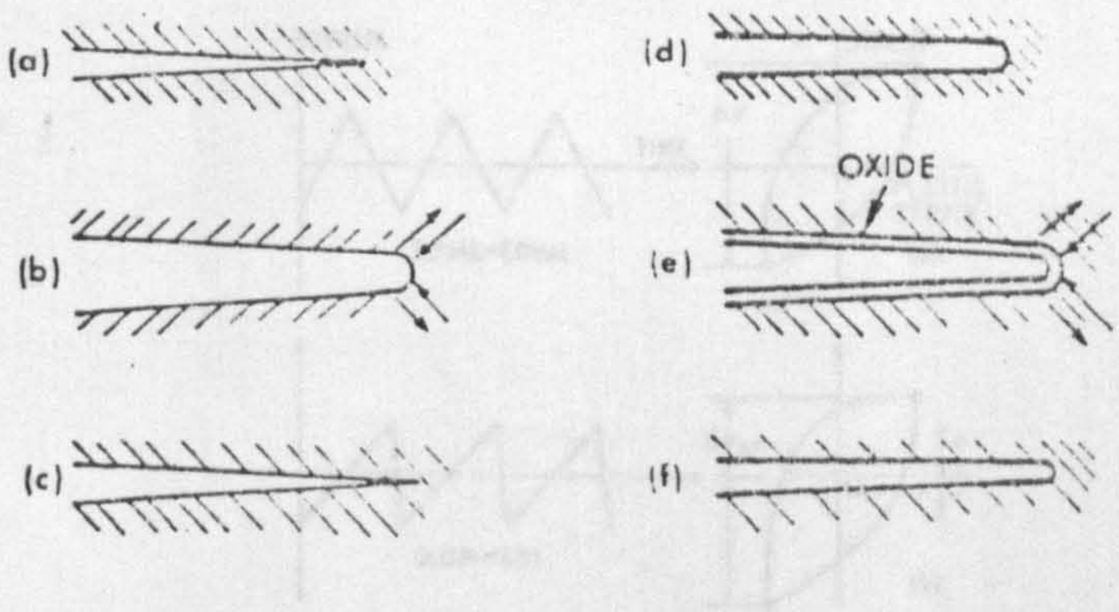

Figure 2.18 Schematic drawing of Stage II crack growth in vacuum (a,b,c) and air (d,e,f) (107)

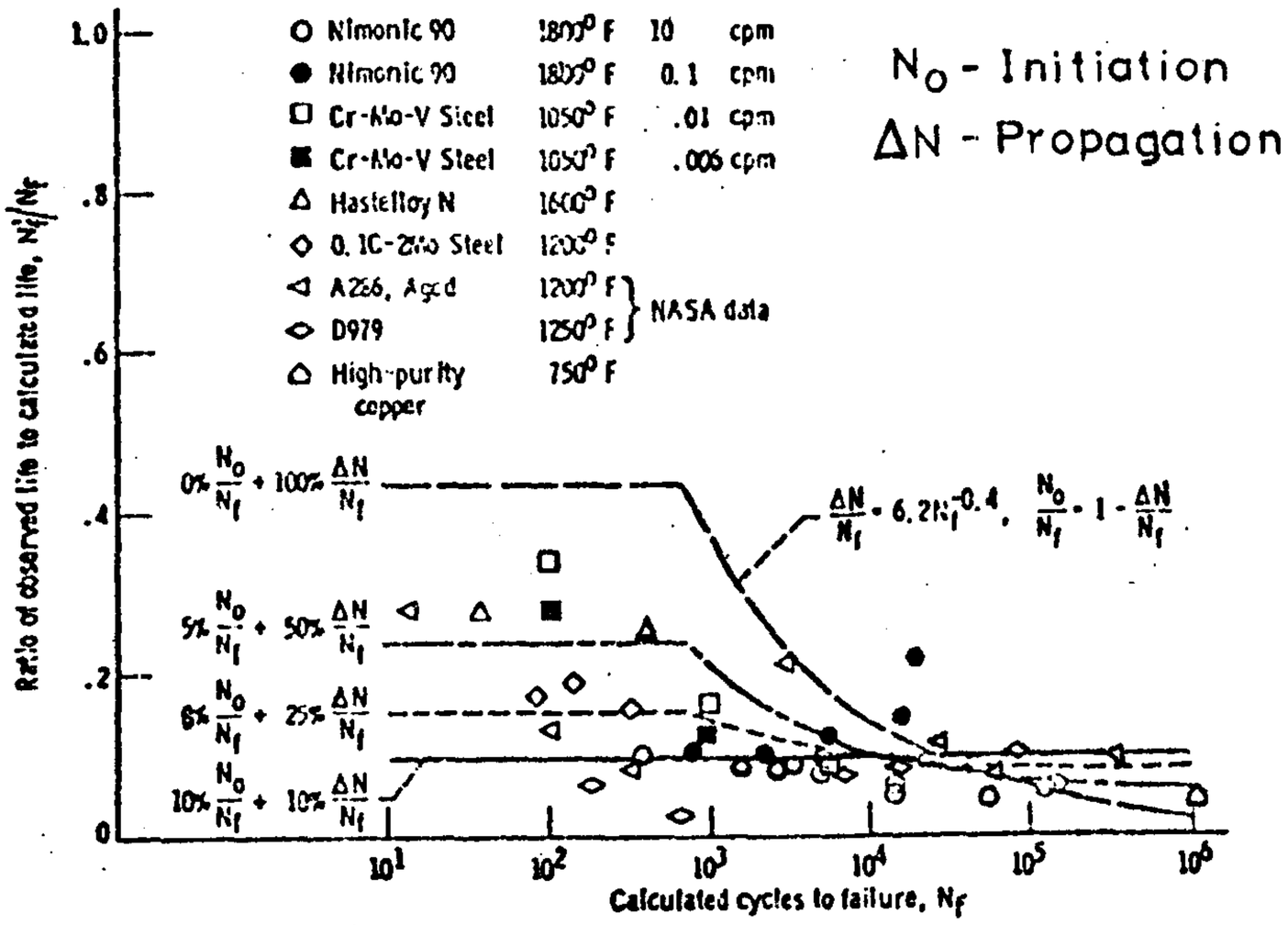

Figure 2.19 High temperature fatigue data and life prediction curves (4)

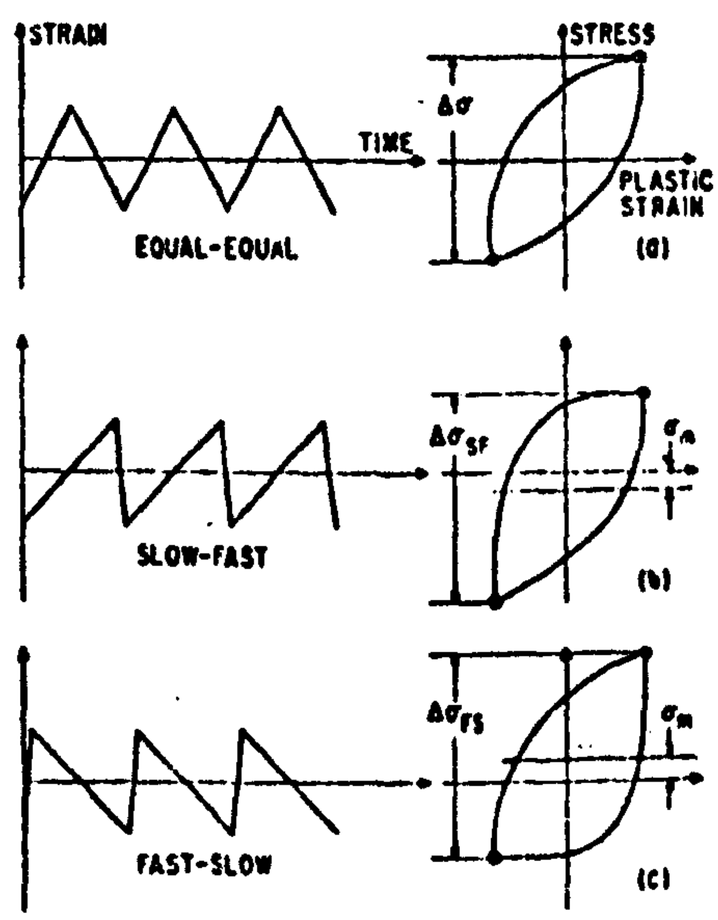

Figure 2.20 Hysteresis loops resulting from various isothermal wave shapes

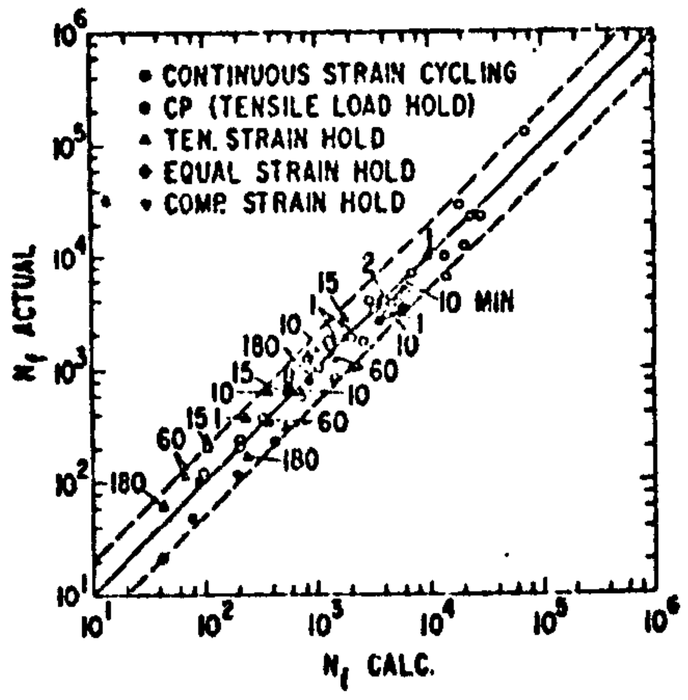

Figure 2.21 Comparison of actual and predicted lives for AISI 304 stainless steel at 595°C (42)

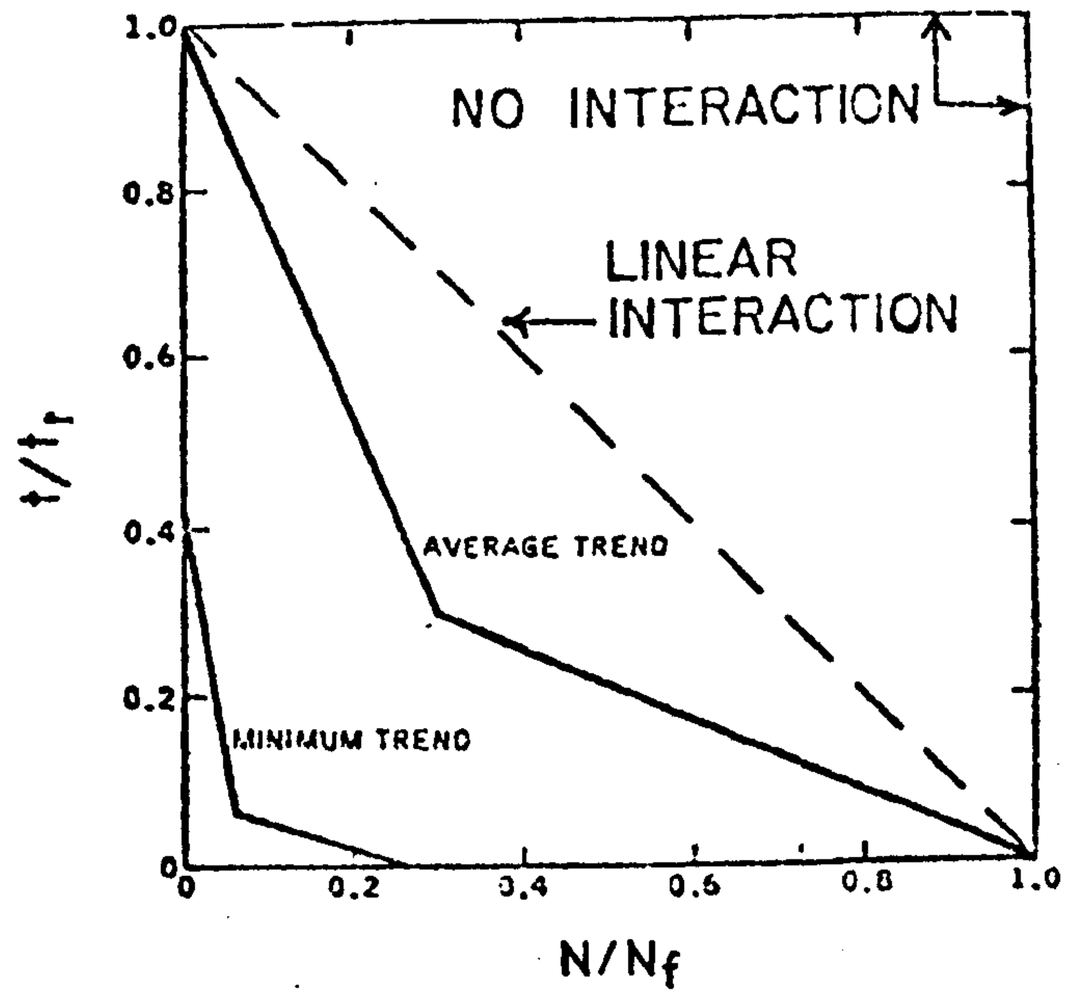

Figure 2.22 Creep fatigue damages interaction plot showing no interaction lines but the linear interaction line the average trend and minimum trend lines (89)

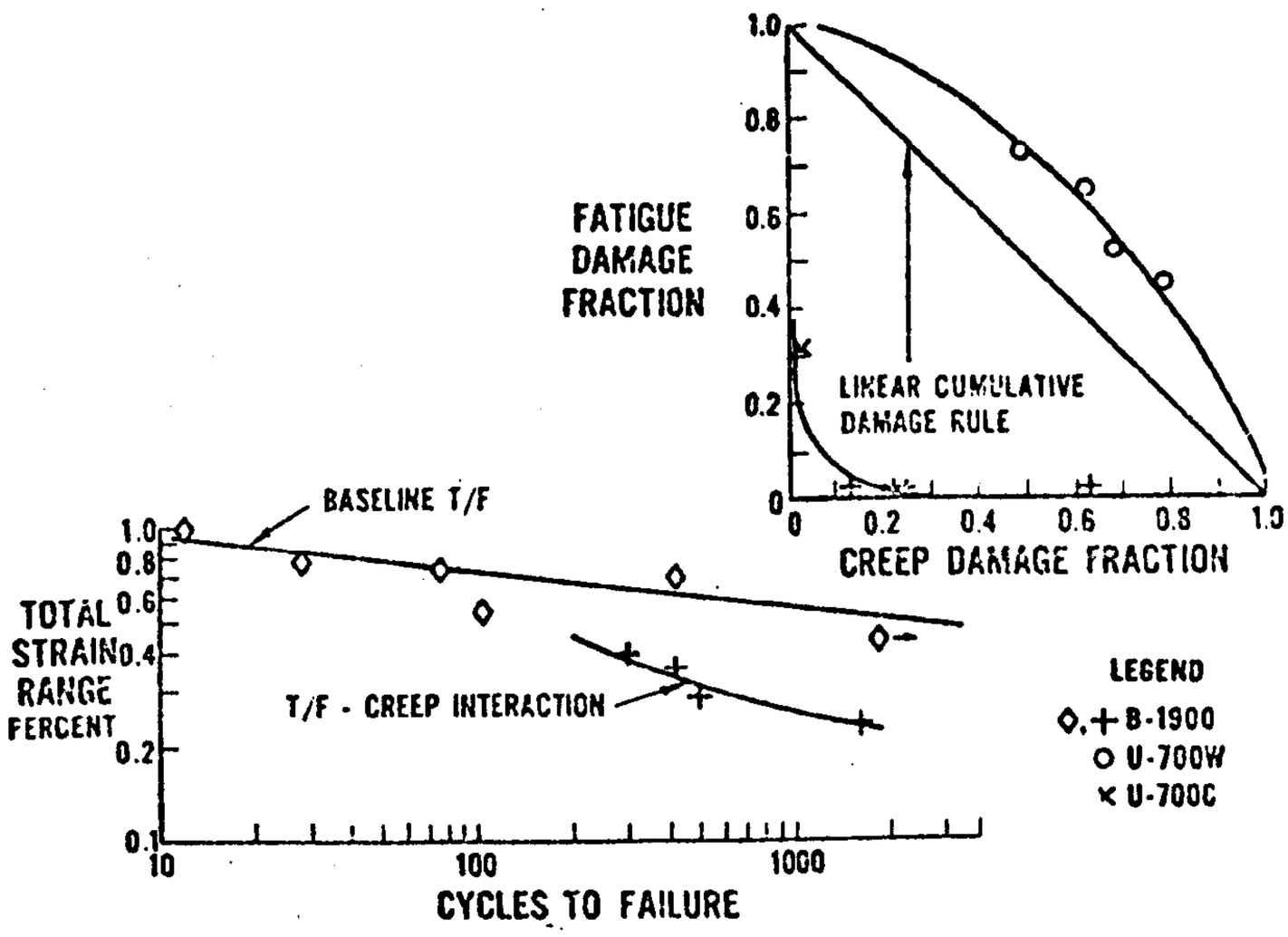

Figure 2.23 THERMAL fatigue creep interaction tests (91)

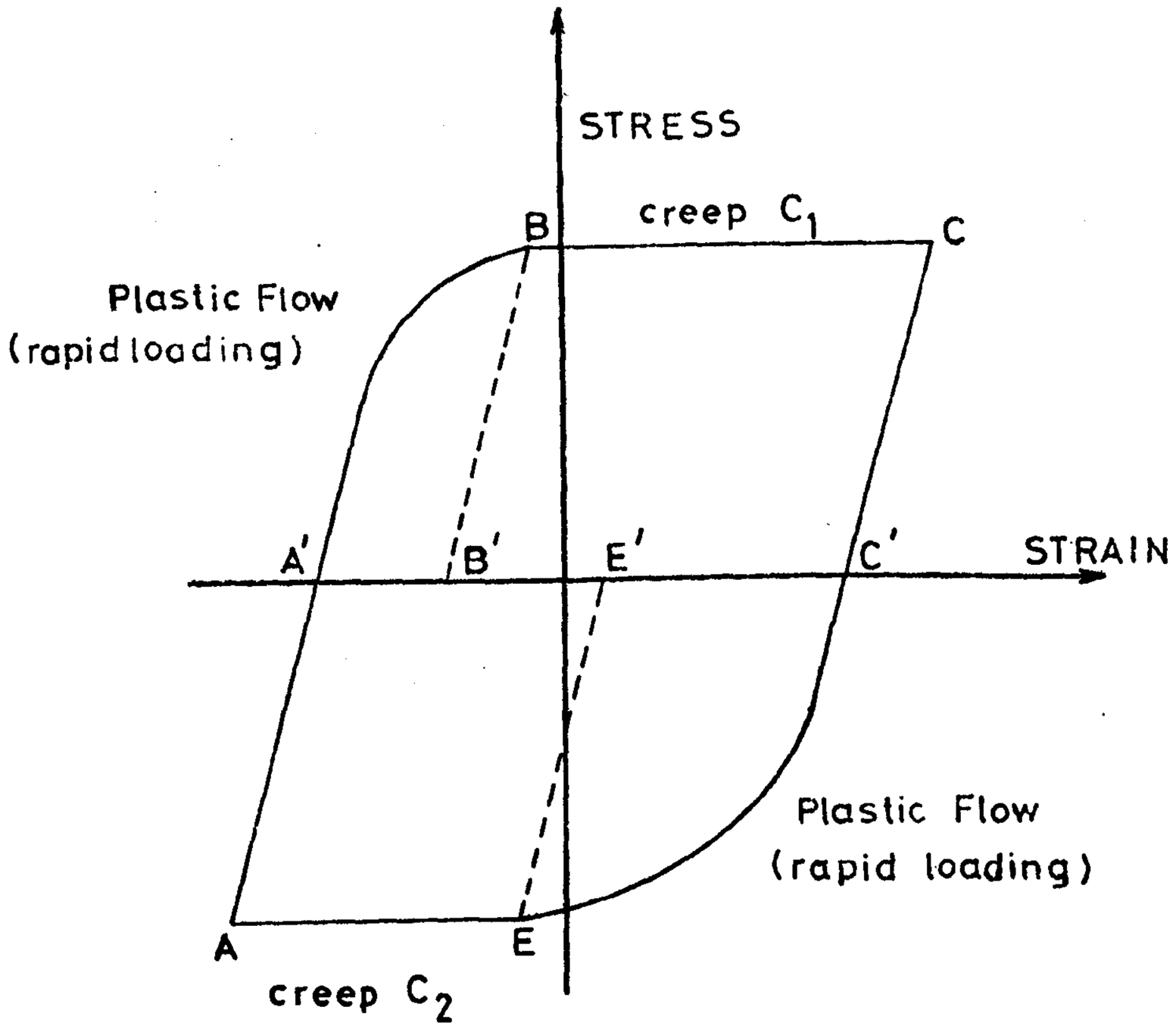

Figure 2.24 Schematic creep-fatigue loop

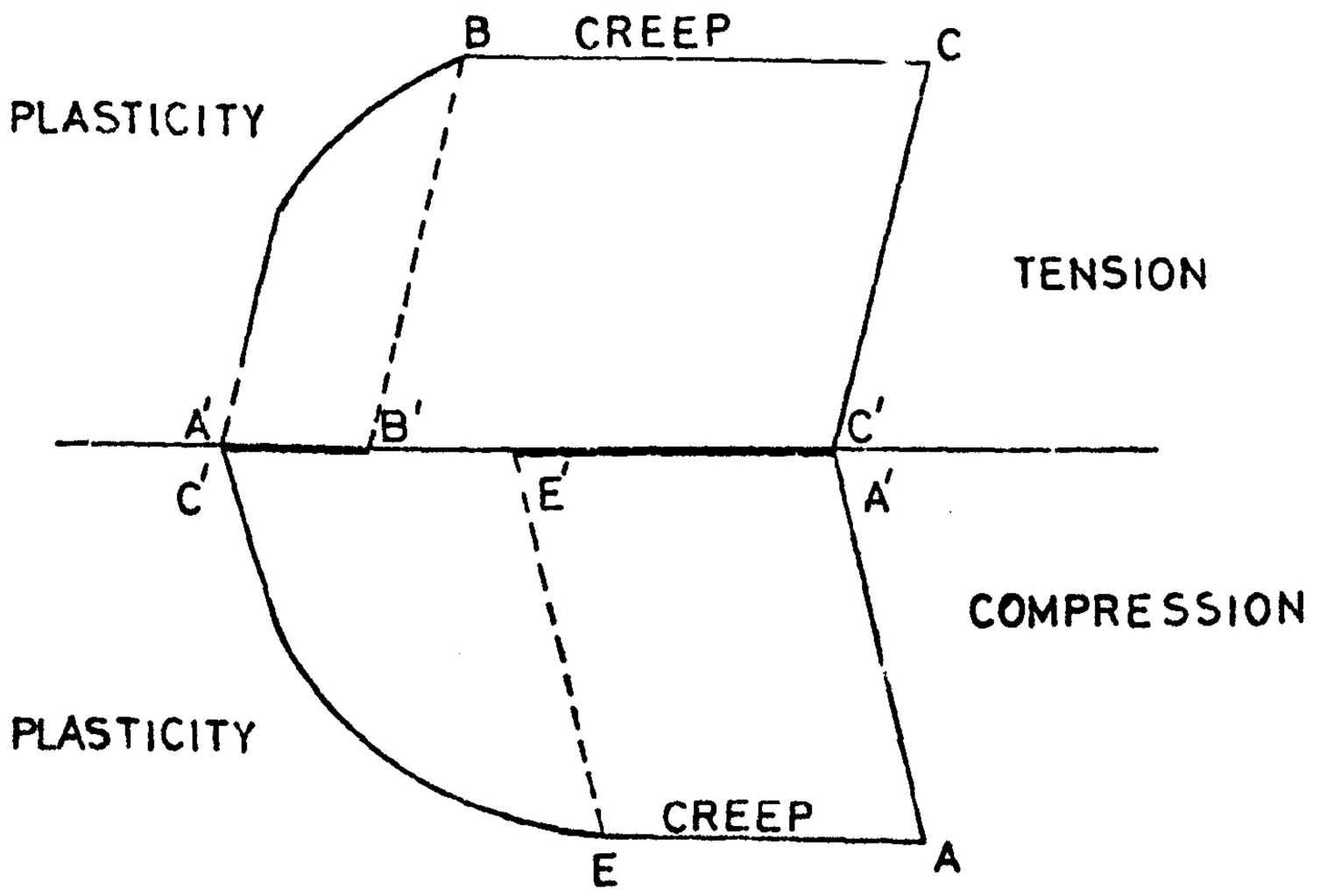

Figure 2.25 Partition of hysteresis loop

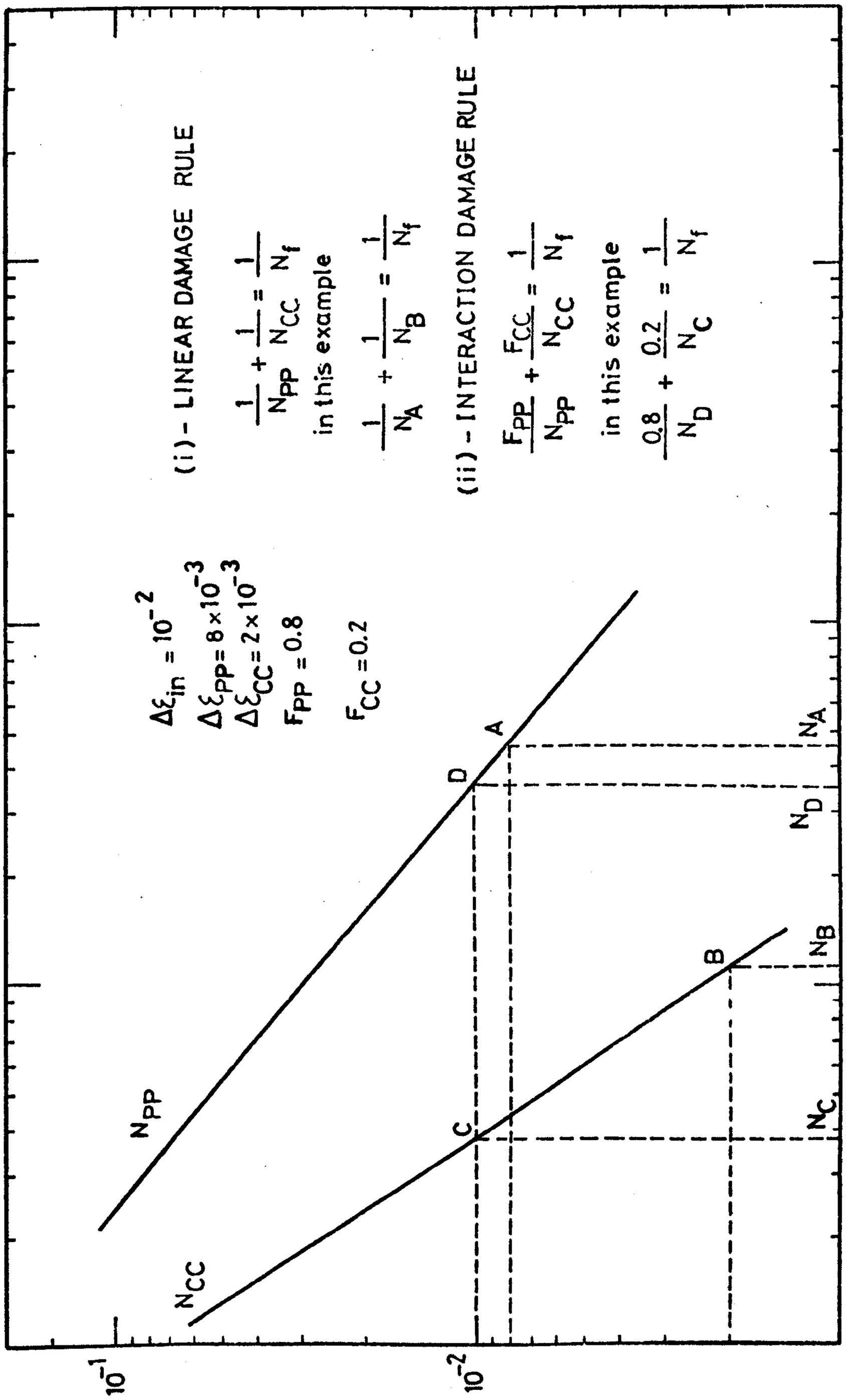

Figure 2.26 A practical example of application of the linear damage rule and the interaction damage rule

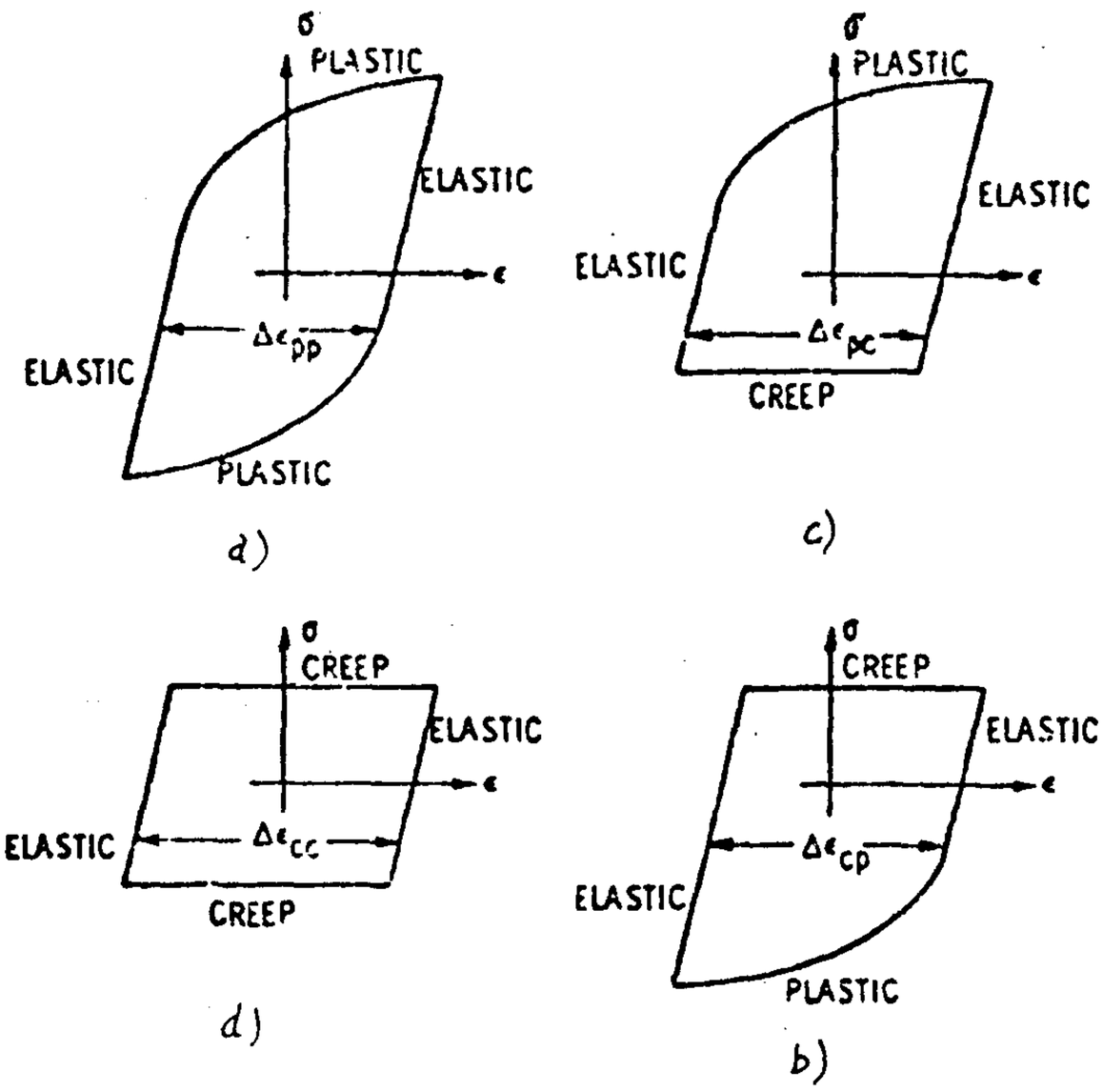

Figure 2.27 Idealized hysteresis loops used to define the individual strainrange versus life relationships

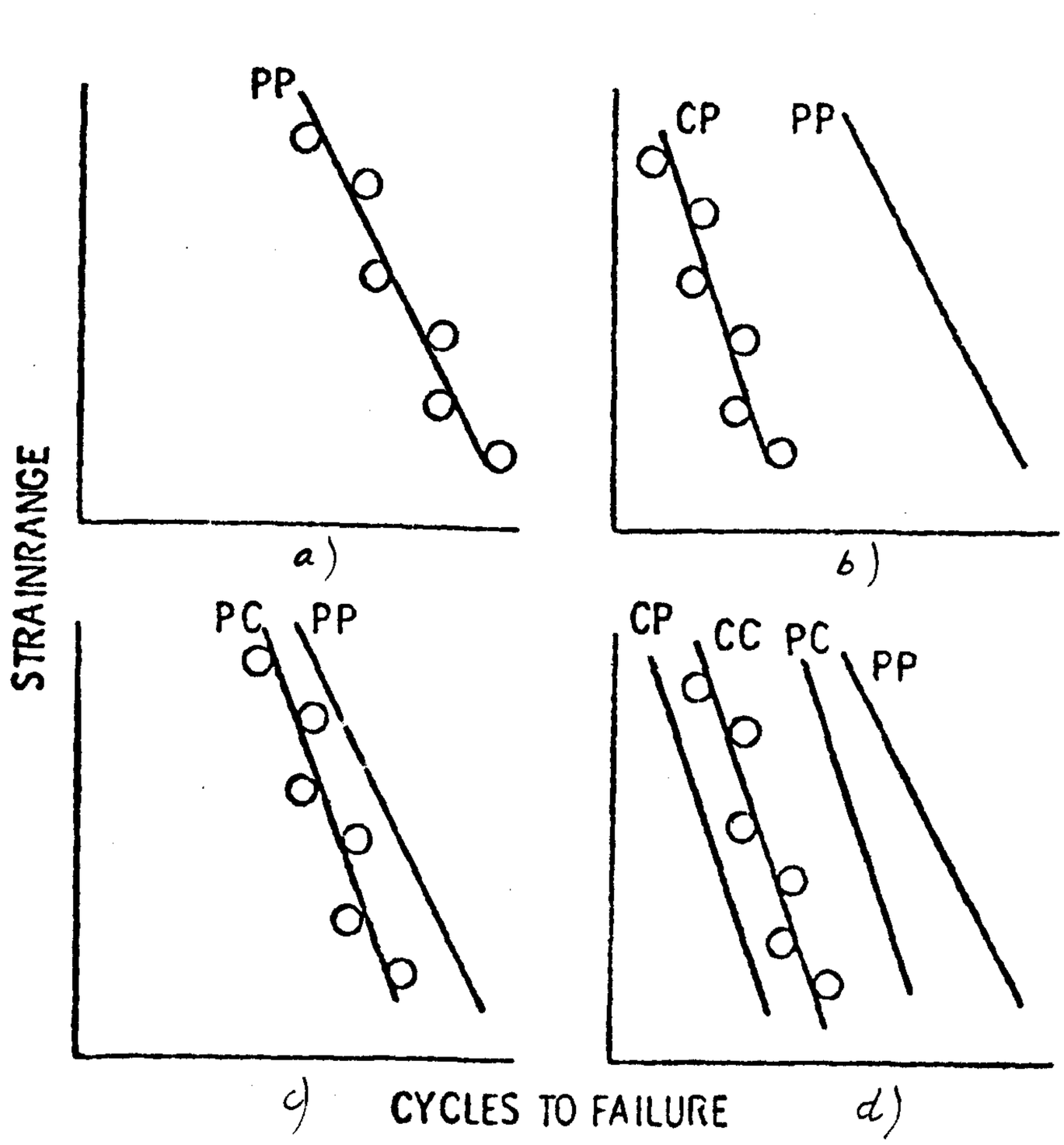

Figure 2.28 Schematic procedure for generating the isothermal partitioned strainrange versus life relationships

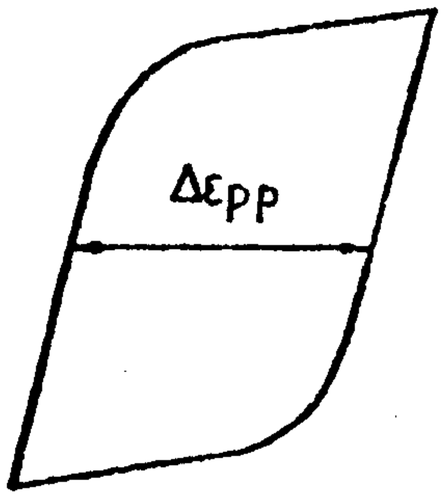

(a) PP CYCLE
HIGH-STRAIN RATE.

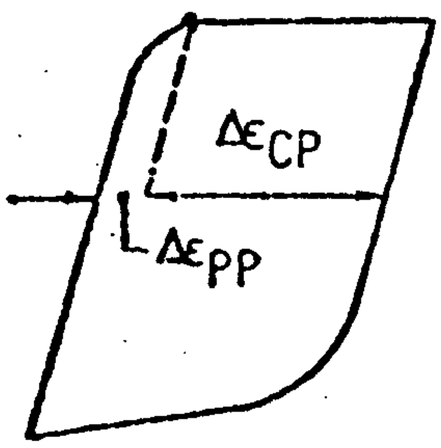

(b) CP CYCLE
STRESS-HOLD.

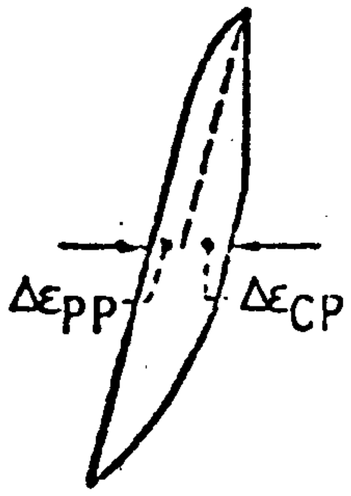

(c) CP CYCLE
STRAIN-HOLD.

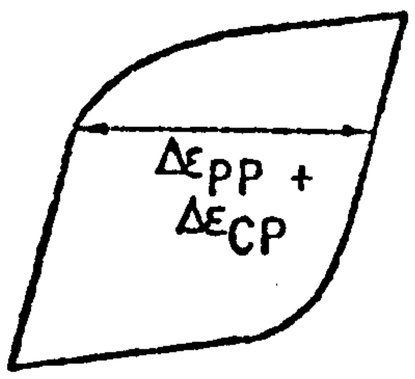

(d) CP CYCLE
LOW/HIGH
STRAINRATE.

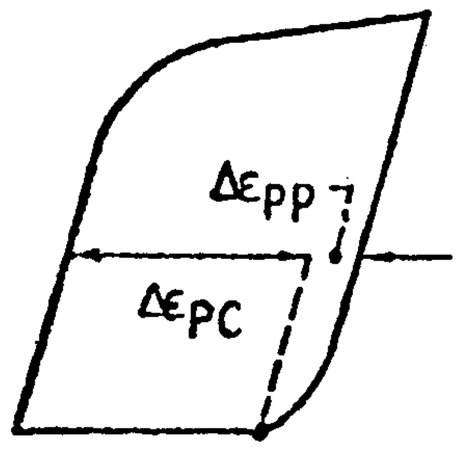

(e) PC CYCLE
STRESS-HOLD.

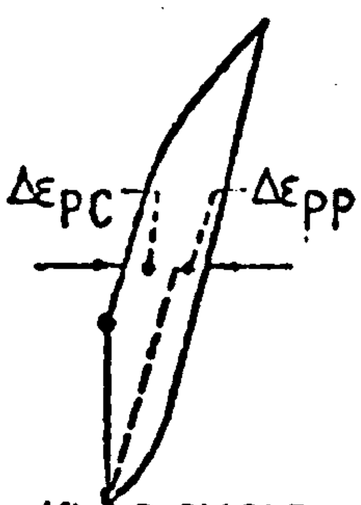

(f) PC CYCLE
STRAIN-HOLD.

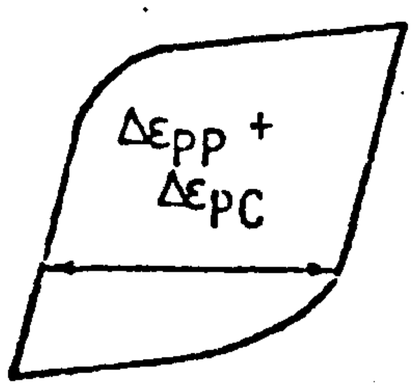

(g) PC CYCLE
HIGH/LOW
STRAINRATE

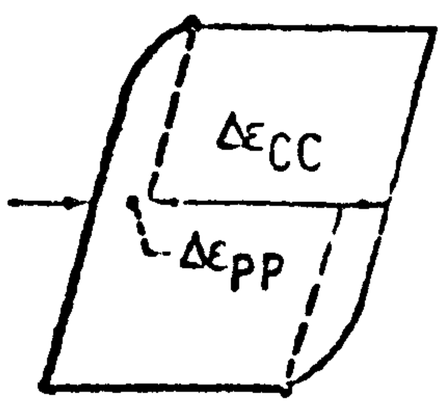

(h) CC CYCLE
STRESS-HOLD.

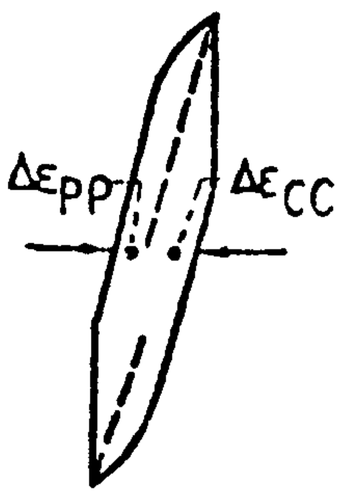

(i) CC CYCLE
STRAIN-HOLD

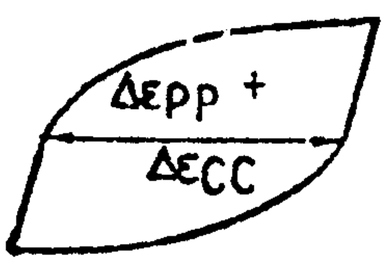

(j) CC CYCLE
LOW STRAINRATE.

Figure 2.29 Examples of isothermal test cycles to determine the partitioned strainrange versus life relationships

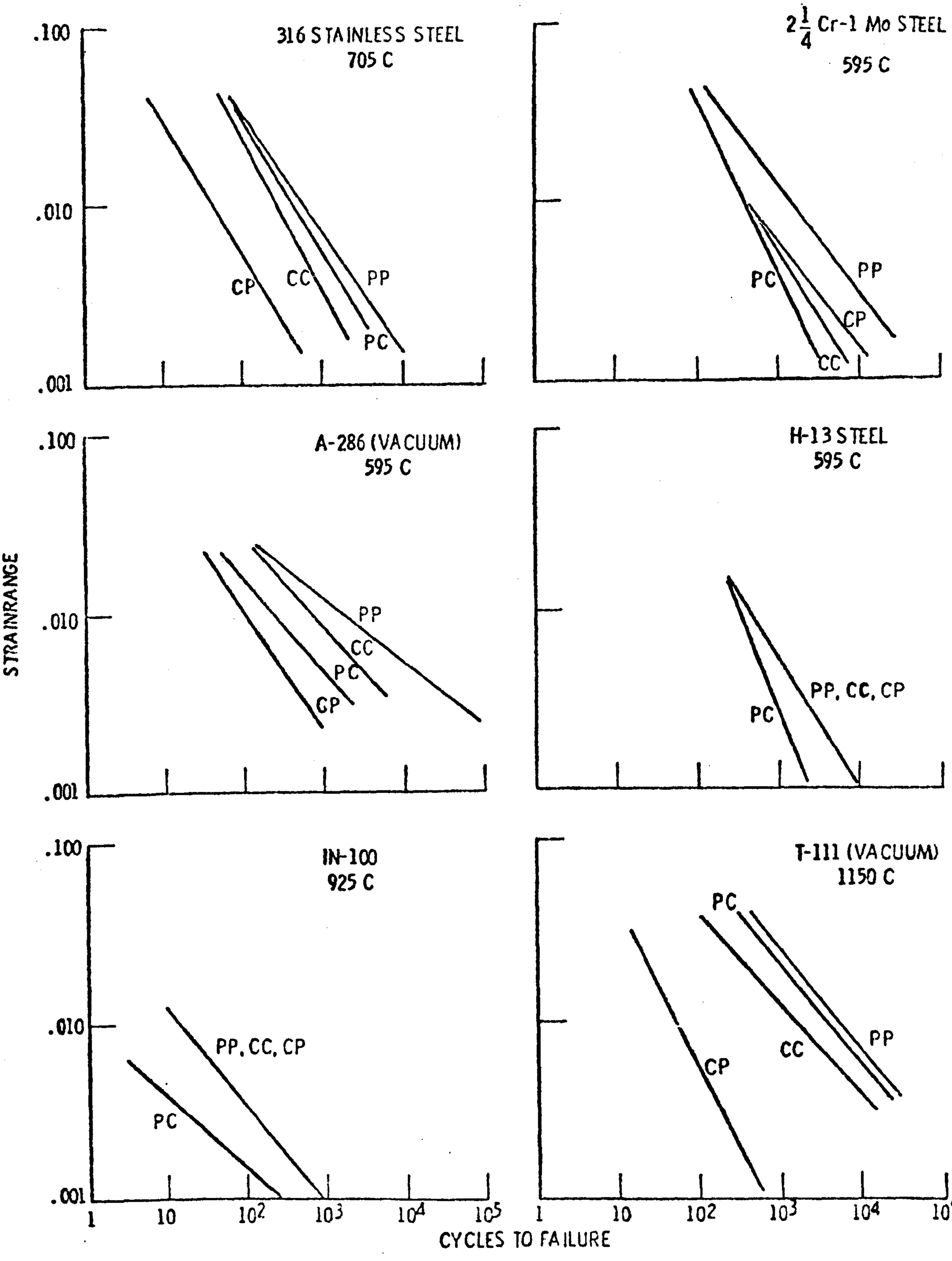

Figure 2.30 Partitioned strainrange - life relationships for six alloys

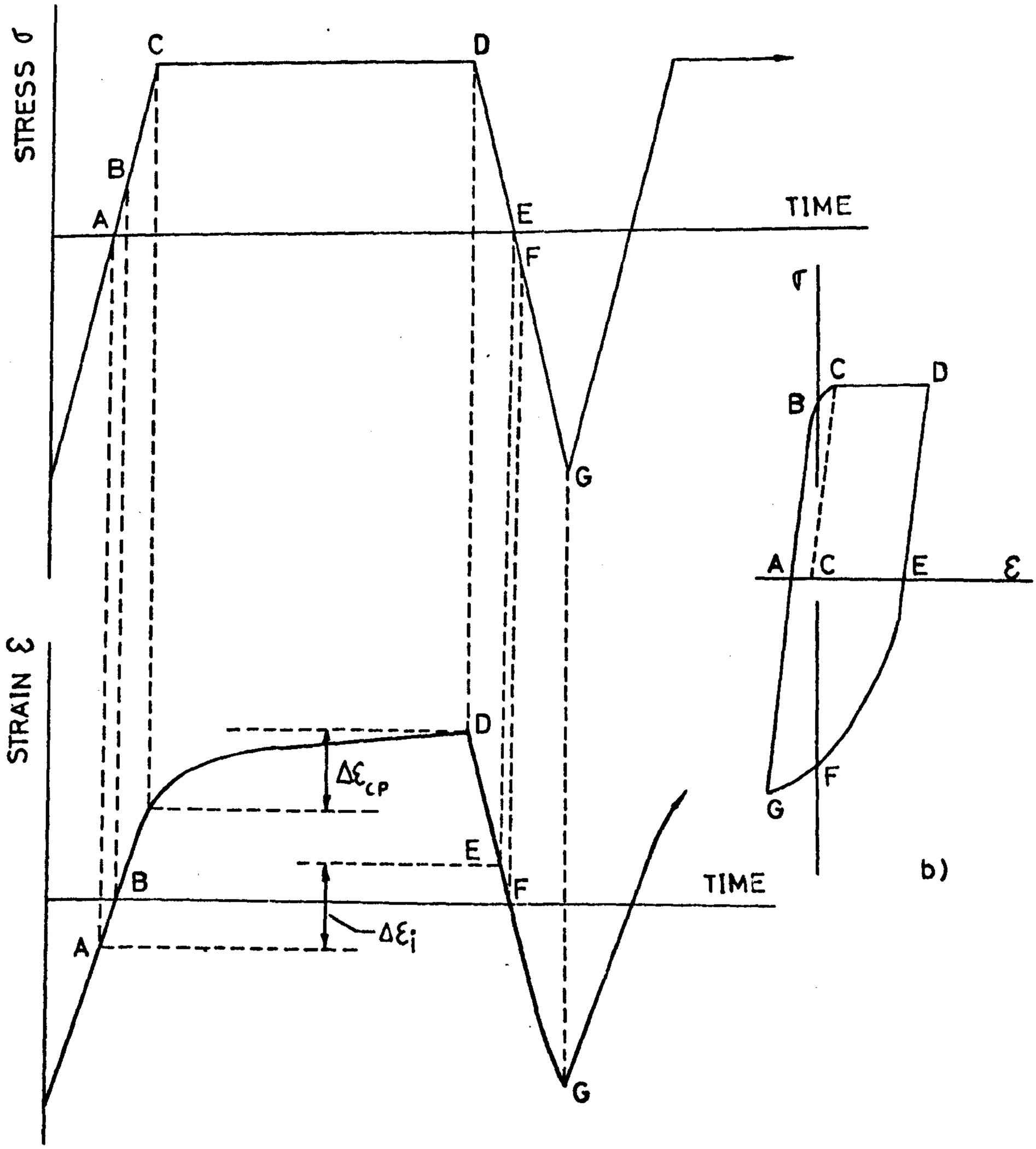

Figure 2.31 Partition of a loop in plots of strain and stress versus time like those obtained in a U V record

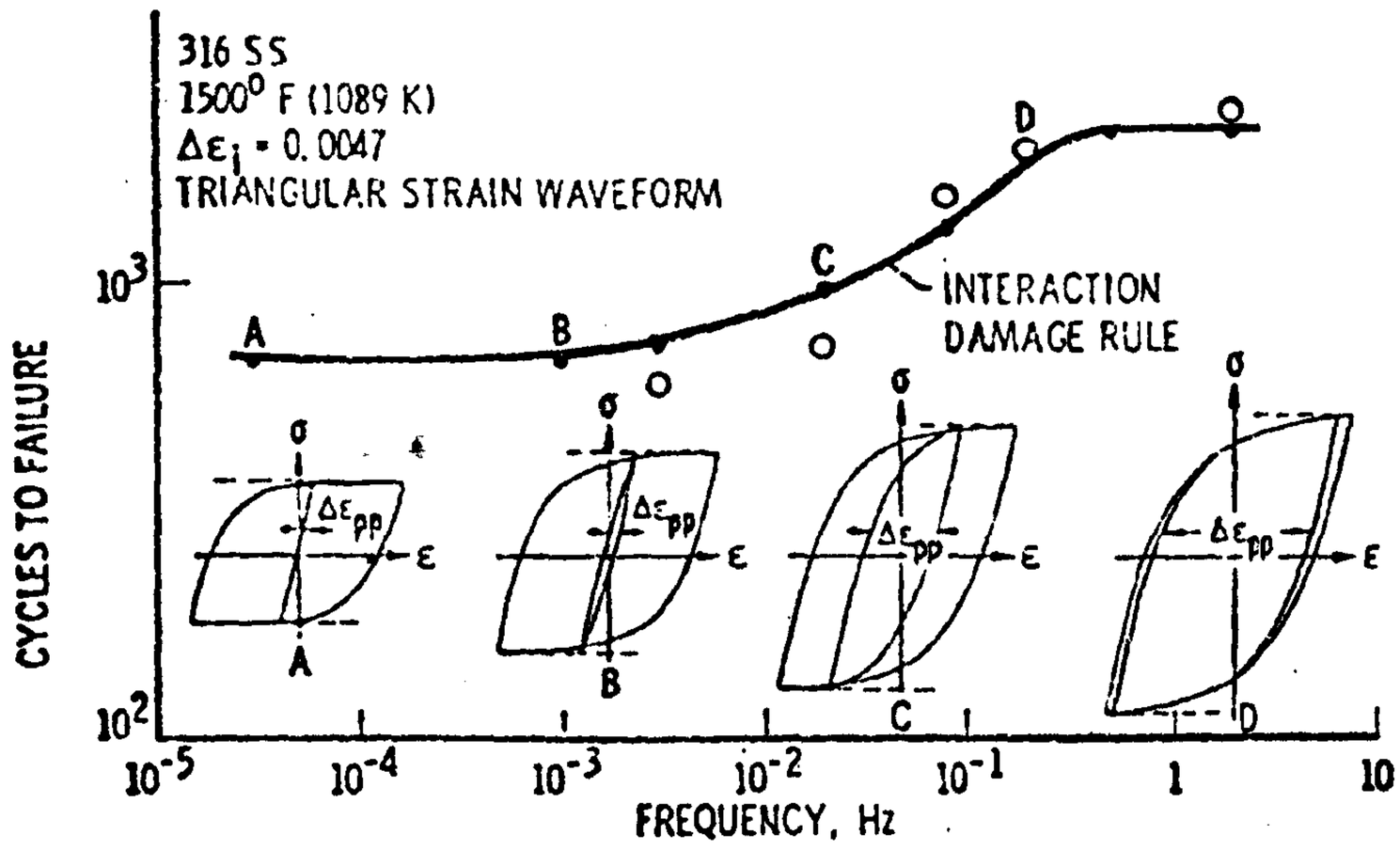

Figure 2.32 Partitioning using rapid cycling hysteresis loop between two stress peaks

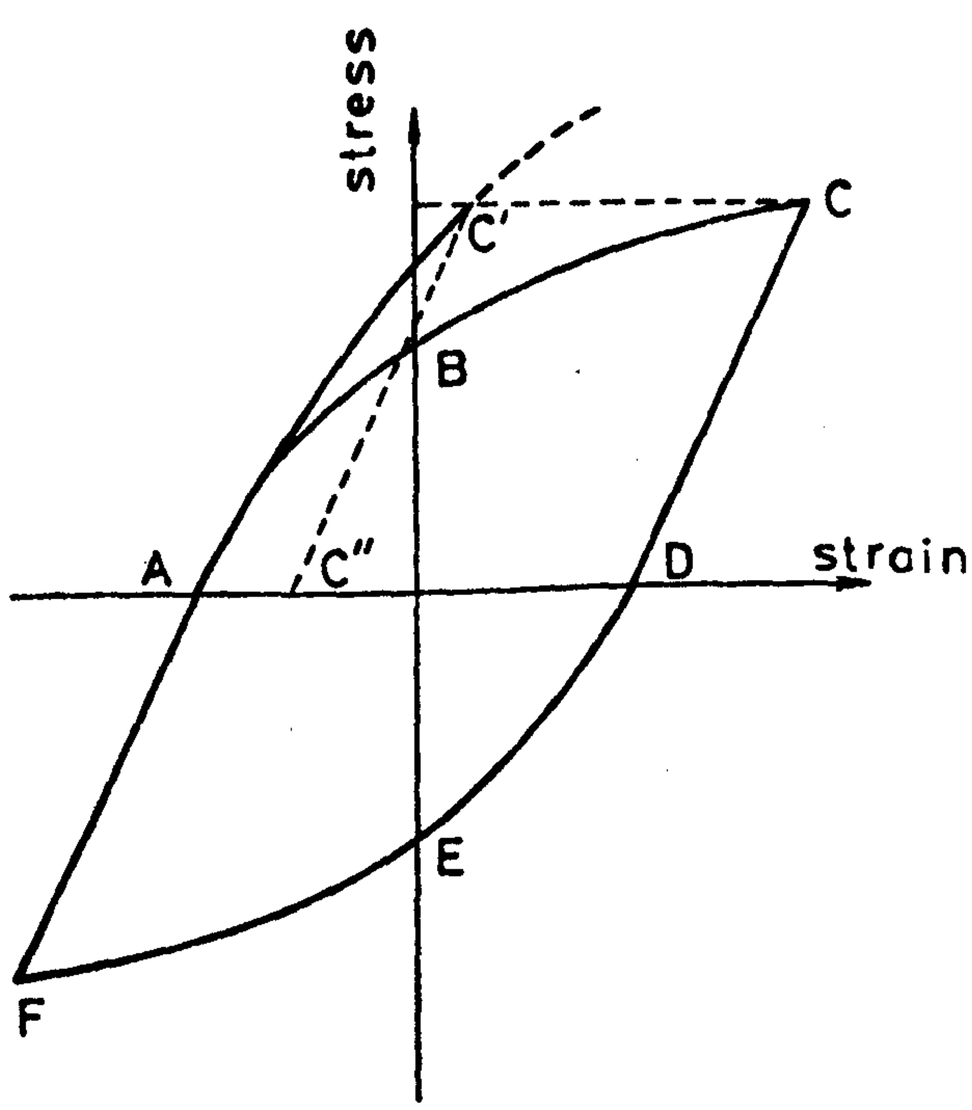

Figure 2.33 Application of the half-cycle rapid load-unload method for partitioning

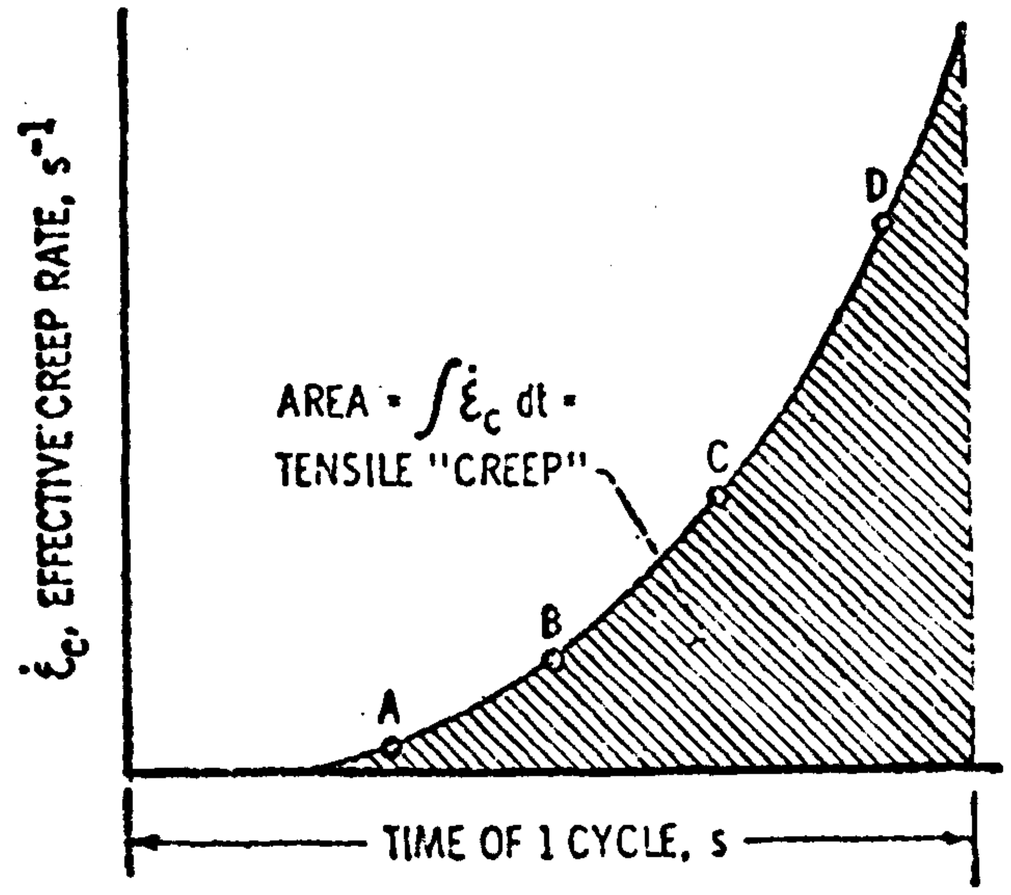

Figure 2.34 Selection of several stress levels along the hysteresis loop where stress hold tests are conducted to determine creep rates on the STEP-STRESS method

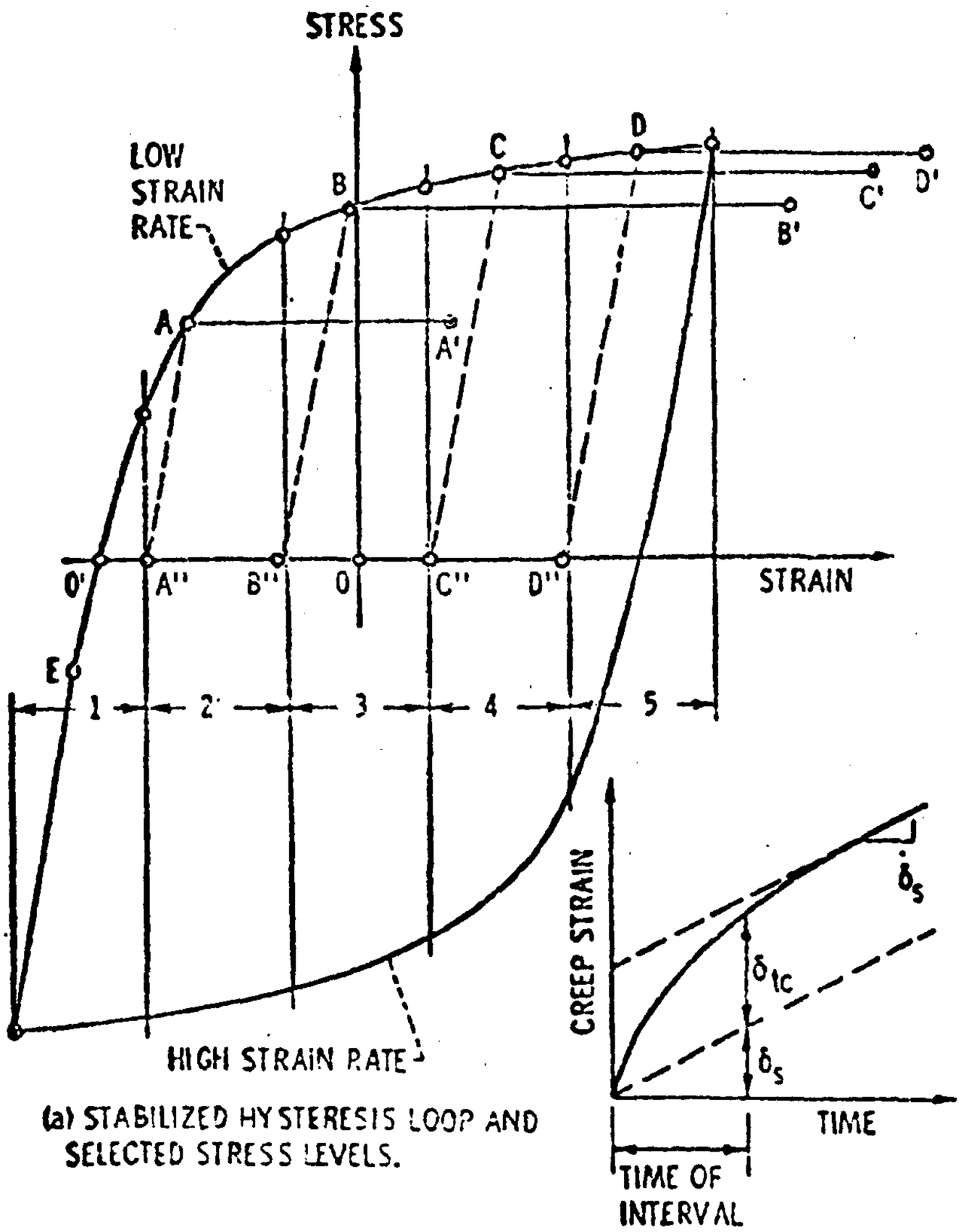

Figure 2.35 Determination of creep within a cycle

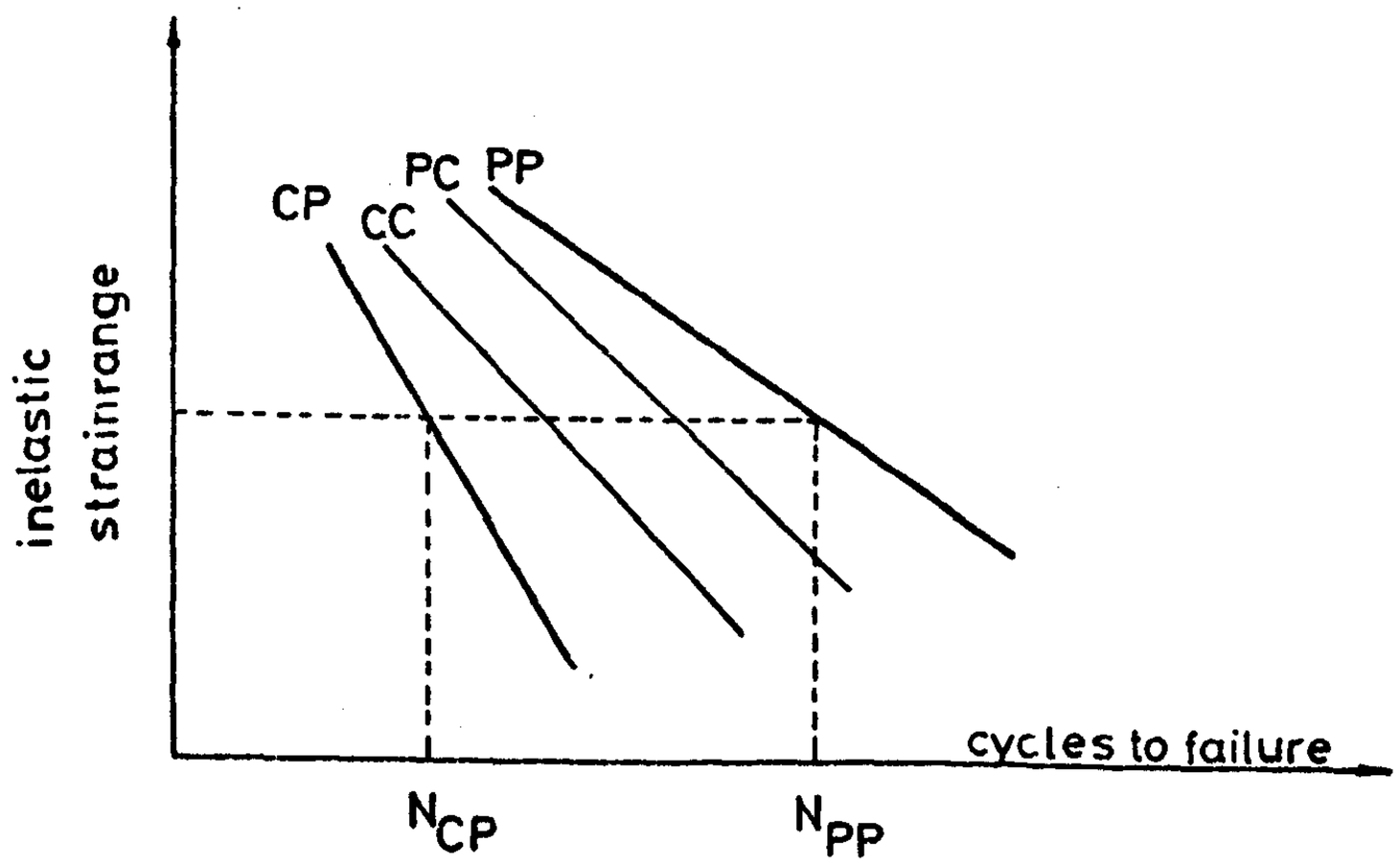

Figure 2.36 Relative position of the strainrange versus life relationships (schematic)

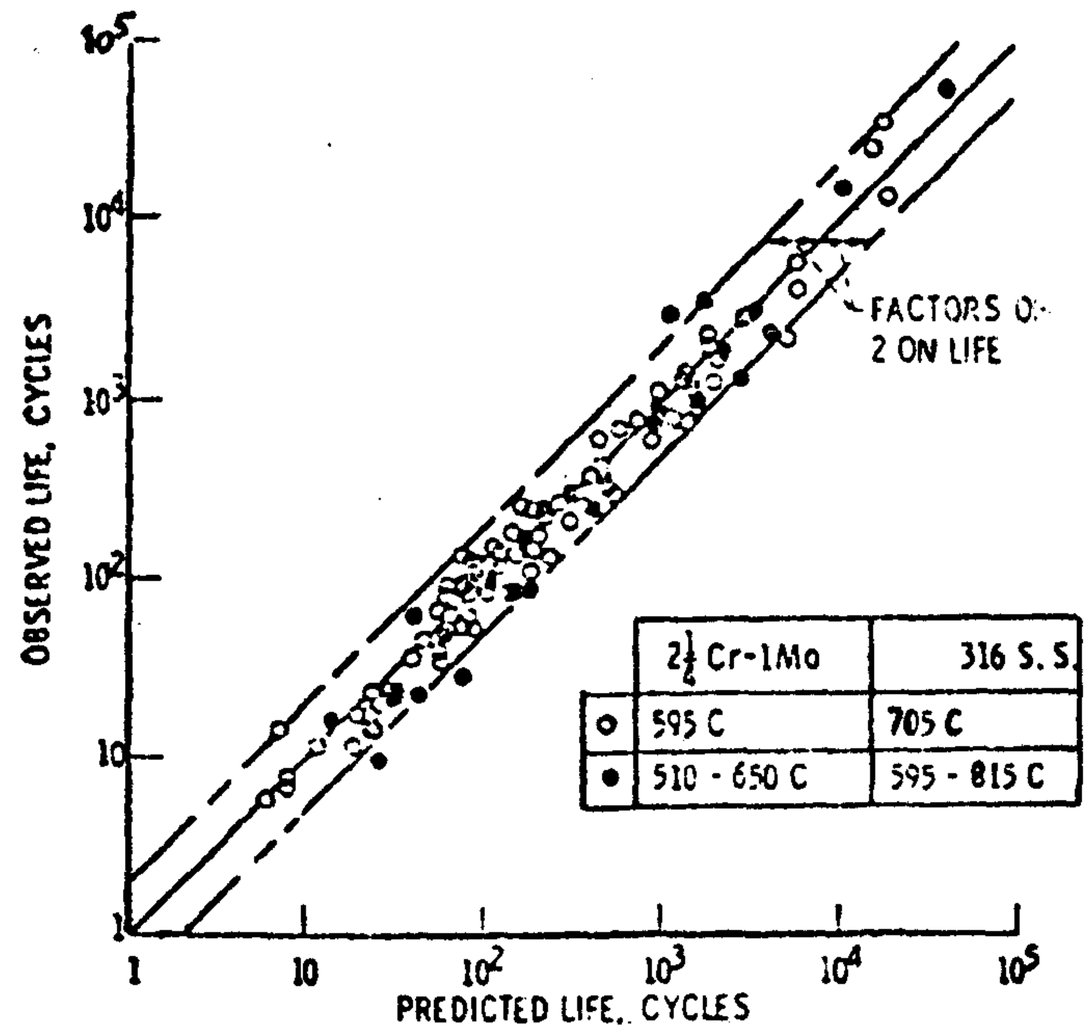

Figure 2.37 Comparison of observed and predicted lives using SrP method for two steels tested at two temperature ranges

TYPE 316 STAINLESS STEEL

SYMBOL		TEMPERATURE, °C	FREQUENCY Hz	INELASTIC STRAINRANGE	CYCLES TO FAILURE
O	a	870	0.02	0.00468	677
	b	815	↓	.00460	730
	c	705		.00420	2100
	d	650		.00400	1636
	e	595		.00356	3507
	f	540		.00484	1264
□	g	705	0.00046	0.00510	666
	h	↓	.0074	.00480	894
	i		.02	.00420	2100
	j		2.0	.00424	1700
Δ	k	815	0.003	0.00464	605
	l	↓	.02	.00460	730
	m		.2	.00464	1950
	n		2.0	.00468	2350

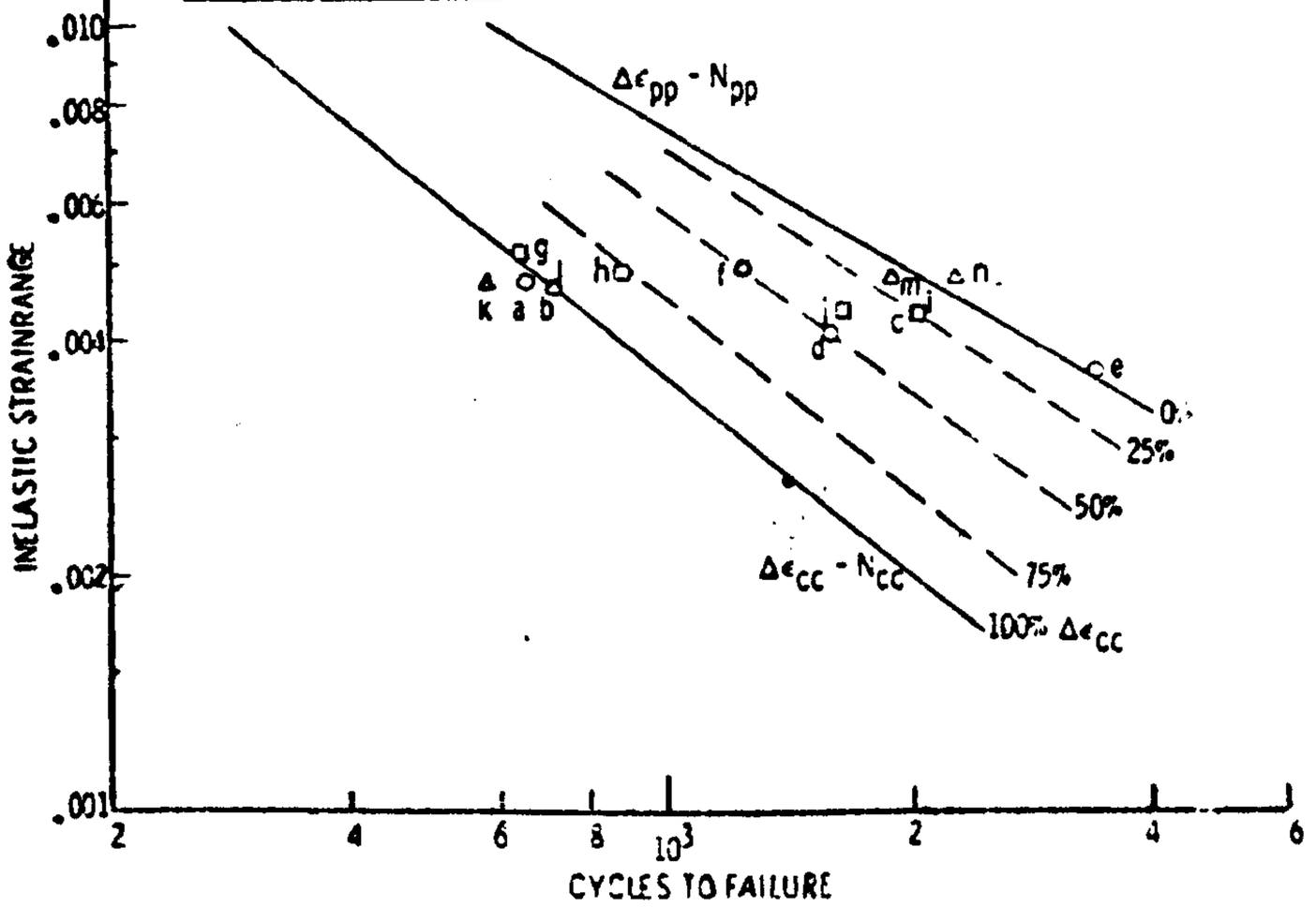

Figure 2.38 Application of the SrP method to continuous strain cycling results

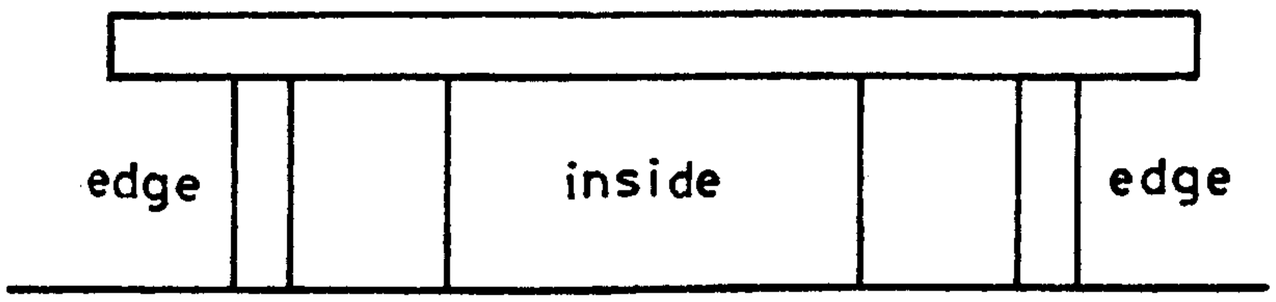

$$\varepsilon_{MECH} \approx \alpha \Delta T$$

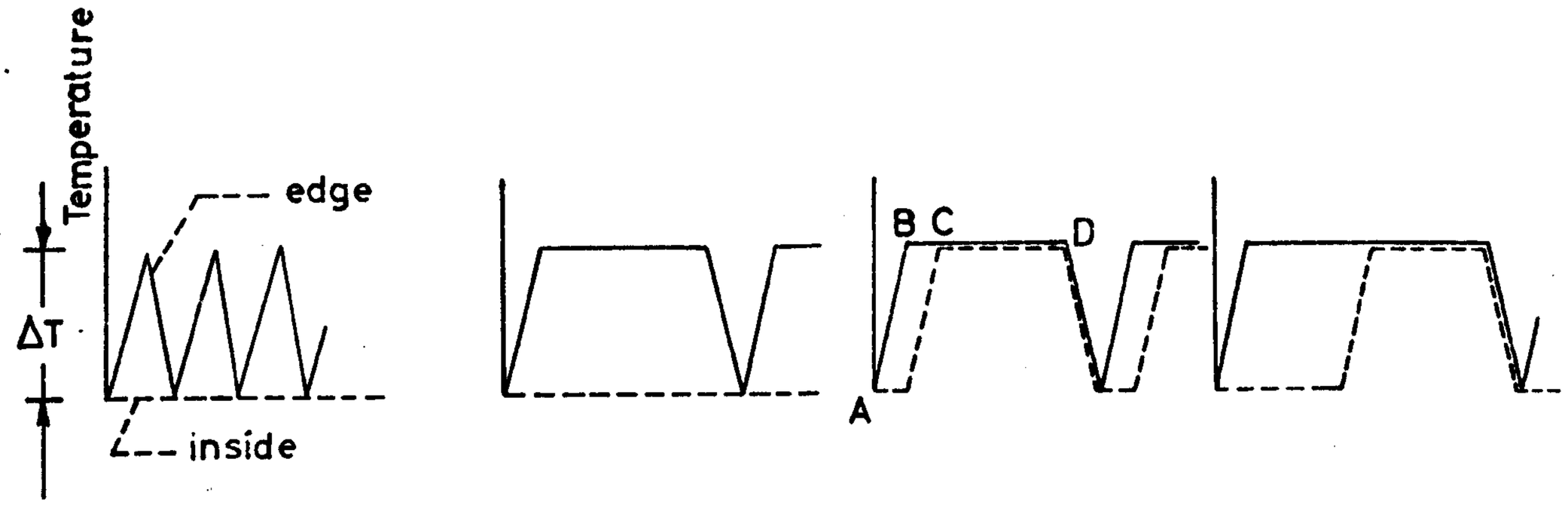

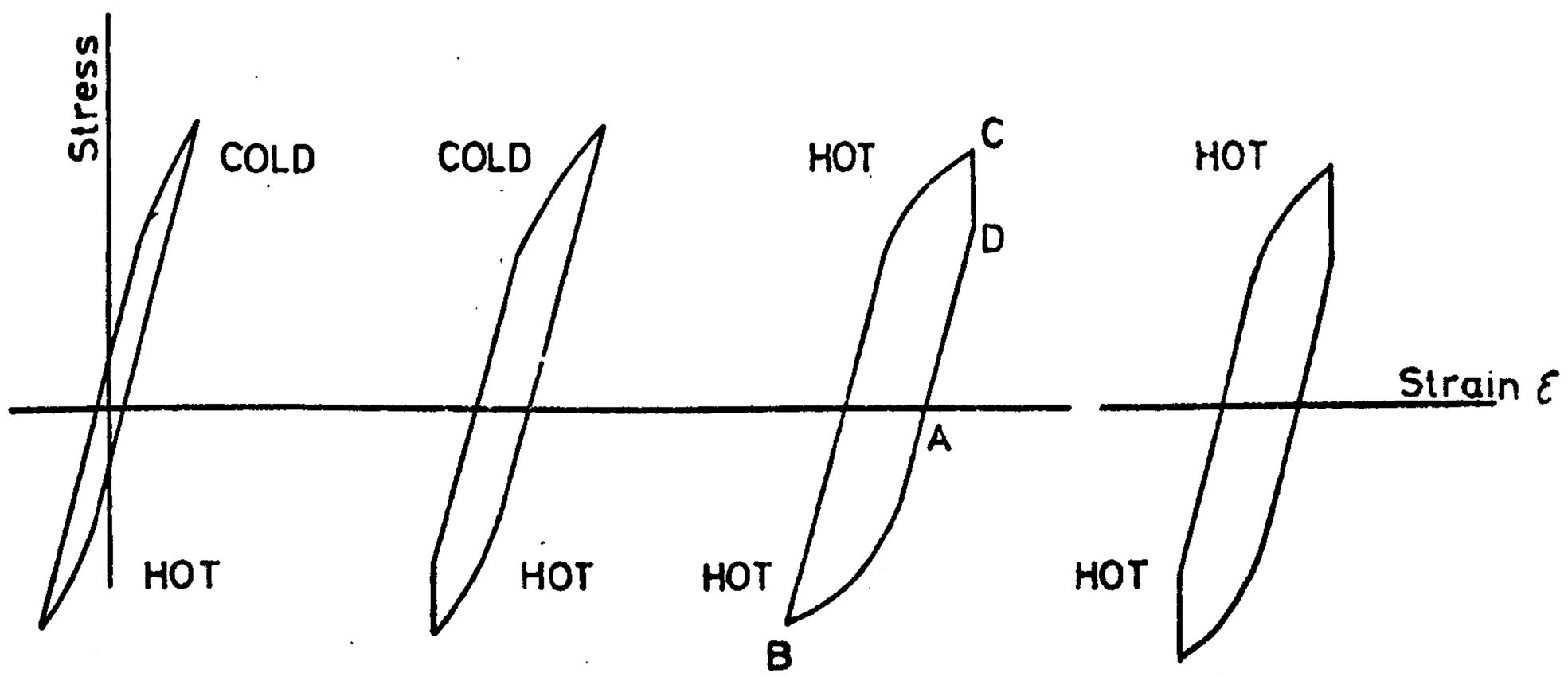

$\Delta\varepsilon_{PP}$ $\Delta\varepsilon_{PP}+\Delta\varepsilon_{PC}$ $\Delta\varepsilon_{PP}+\Delta\varepsilon_{CP}$ $\Delta\varepsilon_{PP}+\Delta\varepsilon_{CC}$

Figure 2.39 Strainrange components produced in the edge of the schematic assembly by several thermal hystories

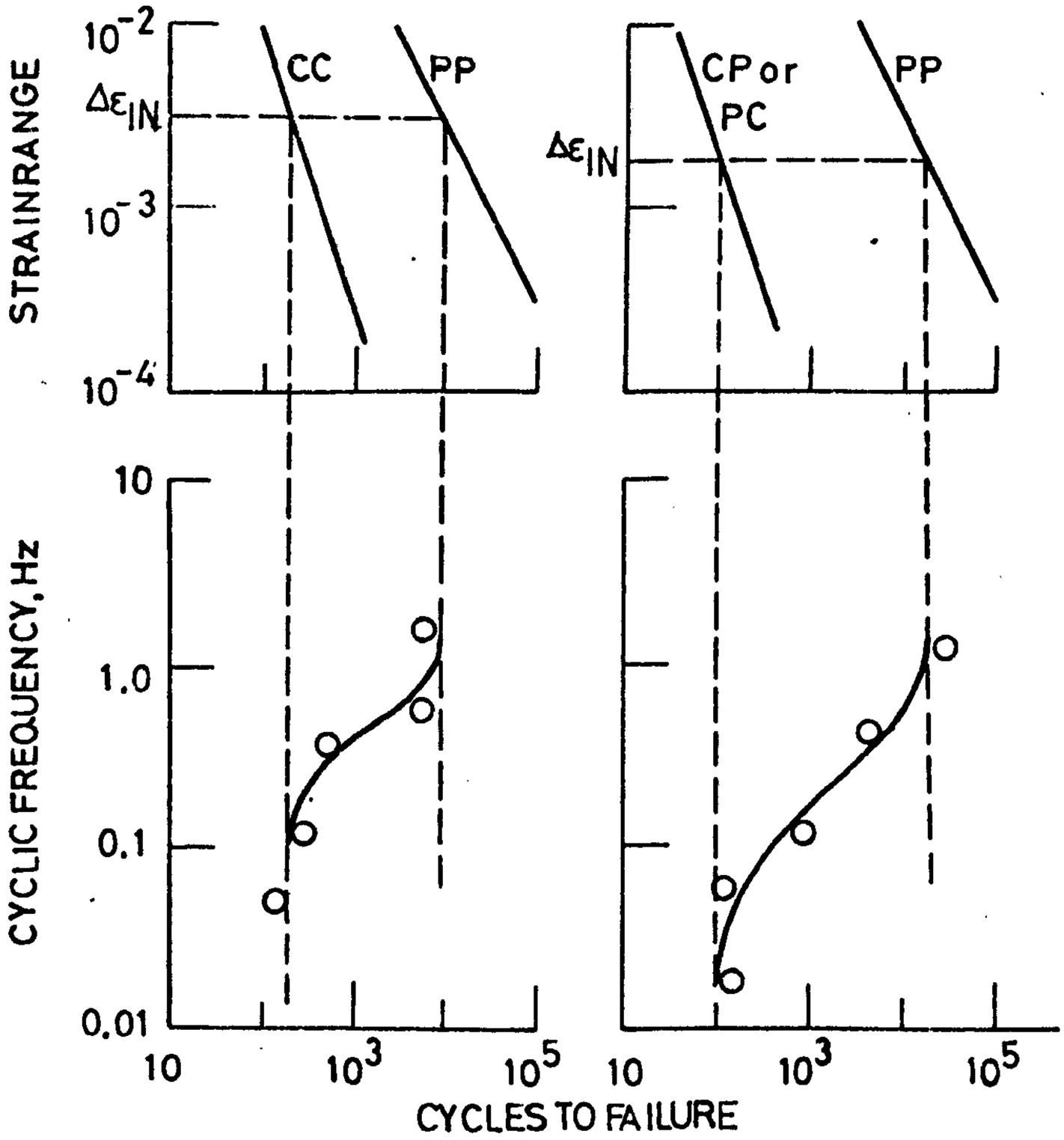

Figure 2.40 Use of partitioned strainrange-life relationships to obtain bounds on life

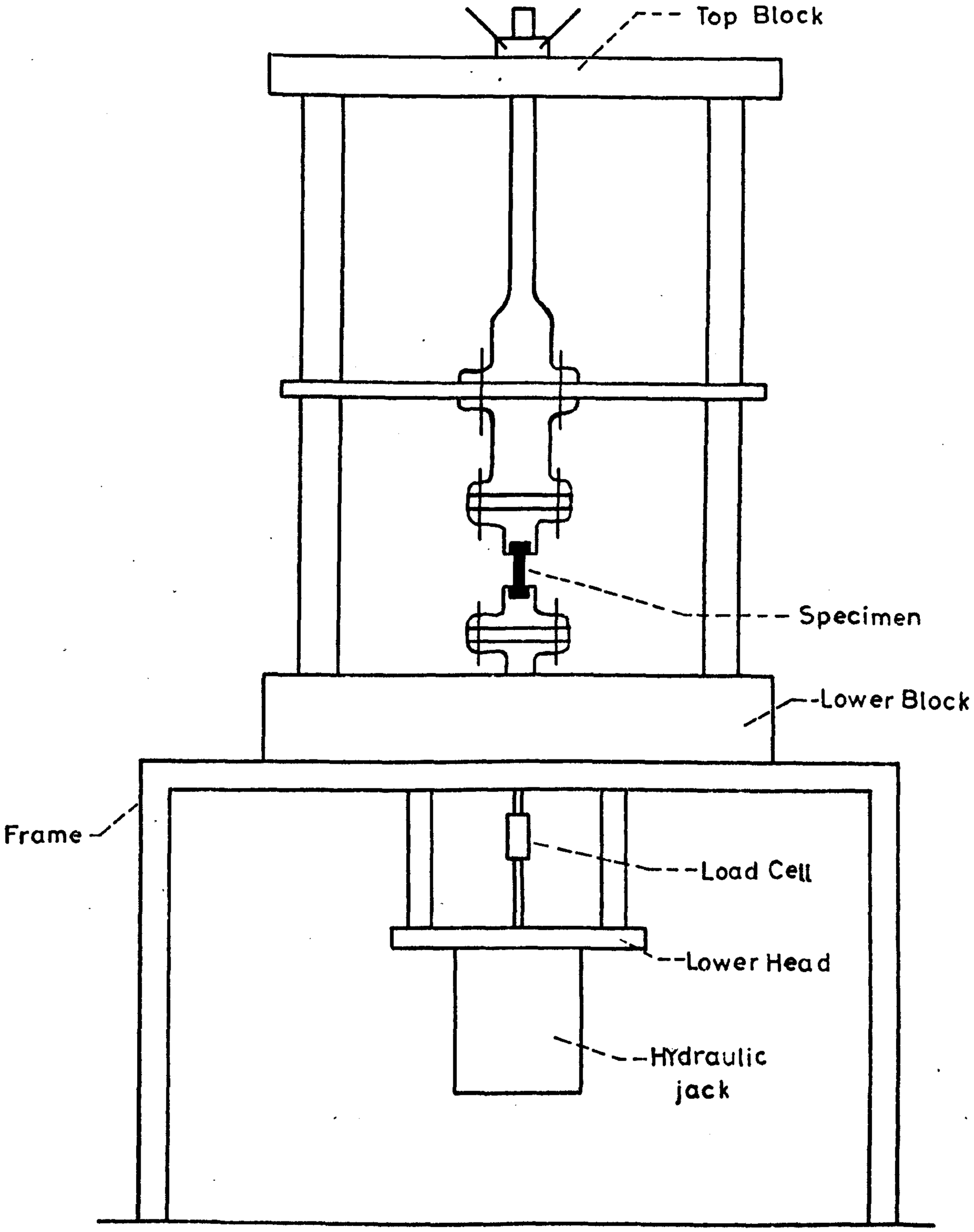

Figure 3.1 Testing Rig for high temperature fatigue tests

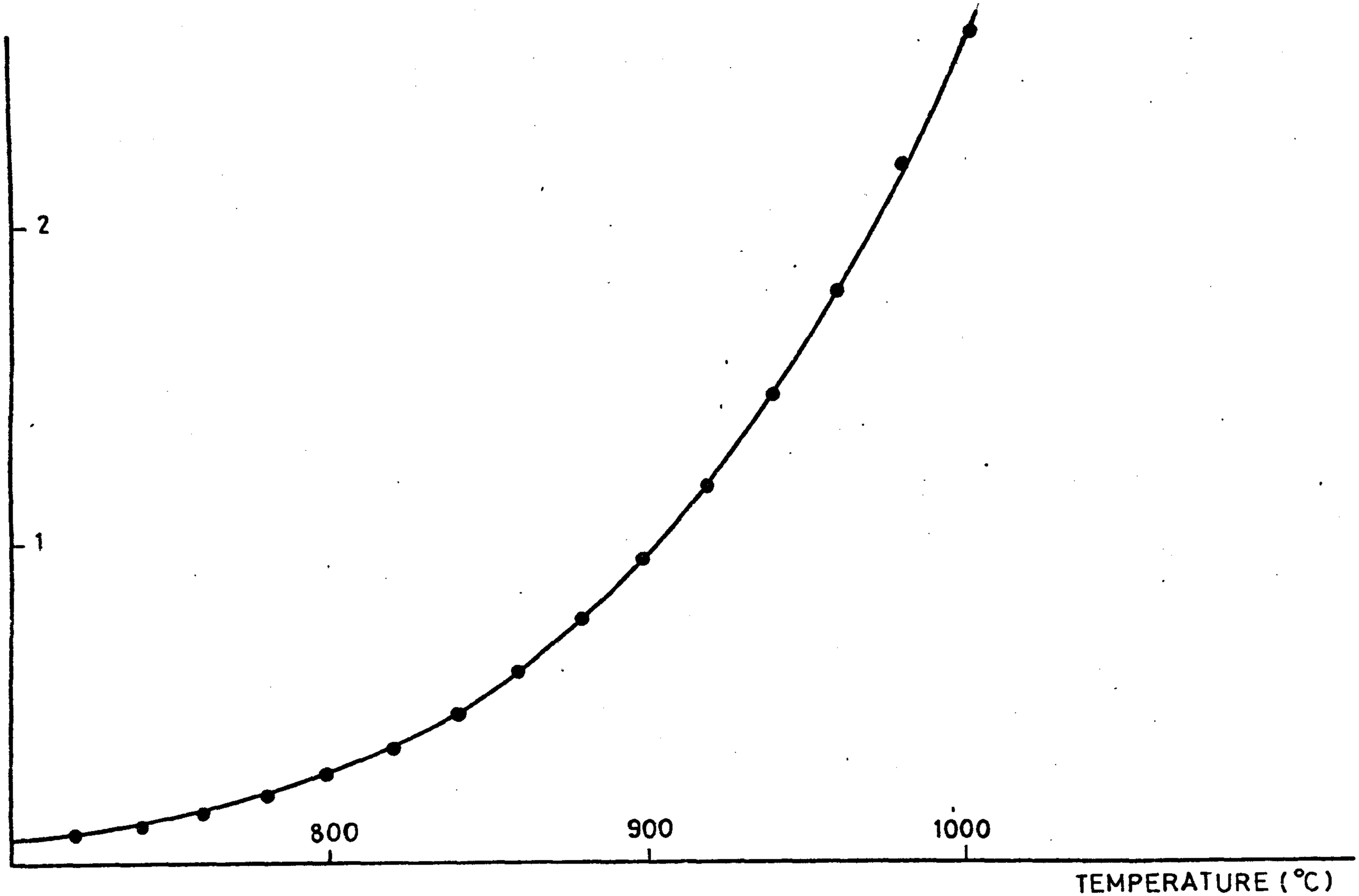

Figure 3.2 GRAPH voltage - temperature

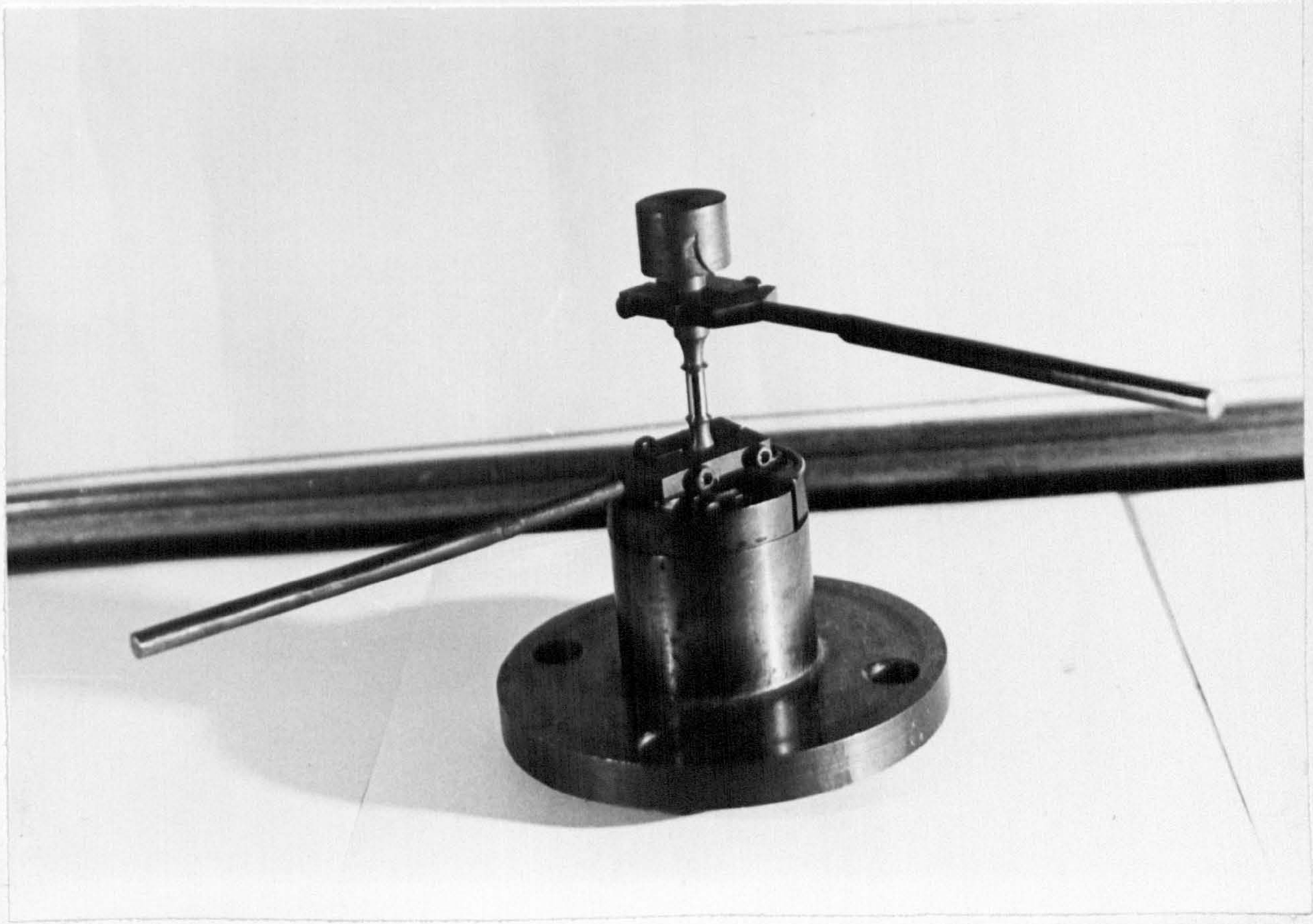

Figure 3.3 - MARM002 specimen mounted in one of the rig grips.
Nimonic rods are attached to the specimen.

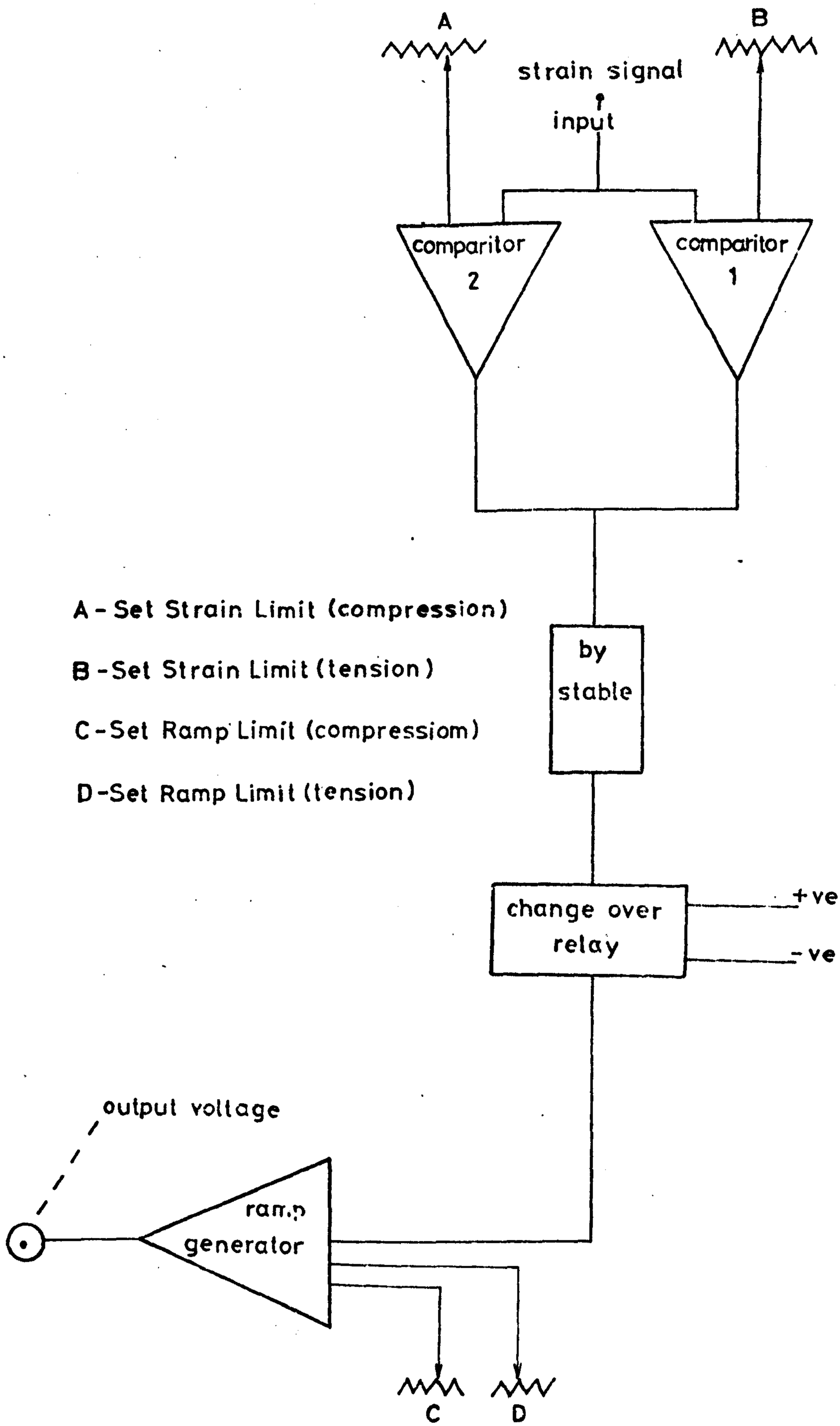

Figure 3.4 Schematic diagram of the circuit employed to generate the PC, CP and CC wave shapes

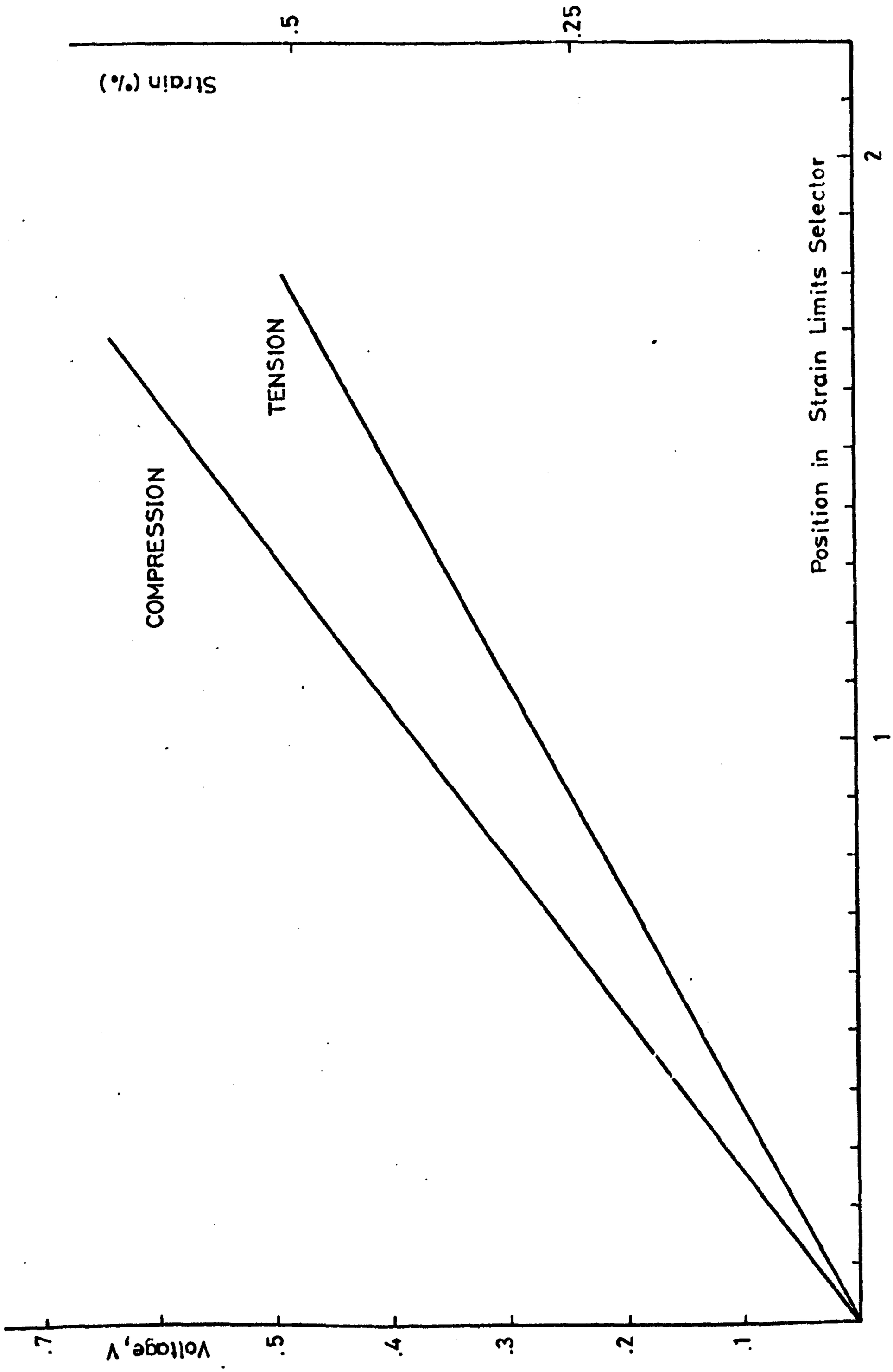

Figure 3.5 Graph strain

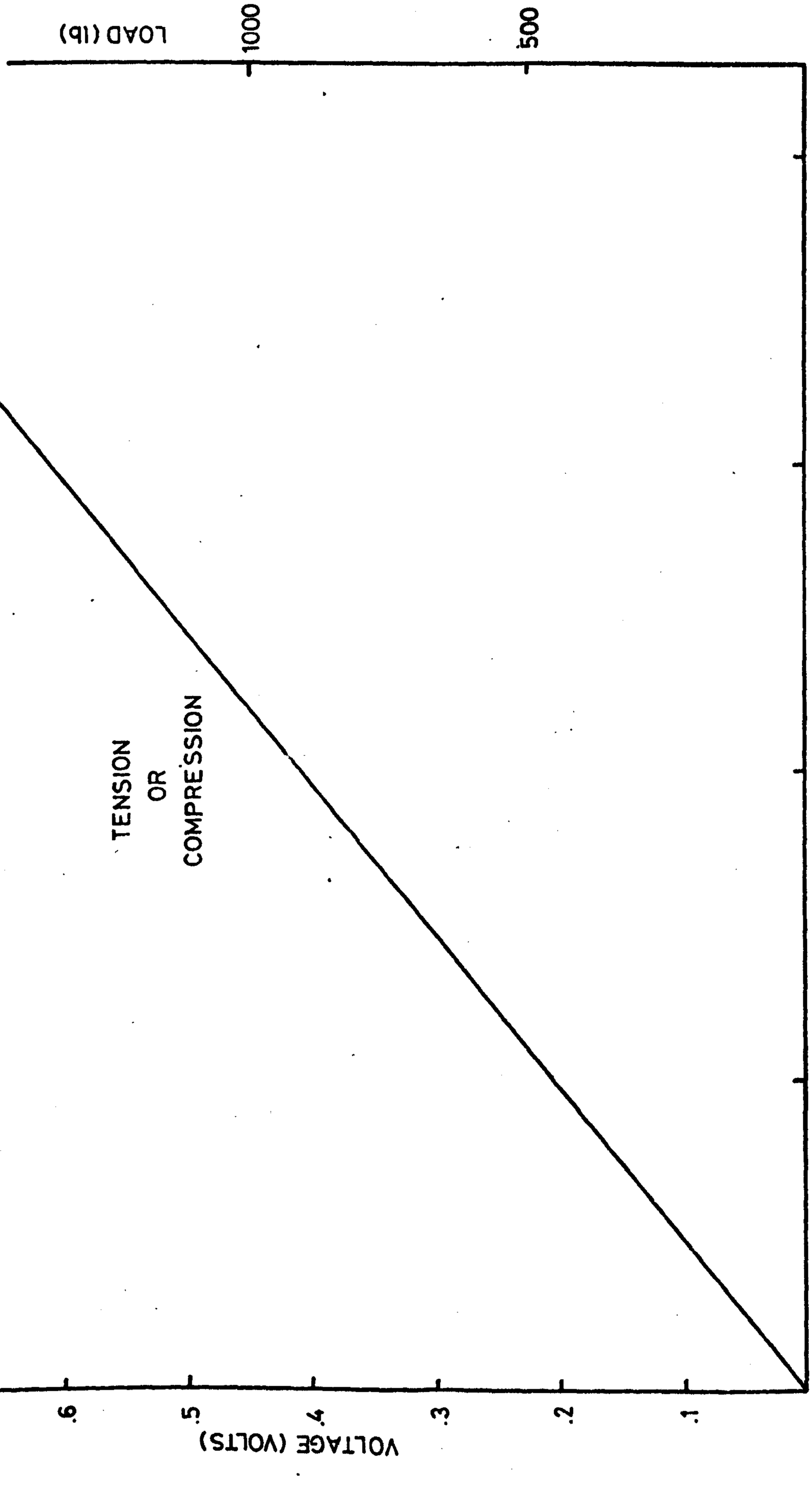

Figure 3.6 Graph load limits - voltage

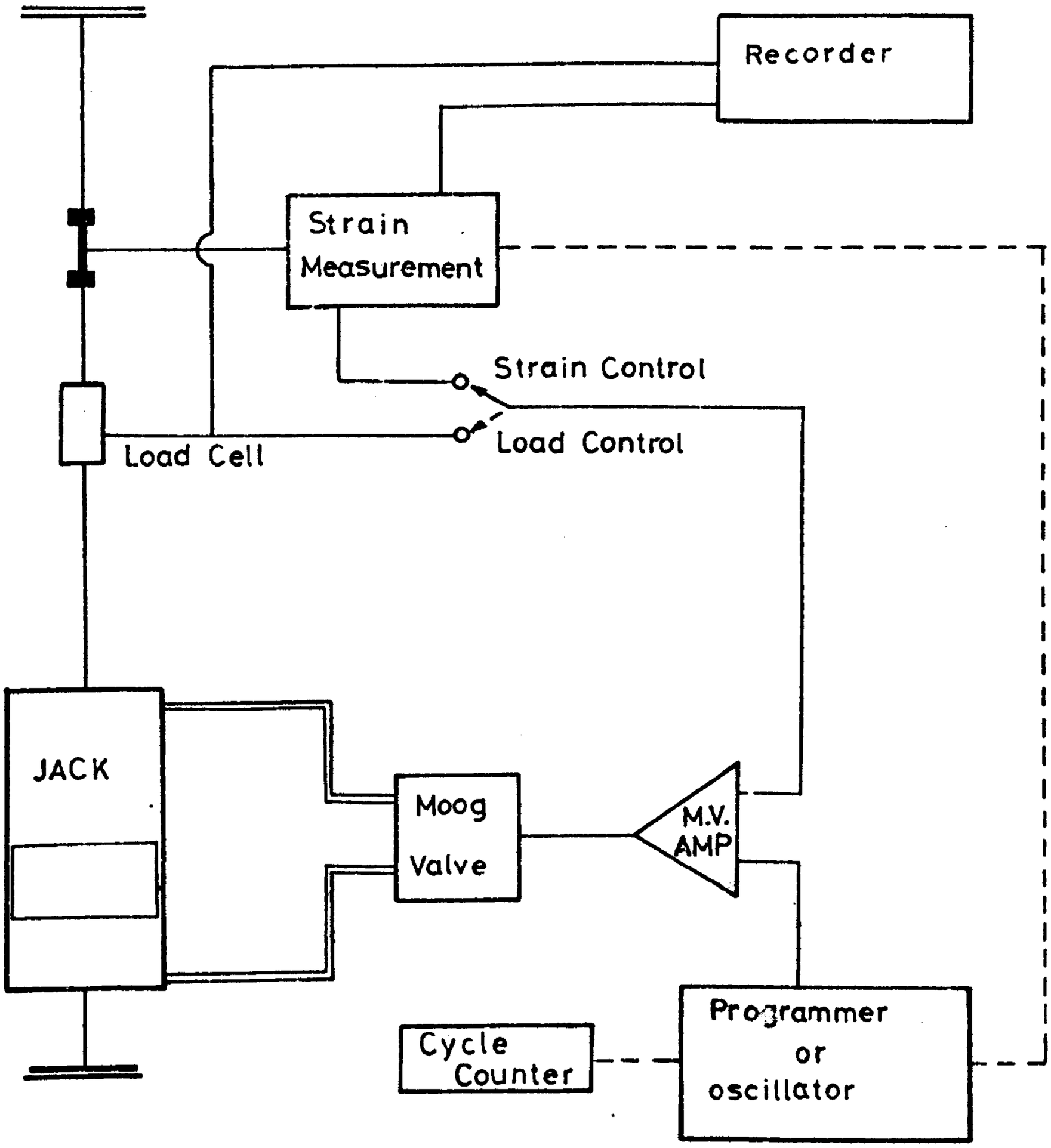

Figure 3.7 Basic block circuit for control systems

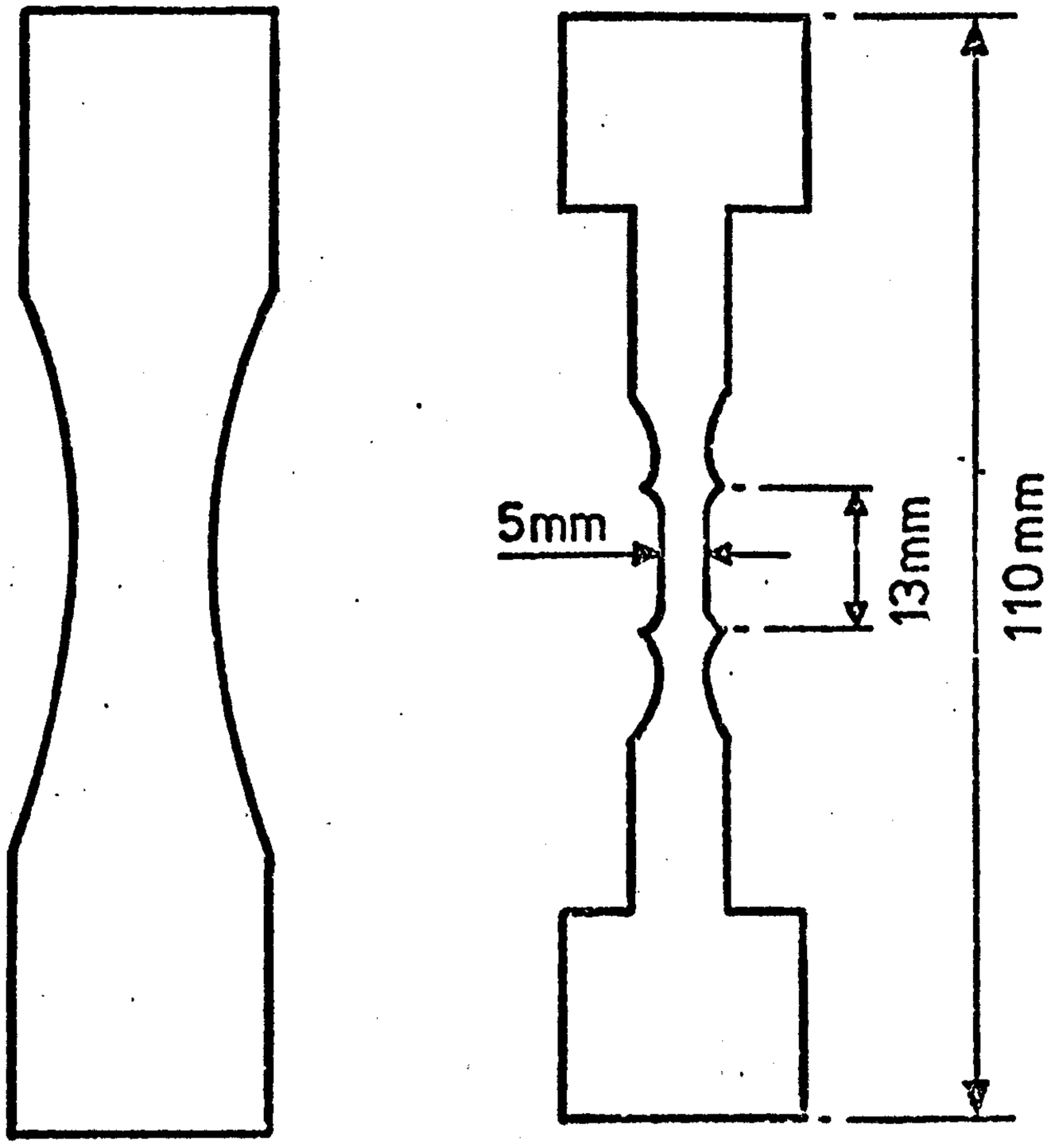

a) AS CAST b) MACHINED

FIG. 4.1 - MAR M 002 SPECIMENS.

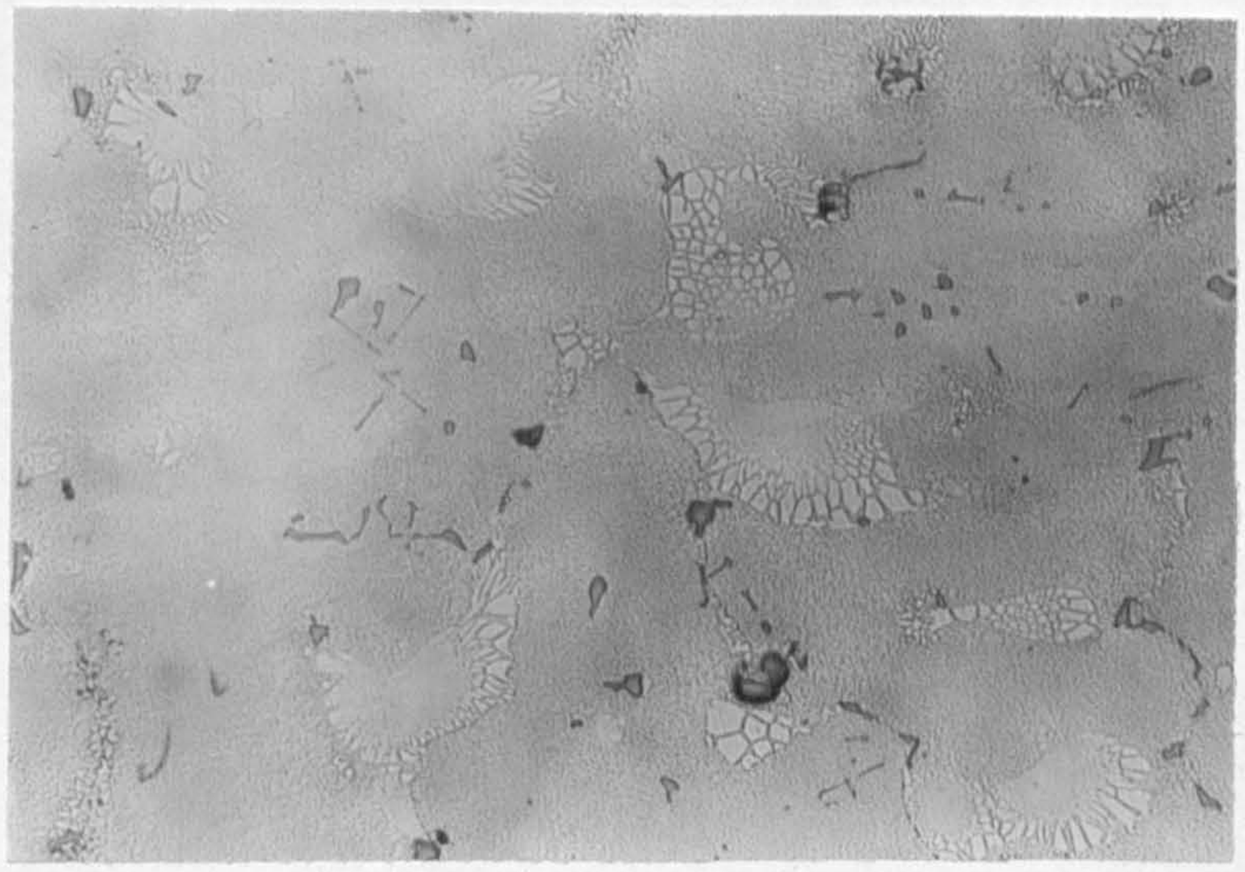

Figure 4.2 - MARM002 microstructure, magnification 200X
Etched in Kalling's reagent

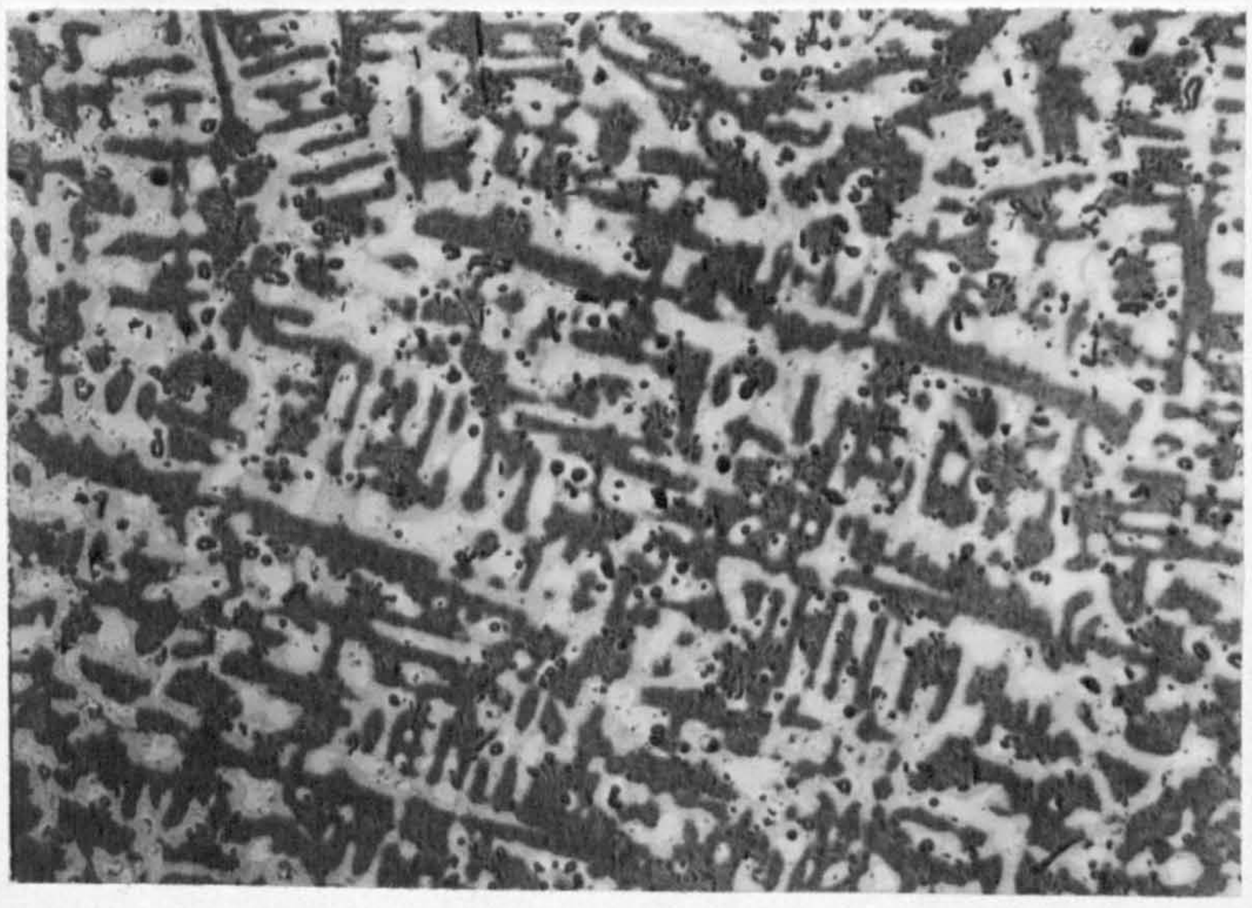

Figure 4.3 - Cast MARM002 microstructure, magnification 100X
Electrolitic etching in glacial acetic acid 15%

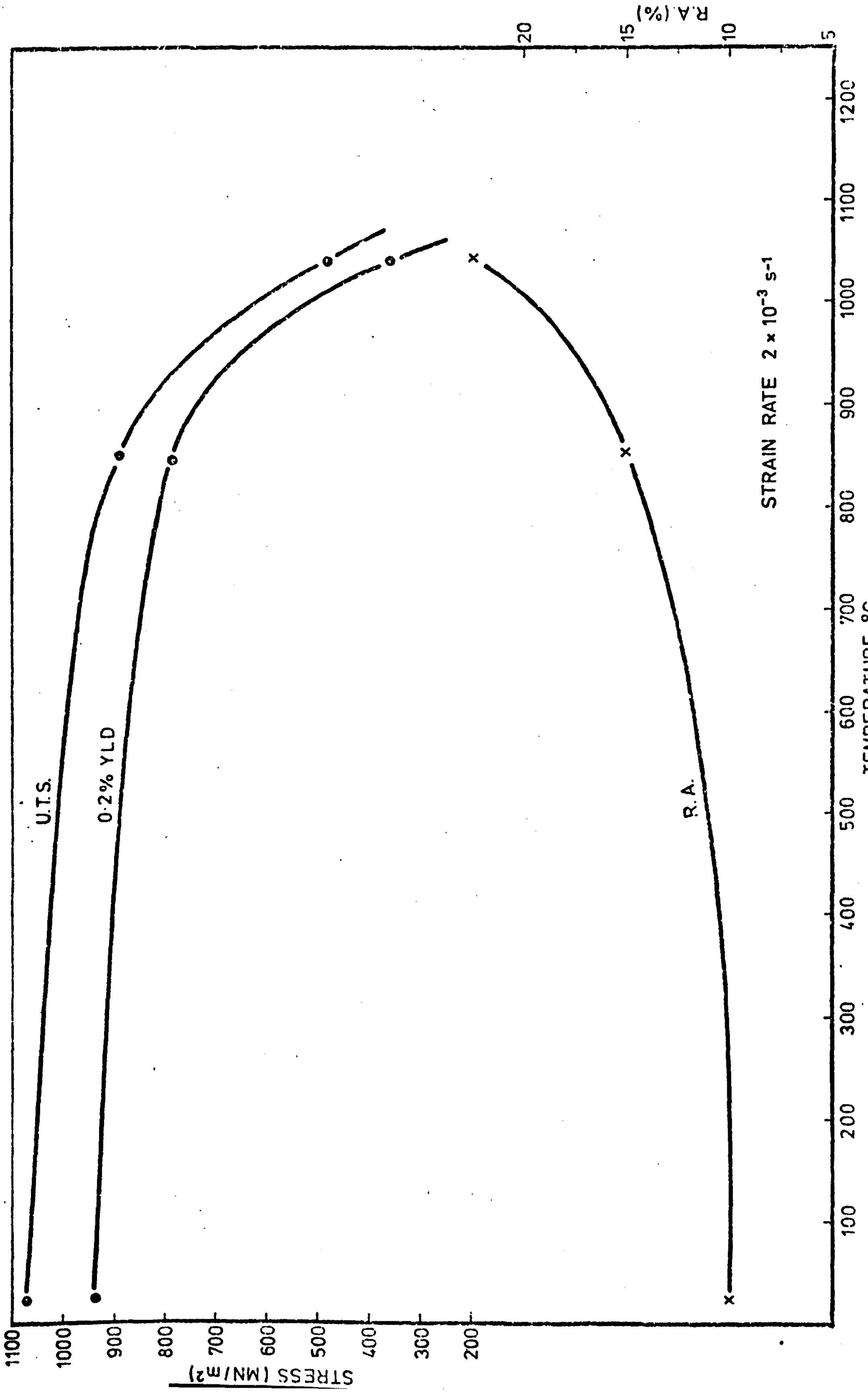

FIG.44 - TENSILE PROPERTIES MAR M002.

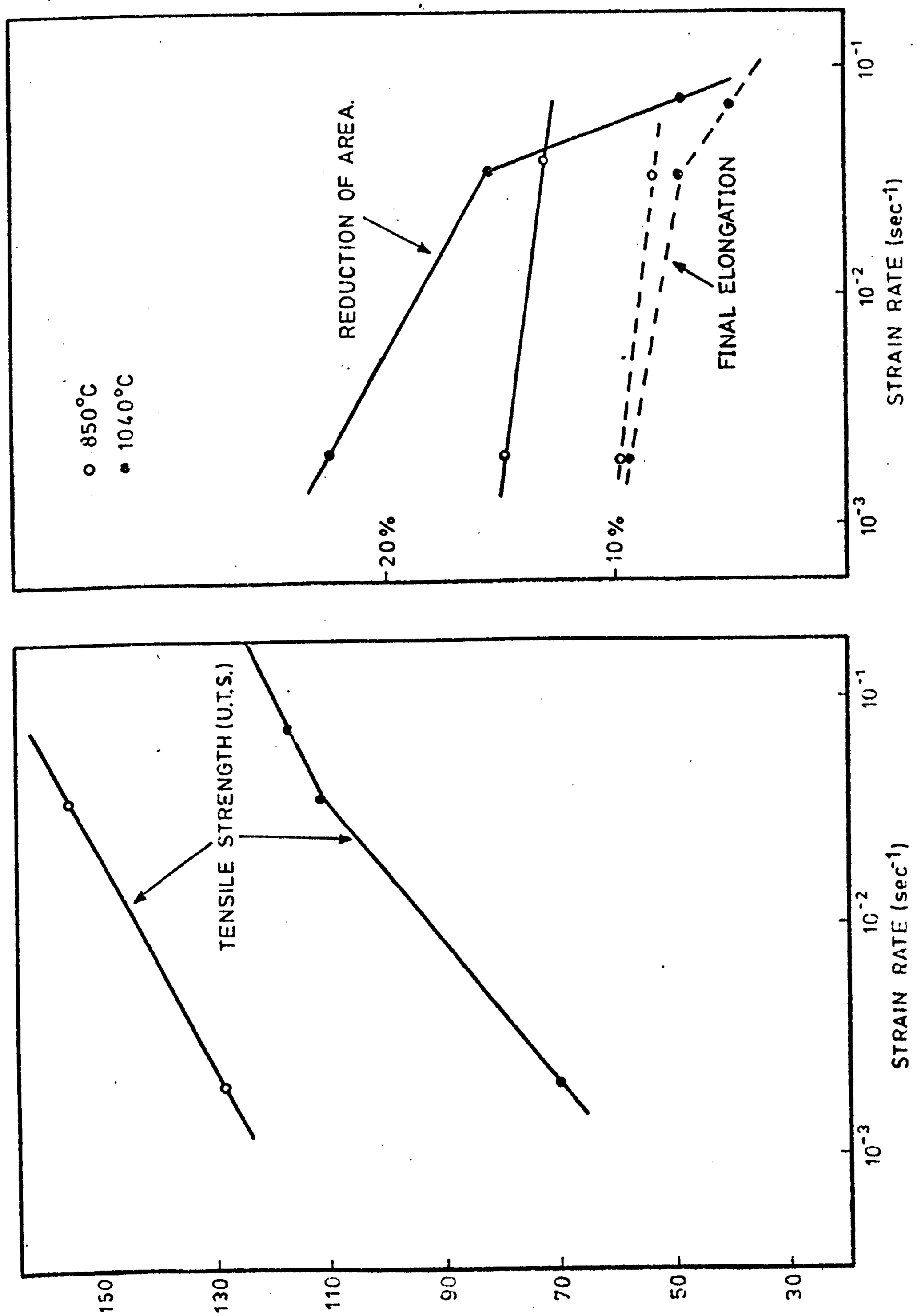

FIG.4.5 – TENSILE PROPERTIES OF MAR M002 AS A FUNCTION OF THE STRAIN RATE.

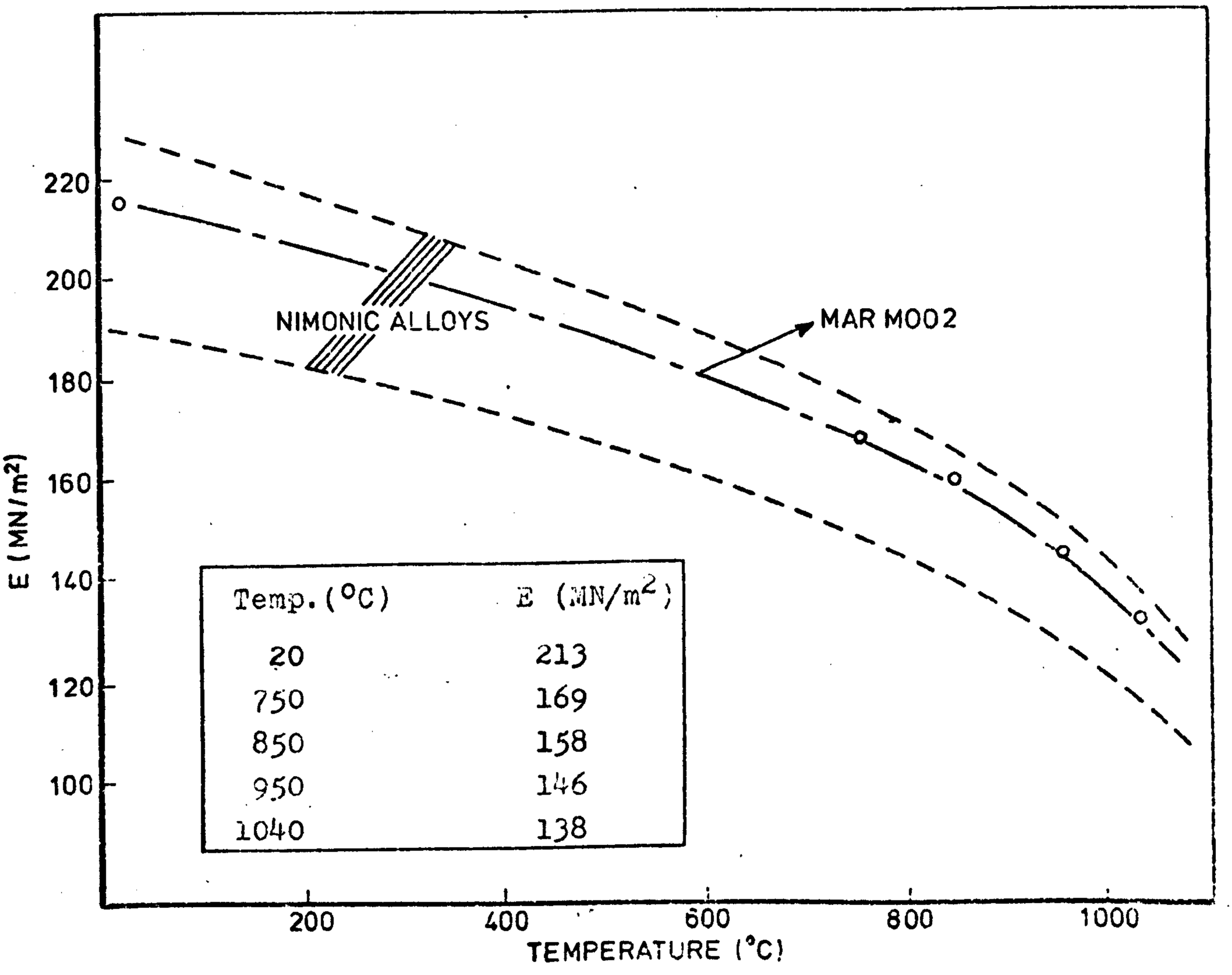

Temp. (°C)	E (MN/m²)
20	213
750	169
850	158
950	146
1040	138

FIG. 4.6 - MAR M002 STATIC YOUNG MODULUS vs. TEMPERATURE

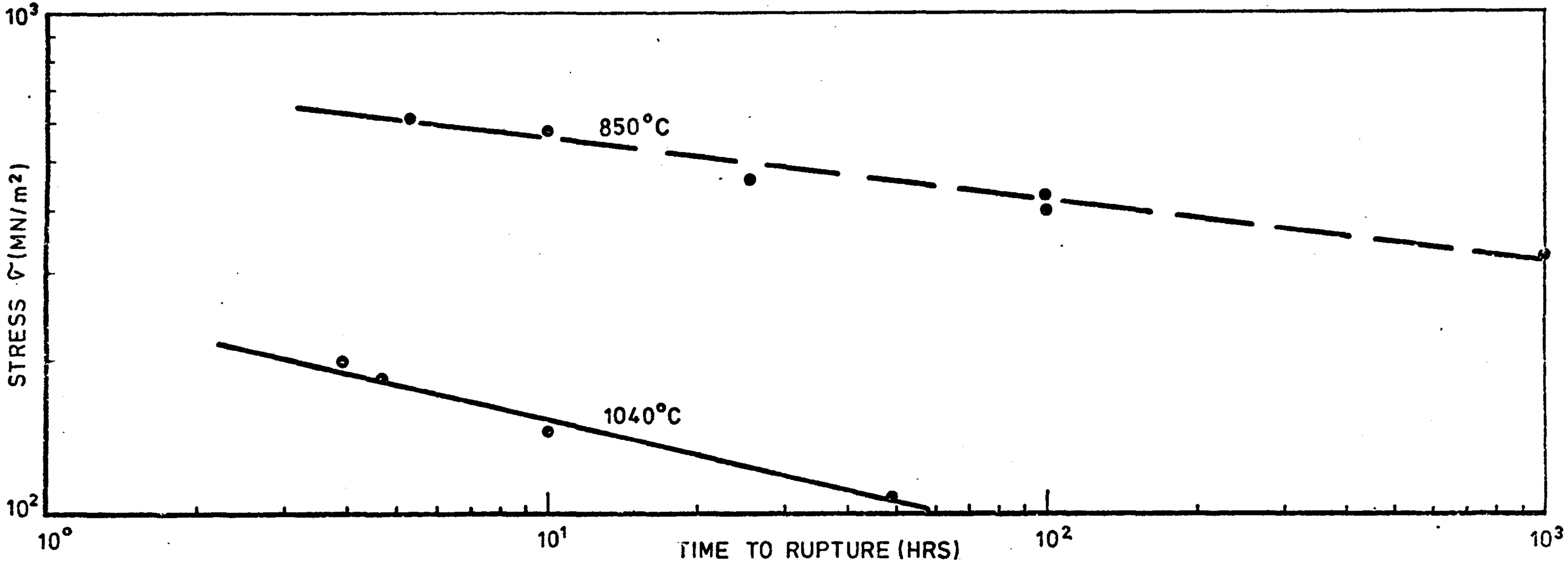

FIG. 4.7- CREEP PROPERTIES AT 850° AND 1040°C OF MAR M002.

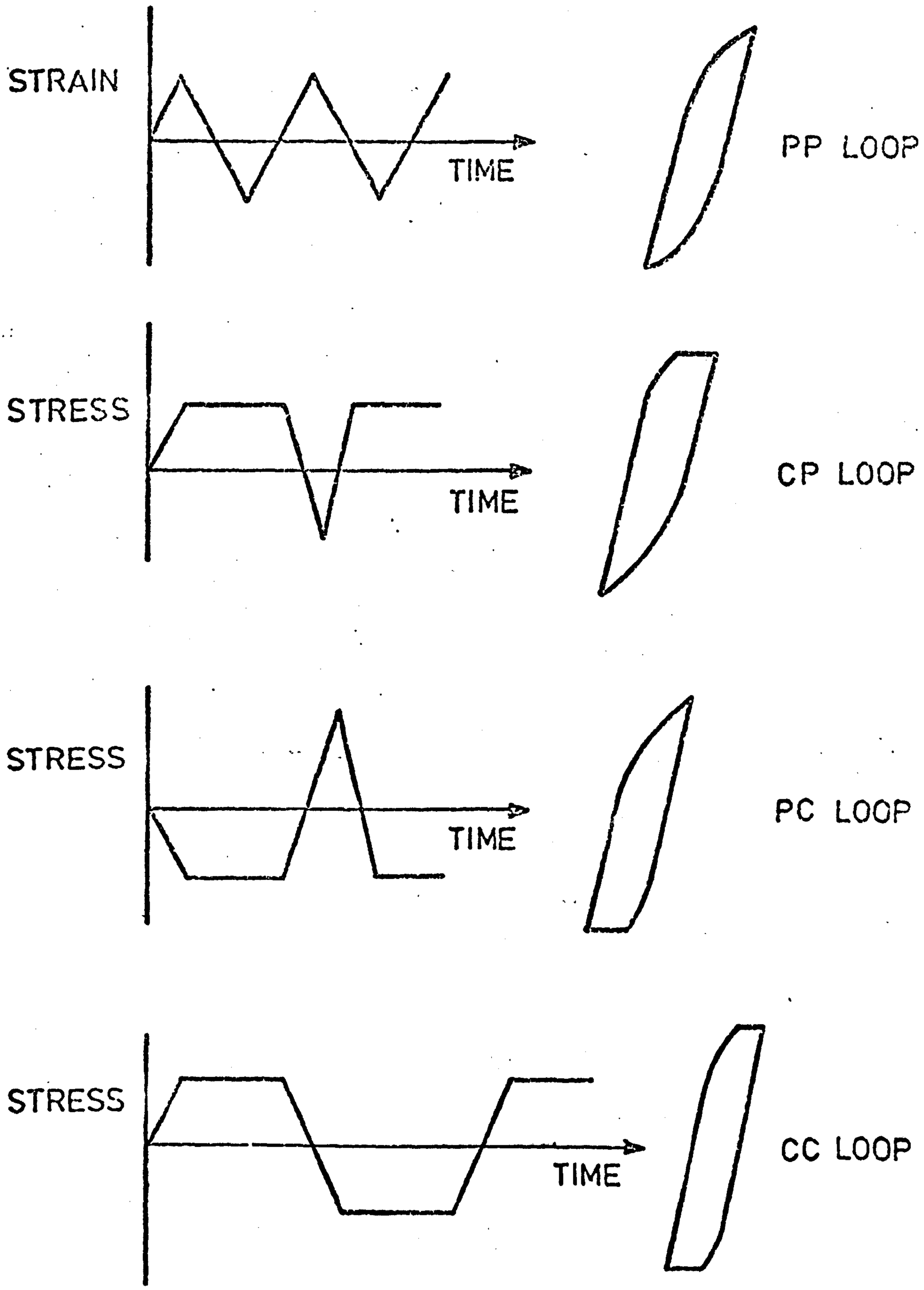

FIG.4.8 - AXIAL STRAIN AND STRESS VERSUS TIME WAVE FORMS FOR THE ISOTHERMAL LOW CYCLE FATIGUE TESTS.

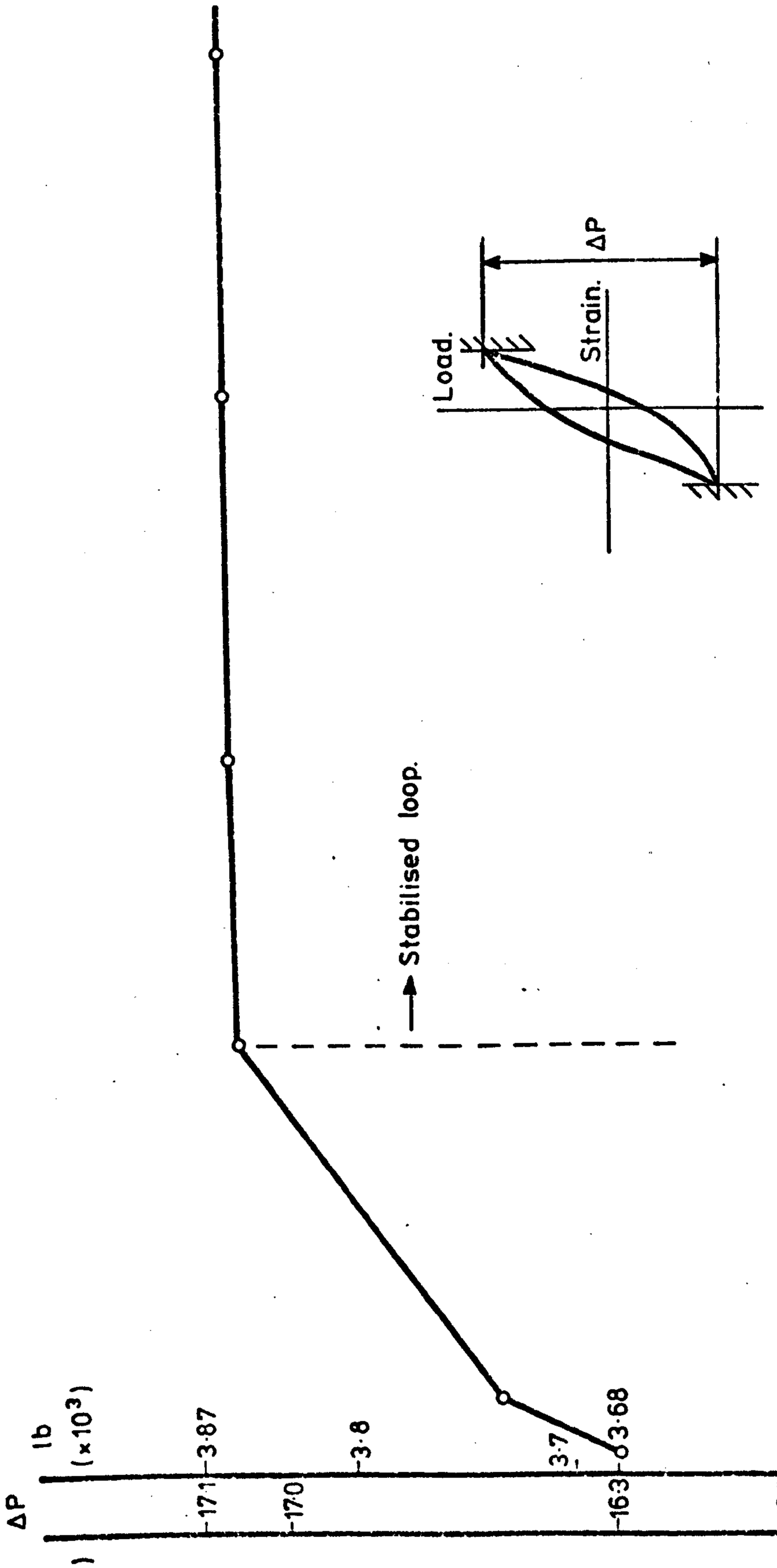

FIG. 4.9 - FREQUENCY RESPONSE AT 850°C FOR A STRAIN CONTROLLED TEST.

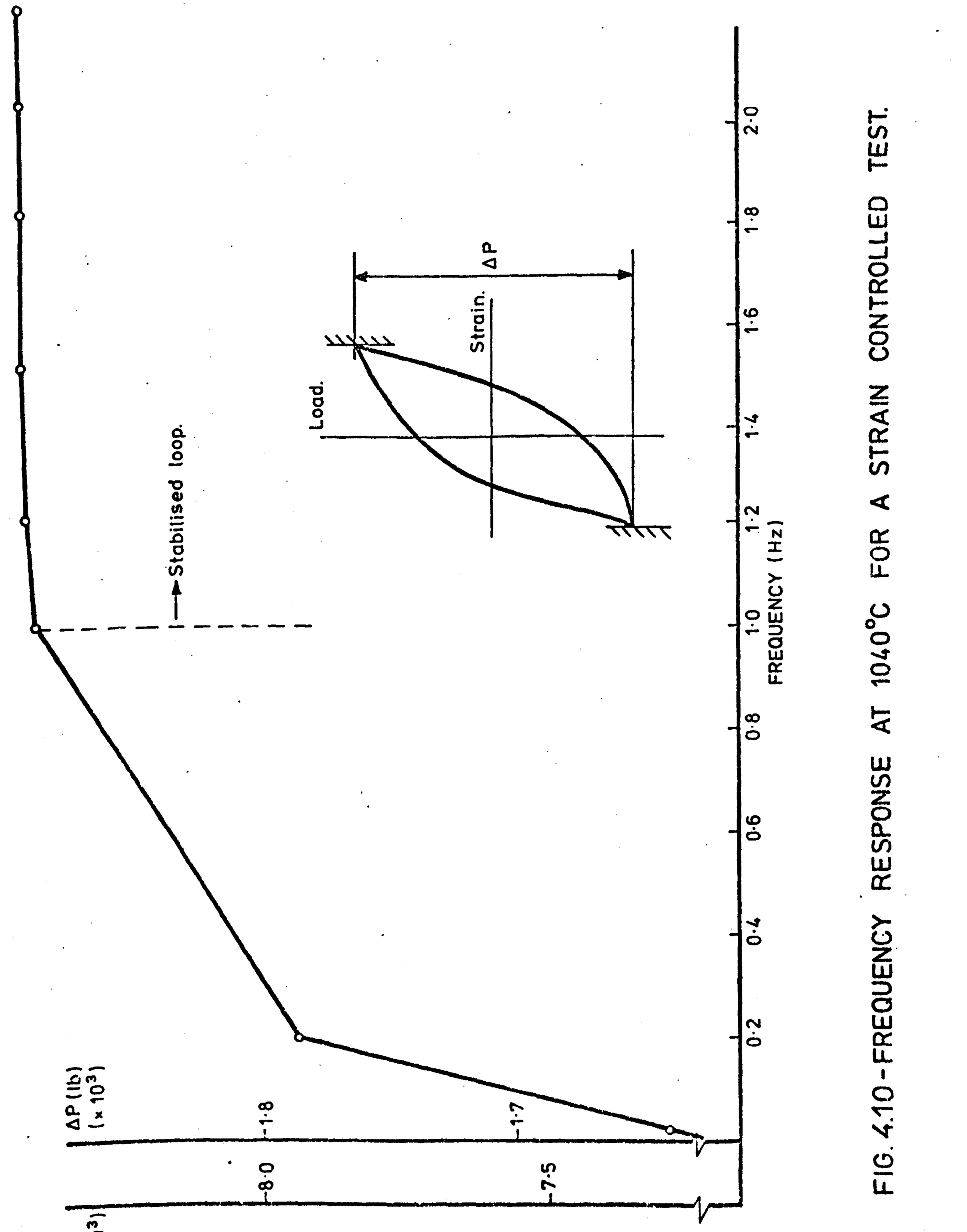

FIG. 4.10 - FREQUENCY RESPONSE AT 1040°C FOR A STRAIN CONTROLLED TEST.

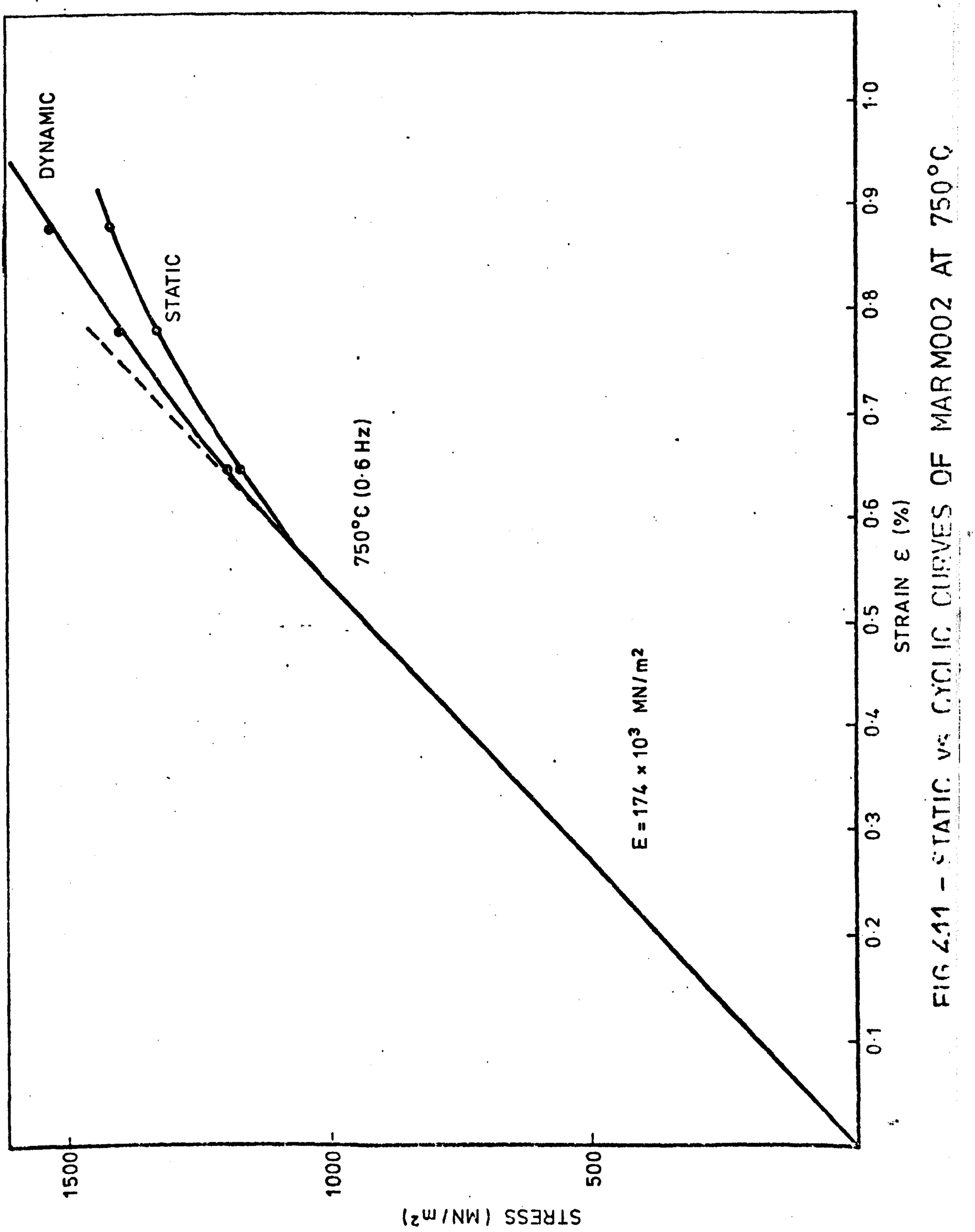

FIG 4.11 – STATIC VS CYCLIC CURVES OF MARMOO2 AT 750°C

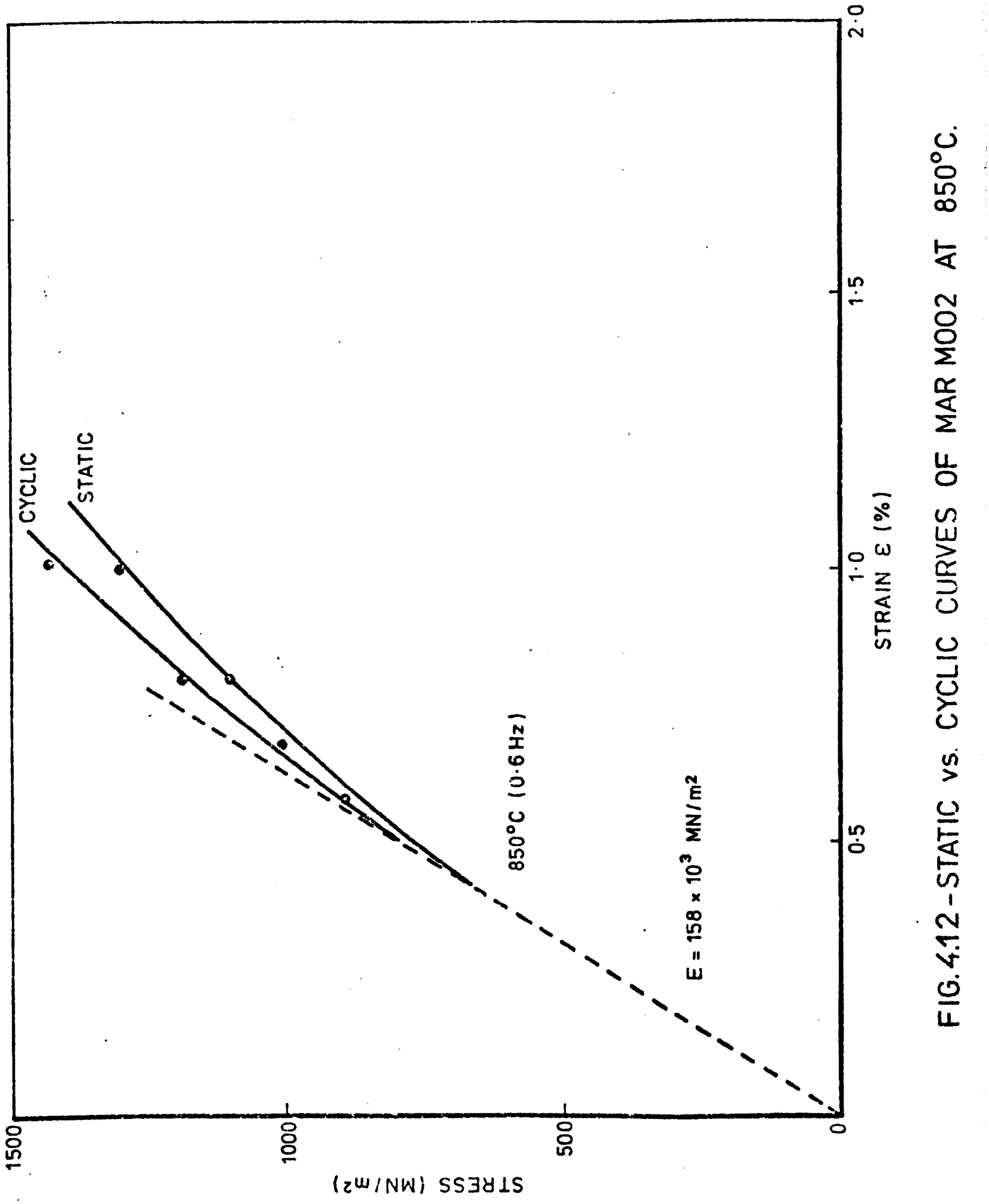

FIG.4.12-STATIC vs. CYCLIC CURVES OF MAR M002 AT

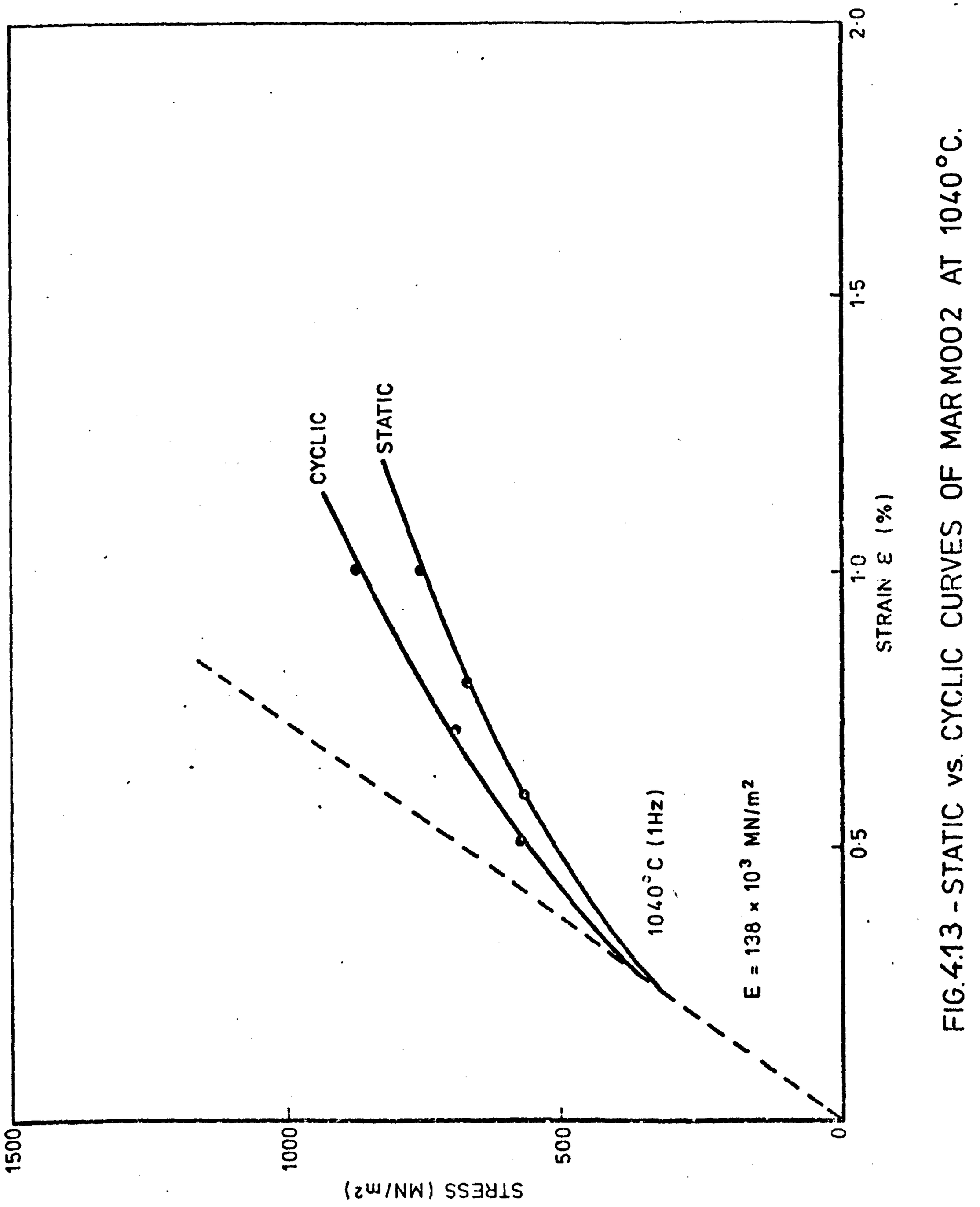

FIG.4.13 - STATIC vs. CYCLIC CURVES OF MAR M002 AT 1040°C.

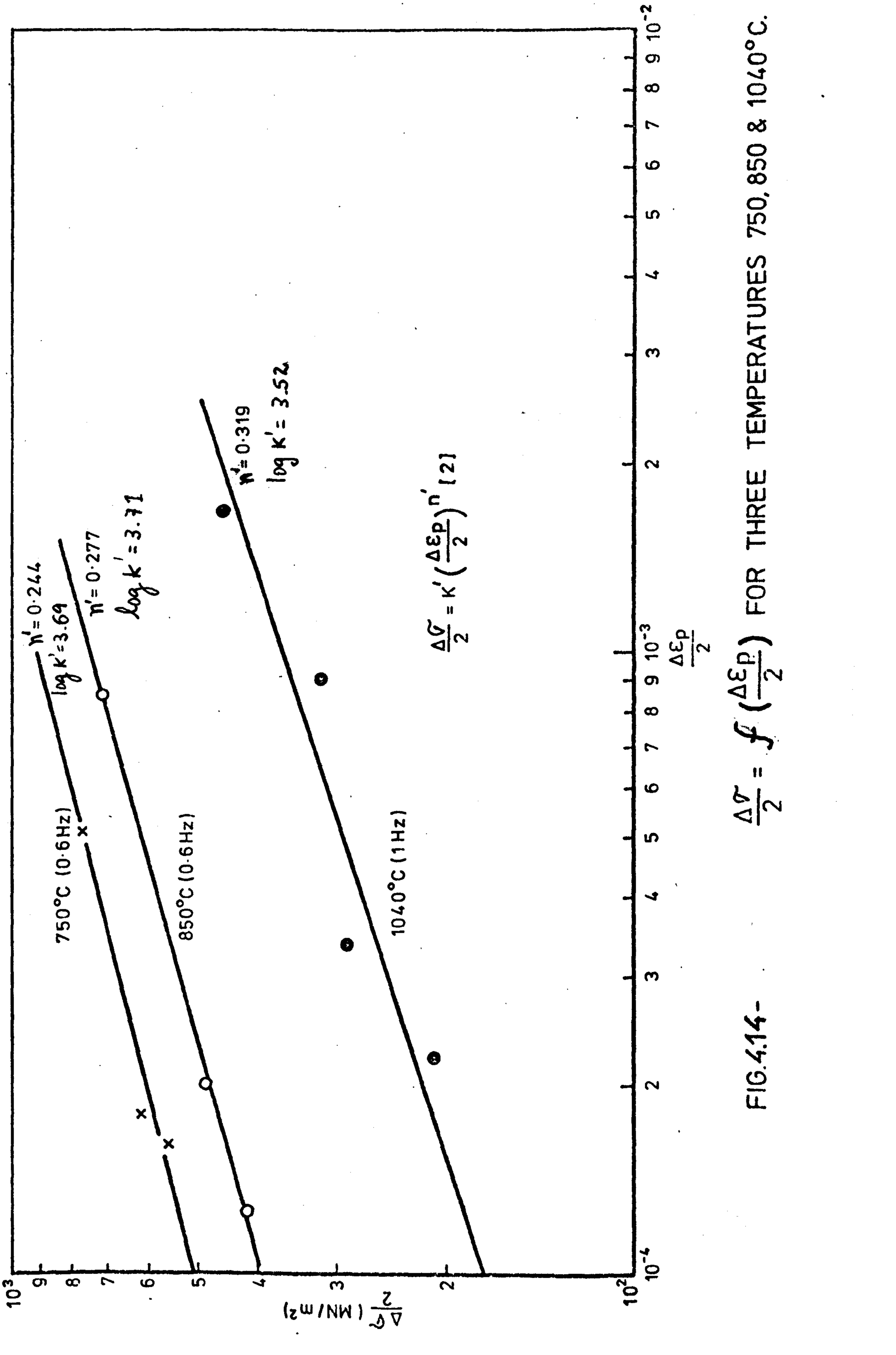
$\frac{\Delta\sigma}{2} = k'\left(\frac{\Delta\varepsilon_p}{2}\right)^{n'}$ [2]
$\frac{\Delta\sigma}{2} = f\left(\frac{\Delta\varepsilon_p}{2}\right)$ FOR THREE TEMPERATURES
$\frac{\Delta\sigma}{2}$ (MN/m²)
$\frac{\Delta\varepsilon_p}{2}$
750°C (0·6Hz)
850°C (0·6Hz)
1040°C (1Hz)
n'= 0·244
log k'=3.69
n'= 0·277
log k'=3.71
n'= 0·319
log k'= 3.52

FIG.4.14-

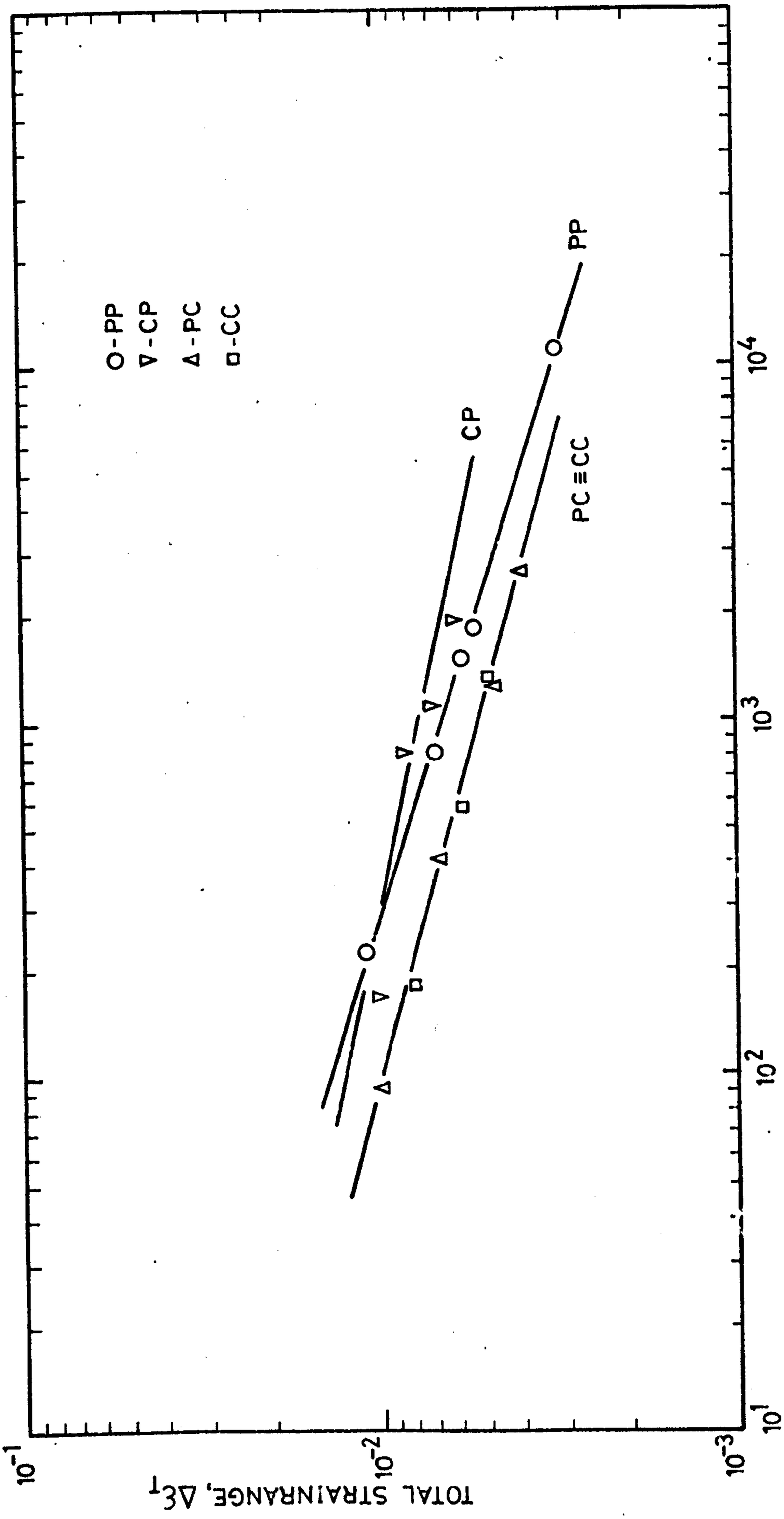

FIG.4.15 – TOTAL STRAINRANGE VS. LIFE RELATIONSHIPS FOR EACH OF THE GENERIC TEST TYPES AT 850°C.

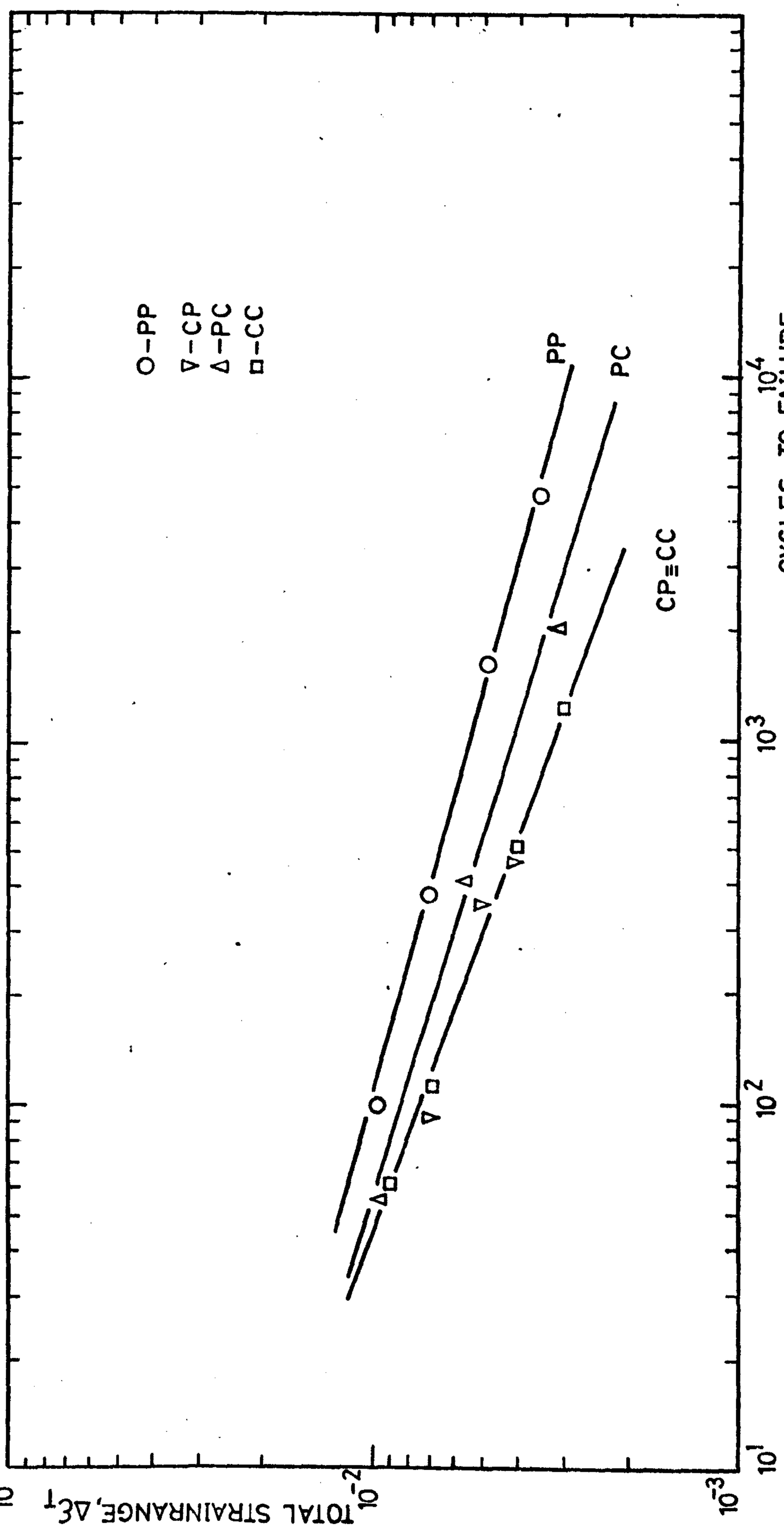

FIG. 4.16 – TOTAL STRAINRANGE VS. LIFE RELATIONSHIPS FOR EACH OF THE GENERIC TEST TYPES AT 1040 °C.

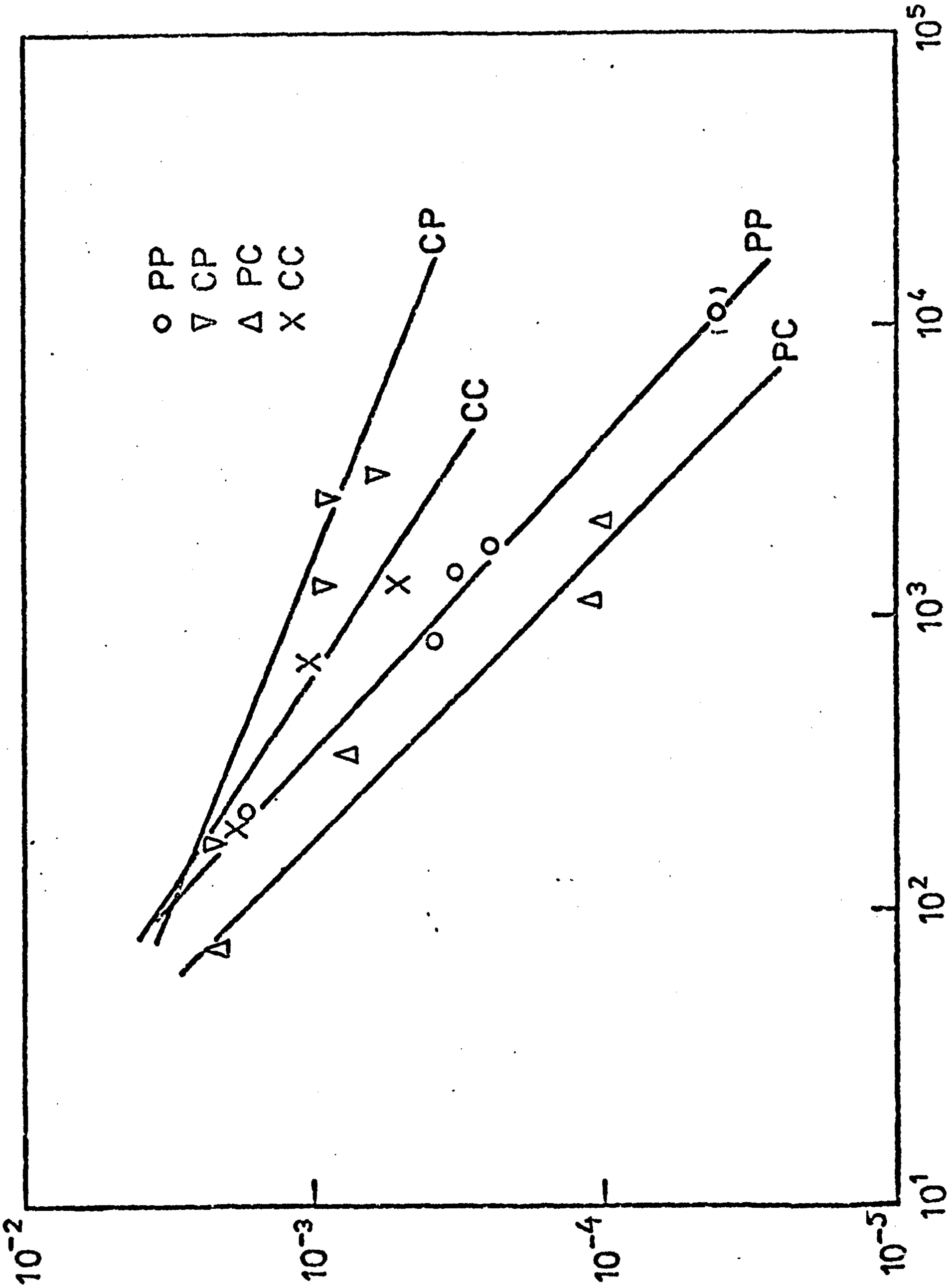

FIG.4.17-STRAINRANGE VERSUS LIFE RELATIONSHIPS FOR EACH OF THE BASIC TESTS AT 850°C.

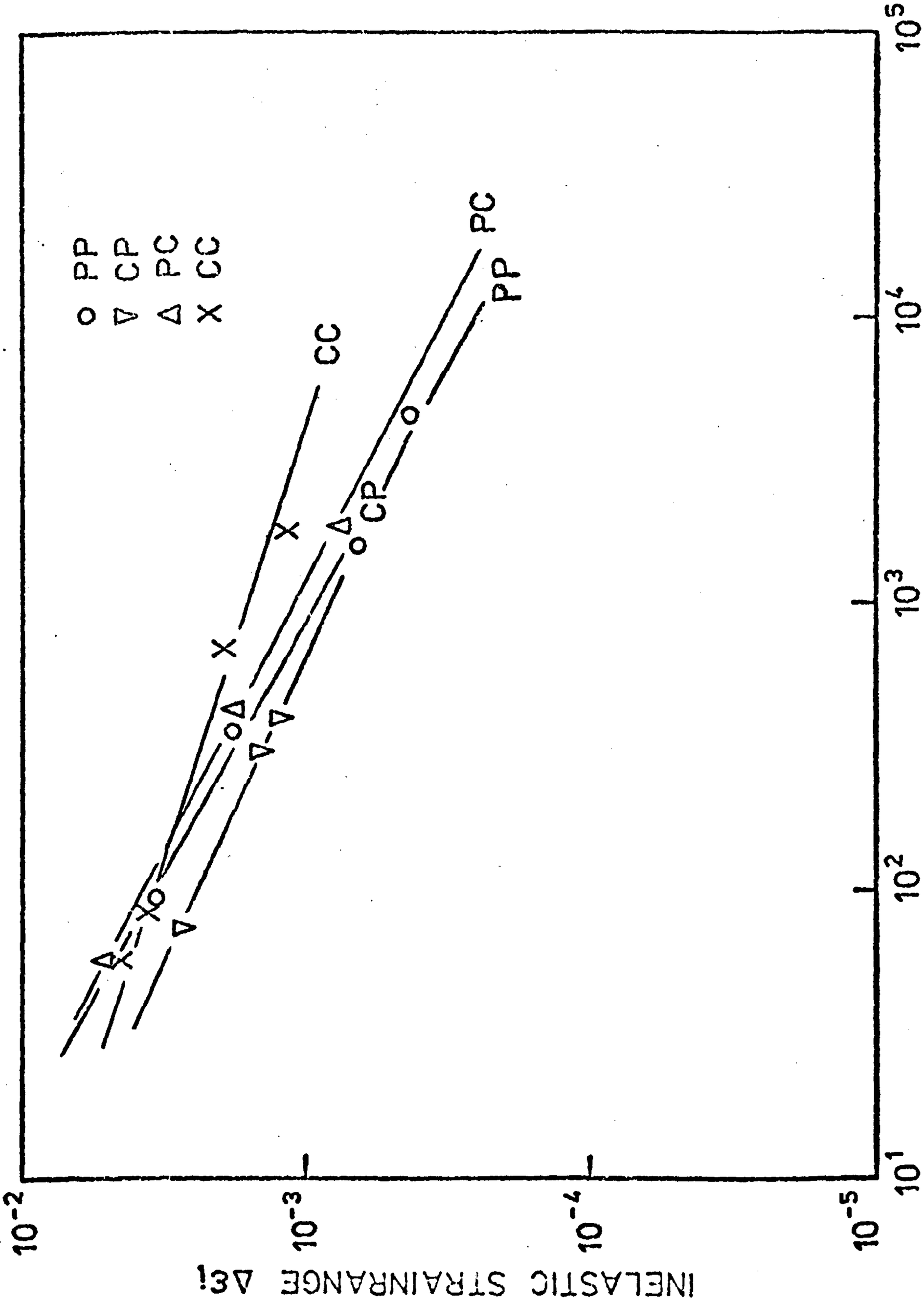

FIG.418-STRAINRANGE VERSUS LIFE RELATIONSHIPS FOR EACH OF THE BASIC TESTS AT 1040°C.

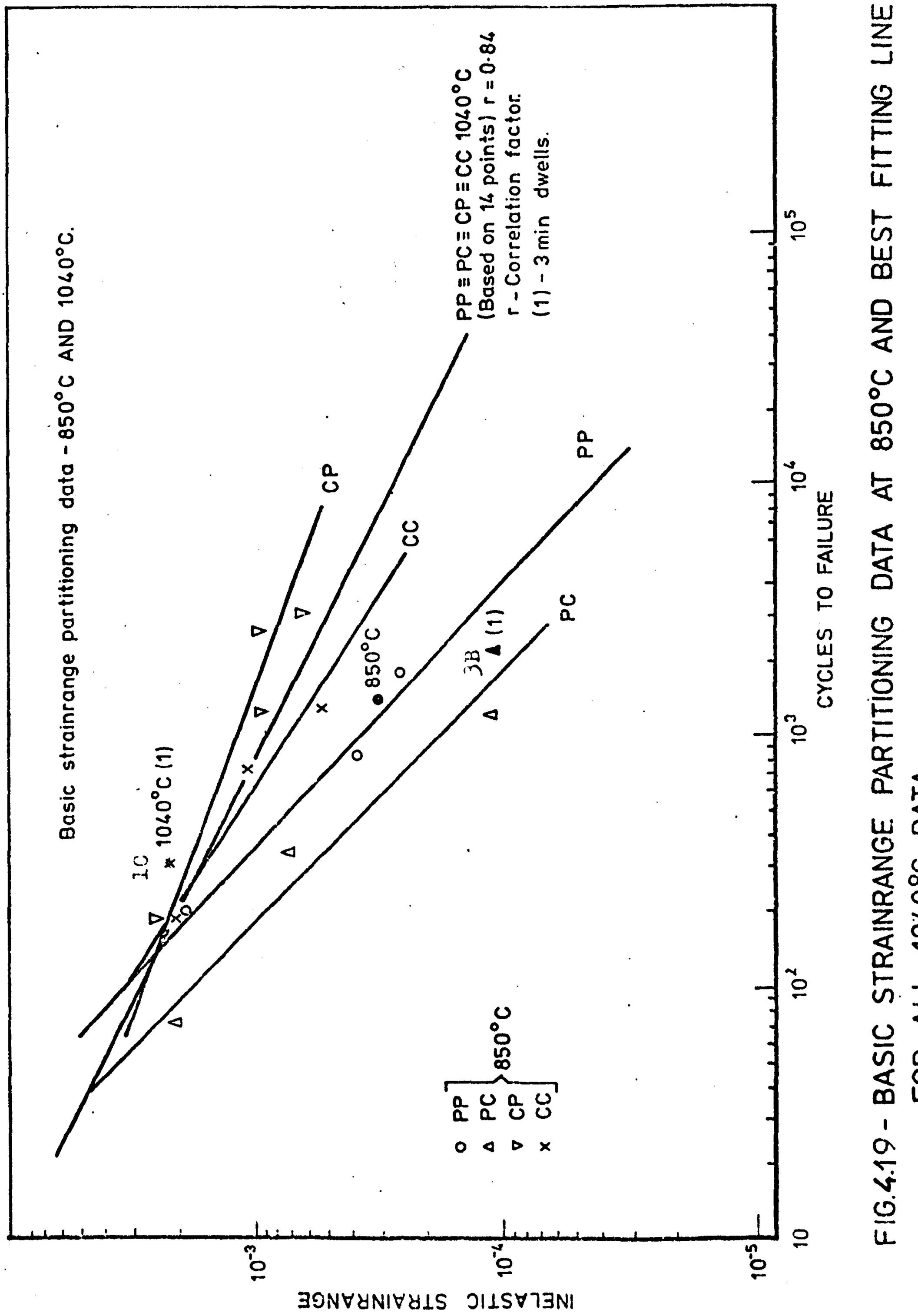

FIG.4.19 - BASIC STRAINRANGE PARTITIONING DATA AT 850°C AND 1040°C AND BEST FITTING LINE FOR ALL 1040°C DATA.

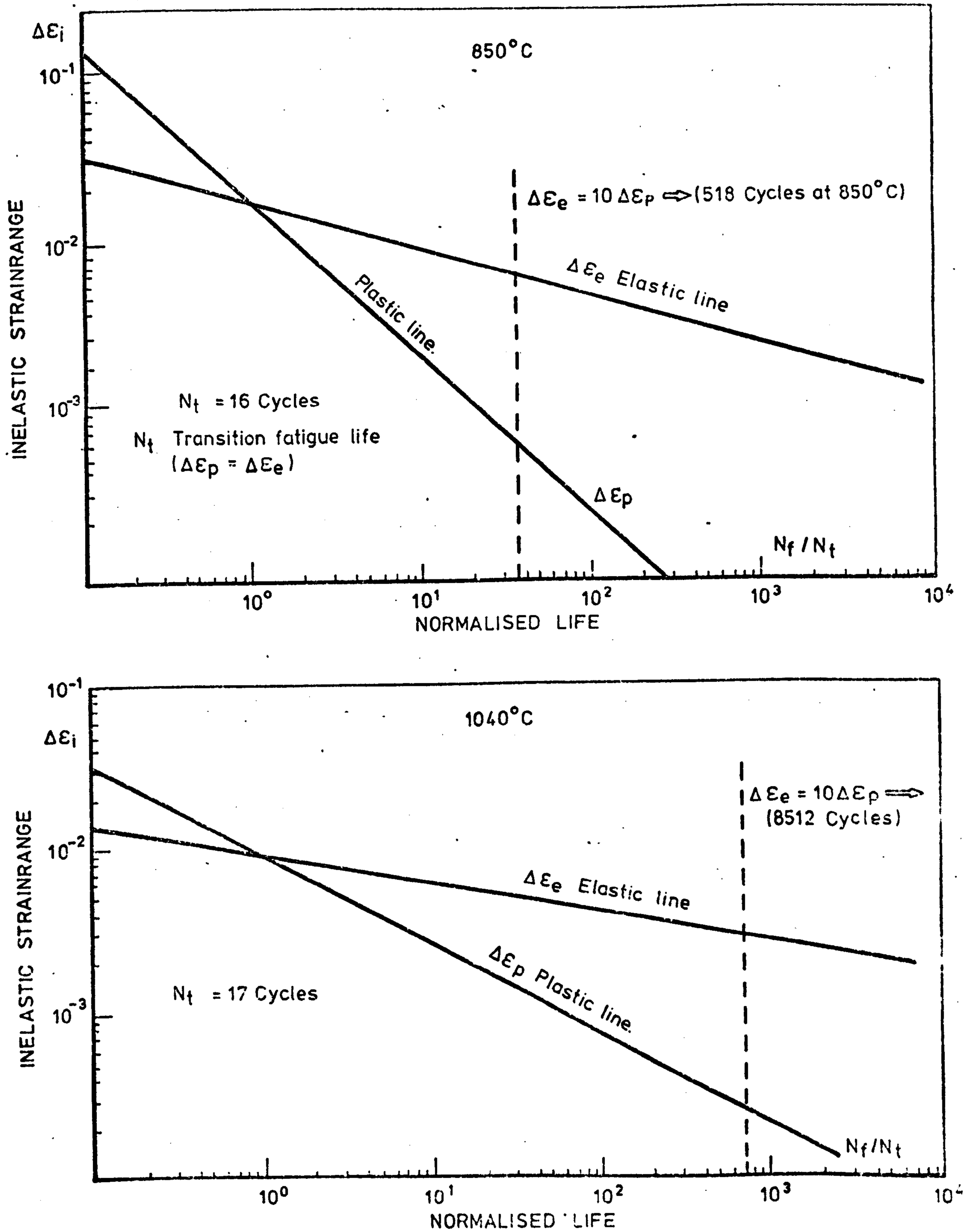

FIG.4.20 - PLASTIC AND ELASTIC LINES AT 850°C AND 1040°C.

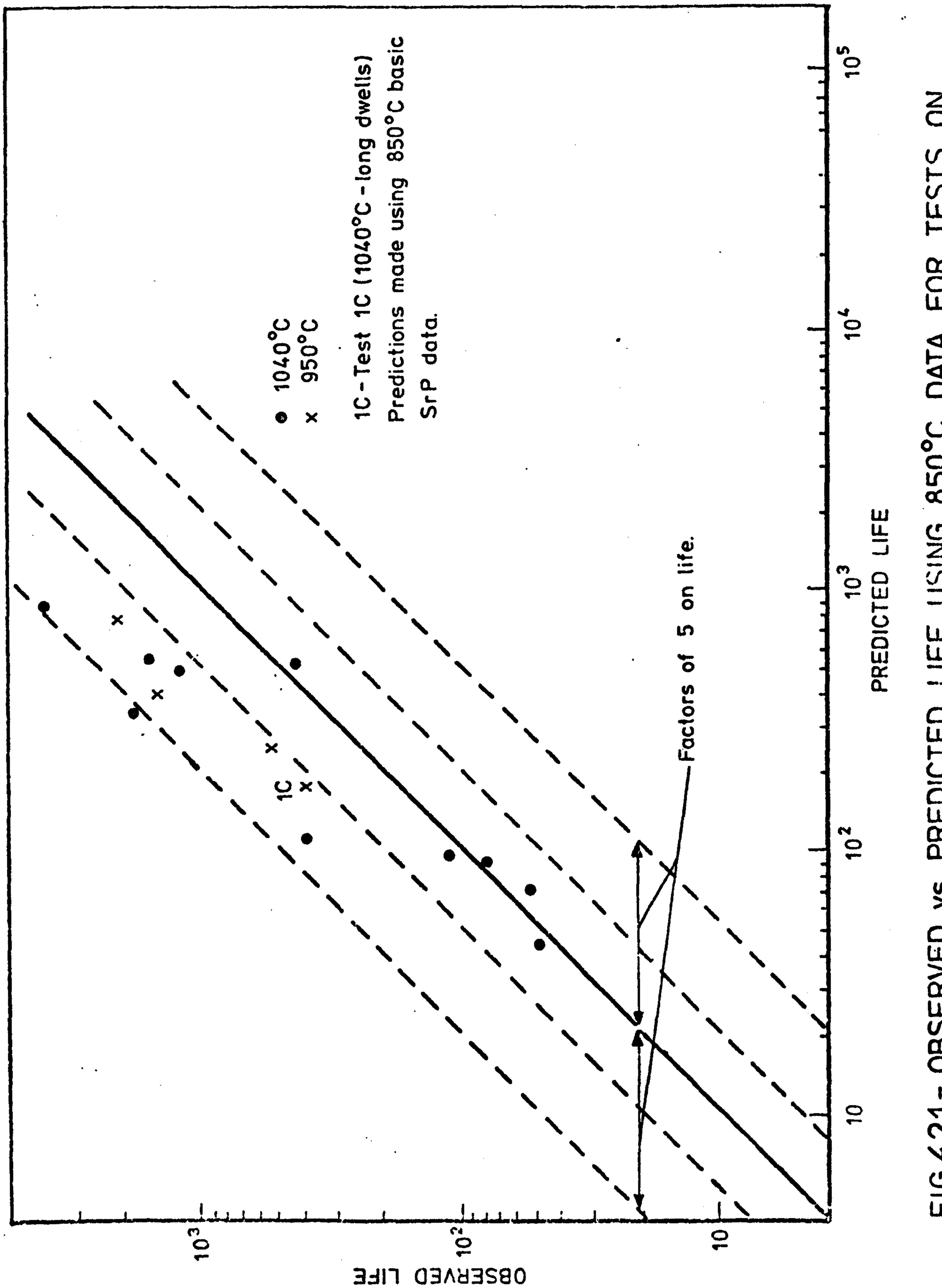

FIG.4.21- OBSERVED vs PREDICTED LIFE USING 850°C DATA FOR TESTS
MAR M002 AT 1040°C AND 950°C.

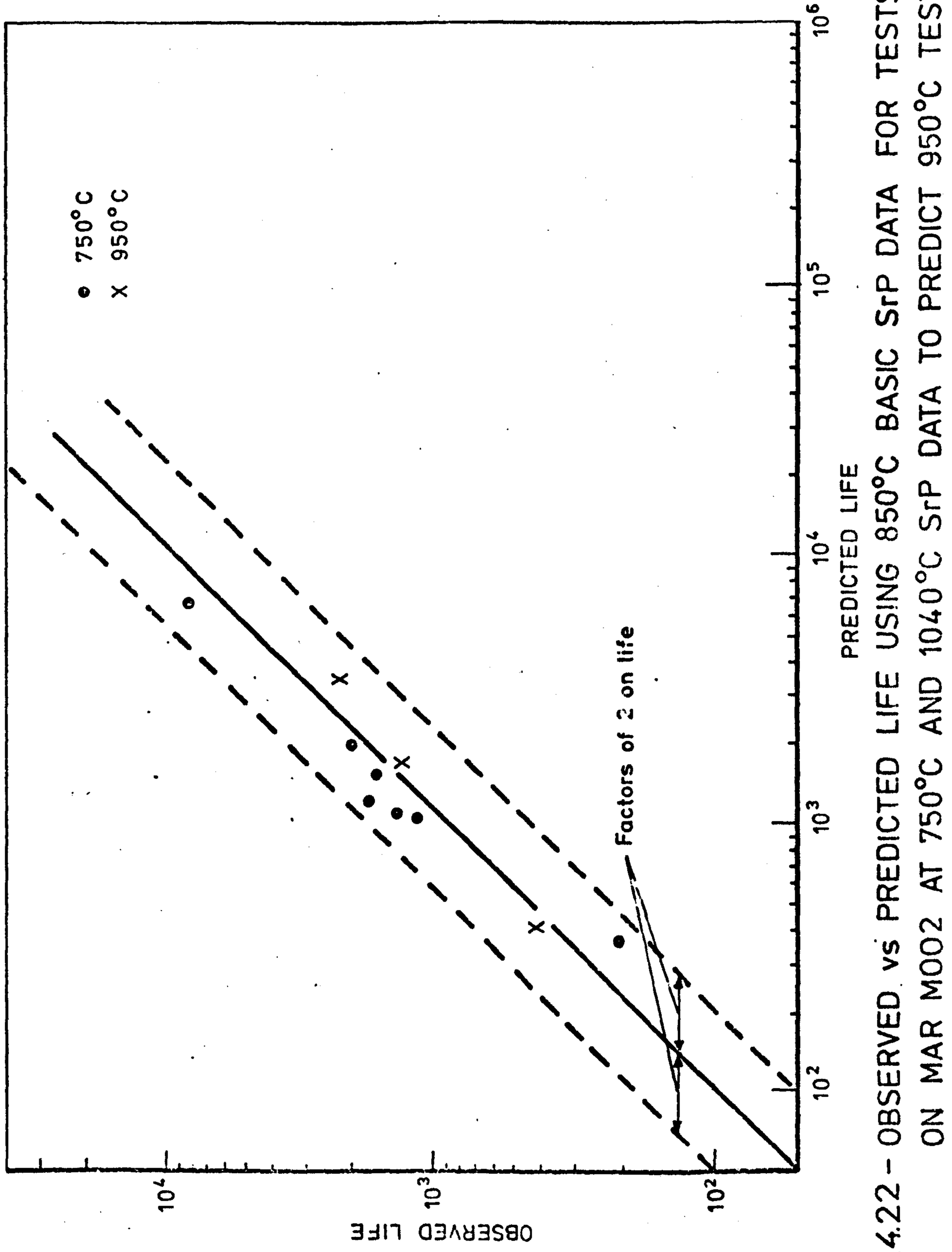

FIG.4.22 – OBSERVED vs PREDICTED LIFE USING 850°C BASIC SrP DATA FOR TESTS ON MAR M002 AT 750°C AND 1040°C SrP DATA TO PREDICT 950°C TEST RESULTS.

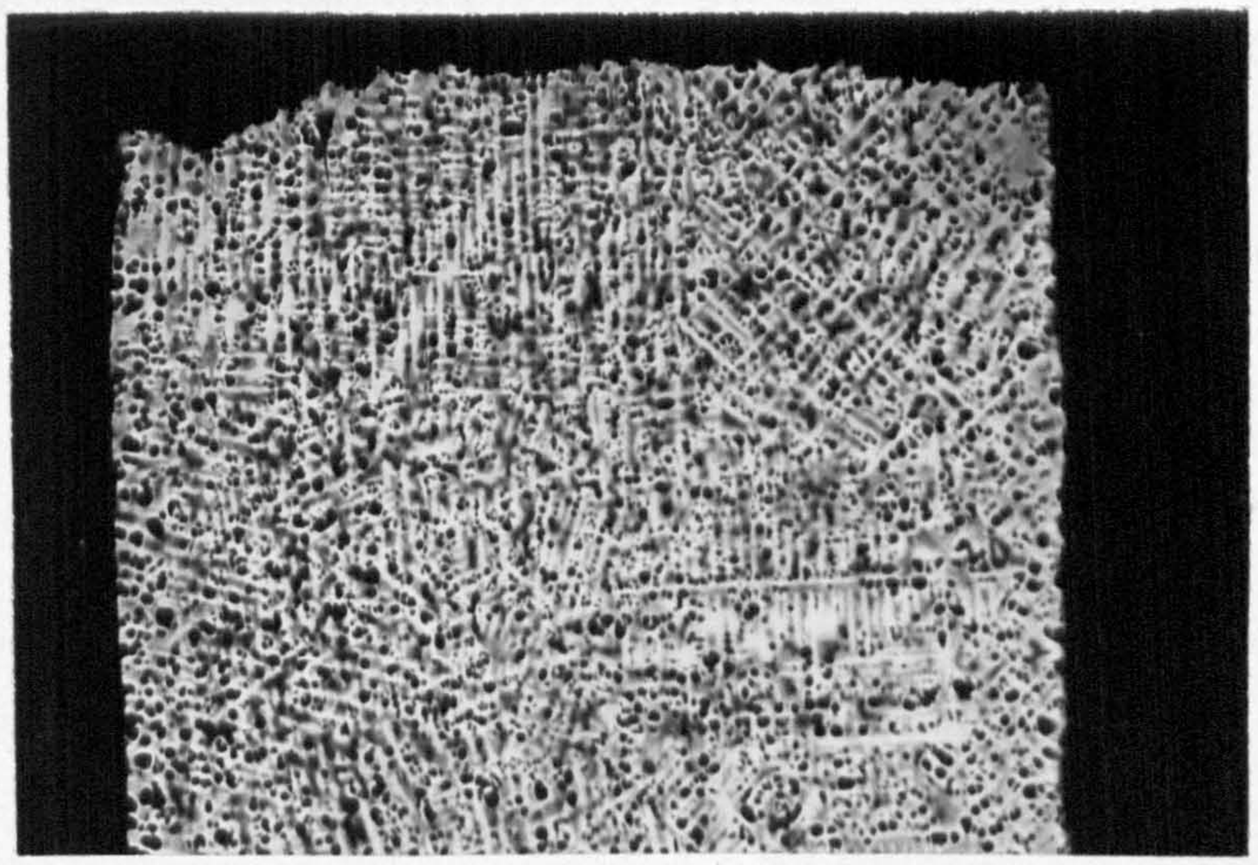

Tensile creep, compressive plastic flow
$\Delta\varepsilon_{cp}$ = 0.020% N = 2173 cycles

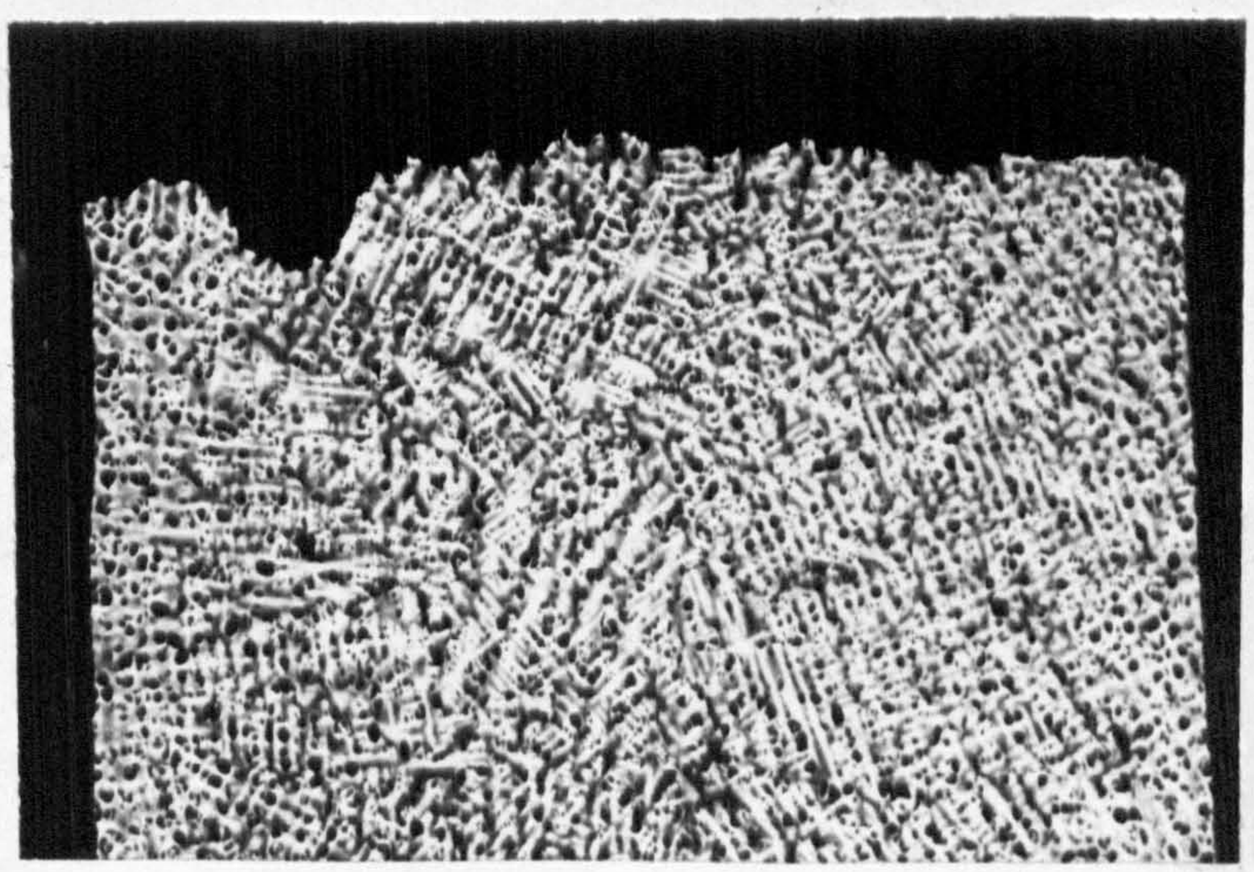

Tensile creep, compressive creep
$\Delta\varepsilon_{cc}$ = 0.024% N = 1377 cycles

Figure 4.23 - Photomicrographs of longitudinal sections of MARM002 specimens tested at 750°C

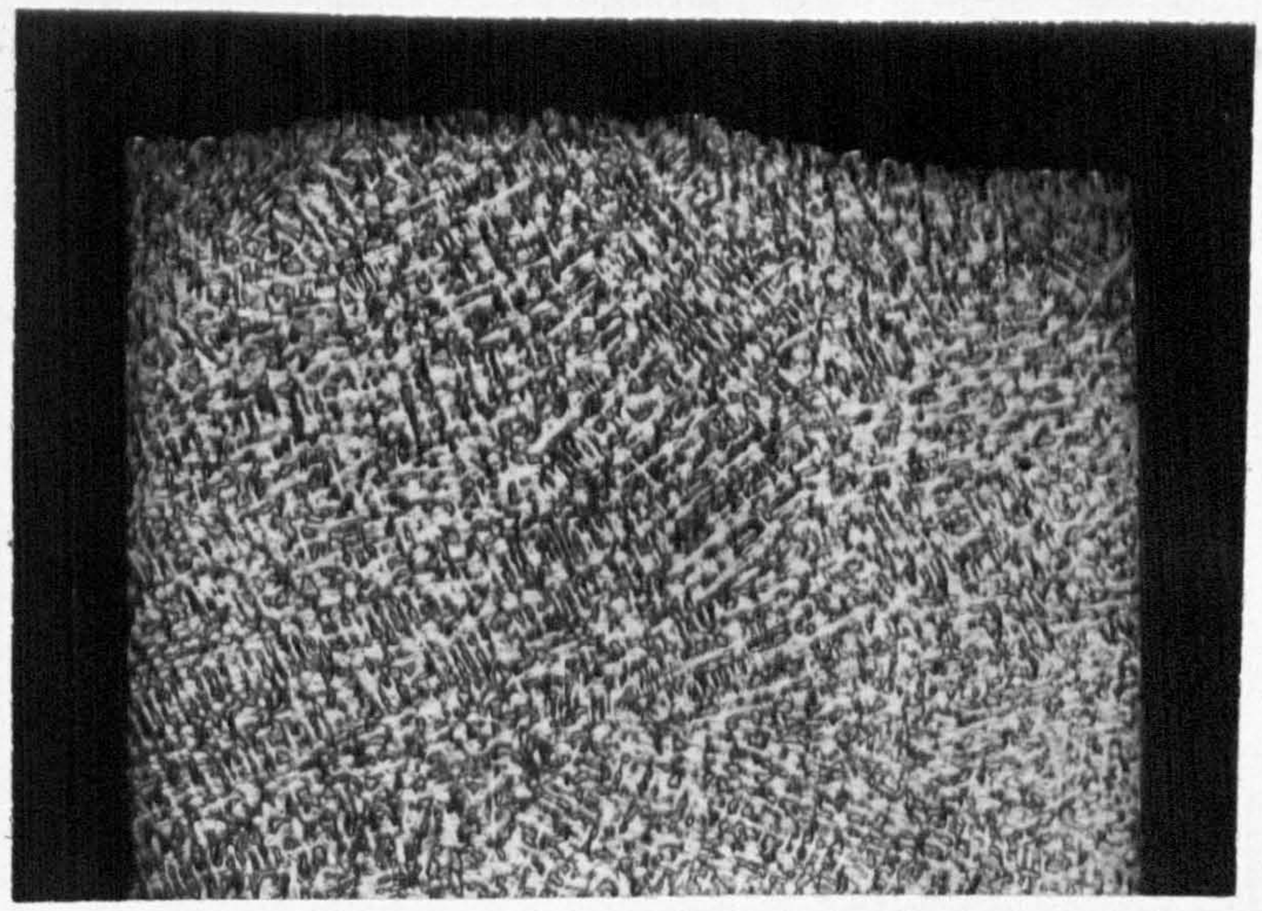

Tensile plastic flow, compressive plastic flow
$\Delta\varepsilon_{pp}$ = 0.004% N = 10960 cycles

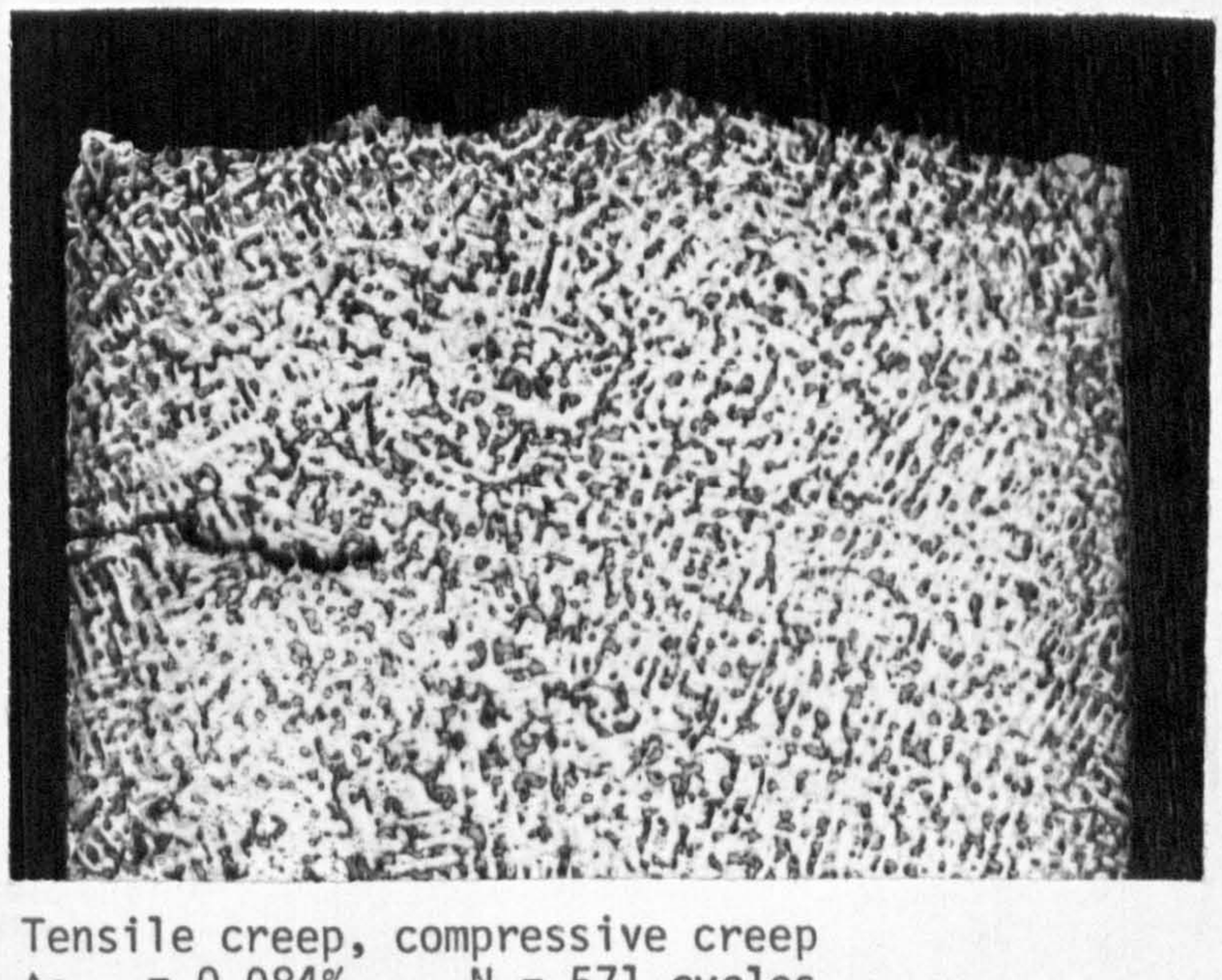

Tensile creep, compressive creep
$\Delta\varepsilon_{cc}$ = 0.084% N = 571 cycles

Figure 4.24 - Photomicrographs of longitudinal sections of MARM002 specimens tested at 850°C

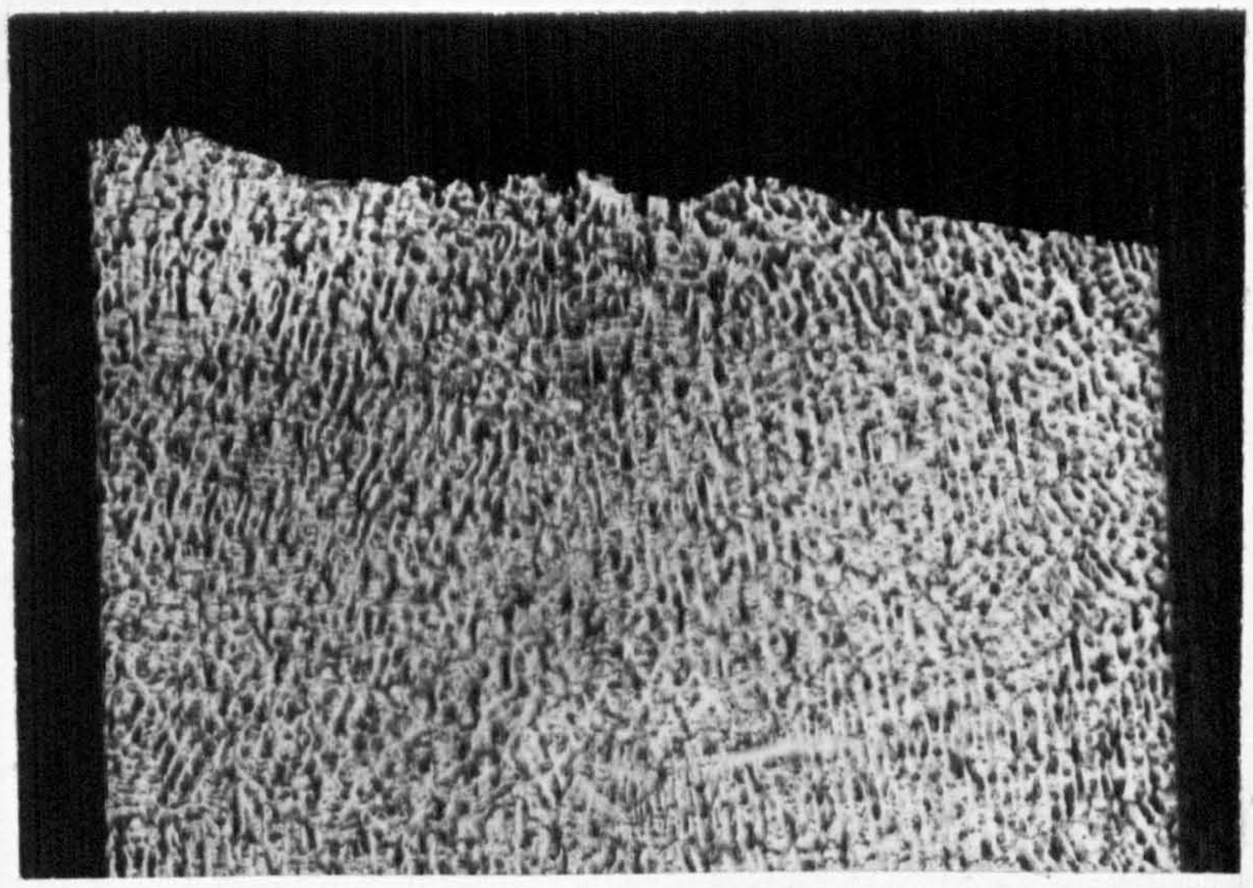

Tensile plastic flow, compressive plastic flow
$\Delta\varepsilon_{pp}$ = 0.044% N = 4600 cycles

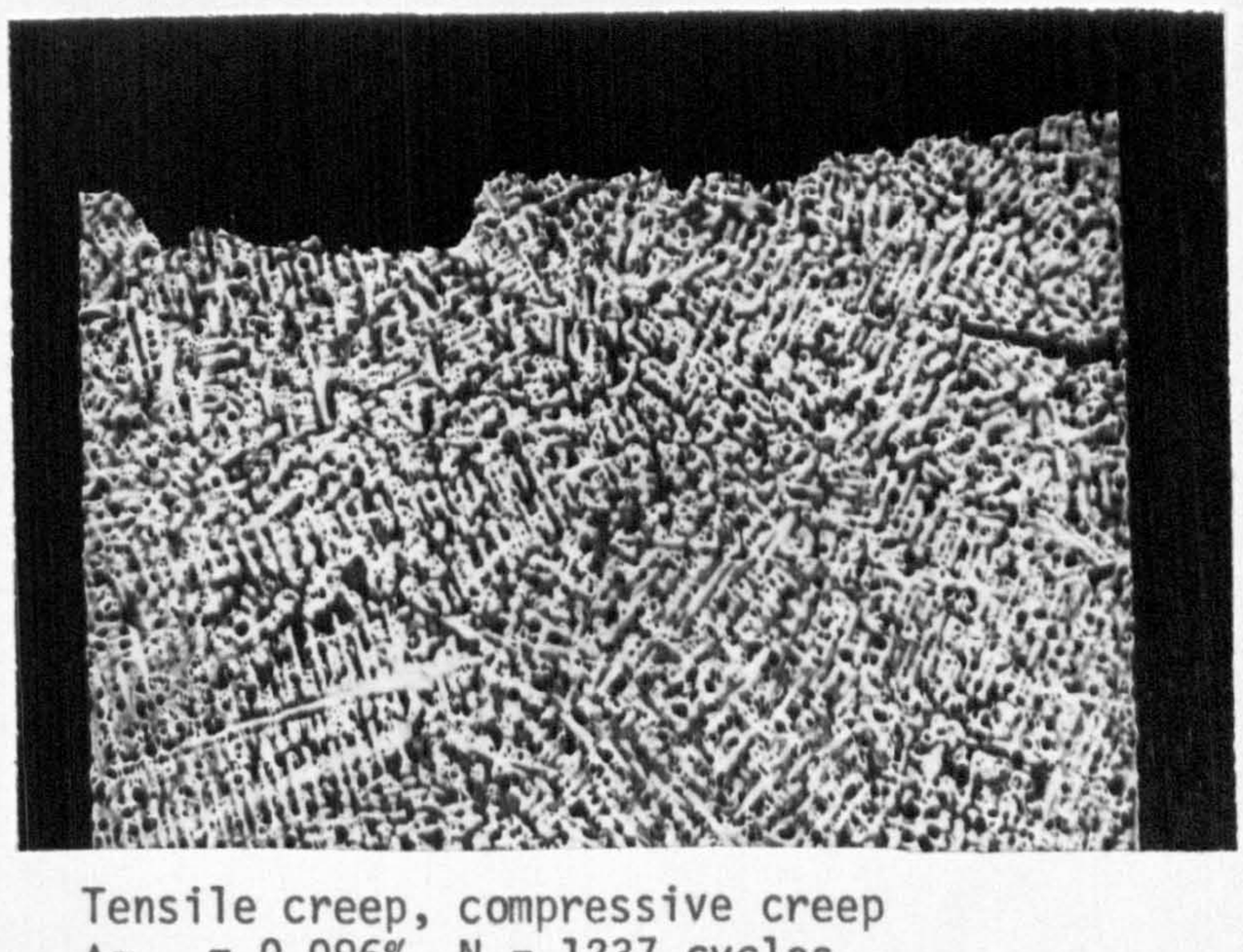

Tensile creep, compressive creep
$\Delta\varepsilon_{cc}$ = 0.096% N = 1237 cycles

Figure 4.25 - Photomicrographs of longitudinal sections of MARM002 specimens tested at 1040°C

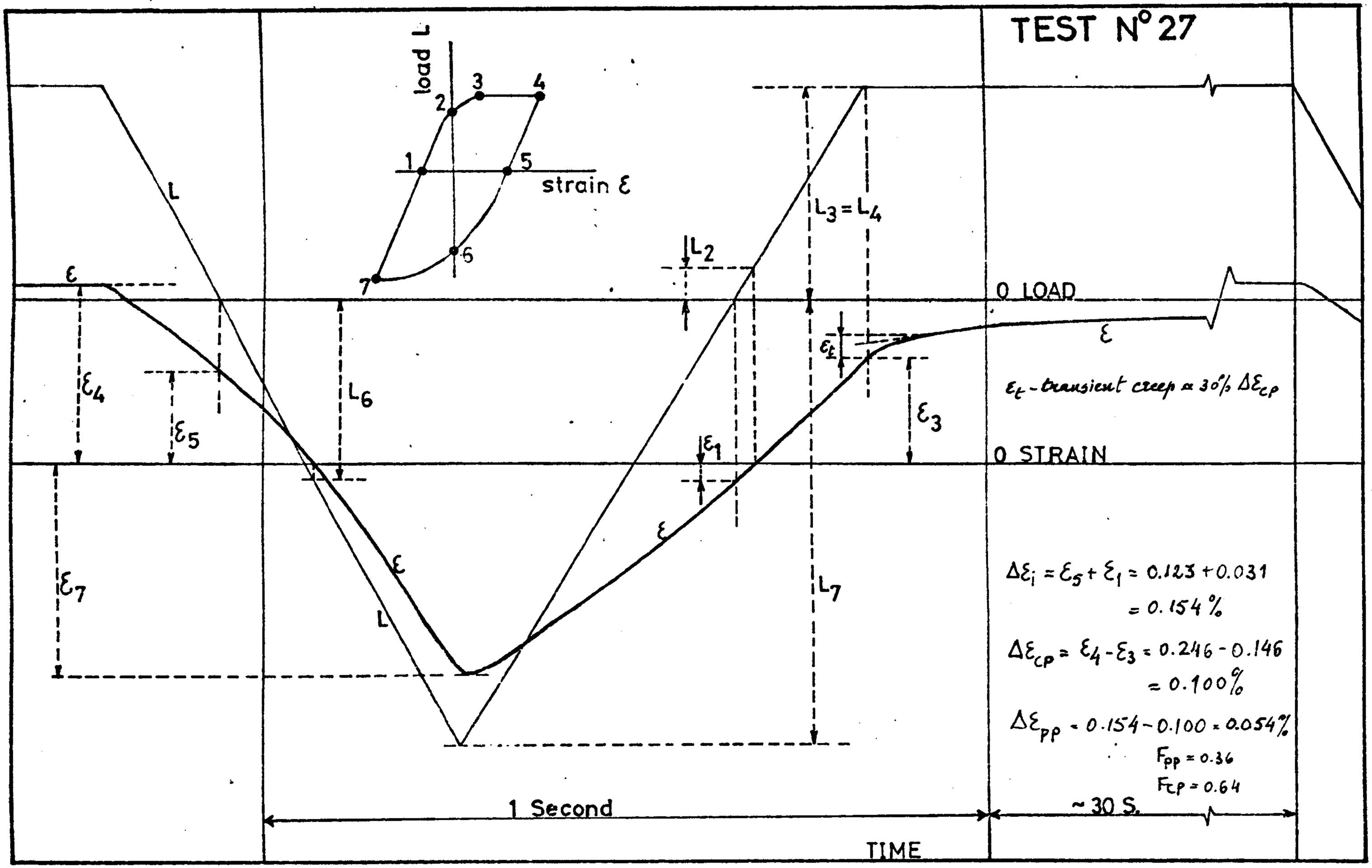

Fig. 4.26 - UV Load and Strain traces for test n°27

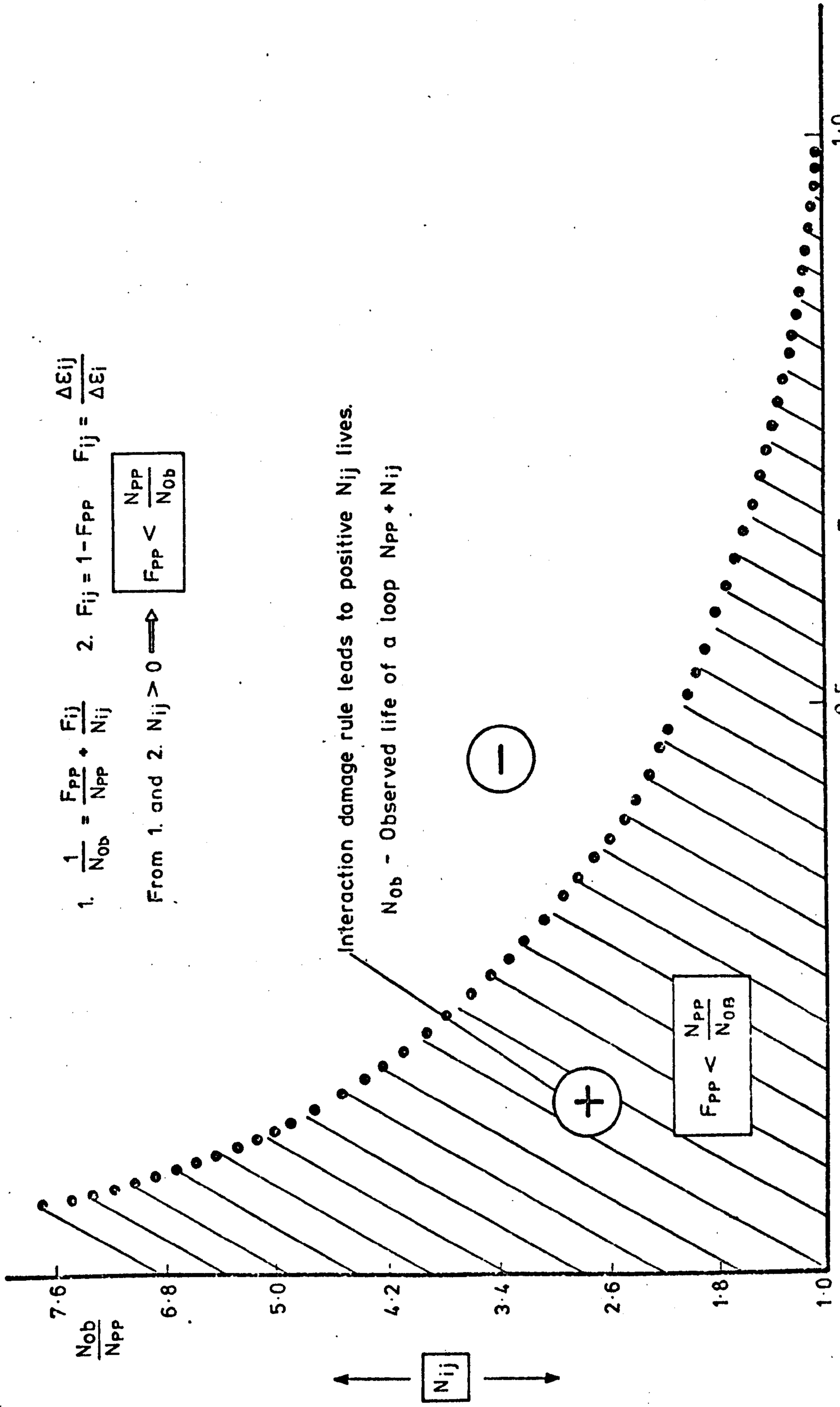

FIG. 5.1 – CONDITION ON F_{PP} LEADING TO EXTRAPOLATED POSITIVE Nij LIVES.

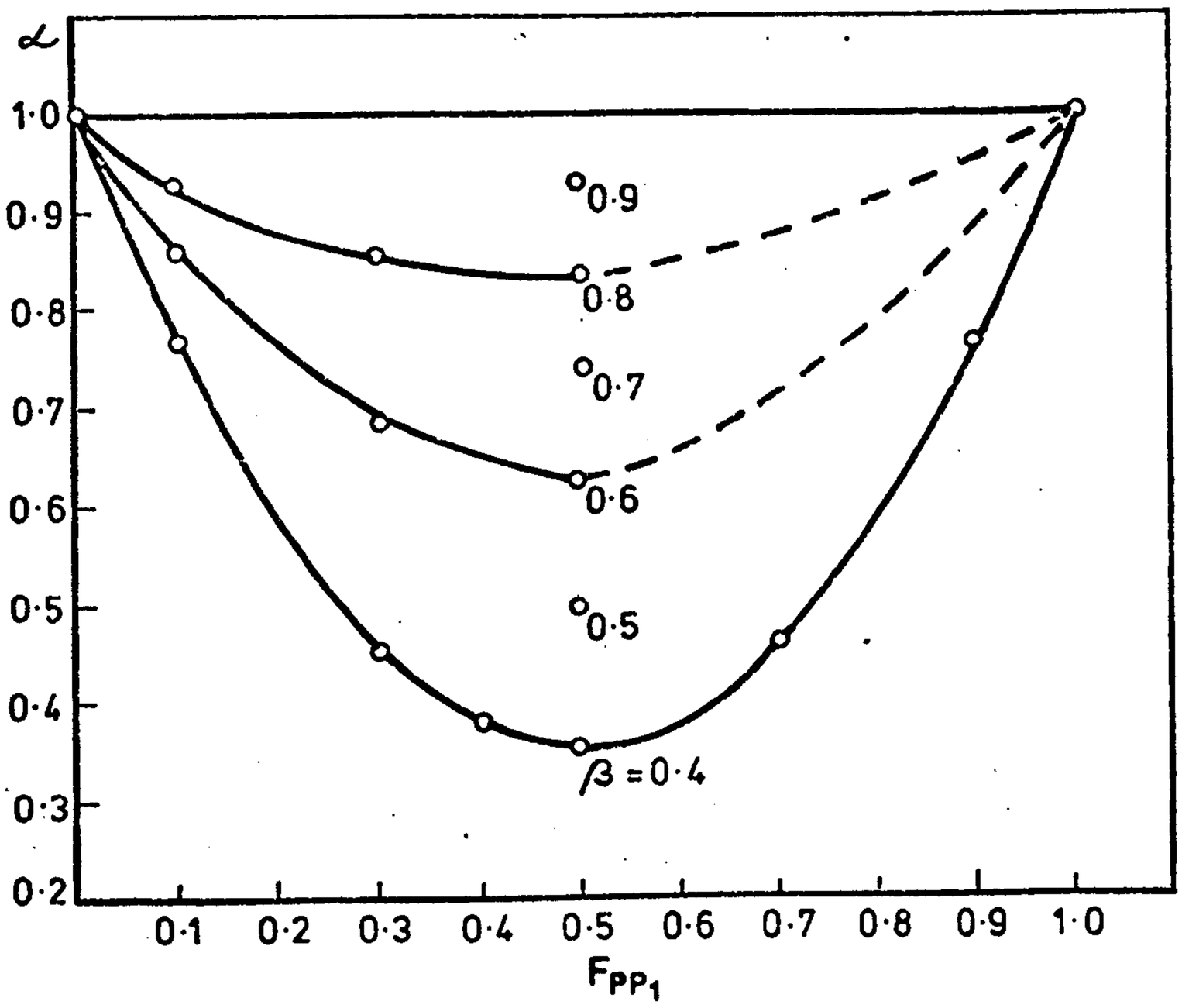

FIG. 5.2 - FUNCTIONS $\alpha = \alpha(F_{PP_1})$ FOR VALUES OF β BETWEEN 0·4 AND 1·0.

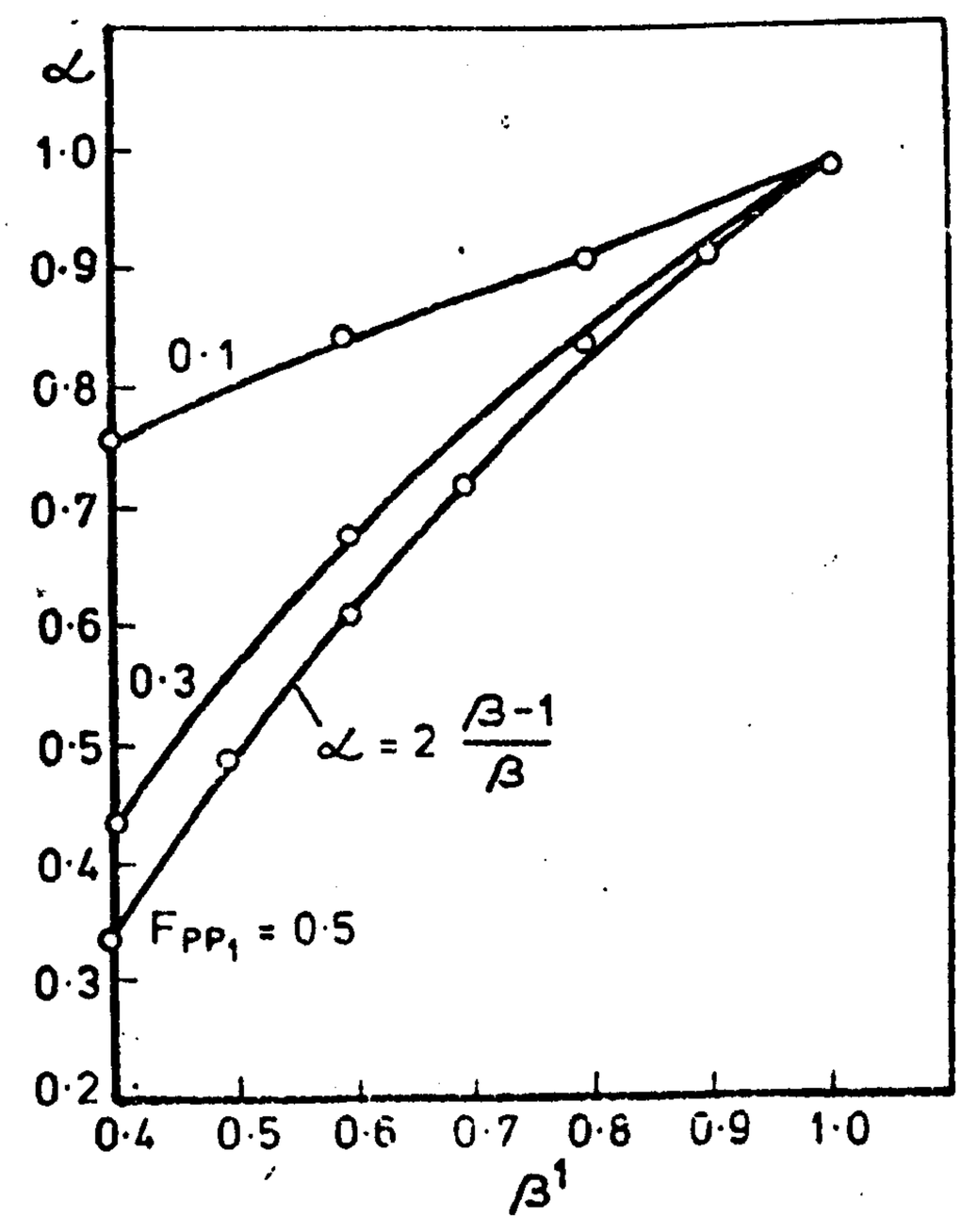

FIG. 5.3 - FUNCTIONS $\alpha = \alpha(\beta)$ FOR VALUES OF F_{PP} BETWEEN 0·1 AND 0·5

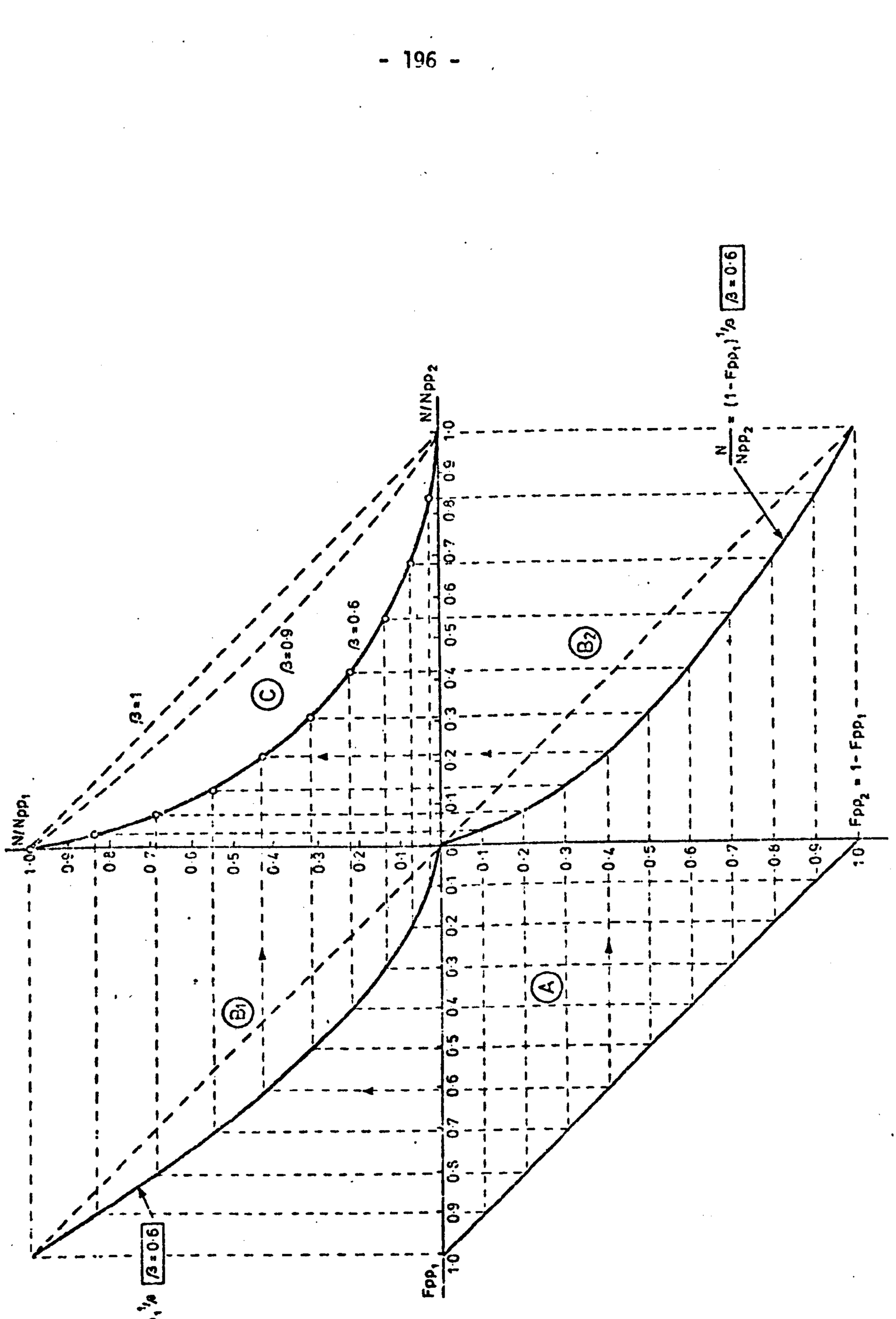

FIG. 5.4 – DAMAGE RULE FOR SIMILAR STRAIN TYPES PP_1 AND PP_2 BOTH OBEYING TO A MANSON-COFFIN TYPE OF STRAIN RANGE vs LIFE EQUATION WITH SLOPES $\beta = 0.6$, 0.9 AND 1.

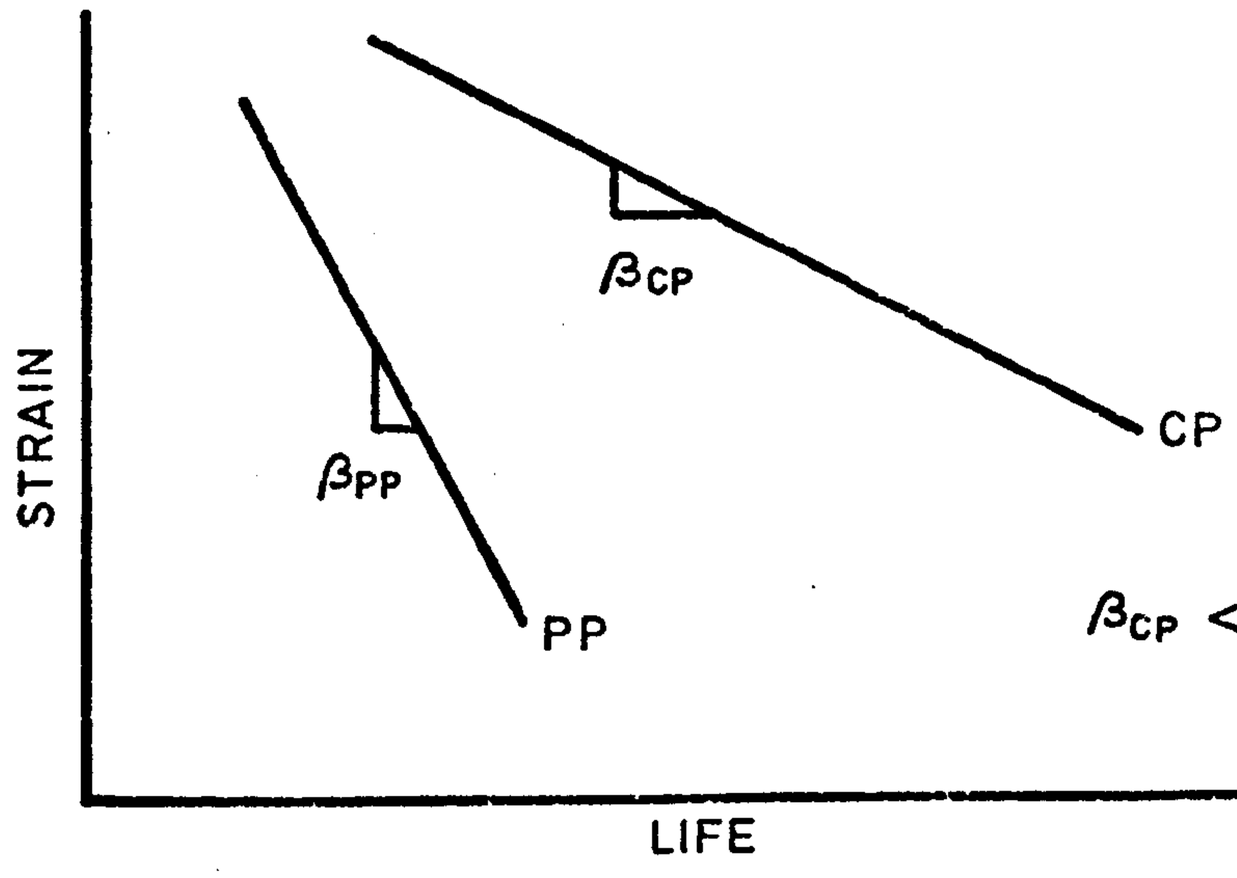

FIG. 5.5 - PP AND CP STRAINRANGE vs LIFE RELATIONSHIPS WHEN CP LIVES ARE GREATER THAN PP ONES. (SCHEMATIC)

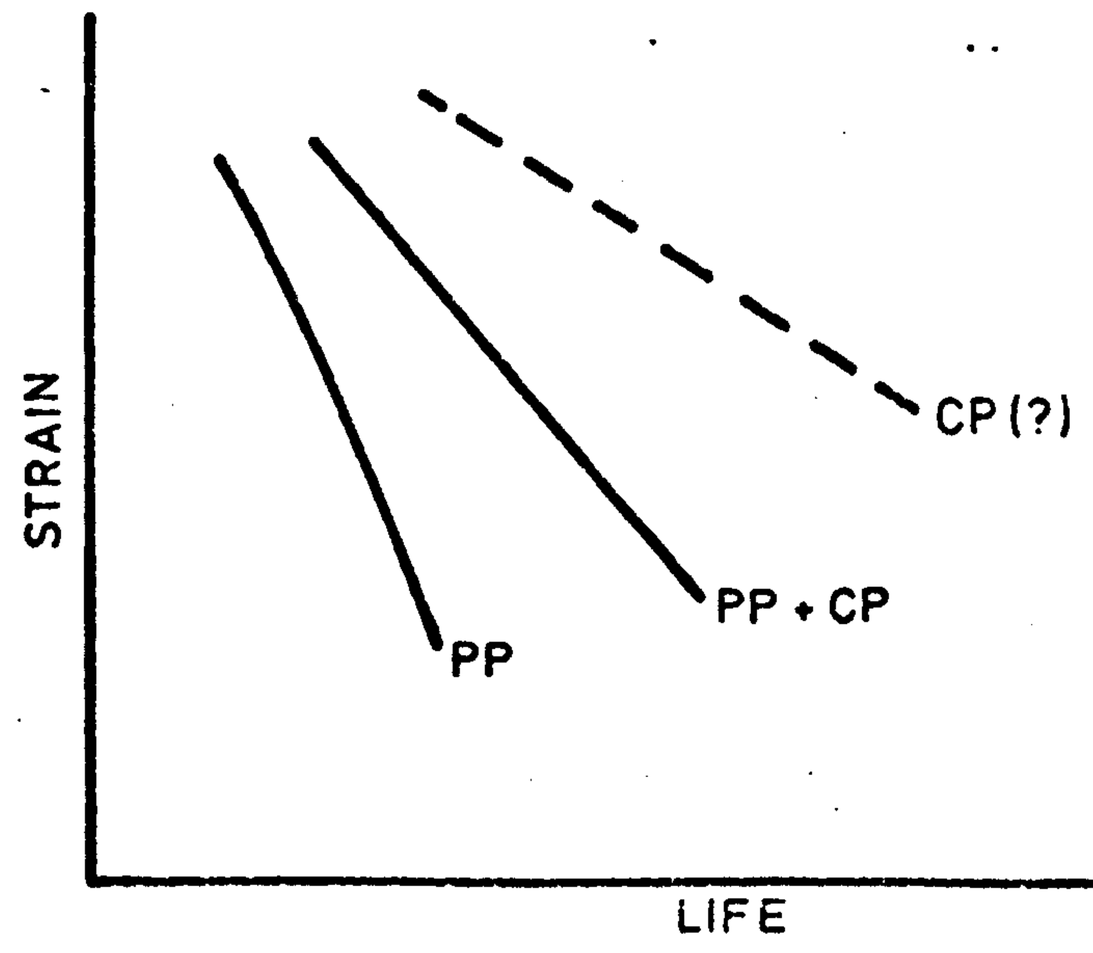

FIG. 5.6 - EXTRAPOLATION TO A 100% CP LINE AS AN UPPER BOUND OF THE SrP BASIC RELATIONSHIPS. (SCHEMATIC)

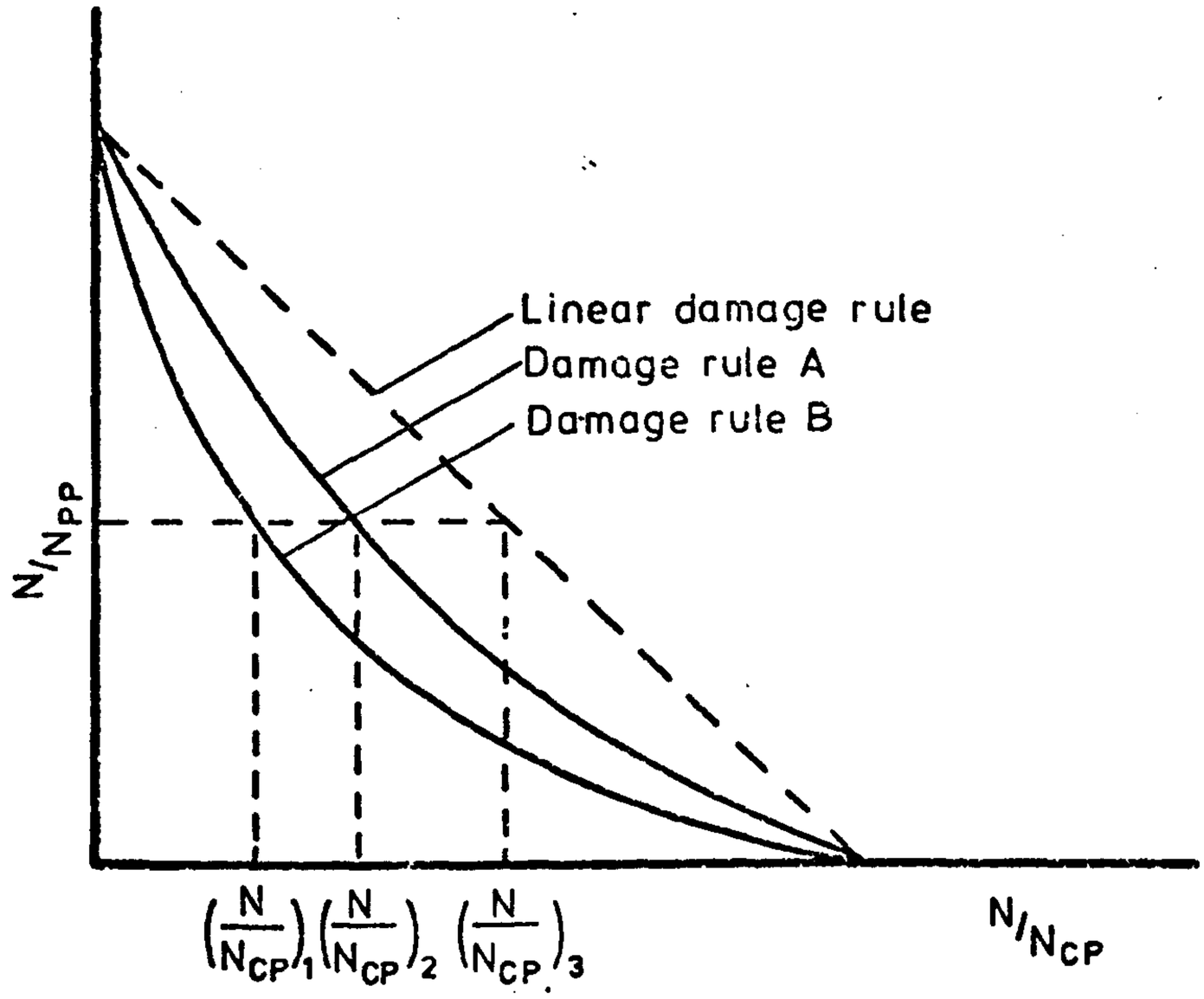

$$\left(\frac{N}{N_{CP}}\right)_2 > \left(\frac{N}{N_{CP}}\right)_1 \Longrightarrow (N_{CP})_2 < (N_{CP})_1$$

FIG. 5.7 - DAMAGE RULES CALCULATED ACCORDING TO FIG. 5.4 USING PP LINE (A) AND CP LINE (B) (SCHEMATIC)

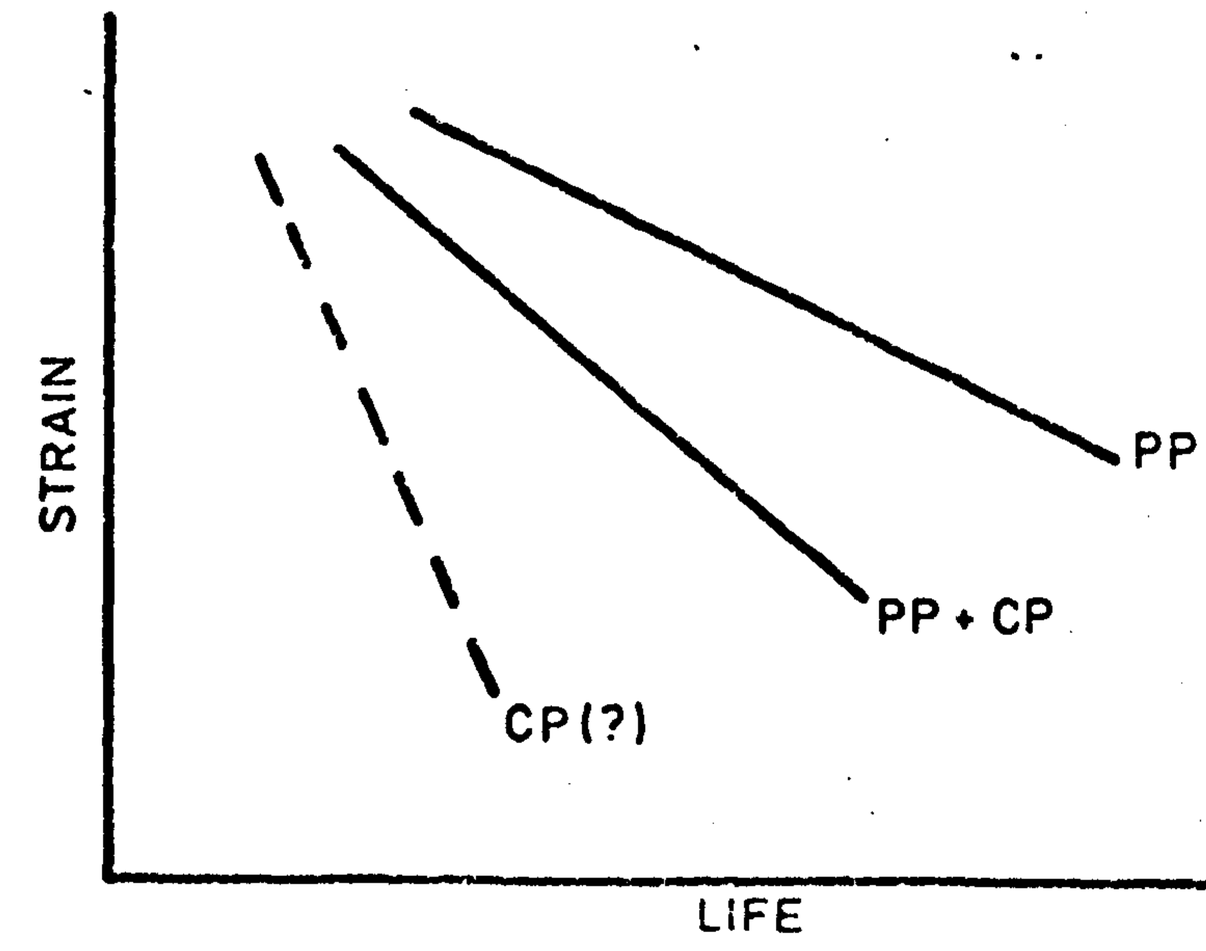

FIG. 5.8 - EXTRAPOLATION TO A 100% CP LINE AS A LOWER BOUND OF THE SrP BASIC RELATIONSHIPS. (SCHEMATIC)

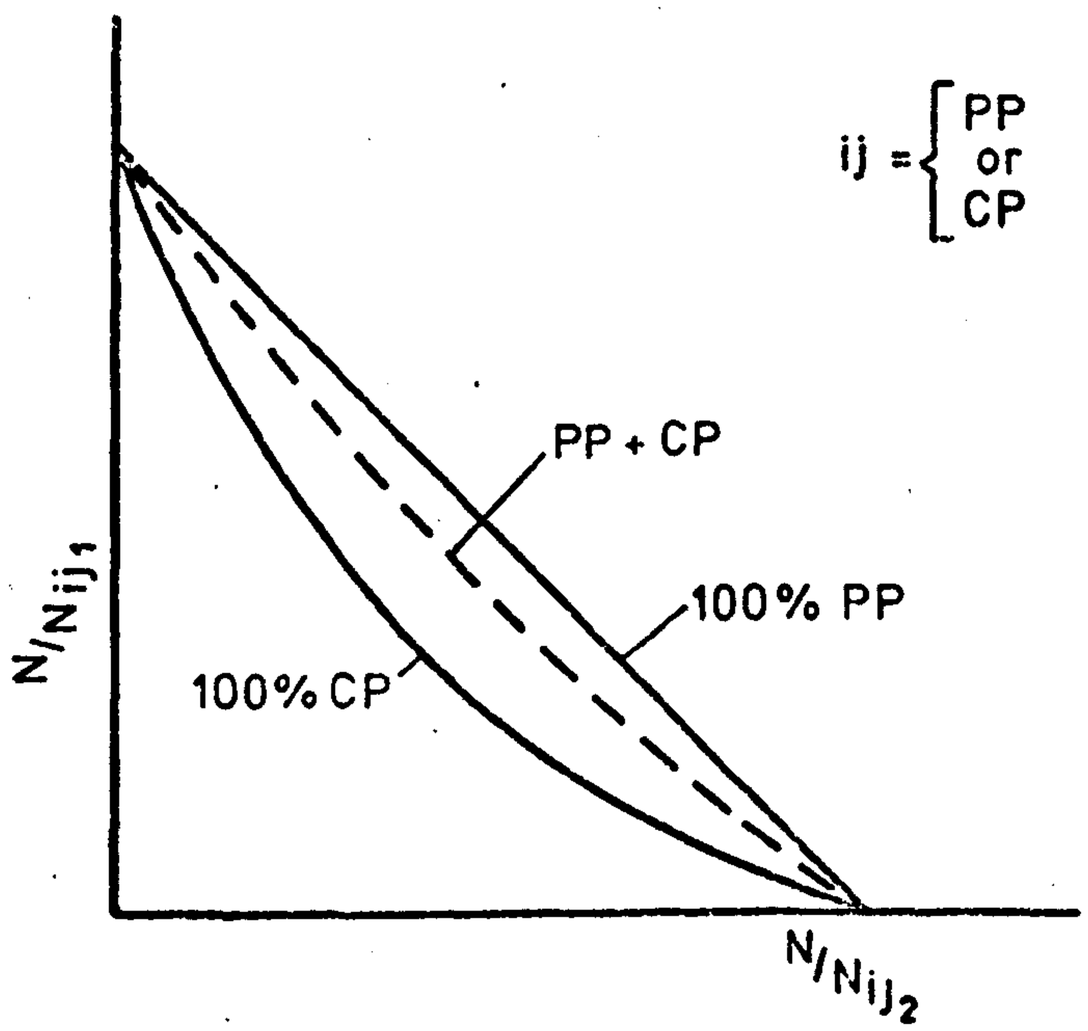

FIG. 5.9 - DAMAGE RULES (SCHEMATIC)

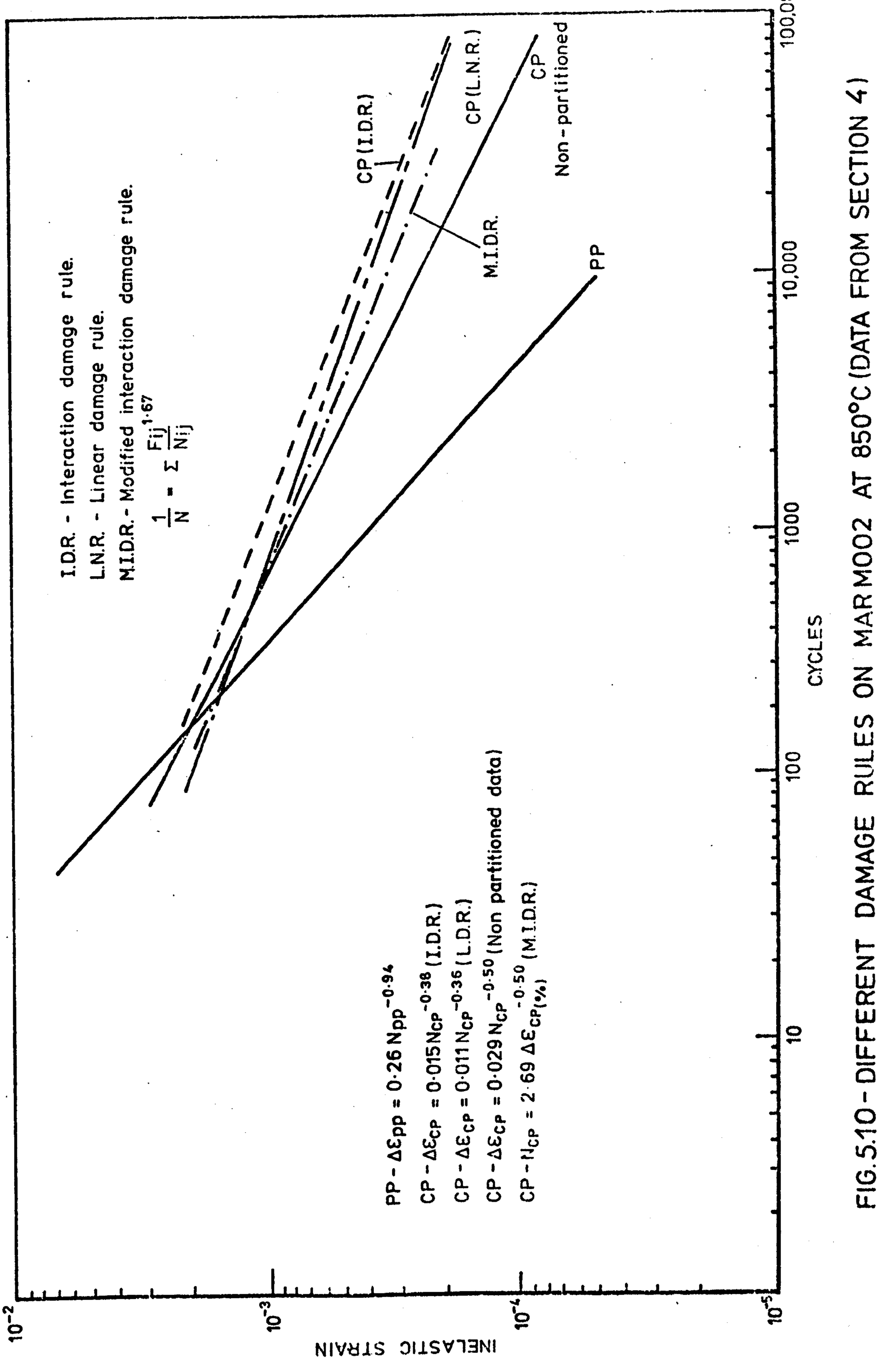

FIG.5.10- DIFFERENT DAMAGE RULES ON MAR M002 AT 850°C (DATA FROM SECTION 4)

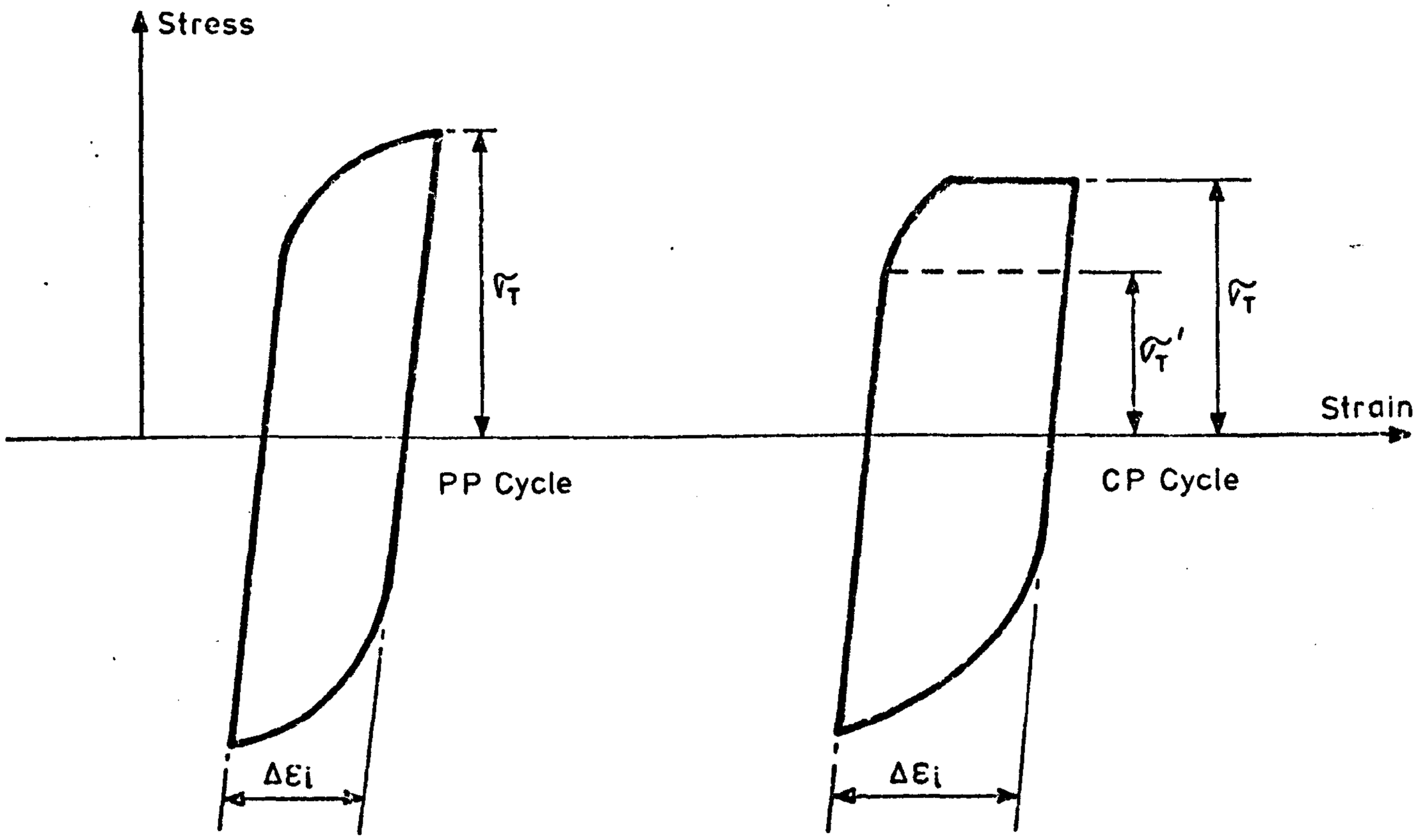

TENSILE HYSTERETIC ENERGY ≃ $\tilde{\sigma}_T \Delta\varepsilon_i$ PP Cycle

$\tilde{\sigma}_T \Delta\varepsilon_i$ PP + CP Cycle (Experimental)

$\tilde{\sigma}_T' \Delta\varepsilon_i$ CP Cycle (Ideal cycle)

FIG. 6.1.-TENSILE HYSTERETIC ENERGIES FOR TWO TYPICAL SrP LOOPS (Schematic)

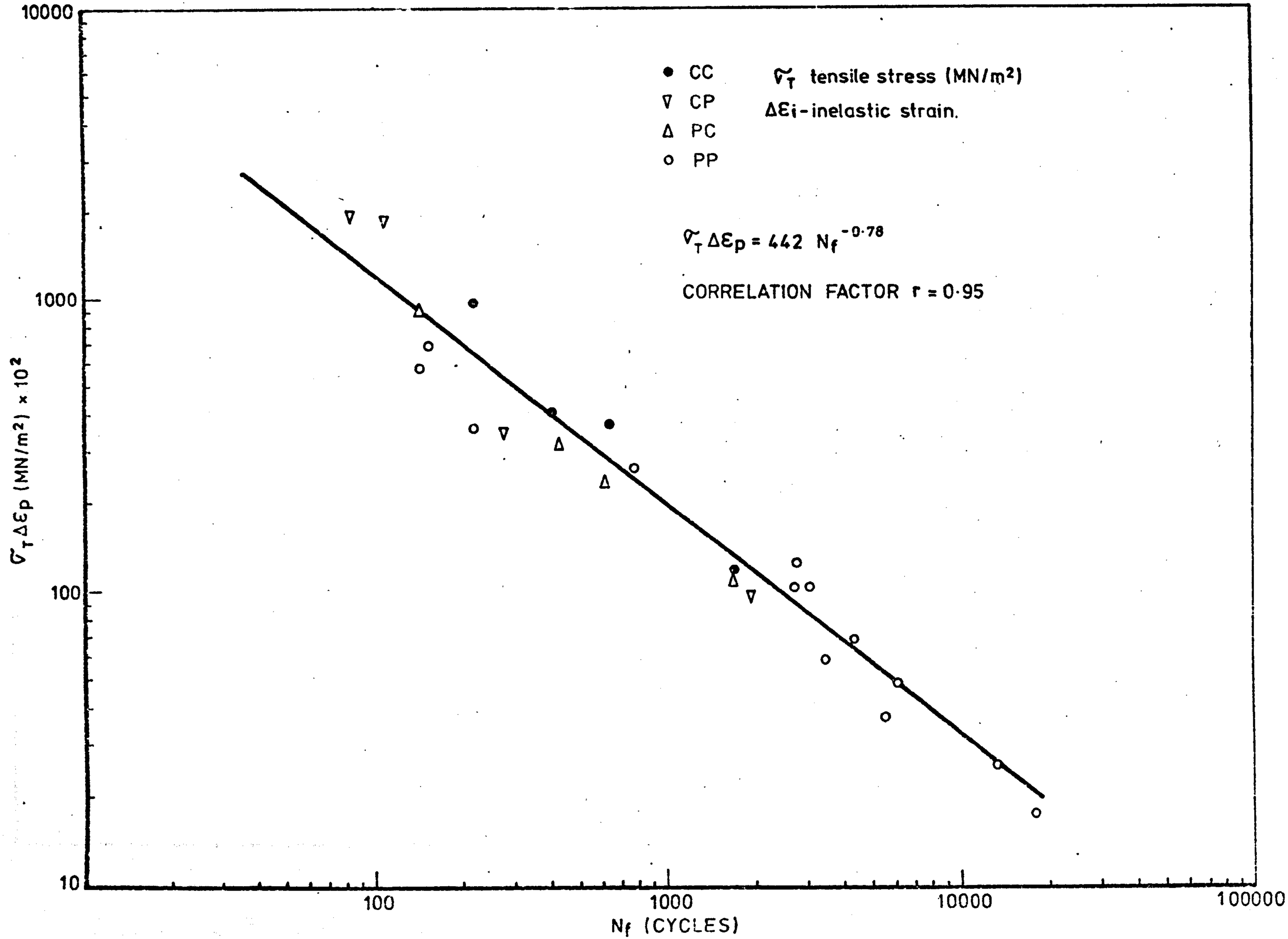

FIG.6.2-OSTERGREN'S METHOD ON A TITANIUM ALLOY, DATA FROM ref 110

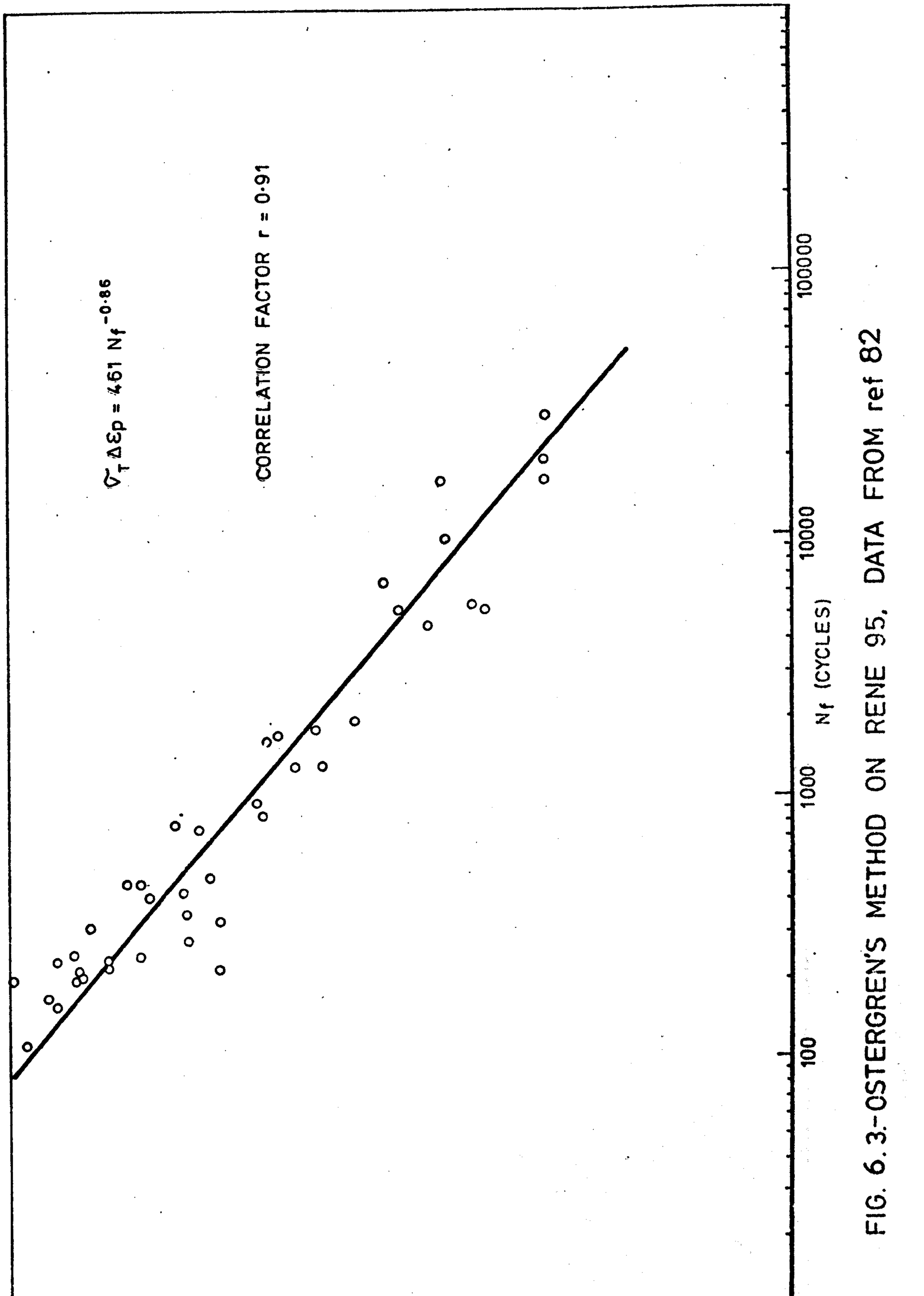

FIG. 6.3.-OSTERGREN'S METHOD ON RENE 95. DATA FROM ref 82

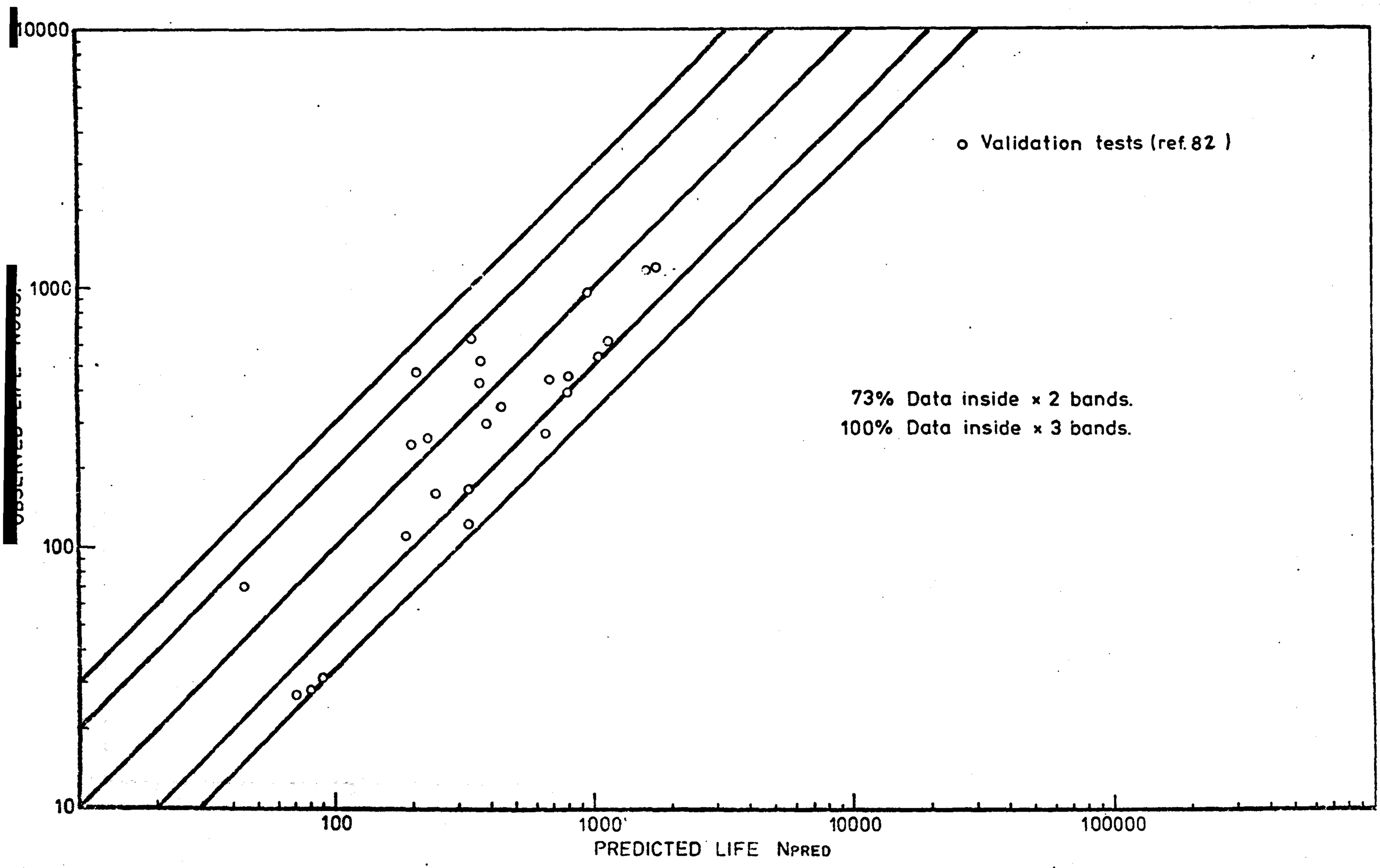

FIG. 6.4 - OSTERGREN'S METHOD ON RENÉ 95, 650°C.

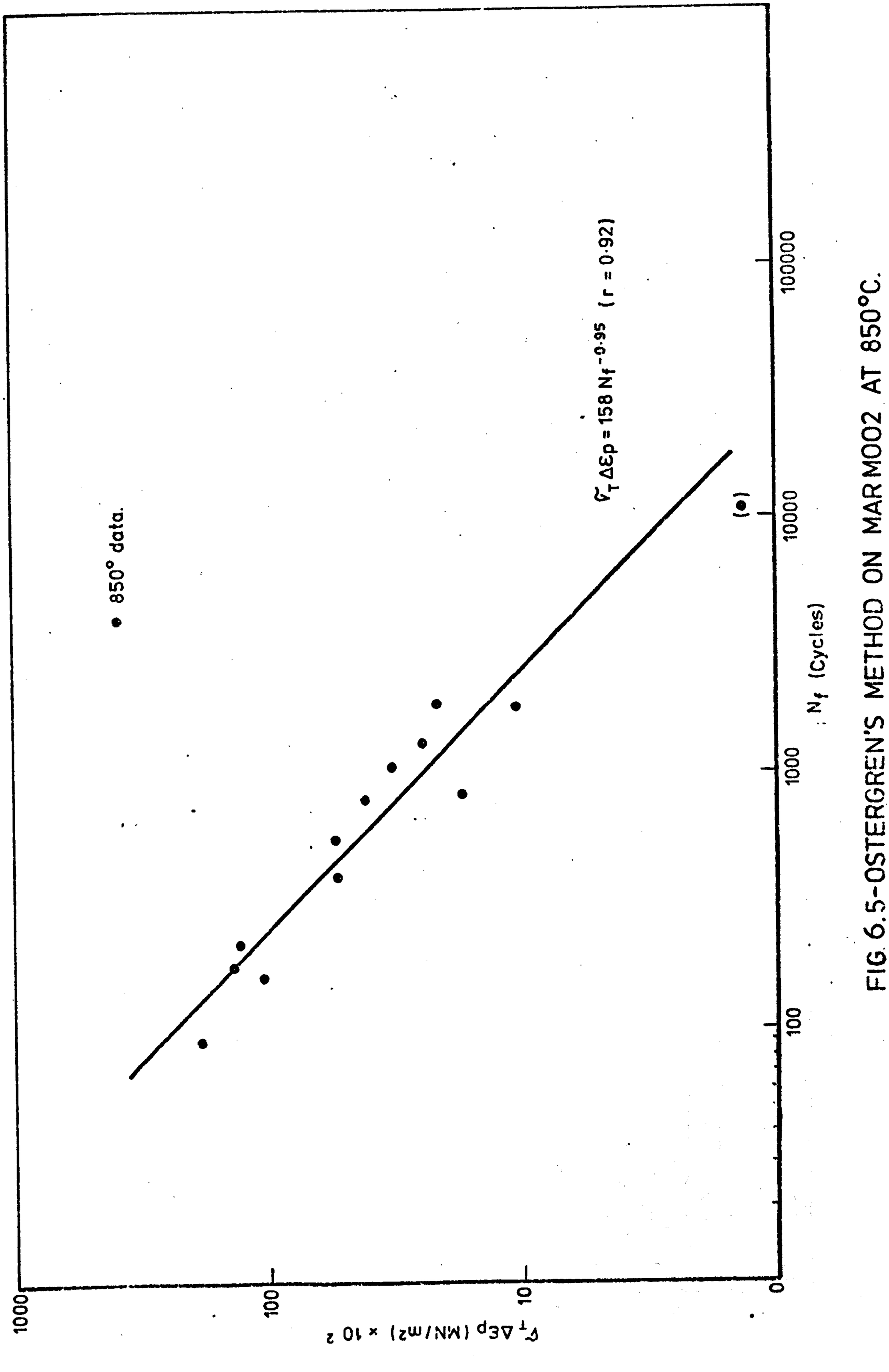

FIG 6.5-OSTERGREN'S METHOD ON MARMOO2 AT 850°C.

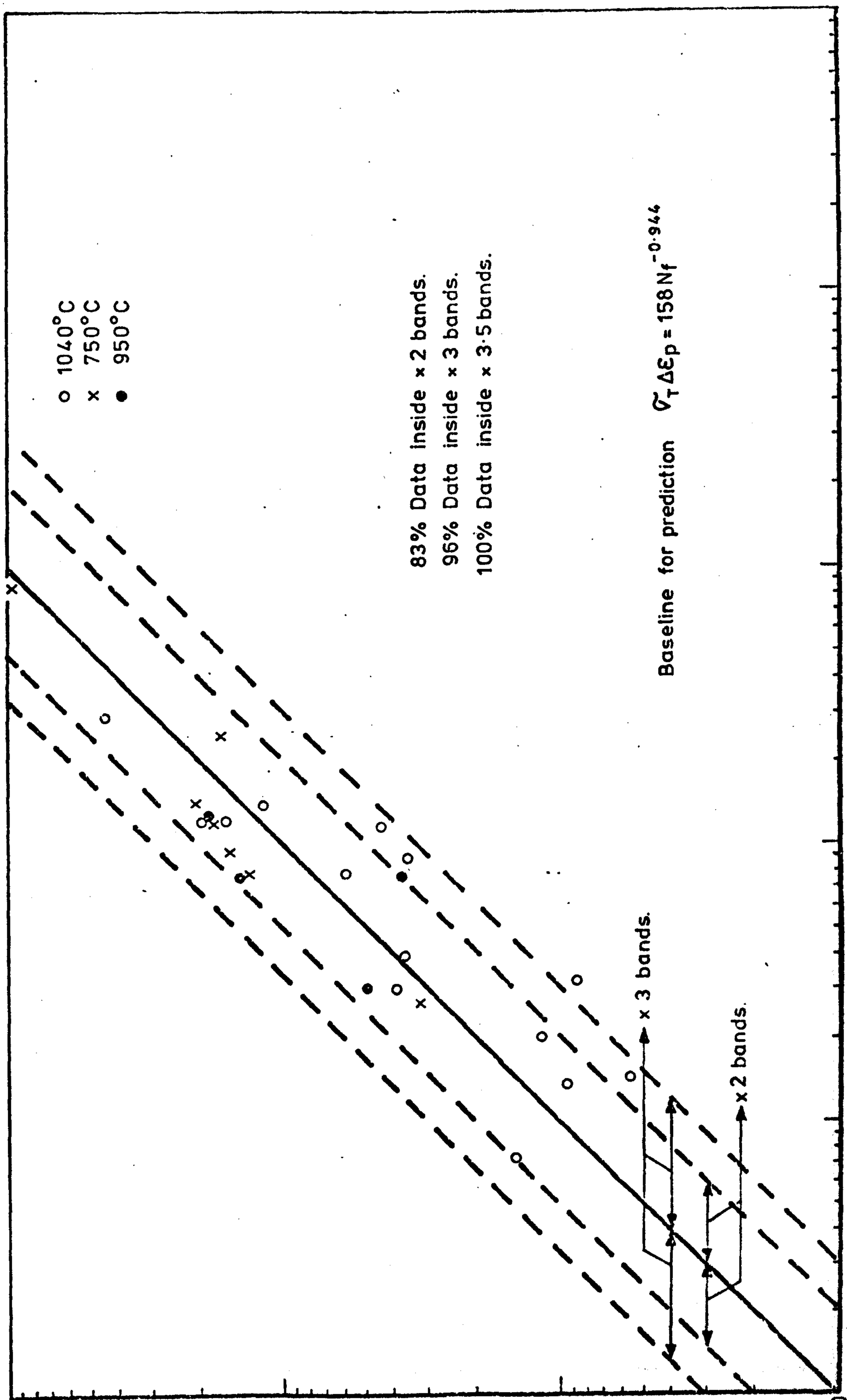

FIG. 6.6 - OSTERGREN'S METHOD ON MAR M002, 750 - 1040°C.

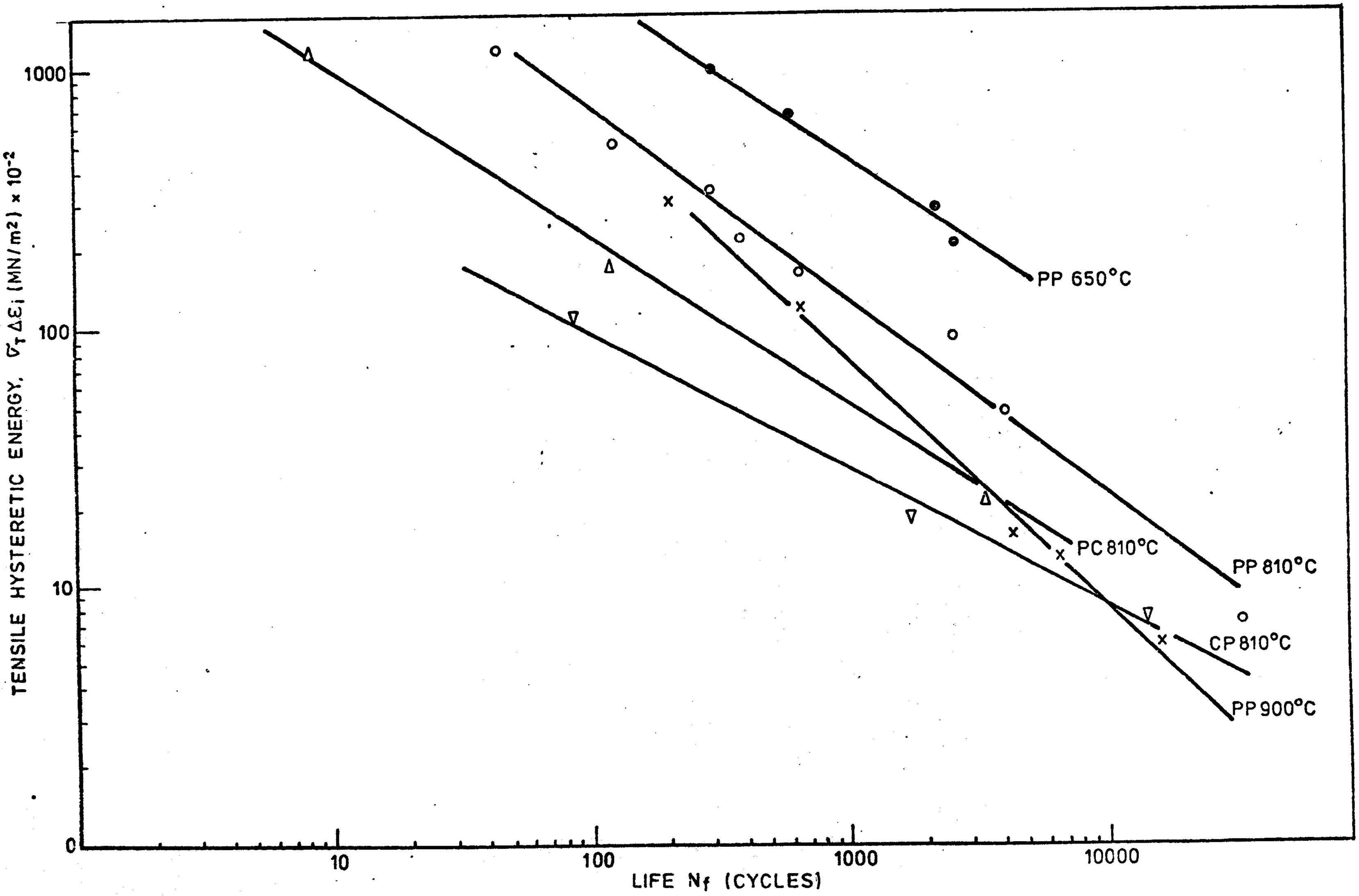

FIG. 6.7-Sr P-OSTERGREN'S METHOD ON NIMONIC 90 (ref. 111)

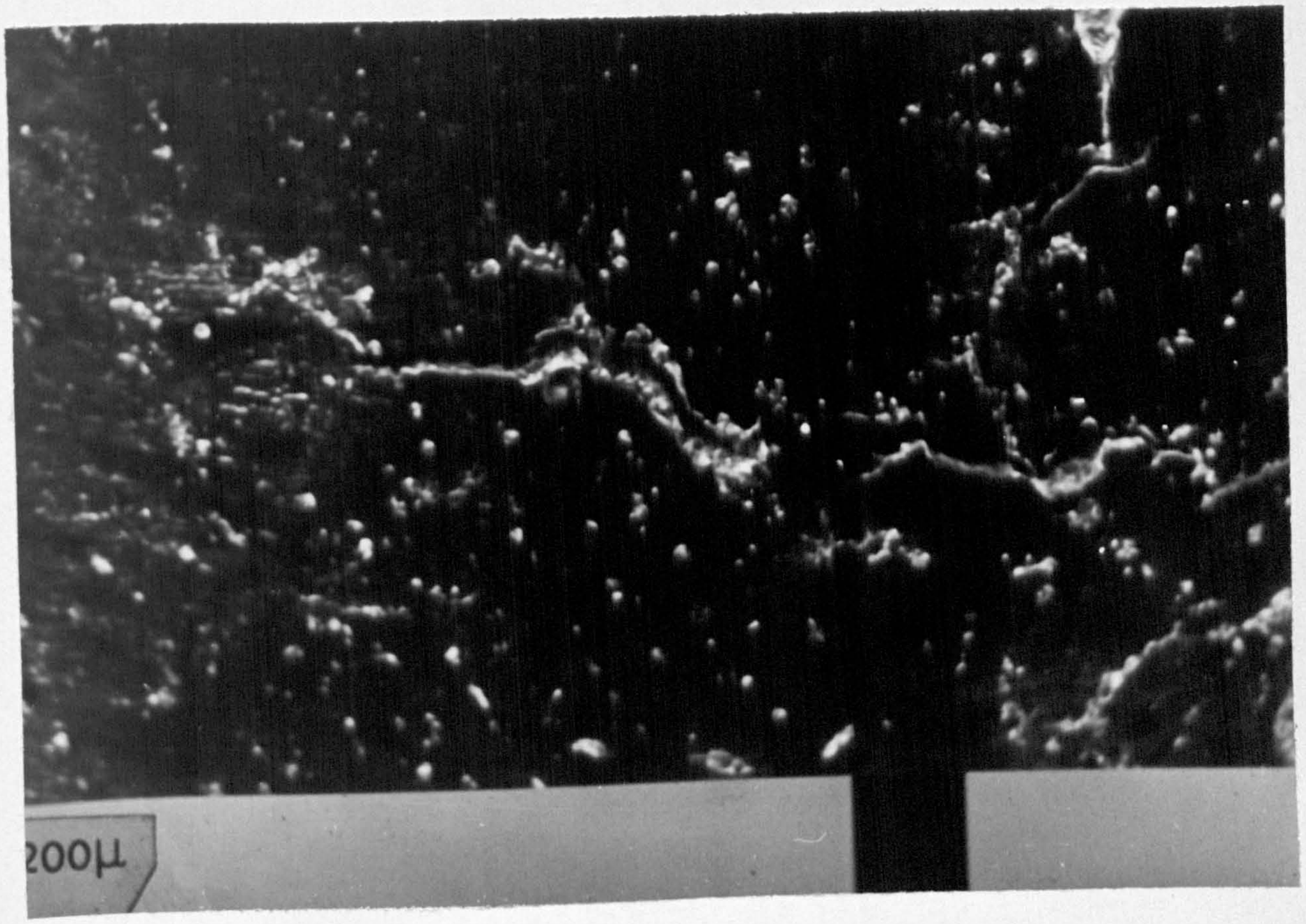

Figure 7.1 - Lateral surface view of cast MARM002 specimen 30 after testing.

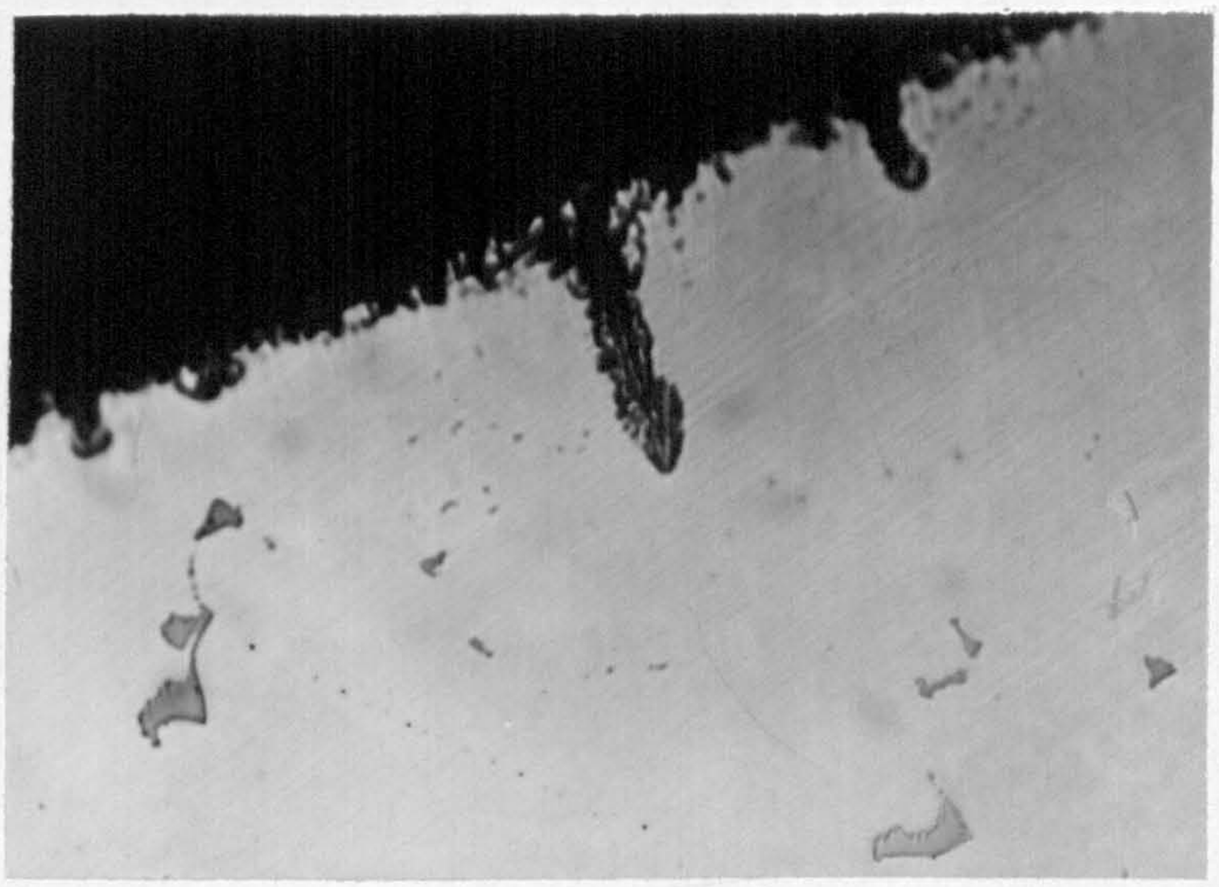

Figure 7.2 - Profile of oxide intrusions. Unetched X500

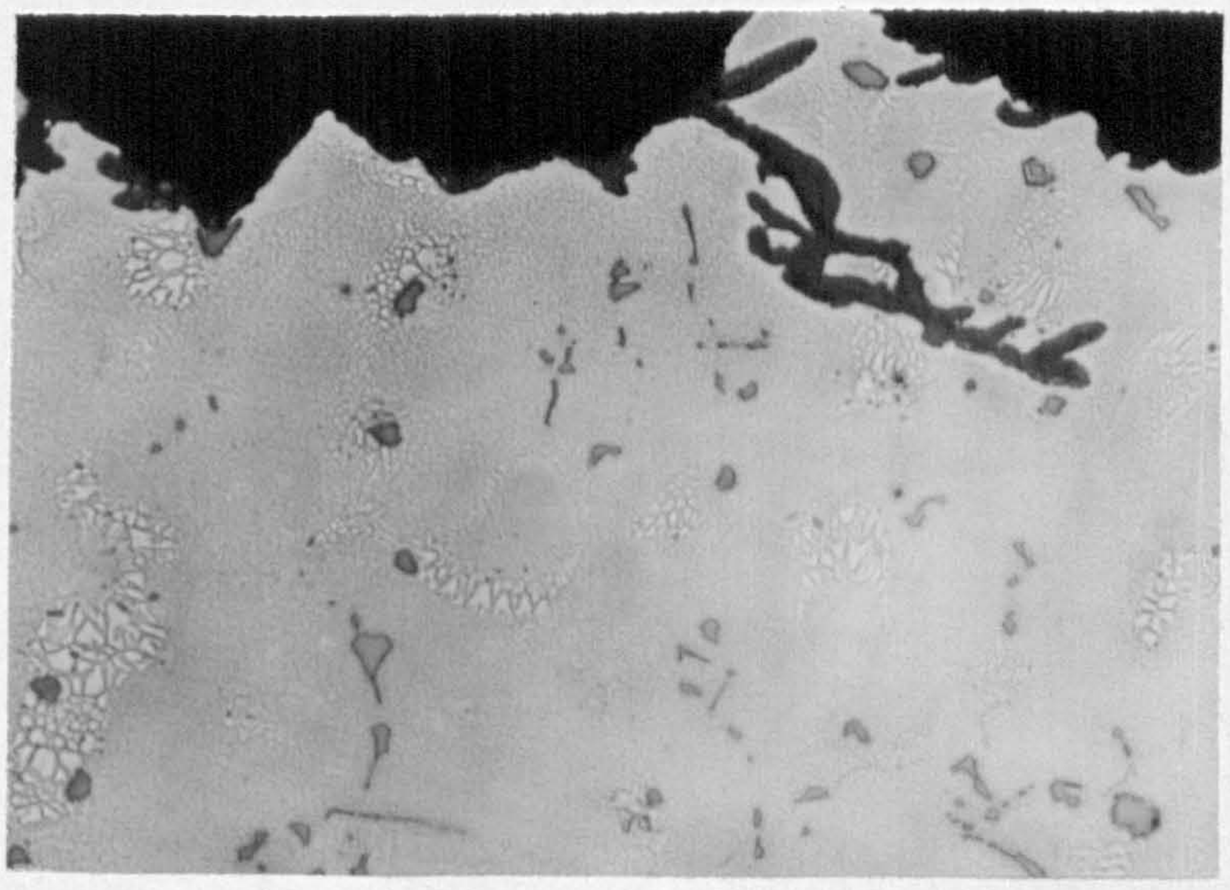

Figure 7.3 - Profile of secondary crack in specimen 46 (200X)
Note deplected area of γ' at periphery of oxide.

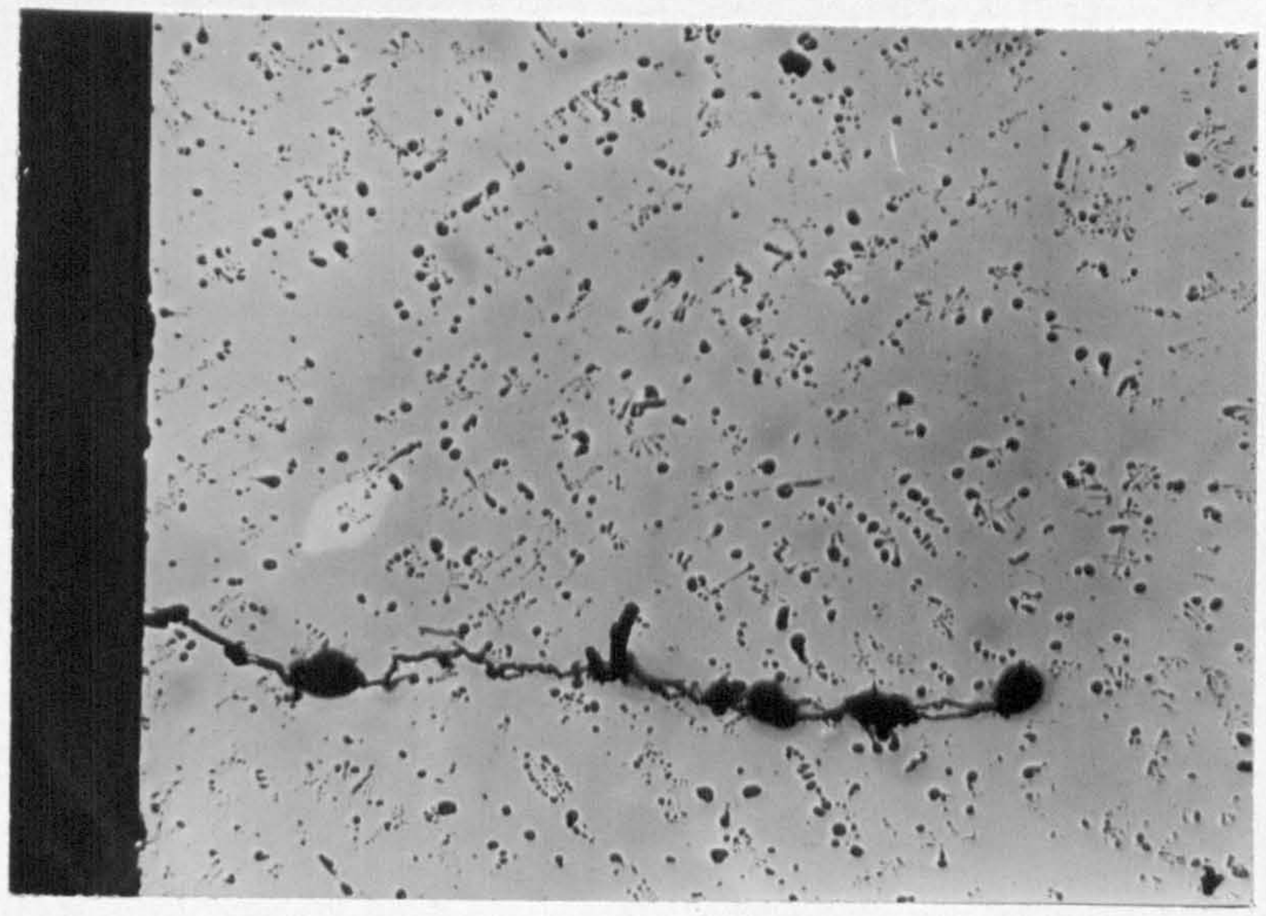

Figure 7.4 - Surface connected secondary crack running through porosity. Magnification 200X

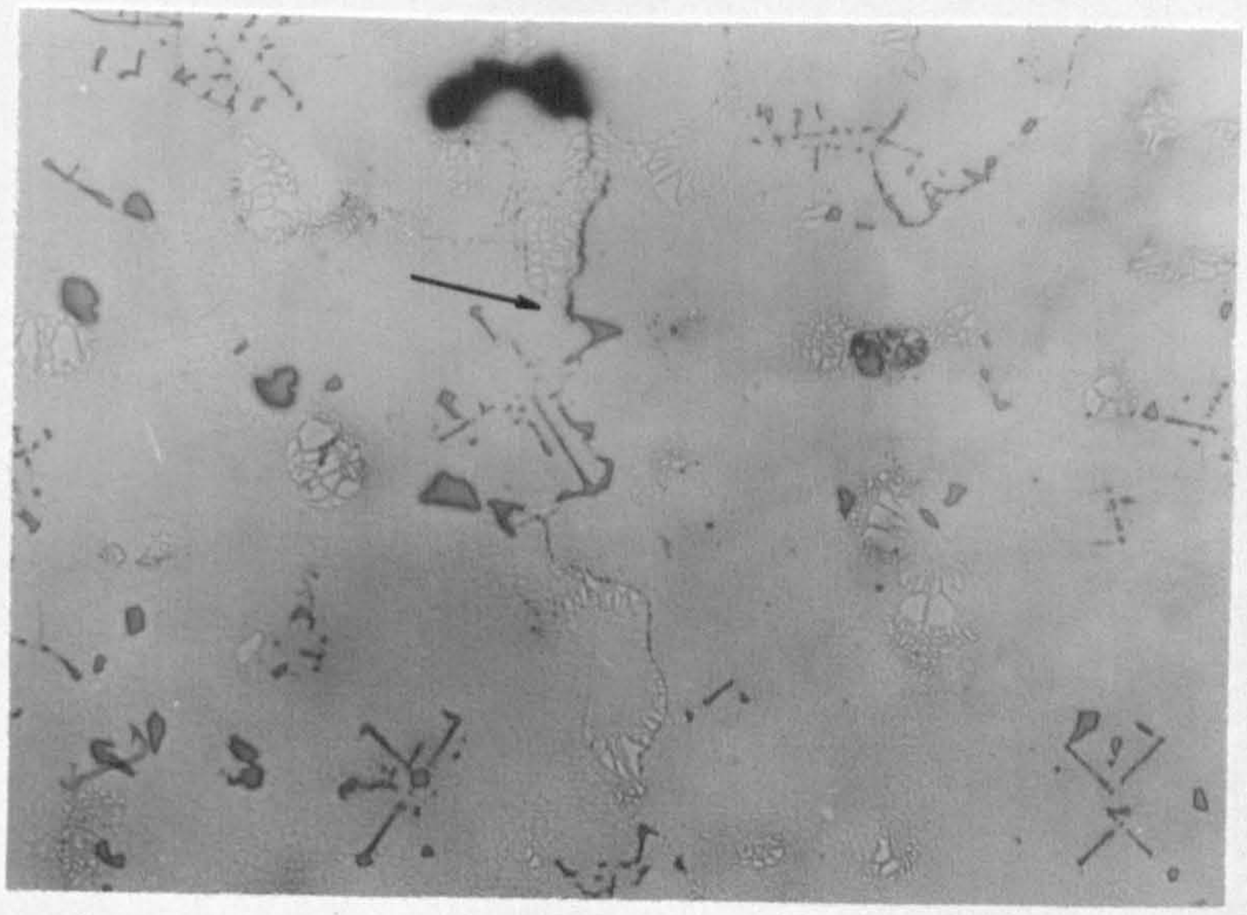

Figure 7.7 - Internal cracks starting at pore and carbide. One crack at sharp carbide and propagated trough $\gamma - \gamma'$ interface. Specimen 41 (200X)

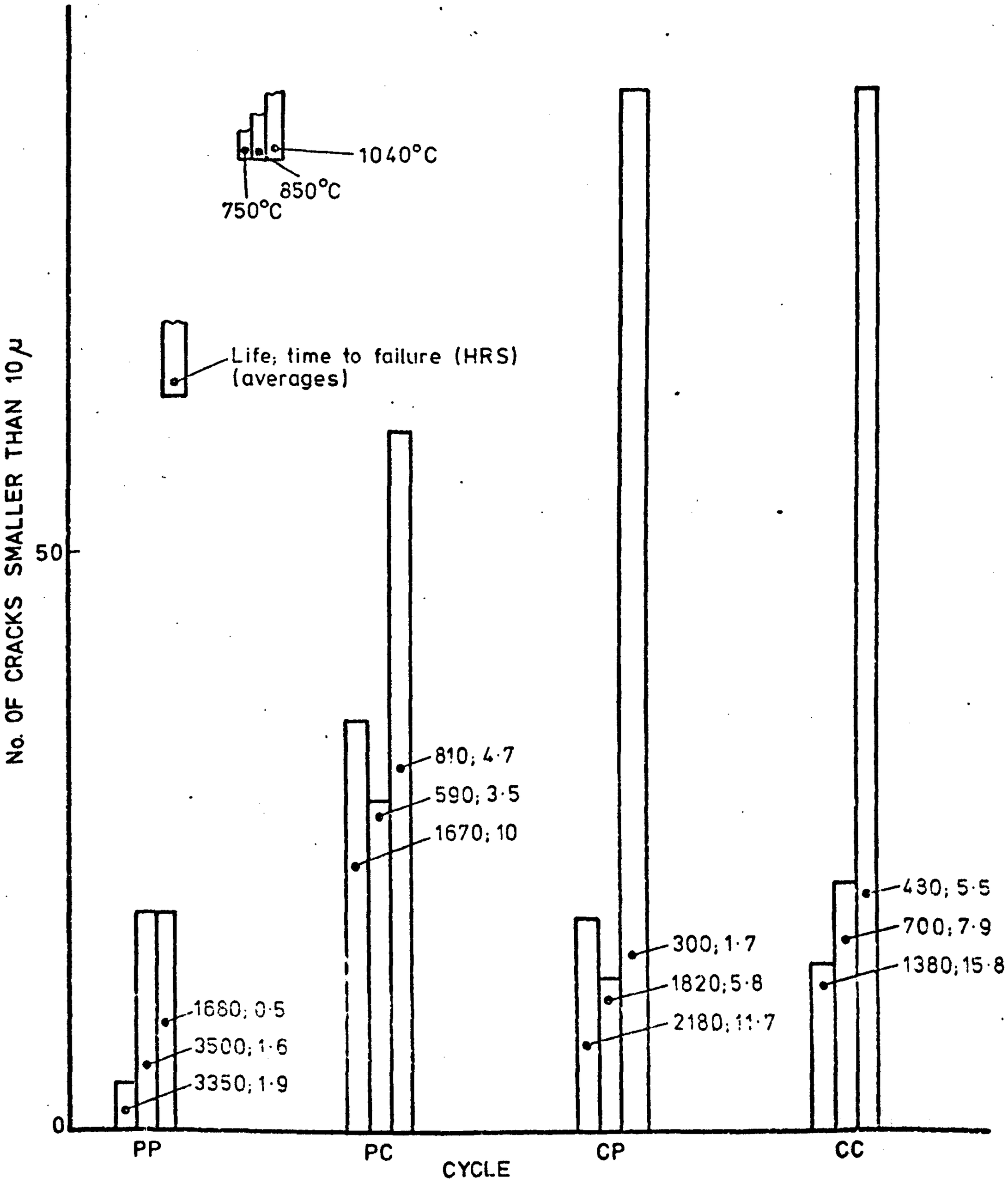

FIG. 7.5 – SECONDARY CRACKS ON LONGITUDINAL SECTIONS (~25mm) OF THE SPECIMENS USED TO DETERMINE THE STRAINRAN vs. LIFE RELATIONSHIPS AT 850 AND 1040°C AND VALIDATION TESTS AT 750°C ON MAR M002.

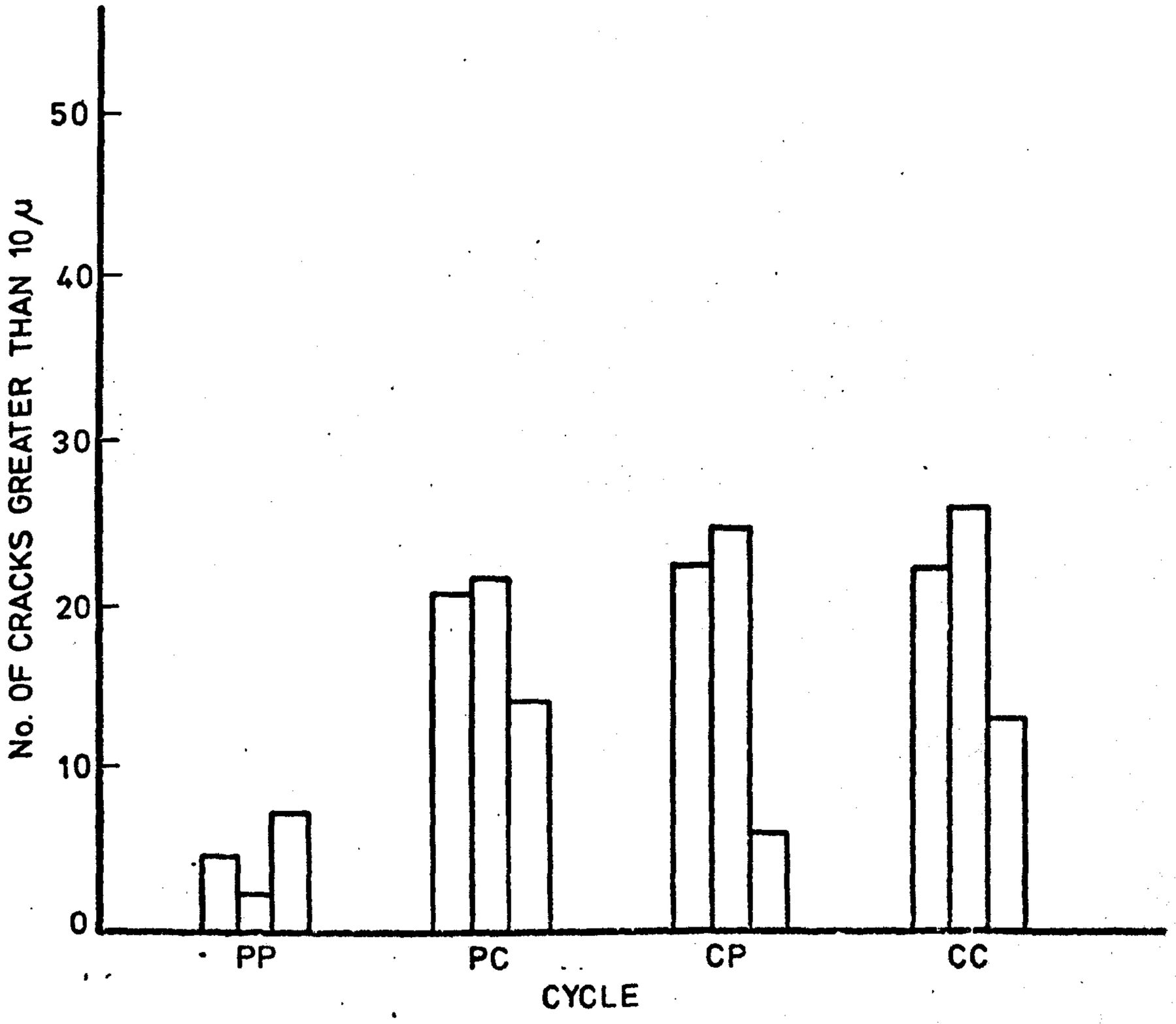

FIG. 7.6 - SECONDARY CRACKS ON THE SAME SPECIMENS OF FIG. 7.5 BUT WITH LENGTH GREATER THAN 10 μ.

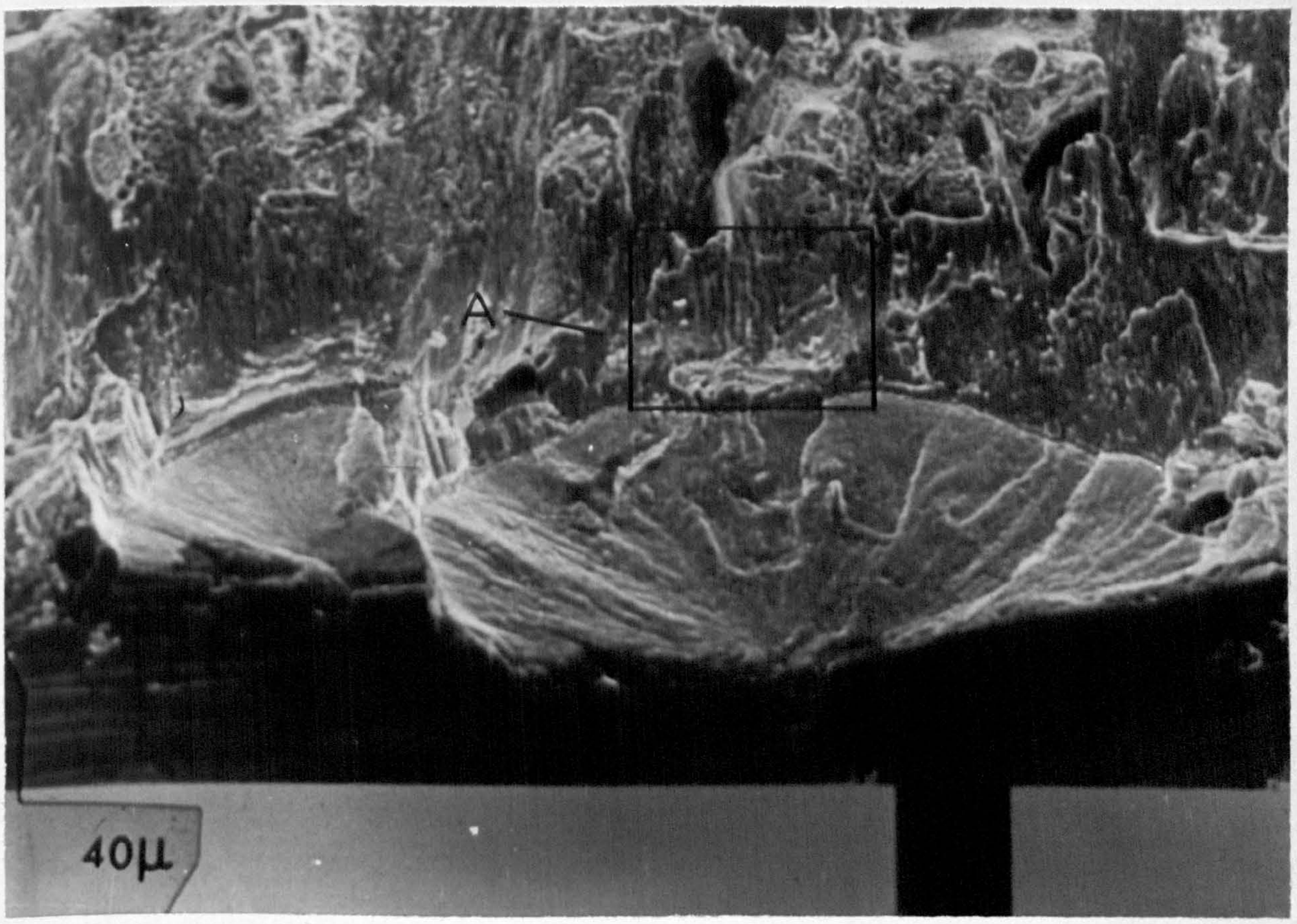

Figure 7.8 - Scanning electron micrograph of specimen 11A indicating transgranular fracture at origin. The outlined region A is shown at a higher magnification in Figure 7.9.

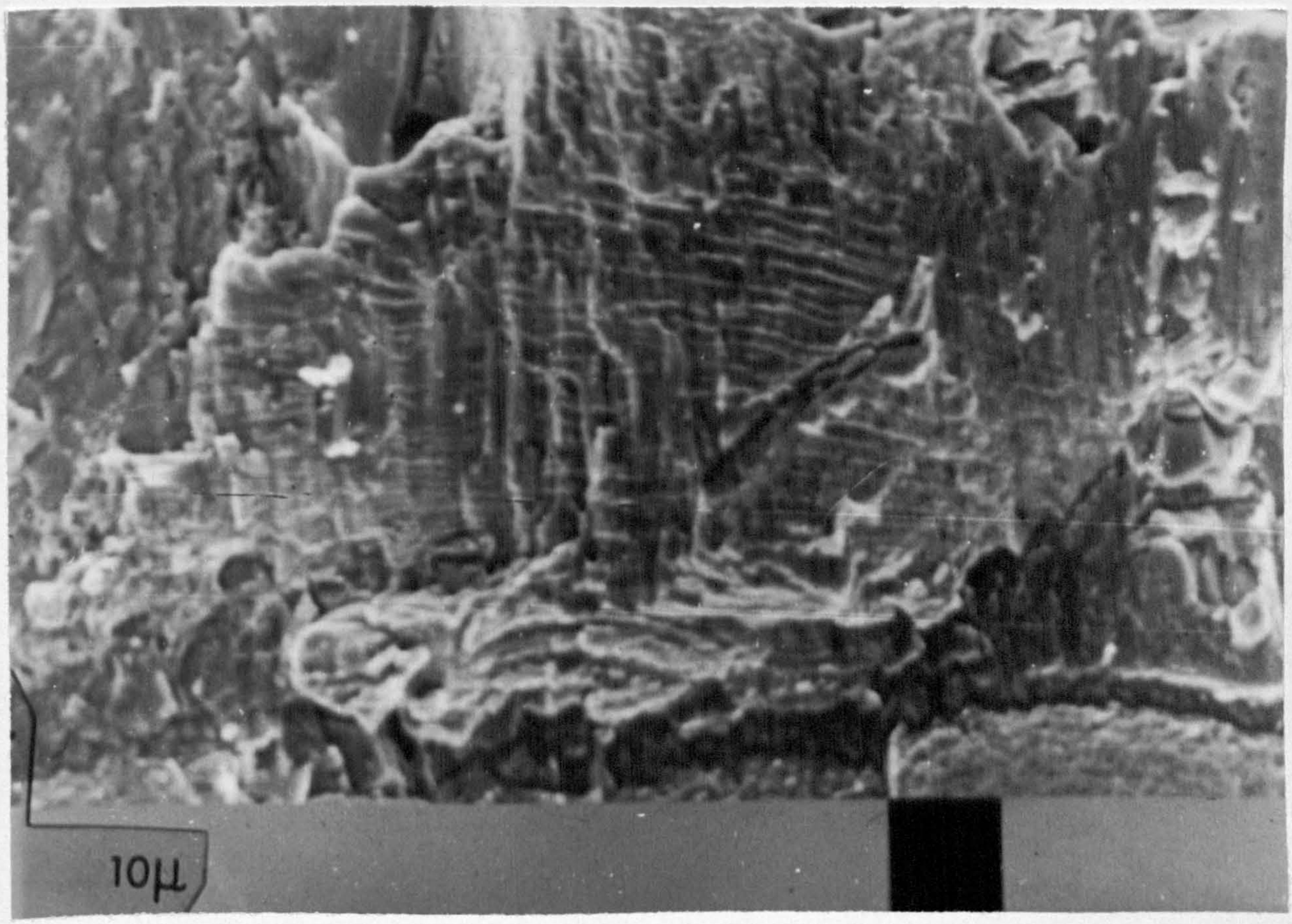

Figure 7.9 - Scanning electron micrograph of specimen 11A.
Area A of Figure 7.8 showing fatigue striactions.

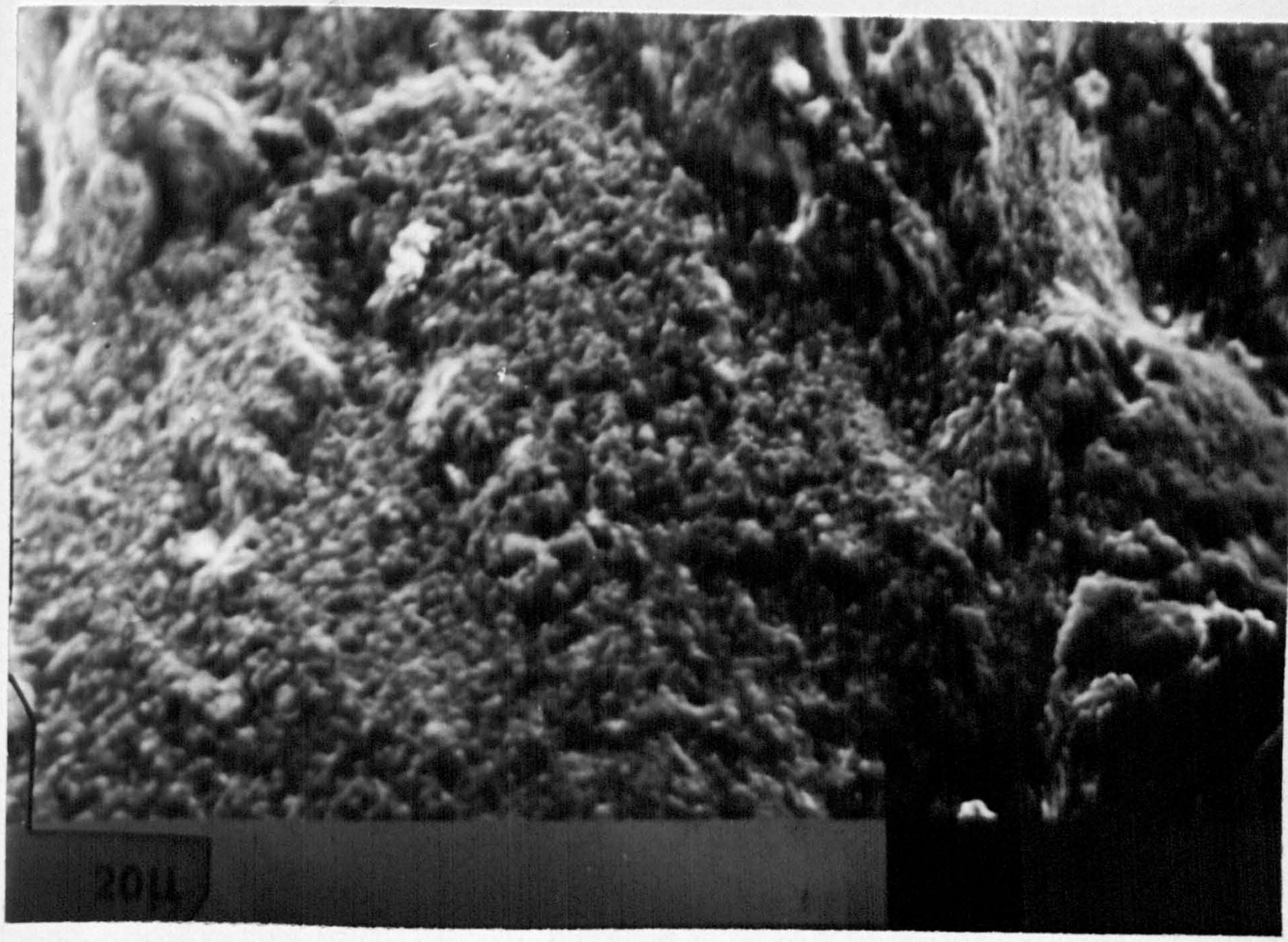

Figure 7.10 - Scanning electron micrograph of specimen 21.
The layer of oxidation products makes it impossible
to determine the mode of fracture

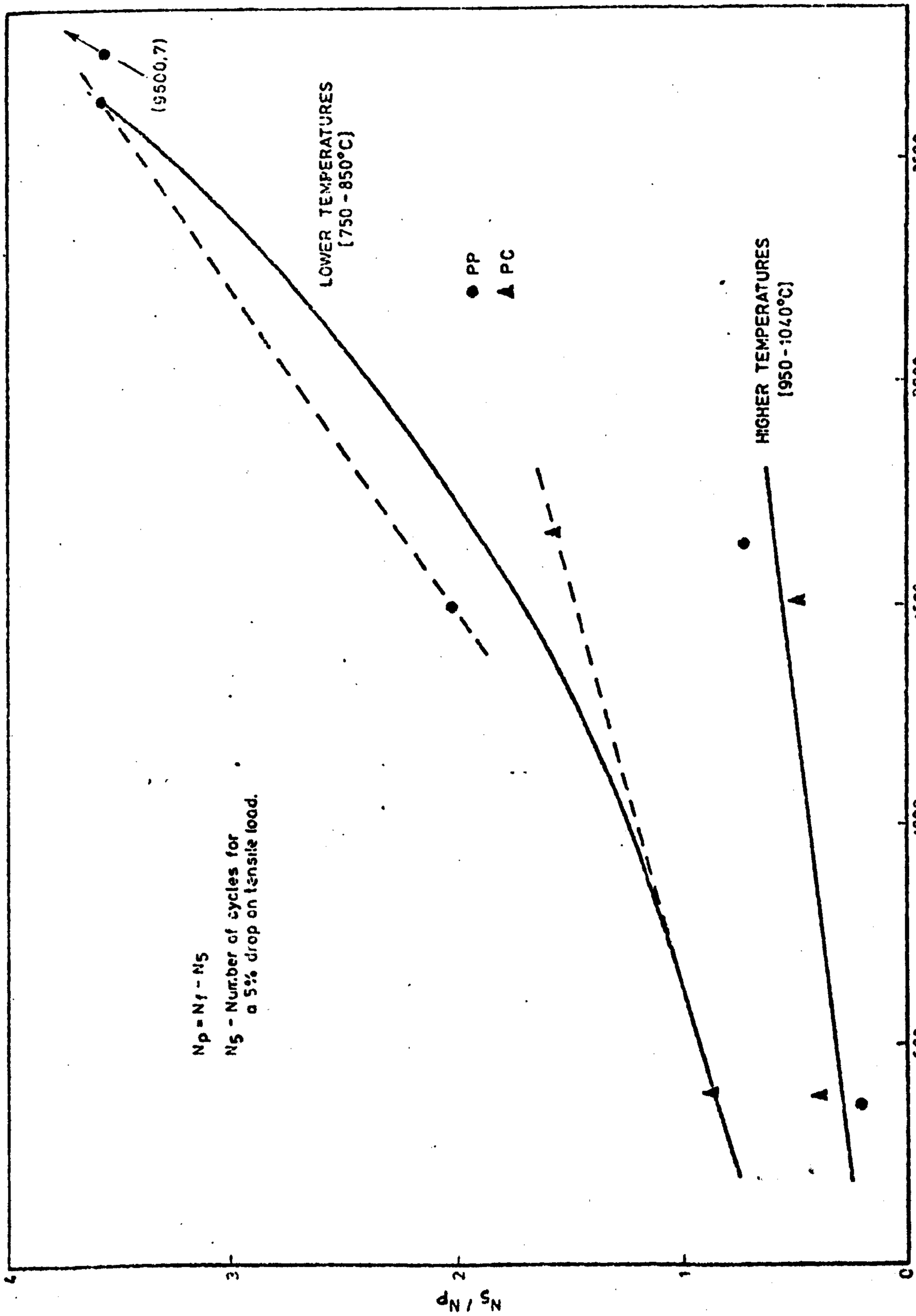

FIG. 7.11 – RATIOS N_5/N_P FOR TWO TEMPERATURE RANGES.

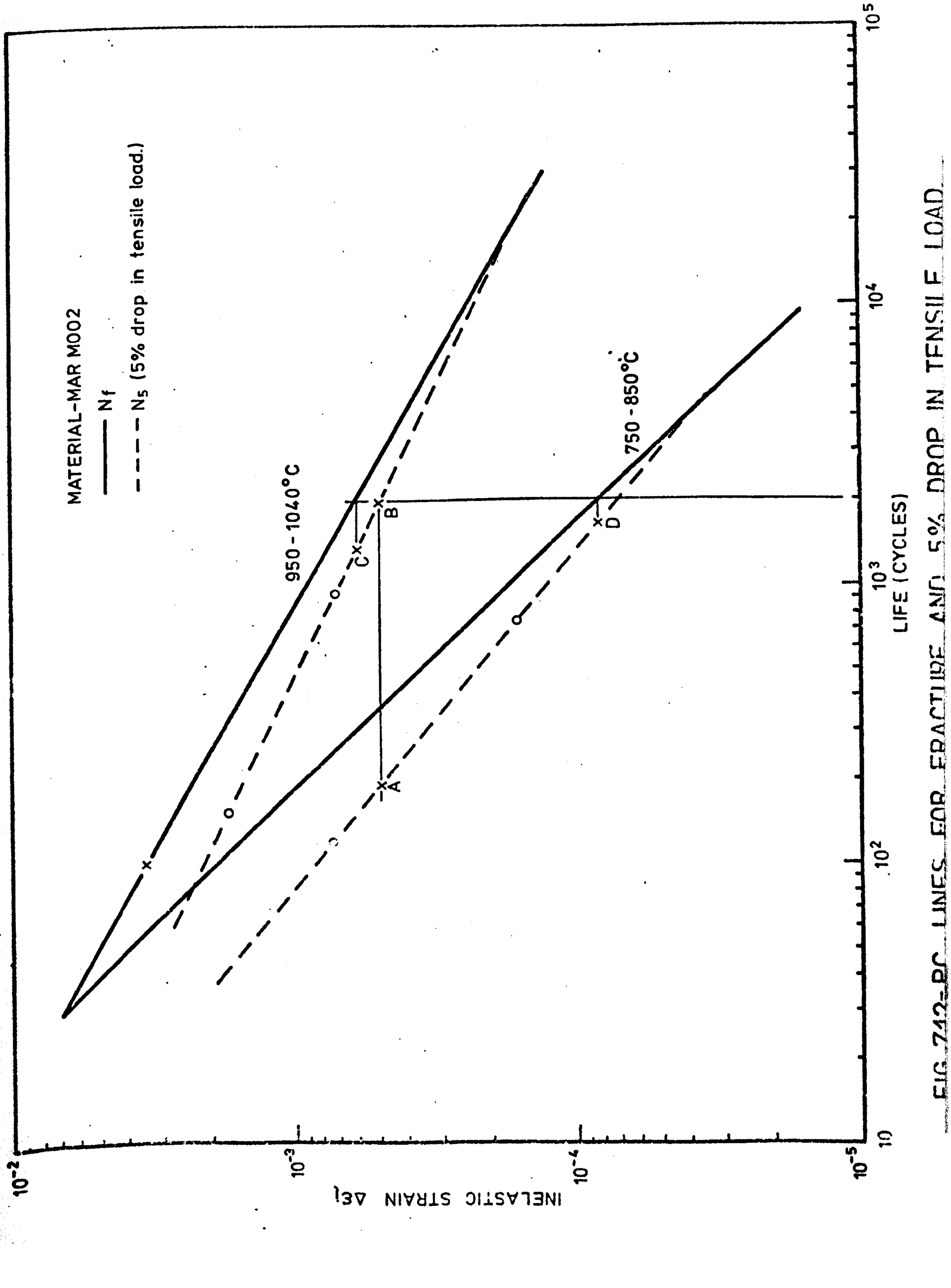

FIG 7.12-BC LINES FOR FRACTURE AND 5% DROP IN TENSILE LOAD

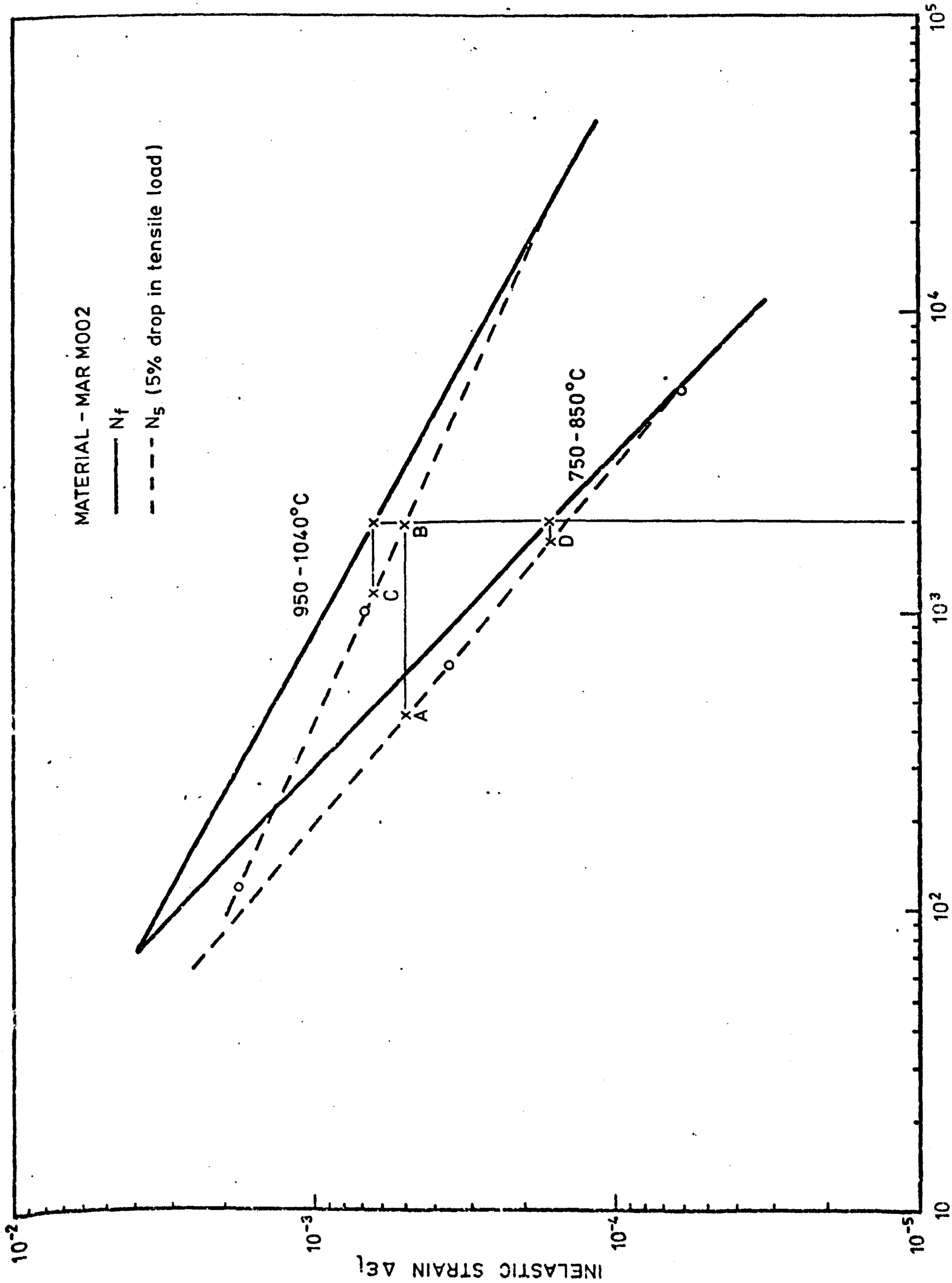

FIG 7.13 - S-P LINES FOR FRACTURE AND 5% DROP IN TENSILE LOAD.

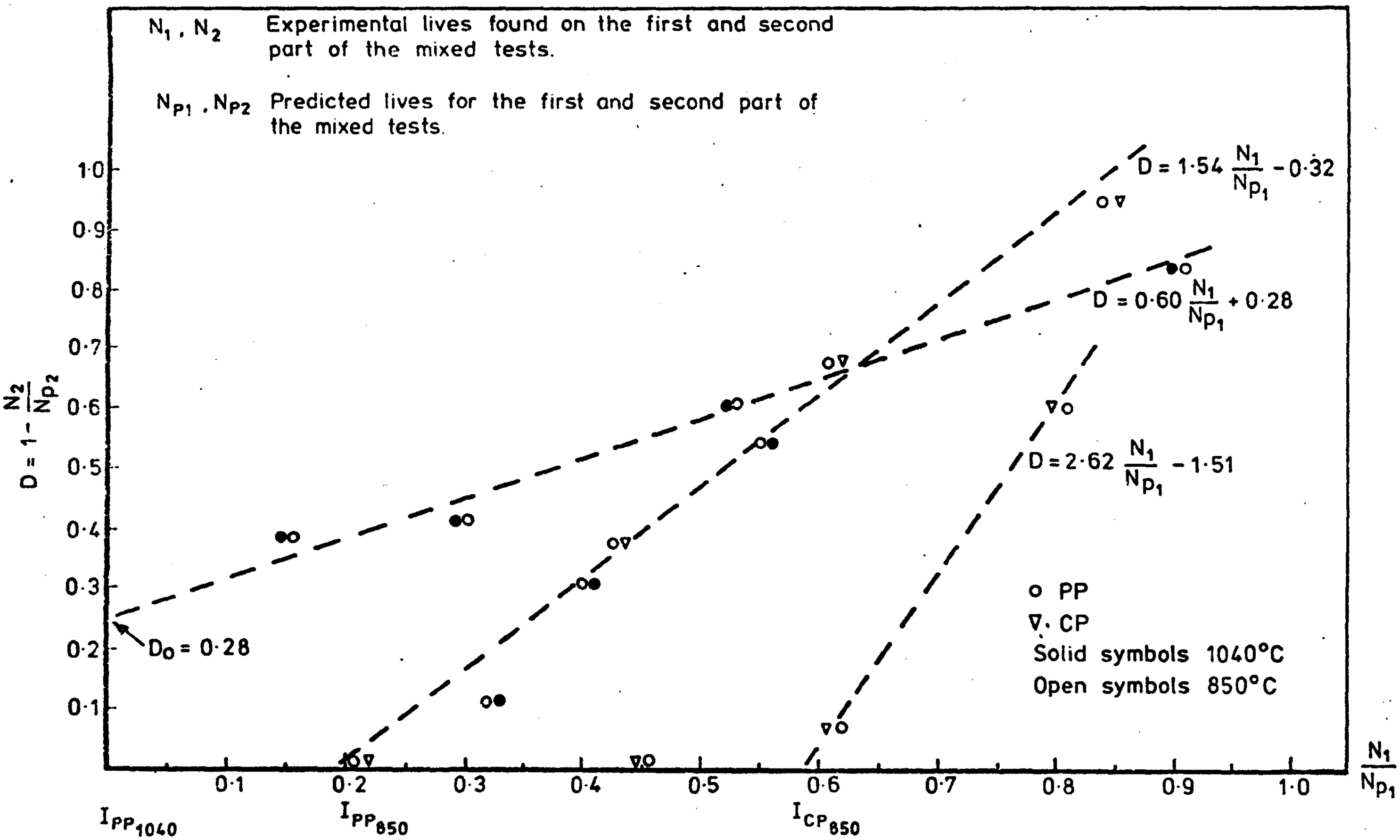

FIG. 7.14 – INITIATION POINTS FOR PP AND CP AT 850°C AND PP AT 1040°C.

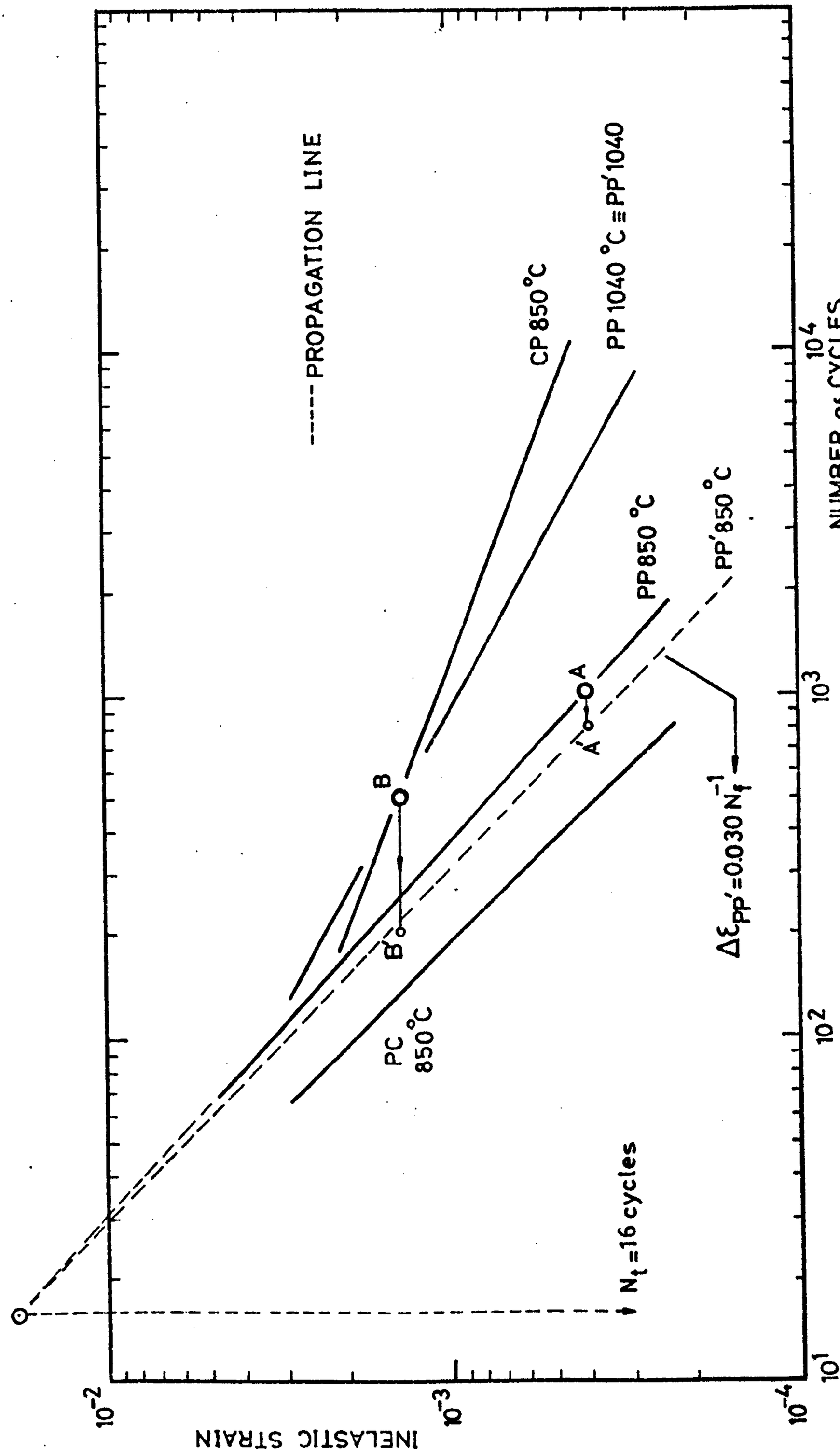

FIG. 7.15 – CONSTRUCTION OF PROPAGATION LINES (PP'850 and PP'1040 °C) BASED ON INFORMATION GIVEN BY THE MIXED TESTS.